UCRL-16969
c.2

University of California

Ernest O. Lawrence Radiation Laboratory

I. THE MEASUREMENT OF INTERNAL CONVERSION COEFFICIENTS UTILIZING SEMICONDUCTOR DETECTORS
II. DECAY SCHEME STUDIES OF THE ODD-MASS GOLD ISOTOPES

TWO-WEEK LOAN COPY

This is a Library Circulating Copy which may be borrowed for two weeks. For a personal retention copy, call Tech. Info. Division, Ext. 5545

Berkeley, California

UCRL-16969 c.2

DISCLAIMER

This document was prepared as an account of work sponsored by the United States Government. While this document is believed to contain correct information, neither the United States Government nor any agency thereof, nor the Regents of the University of California, nor any of their employees, makes any warranty, express or implied, or assumes any legal responsibility for the accuracy, completeness, or usefulness of any information, apparatus, product, or process disclosed, or represents that its use would not infringe privately owned rights. Reference herein to any specific commercial product, process, or service by its trade name, trademark, manufacturer, or otherwise, does not necessarily constitute or imply its endorsement, recommendation, or favoring by the United States Government or any agency thereof, or the Regents of the University of California. The views and opinions of authors expressed herein do not necessarily state or reflect those of the United States Government or any agency thereof or the Regents of the University of California.

Research and Development

UCRL-16969

UNIVERSITY OF CALIFORNIA

Lawrence Radiation Laboratory
Berkeley, California

AEC Contract No. W-7405-eng-48

I. THE MEASUREMENT OF INTERNAL CONVERSION COEFFICIENTS UTILIZING SEMICONDUCTOR DETECTORS

II. DECAY SCHEME STUDIES OF THE ODD-MASS GOLD ISOTOPES

Arthur Judd Haverfield

(Ph.D. Thesis)

November 10, 1966

I. THE MEASUREMENT OF INTERNAL CONVERSION COEFFICIENTS UTILIZING SEMICONDUCTOR DETECTORS

II. DECAY SCHEME STUDIES OF THE ODD-MASS GOLD ISOTOPES

Contents

Abstract v

I. Introduction 1

II. The Measurement of Internal Conversion Coefficients Utilizing Semiconductor Detectors 2

A. Semiconductor Detectors 2

B. Methods of ICC Measurement with Semiconductor Detectors 3

1. K/L Ratio 4

2. Conversion-Electron-to-Gamma-Ray Ratio 5

3. X-Ray-to-Gamma-Ray Ratio 6

4. Coincidence Measurements 8

5. Other Methods 8

C. An Internal Conversion Coefficients Spectrometer Employing Semiconductor Detectors 11

1. Method 11

2. Description of Apparatus 12

3. Calibration of Apparatus 26

4. Examples of Use 33

5. Limits of Accuracy and Possible System Improvements 37

D. Conclusion 40

III. Decay Scheme Studies of the Odd-Mass Gold Isotopes 41

A. Theory 41

1. Simple Shell Model 42

2. Core-Excitation Model 43

3. Kisslinger and Sorensen Treatment 48

4. Semimicroscopic Description 49

B. Experimental Techniques and Apparatus 50
1. Source Preparation 50
2. Apparatus 52
C. Experimental Results 53
1. ^{199}Au 53
2. ^{197}Au 64
3. ^{195}Au 78
4. ^{193}Au 98
D. Comparison of Experiment and Theory 105
1. Energy Levels 105
2. Transition Probabilities 117
3. Magnetic Moments 126
4. Log ft Values 127
5. Rotational Model 128
E. Conclusion 130
Acknowledgements 131
Appendicies 133
A. The Internal Conversion Coefficient as a Means of Multipolarity Determination 133
1. Basic Theory 133
2. Theoretical Calculations of ICC 135
3. Experimental Methods of ICC Measurement 137
B. Spectrometer Calibration 146
1. Introduction 146
2. Gamma-Ray Energy Calibration 147
3. Electron Energy Calibration 157
4. Gamma-Ray Relative-Intensity Calibration 159
5. Conversion-Electron Relative Intensity Calibration 172
6. ^{177m}Lu 175
References 183

I. THE MEASUREMENT OF INTERNAL CONVERSION COEFFICIENTS UTILIZING SEMICONDUCTOR DETECTORS

II. DECAY SCHEME STUDIES OF THE ODD-MASS GOLD ISOTOPES

Arthur Judd Haverfield

Lawrence Radiation Laboratory
University of California
Berkeley, California

November 10, 1966

ABSTRACT

The application of semiconductor detectors to measurements of internal conversion coefficients has been extensively discussed, with particular emphasis being placed upon a spectrometer employing both Si(Li) and Ge(Li) detectors for the simultaneous observation of conversion electrons and gamma rays. The construction, calibration and use of such a spectrometer were described. Possible improvements in this system were also discussed. It was found that this type of spectrometer is best suited for ICC measurements of transitions following electron-capture decay, but may still be useful in cases of beta or positron decay.

The level schemes of the odd-mass gold isotopes of mass 199, 197, 195 and 193 were examined from the decay of the respective odd-mass platinum and mercury isotopes. The measurement of numerous internal conversion coefficients permitted the assignment of spin and parity values to many of these levels. The systematic trends of many of the nuclear phenomena associated with these isotopes were examined as a function of neutron number. The experimental data were compared to the various theoretical approaches applicable to this region of nuclei.

The internal conversion process was discussed along with the various experimental methods of ICC measurement.

The calibration of semiconductor detectors for energy and intensity measurements was discussed. Extensive tables of standards for these calibration procedures were presented.

I. INTRODUCTION

The nuclear sciences have profited greatly from important instrumental advances in recent years. Among the most important of these in the area of nuclear spectroscopy had been the recent development of lithium-drifted semiconductor detectors. The applicability of these detectors to a wide range of experimental problems has already been well demonstrated. Their high resolution has made them invaluable in both singles and coincidence configurations. In Section II of this work the potential of these detectors in the measurement of internal conversion coefficients (hereafter denoted in both singular and plural forms by ICC) is examined, and a device for making such measurements is described. To aid the reader in evaluating the merit of this system, a general discussion of the ICC and the various methods of its measurement is presented in Appendix A.

A major purpose of nuclear spectroscopy is to provide those parameters of nuclear decay which will be of value in the formulation or refinement of nuclear theory. The study of nuclear level schemes in the platinum-gold-mercury region is of particular importance in the formulation of a consistent theory which will span the change from the shell-model region of the lead isotopes to the deformed region covered by the Bohr-Mottelson unified theory. To this end, we have studied the level schemes of a number of the odd-mass gold isotopes. In Section III we discuss the theoretical approaches being taken toward this region as well as the present experimental results.

Throughout this work the importance of the lithium-drift semiconductor detector has been stressed. The utilization of these devices for the measurement of the energy and relative intensity of gamma rays or conversion electrons requires standards and a standard method of analysis. In Appendix B we present the method of calibration used for our detectors as well as tables of standards for energy and intensity determinations.

II. THE MEASUREMENT OF INTERNAL CONVERSION COEFFICIENTS UTILIZING SEMICONDUCTOR DETECTORS

A. Semiconductor Detectors

The past four years have seen the accomplishments made possible through the use of semiconductor detectors grow into a list of considerable length. They have been utilized in almost every type of nuclear measurement which requires the observation of photons or particles. The benefits to the nuclear sciences have been enormous. Experiments which would have been impossible or which, at the least, would have required extremely elaborate equipment just a few years ago may now be undertaken with relative ease. While several types of semiconductor detectors have been developed we shall focus our discussion on those made by the lithium-drift technique.[1] The present level of sophistication of the lithium-drifted germanium detector has been attained through the work of a number of groups; primarily those at Chalk River, Argonne National Laboratory, and the Lawrence Radiation Laboratory in both Livermore and Berkeley. The development of lithium-drifted silicon detectors has been advanced by many small groups as well as those above.

Since there have been numerous published articles describing the theory, fabrication and use of semiconductor detectors, it would be of little value to include another such discussion at this point. However, we do feel that a brief mention of some of the major references might be of some value. Such a discussion is bound to have serious omissions, but will, it is hoped, be sufficiently complete to indicate the path for the reader to follow for information on a particular topic.

Any discussion of Ge(Li) detectors must begin by referring to the first published works on this subject. These were the articles by Freck and Wakefield[2] and Webb and Williams.[3] It is interesting to note how the field has progressed since Ref. 2 reported a Ge(Li) detector of 1.5 cm^2 × 1.5 mm depletion thickness, which exhibited a resolution (full-width at half maximum of the full-energy peak) of 21 keV at 662 keV. The first two references were followed by the first of a series of articles by Ewan and Tavendale[4] in which they described a detector having a depletion depth

of 8 mm and a resolution of 6 keV at 1.333 MeV. The first discussion of an isotope other than a standard for which a Ge(Li) detector was used to examine the gamma-ray spectrum is presented in this work. In general, these articles are primarily important from a historical point of view.

While the early work in the development of Si(Li) detectors was slanted toward their use in heavy charged-particle spectroscopy, it was immediately noted that they could serve quite well for detection of electrons. Among the first articles on Si(Li) detectors were those by Elliot,[5] Bailey et al.,[6] and Blankenship and Borkowski.[7]

There have been numerous general review articles and books published on the subject of semiconductor detectors and their application to nuclear spectroscopy. With regard to the detector itself (theory, fabrication, etc.), the following reviews are of considerable value. The books by Taylor,[8] Dearnaley and Northrop,[9,10] and Price[11] cover the subject quite extensively. Goulding[12] has presented a detailed description of these detectors, their fabrication, and optimization of the associated electronics. The review articles which place considerable emphasis on the experimental uses of semiconductor detectors are those by Ewan and Tavendale,[13] Shirley,[14] Gibson et al.,[15] Jungclaussen[16] and Hollander.[17] Also the forthcoming review articles by Ewan[18] and Camp[19] will be of great interest to the nuclear spectroscopist.

B. Methods of ICC Measurement with Semiconductor Detectors

In the present discussion, we will touch upon many of the published methods of ICC measurement using semiconductor detectors. At this point we shall exclude one method for which we reserve the remainder of Section II. The following discussion will emphasize the improvements in measurements brought about by the new detectors. For a discussion of the individual methods, the reader is directed to Appendix A of this thesis.

1. K/L Ratio

The measurement of the K/L ratio is one which can be done with relative ease using Si(Li) or phosphorous diffused silicon detectors. The resolution of these detectors is sufficient to allow separation of K and L lines for nuclides greater than about 20 in Z (depending upon the energy and intensity of the transition in question). The silicon detector has the distinct advantage over magnetic spectrometers in the multichannel acquisition of data which permits the study of short-lived activities. The solid angle of the detector can also be made large, thus allowing the use of weak samples.

However, there are certain problems involved in the use of these detectors for K/L ratio measurements. The resolution is such that it is difficult to observe the internal-conversion electron lines in the presence of an intense beta or positron continuum. Therefore, weakly-converted transitions or moderately - converted, weak transitions are particularly unsuitable cases for K/L measurement when the nuclide in question has a strong beta branch higher in energy than the transition of interest. Also in cases where Z is less than 60, resolution of L and M+N+ lines is presently very difficult. When one is unable to resolve these lines an estimate of the contribution to the L line from M,N, and higher shells must be made. In general the relationship[20] $(M+N+\ldots)/L \approx 1/3$ is used. However, it is important to note that although the photopeak efficiency for gamma rays in silicon is quite small, it still is such that a significant contribution to the (L+M+...) line may arise from the gamma ray itself. This point is particularly important in cases where the transitions of interest have very small ICC. Thus, one must experimentally subtract the gamma contribution to the electron spectrum.

The references to K/L ratio measurements with semiconductor detectors are already numerous. To indicate some of the prominent articles we point out the work by Harpster[21] and Durosinmi-Etti et al.[22]

2. Conversion Electron to Gamma Ray Ratio

To the present time, the conversion electron to gamma ray ratio has been the prime method of ICC measurement utilizing semiconductor detectors. This method has allowed the experimenter to take advantage of the high resolution of the Ge(Li) detector for gamma rays in combination with the high resolution of magnetic spectrometers for conversion electrons. The following three techniques have been used to relate the spectra obtained from the two systems.

(a) Internal standard-transition having known ICC. If one transition in the nuclide of interest has an ICC which has been measured accurately by some means (e.g. internal-external conversion) or for which the multipolarity (and thus the theoretical ICC) can be assumed, its ICC value may be used to relate electron and gamma-ray data. This method has been successfully employed by van Nooijen[23] et al., it measure the ICC of twenty one transitions in the decay of ^{86}Y to ^{86}Sr. This was not a favorable case due to the low ICC and complex decay scheme. Their quoted accuracy is 8% - 10% for the ICC of prominent transitions. This technque is also valuable if one group of workers examines the gamma-ray spectrum while another group has observed the conversion electrons.

(b) Internal standard. One may also relate the conversion electron and gamma ray spectra through the use of a mixed source (one in which a small amount of a nuclide having a well known conversion coefficient is mixed with the nuclide of interest). Brown and Ewan[24] have used this method to determine the K-ICC of the 605-keV transition in the decay of ^{134}Cs by using a composite source of ^{134}Cs and ^{137}Cs. The K-ICC of the 662-keV transition from ^{137}Cs decay is well known. The 605-keV transition was then used to normalize the conversion electron and gamma-ray data from a source of ^{134}Cs alone, giving the ICC of the other transitions in the scheme.

(c) External standard. In cases where one is unable to use the mixed source technique due to interference between the standard and transition of interest in either the electron or gamma-ray spectra or where a limited amount of the nuclide precludes production of two sources (one with standard,

one alone) having sufficient intensity to be measured by the magnetic spectrometer, the standard may be measured separately. In this external standard technique care must be taken to maintain constant geometrical detection conditions between standard and unknown. Examples of this technique are the recent measurements by Yamazaki and Hollander[25,26] of the K-ICC of the 80-keV transition from the decay of ^{166}Ho and the 208-keV transition from ^{237}U using ^{203}Hg and ^{198}Au respectively. In the first case-the mixed-source technique was not used due to the overlap of the gamma ray of interest and the K-X-rays from the standard.

The conversion-electron-to-gamma-ray method depends upon the ability to determine the relative intensities of both conversion electrons and gamma rays. The Ge(Li) detector has, of course, provided a great increase in resolving power for complex gamma-ray spectra over the NaI(Tl) detectors. This permits analysis of most spectra for relative intensities. The methods of gamma-ray detection which have extremely high resolving ability (i.e. curved crystal, external conversion) do not have as good a signal-to-noise ratio as the Ge(Li) detector, and thus, the ability to determine the intensities of the weaker transitions in the spectrum is hindered. Another drawback of the latter detection methods is the fact that radioactive sources required must be considerably stronger than those required for Ge(Li) detectors.

Thus, the Ge(Li) detector, providing the ability to determine relative gamma-ray intensities to an accuracy of approximately 3%, has greatly improved the conversion electron to gamma ray ratio as a method of routinely determining ICC. An extension of this method will be discussed in Section II-C of this thesis.

3. X-Ray - to - Gamma-Ray Ratio

Since the X-ray - to - gamma-ray ratio method of ICC determination again depends upon the ability to determine the relative intensities of peaks in the photon spectrum, it is expected that the semiconductor detector will be of great value in this type of measurement. It is now possible to obtain peak widths (FWHM) of 0.6 - 0.9 keV in the X-ray region using either Ge(Li)

or Si(Li) detectors. This permits resolving of K_α and K_β X-rays from elements having Z = 30-40. Thus, only in very unusual cases will gamma rays interfere with analysis of the X-rays. The high resolution of the semiconductor detector also permits resolution of the X-ray and its associated backscatter peak. It has been noted that the poor resolution of the NaI(Tl) detector has caused ICC determined by this technique to be systematically high, presumably due to that area of the X-ray peak arising from inclusion of backscattered photons. However, it is not solely the resolution which makes semiconductor detectors valuable for these measurements. The presence of iodine X-ray escape peaks in the NaI(Tl) photon spectra contributes to difficulties in intensity analysis. For Ge(Li) detectors the probability of escape of the corresponding Ge X-ray (9.9 keV) is very small and such a phenomenon has not been observed. Thus, in general, the gamma-ray spectra taken on Ge(Li) detectors are much "cleaner" and easier to analyze for intensities.

The sensitivity of the surface lattice sites of the Ge(Li) detector to contaminants has caused the need for a permanent closed vacuum chamber for the detector. While some detectors have actually been encapsulated, the normal procedure has been to place them in a vacuum-tight cryostat. Either of the methods of protection cause an increased "window" (absorption layer) through which X-rays must pass. To avoid this problem, one may use one of the more rugged Si(Li) detectors and be able to place the source within the cryostat. The Si(Li) detectors presently available have quite thin windows. They show a maximum in the photopeak efficiency curve at approximately 15-20 keV in comparison to the maximum at 60-70 keV for "thin window" Ge(Li) detectors in cryostats with 0.010 in. thick Be windows. In general, however, the Si(Li) detector is not as useful for this type of ICC measurement as the Ge(Li) detector in cases where the gamma ray (which is to be compared in intensity to the X-ray) is fairly high in energy. Thus, the Si(Li) detector would be best for cases with $Z < 65$ and $E_\gamma < 100$ keV.

Due to the great interest in using semiconductor detectors for the analysis of complex spectra, there has been little work reported on their

utilization on very simple decays, where this method of ICC measurement is useful. Yamazaki and Hollander,[26] however, have determined the K-ICC of the 208-keV transition in the decay of ^{237}U by this method and find it in good agreement with the value obtained from the external standard-conversion-electron-to gamma-ray ratio measurement.

4. Coincidence Measurements

If the nuclide of interest has two transitions in cascade, the measurement of coincidences between the gamma rays of one transition and conversion electrons of the other can be used to determine the total ICC from relation

$$N_{e_2\gamma_1} = N_{\gamma_1} \frac{\alpha_2}{1+\alpha_2} (\omega\epsilon)_{e_2}$$

where $N_{e_2\gamma_1}$ is the number of conversion electrons from the second transition of the cascade which are in coincidence with the preceding gamma rays; N_{γ_1} is the number of gamma rays observed from the first transition; α_2 is the total ICC of the second transition; and $(\omega\epsilon)_{e_2}$ is the full-energy peak efficiency for conversion electrons from the second transition. This general method has been employed by Bosch et al.,[27,28] as well as Sen et al.[29,30,22] to measure a number of ICC. In their work, both groups have used silicon detectors for the observation of conversion electrons. This has permitted acquisition of the coincident electron spectrum in a multichannel manner, thus, avoiding the slow point - by - point scanning of the magnetic spectrometer. The errors estimated for the ICC values determined using the silicon - NaI(Tl) coincidence combination is about 7 per cent.

5. Other Methods

While the work on utilizing semiconductor detectors for some of the other methods of ICC measurements has thus far not been extensive, we feel some brief mention must be made of the potential value of these detectors for the following types of ICC measurement.

(a) L - subshell ratio. The good resolution for conversion electrons presently obtainable with Si(Li) detectors in conjunction with field-effect

transistor (FET) preamplifiers (~ 1.4 keV at 100 keV) indicates that for transitions in high Z nuclides it should be possible to measure $(L_I + L_{II})/L_{III}$ ratios as an indicator of multipolarity. This should be extremely useful for many of the short-lived heavy elements. As an indication of this potential, we include in Fig. 1 the electron and gamma-ray spectrum of ^{237}U decay taken with a Si(Li) detector.[31]

(b) Conversion-electron - peak - to - beta - distribution ratio. As indicated by Bertolini et al.[32] low energy scattering of electrons was the initial problem to be overcome in using Si(Li) detectors for accurate beta spectrum measurements. It has been shown that this problem can be overcome by a number of means.[33,34] Thus, if one were to devise the proper experimental arrangement, it should be possible to measure the entire beta spectrum as well as the superimposed conversion lines in a single measurement. This method of ICC measurement could then be extended to weak or short-lived sources.

(c) Internal-external conversion. The usual internal-external conversion method employing high-resolution magnetic spectrometers, while quite accurate, is very inefficient. Since it has been shown that Si(Li) detectors can be used in external conversion measurements,[31,35] it is tempting to think that they could be employed in this method of ICC measurement for cases where source strength or half life is a problem. Due to its moderate insensitivity to gamma rays the Si(Li) detector may be placed quite near the converter foil used in this measurement, thus yielding a good efficiency for the external conversion electrons. Another advantage with the Si(Li) system is the fact that the entire external conversion spectrum can be taken in a single measurement. While the Si(Li) detector does not offer the very high resolution of magnetic spectrometer, it does have advantages which may yet make it a useful tool in internal-external conversion measurements.

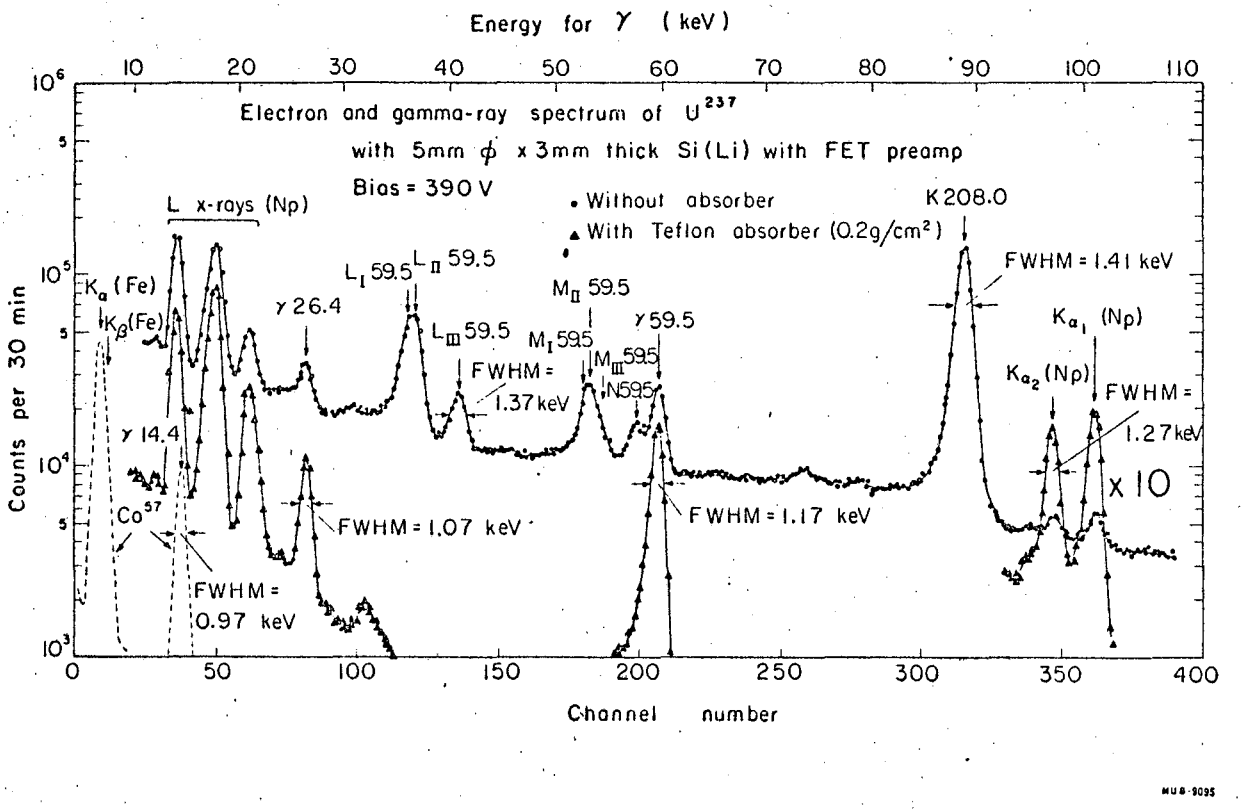

Fig. 1. Conversion-electron and gamma-ray spectrum of ^{237}U.

C. An Internal Conversion Coefficient Spectrometer Employing Semiconductor Detectors

1. Method

In Section II-B we have discussed the conversion-electron-to-gamma-ray-intensity ratio as a means of utilizing semiconductor detectors in the measurement of ICC. The methods described have taken advantage of the high resolution of magnetic spectrometers for conversion electrons as well as the high resolution of Ge(Li) detectors for gamma rays. The accuracy of this type of measurement is quite good, with errors of only 3-5% possible in the best cases. This accuracy is sufficient to provide a test of ICC theory. However, this measurement does require the use of magnetic spectrometers with their associated low efficiency and slow scanning rate. In many experiments, one initially desires ICC values which are sufficiently accurate to allow differentiation of possible multipolarities and thus, the formulation of a consistent level scheme. This type of experiment is one of major difficulty if the half life of the nuclide in question is moderately short and one attempts to use a magnetic spectrometer. Since a complete scanning of the conversion electron spectrum may take a prohibitively long time, a detailed knowledge of the gamma-ray spectrum is usually a necessity before the conversion electrons are observed. With the advent of the Si(Li) detector, with its good resolution, high efficiency, and multichannel acquisition of data, it has become possible to observe the entire conversion electron spectrum in a single measurement. The thought of applying the combination of Ge(Li) and Si(Li) detectors for the simultaneous observation of gamma rays and conversion electrons was immediately put forth. A direct extension of this type of observation is the use of relative intensities of the gamma ray and its corresponding conversion electron to determine the ICC.

In this section we shall discuss a device utilizing both Ge(Li) and Si(Li) detectors capable of measuring ICC to an accuracy of 10-15%. In this method, the radioactive source is positioned directly between the two detectors and within the vacuum chamber surrounding the Si(Li) detector.

The conversion-electron and gamma-ray spectra are simultaneously accumulated and the areas of the gamma ray and its corresponding conversion electron line are measured.

The ICC is then found from

$$\alpha = \frac{A_e}{(\omega\epsilon)_e} \frac{(\omega\epsilon)_\gamma}{A_\gamma}$$

where A_e is the area under the conversion electron peak.

A_γ is the area under the corresponding gamma-ray peak.

$(\omega\epsilon)_e$ is the detection efficiency of the Si(Li) system for electrons in the full-energy peak (including geometric factor).

$(\omega\epsilon)_\gamma$ is the detection efficiency of the Ge(Li) system for gamma rays in the full-energy peak (including geometric factor).

Thus it is possible to simultaneously determine, knowing the efficiencies of the two detectors as functions of the energy of incident radiations, all of the ICC for the transitions observed in a given region of the energy spectrum. If constant geometry is maintained between efficiency calibration and experimental measurement, there is no need for applying the mixed source technique or, with the exception of occasional general system checks, running external standards. The importance of this method for the rapid general determination of ICC and especially for ICC determinations in short-lived decays is quite obvious.

2. Description of Apparatus

A photograph of the original design[36] of the spectrometer is shown in Fig. 2 and a scale drawing is shown in Fig. 3. It consisted of a small vacuum chamber of dimensions 8 in. long × 6.25 in. high × 5 in. deep, in which were mounted, in 180° fixed geometry, Si(Li) and Ge(Li) detectors. The detectors were fabricated here at Berkeley by the methods discussed by Goulding.[12] A 1/16 -inch aluminum absorber was placed in front of the Ge(Li) detector to prevent observation of conversion-electron lines in the gamma-ray spectrum. In order to minimize the loss of scattered electrons at the

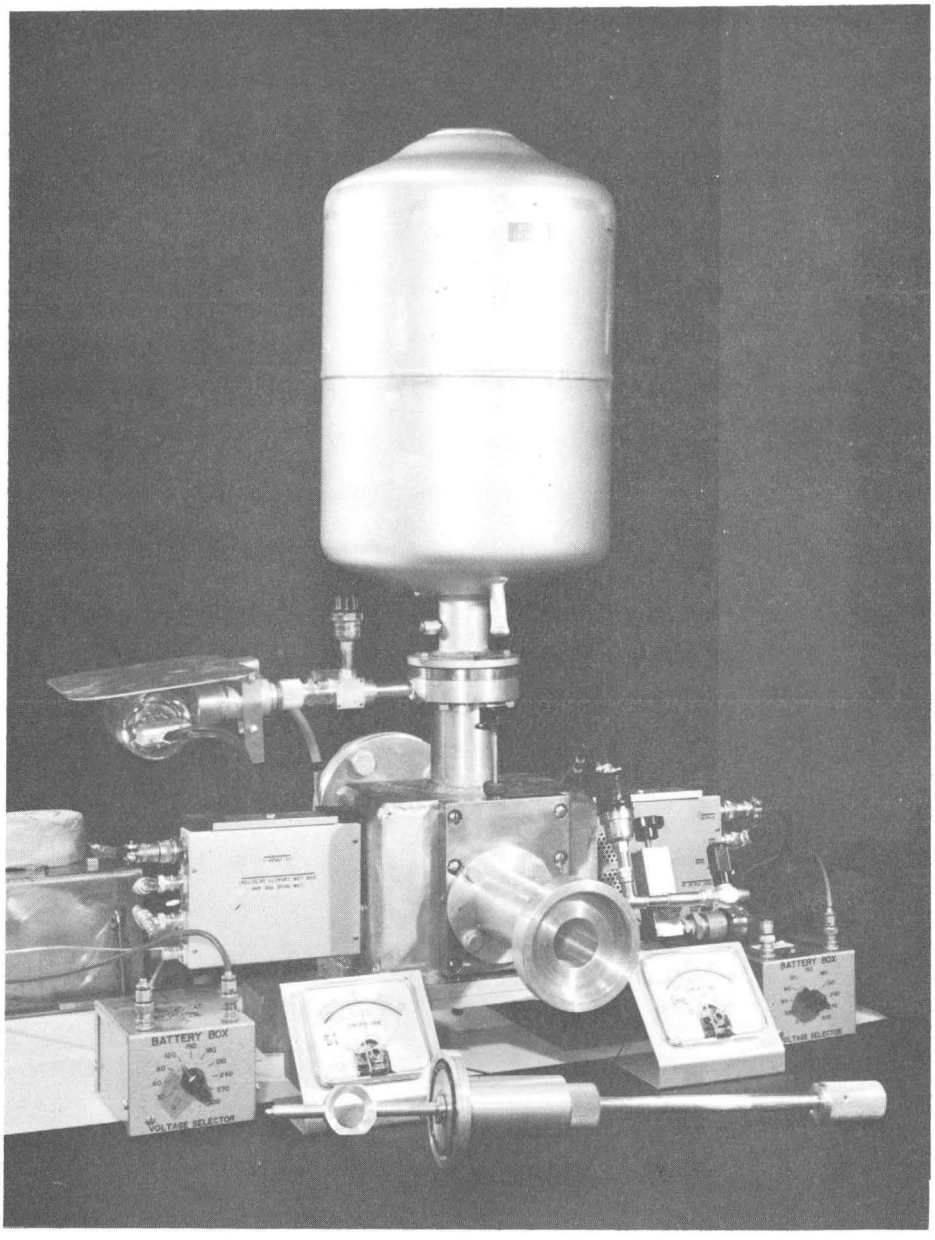

ZN-5190

Fig. 2. Photograph of original design of the conversion-coefficient spectrometer.

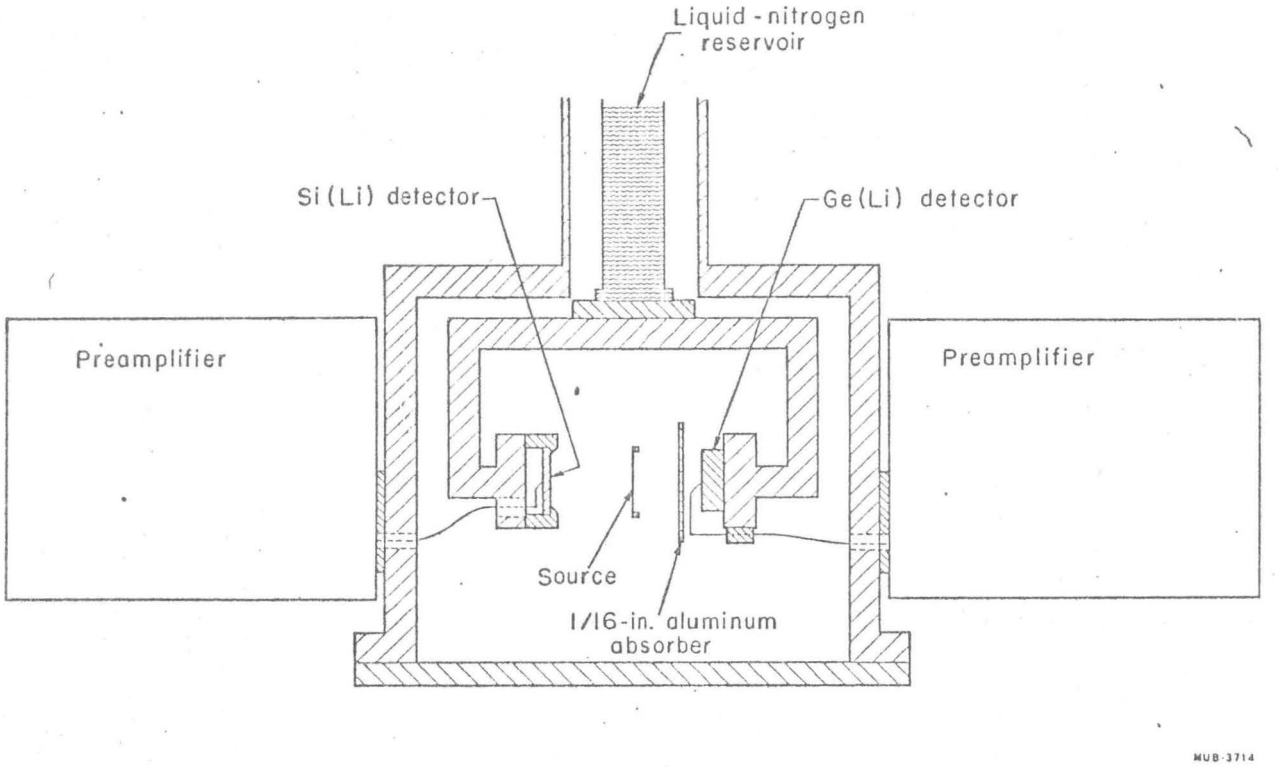

Fig. 3. Schematic scale drawing of the original design of the conversion-coefficient spectrometer.

edges of the Si(Li) crystal, we placed a 5/16 -inch diameter aluminum collimator in front of the crystal. By doing this, we hoped to increase the fraction of electrons which enter the crystal and deposit their full energy within the depletion region, and thus, contribute to the full-energy peak in the resulting electron spectrum. The vacuum chamber was maintained at a pressure of approximately 2×10^{-6} mm with use of a standard oil diffusion pump, separated from the chamber by two cold-traps in series to minimize deposition of pump oil on the detectors. Active sources were introduced into the vacuum chamber through an air lock of conventional design, which was evacuated by a separate roughing pump. The source holder, seen in the foreground of Fig. 2, was designed so as to assure reproducible positioning of the source directly between the two detectors. The source-to-Si(Li)-detector distance was 0.594 in. and the distance to the Ge(Li) detector was 1.177 in. The detectors were cooled with the use of a 10-liter gravity feed liquid nitrogen reservoir of commercial manufacture.[37] The Ge(Li) detector was kept at "liquid nitrogen temperature" (77° K), while the Si(Li) detector was maintained at 208° K, at which temperature the resolution was found to be optimum, by the introduction of a heat leak at the Si(Li) detector mount. The performance of the original design, with Ge(Li) and Si(Li) detectors of 4 cm^2 by 5 mm deep and 1 $cm^2 \times 3$ mm deep respectively, is shown in Fig. 4. In the conversion-electron spectrum the K,L, and M electron lines of the 279-keV transition in the decay of ^{203}Hg are resolved, with a resolution of 4.2 keV. The resolution of the 279-keV photon is seen to be 4.6 keV.

The great sensitivity of the surface of the Ge(Li) detector to contaminants made the above design undesirable. If an inexperienced operator were to open the source insert gate without first closing the air lock to the roughing pump, the different pumping rates would cause pump oil to be drawn into the vacuum chamber. To recover the Ge(Li) detector, the entire apparatus would have to be brought to room temperature, and the Ge(Li) detector would have to be removed, cleaned and re-etched (possibly redrifted).

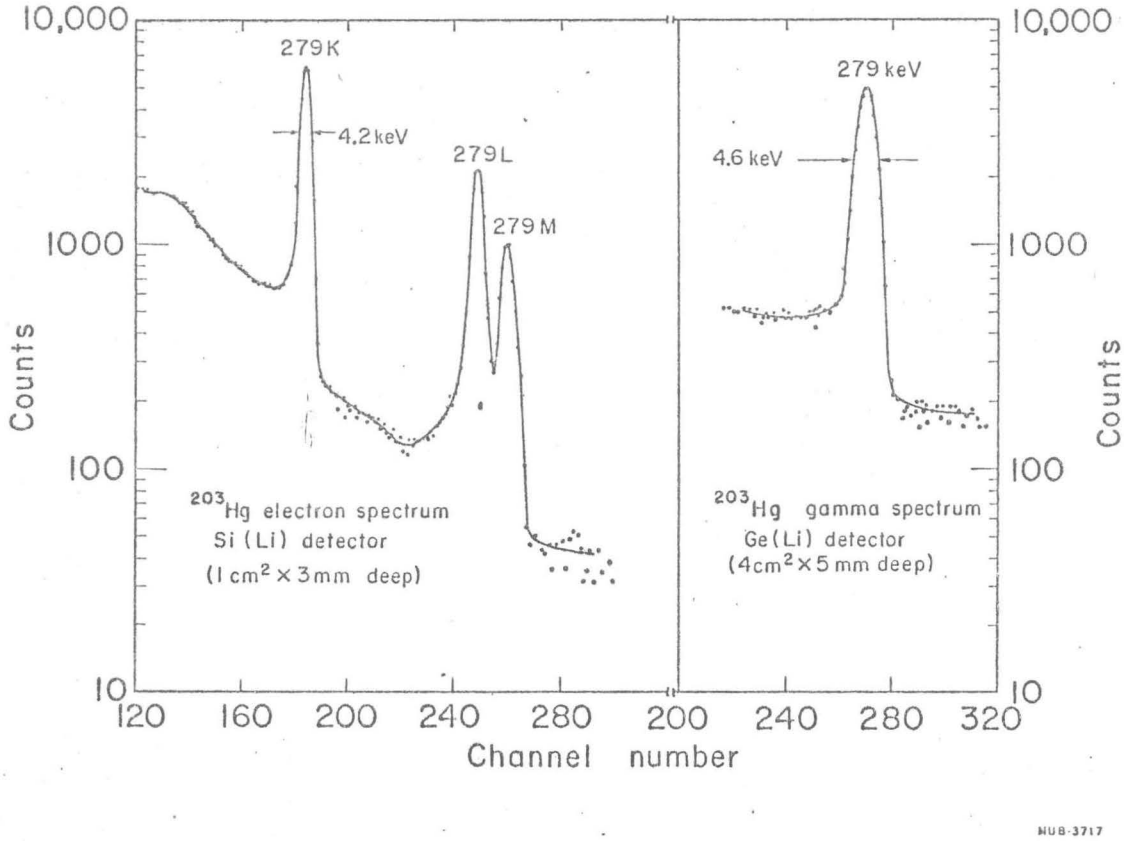

Fig. 4. ^{203}Hg partial conversion-electron and gamma-ray spectra taken simultaneously with original conversion-coefficient spectrometer.

While the rugged Si(Li) detector, with its varnish covering, could be cleaned without removing it from the chamber, the removal and subsequent replacing of the Ge(Li) detector would necessitate a complete recalibration of the system. With this in mind the conversion coefficient spectrometer was modified.

A photograph of the modified spectrometer is shown in Fig. 5 and a scale drawing shown in Fig. 6. In this design the internal Ge(Li) detector and its cooling arm have been removed from the original chamber, the original end wall removed and replaced with a new wall having a 1.75-inch deep "well" positioned directly opposite the Si(Li) detector. A Ge(Li) detector in its own holder, of Berkeley design,[38] is then capable of being positioned reproducibly in this well. Thus, the Ge(Li) detector has its own vacuum system and is not subject to possible contamination within the chamber. Since this reduces the quality of vacuum needed in the main chamber, the oil diffusion pump was replaced by another roughing pump. The final pressure in the chamber was approximately 1×10^{-3} mm. However, it was found that after a long period of pumping, an oil film began to form on the surface of the Si(Li) detector in spite of two cold-traps between pump and chamber. This was observed from increased energy degradation and "tailing" of the electron lines. To remove the need for numerous cleanings of the detector, we have obtained a cryosorption vacuum pump of type designed by R. Hintz and co-workers at the Lawrence Radiation Laboratory.[39] This is a large molecular sieve pump containing approximately 15 lbs. of sieve material. It is capable of evacuating a 200 liter chamber from atmospheric pressure to 1 micron within a period of 8-10 minutes. In Fig. 7 we show a photograph of this pump, and in Fig. 8 we show a photograph of the pump in its normal experimental position.

In order to improve the resolution of the Si(Li) detector, we have incorporated into the system a preamplifier of the type described by Elad,[40,41] which employs in its first stage a field-effect transistor (FET) which is cooled to 77° K and contained within the vacuum chamber to reduce system capacitance. A schematic diagram of this preamplifier is shown in Fig. 9. In Figs. 10, 11, and 12 we show spectra obtained using the Si(Li)

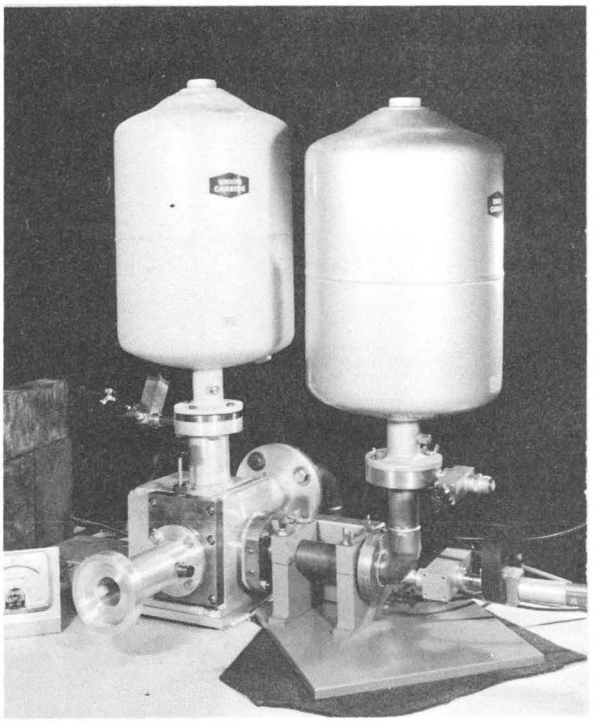

(a)

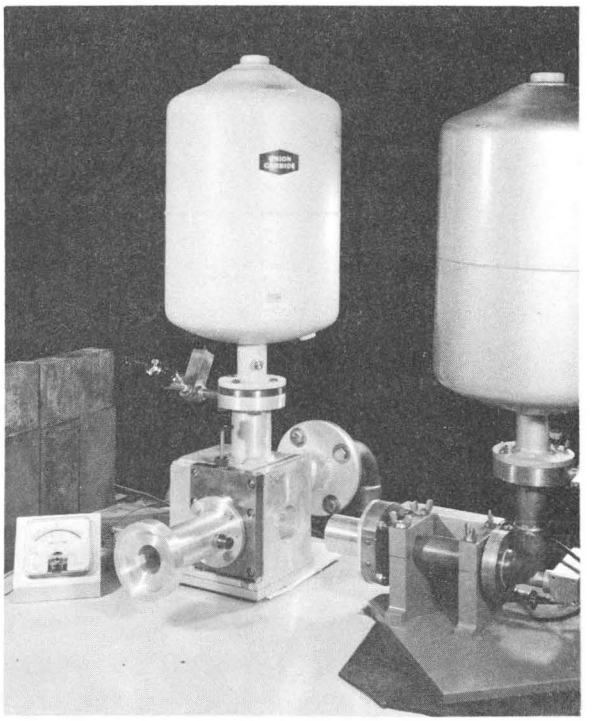

(b)

ZN-4764

Fig. 5. Photograph of modified conversion-coefficient spectrometer.

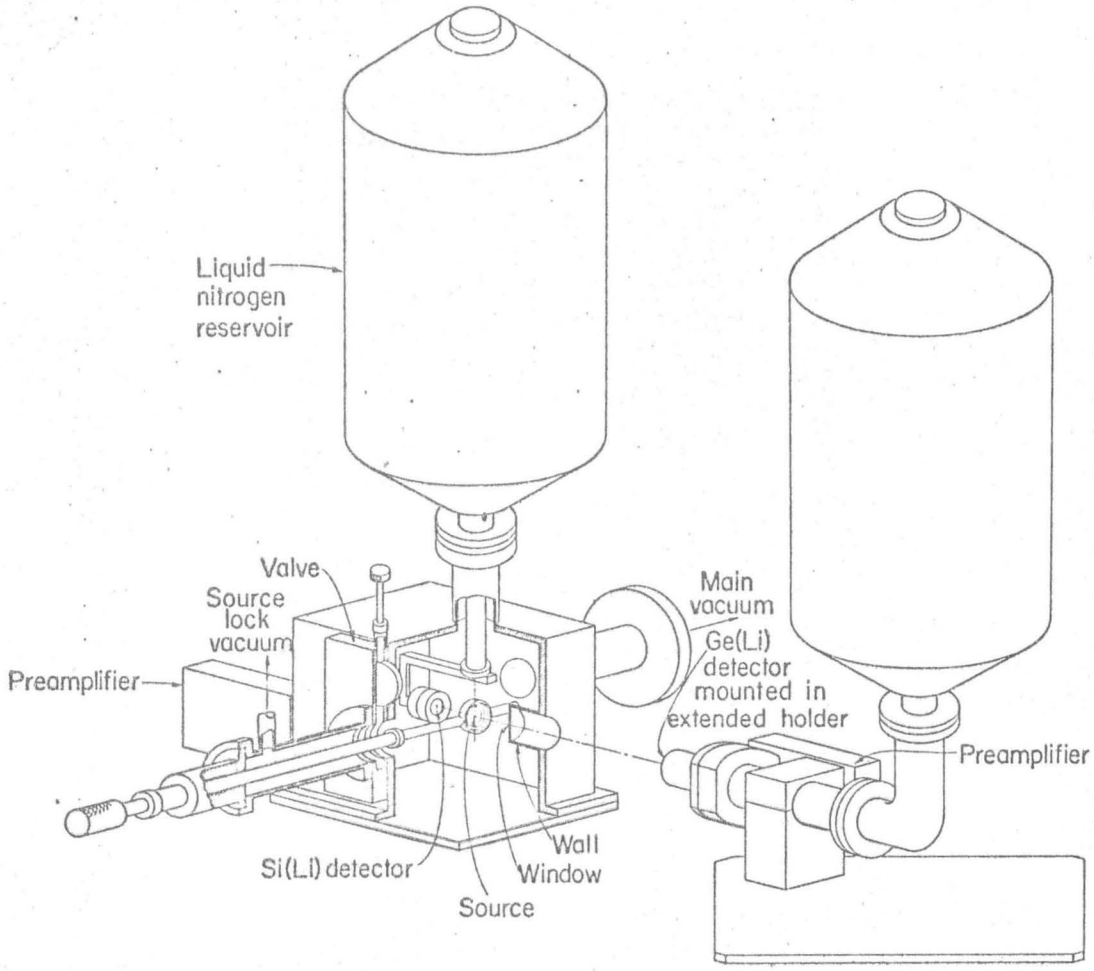

Fig. 6. Schematic scale drawing of modified conversion-coefficient spectrometer.

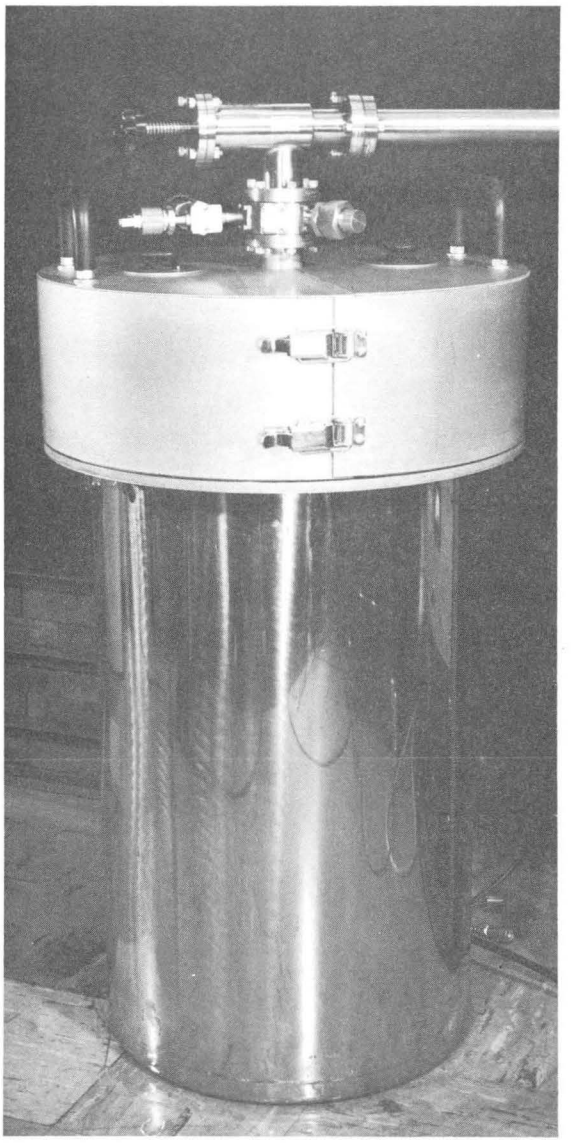

ZN-6006

Fig. 7. Photograph of cryosorption vacuum pump.

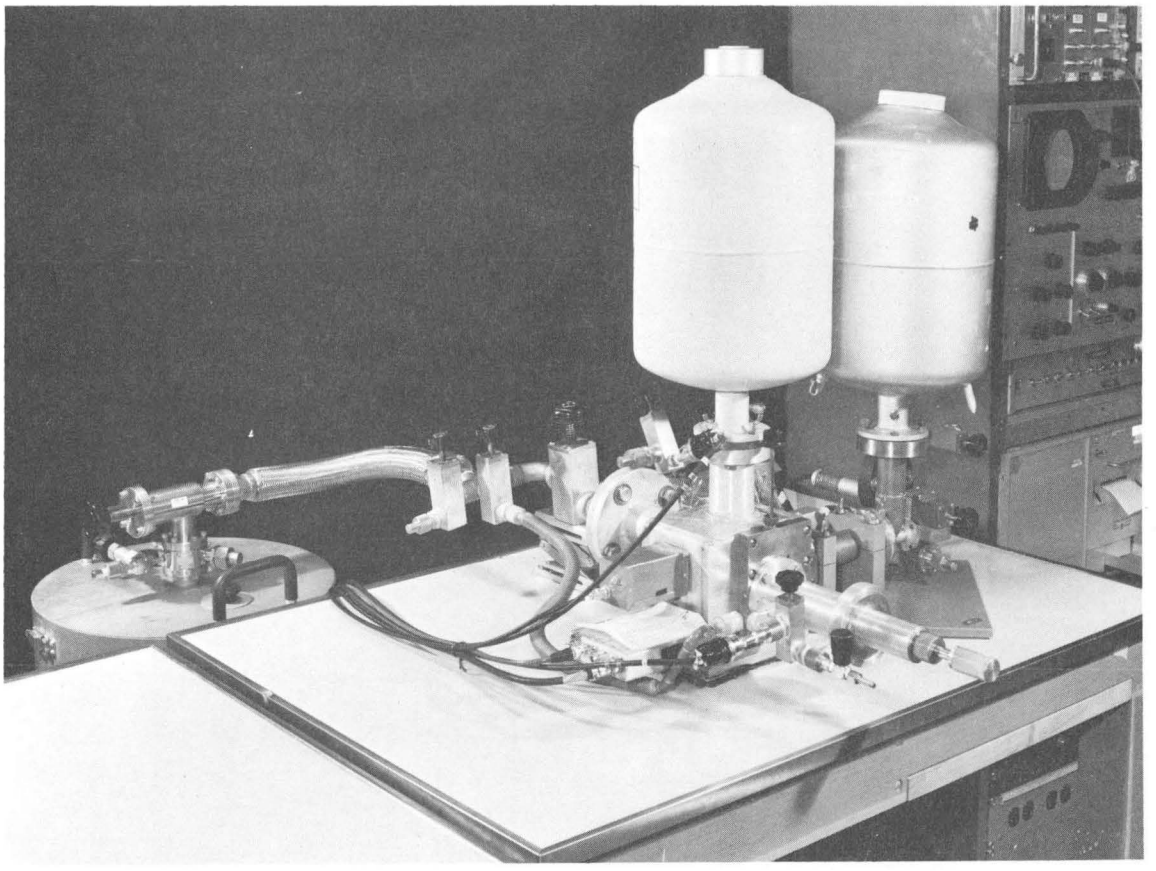

ZN-6007

Fig. 8. Photograph of experimental vacuum system employing cryosorption pump.

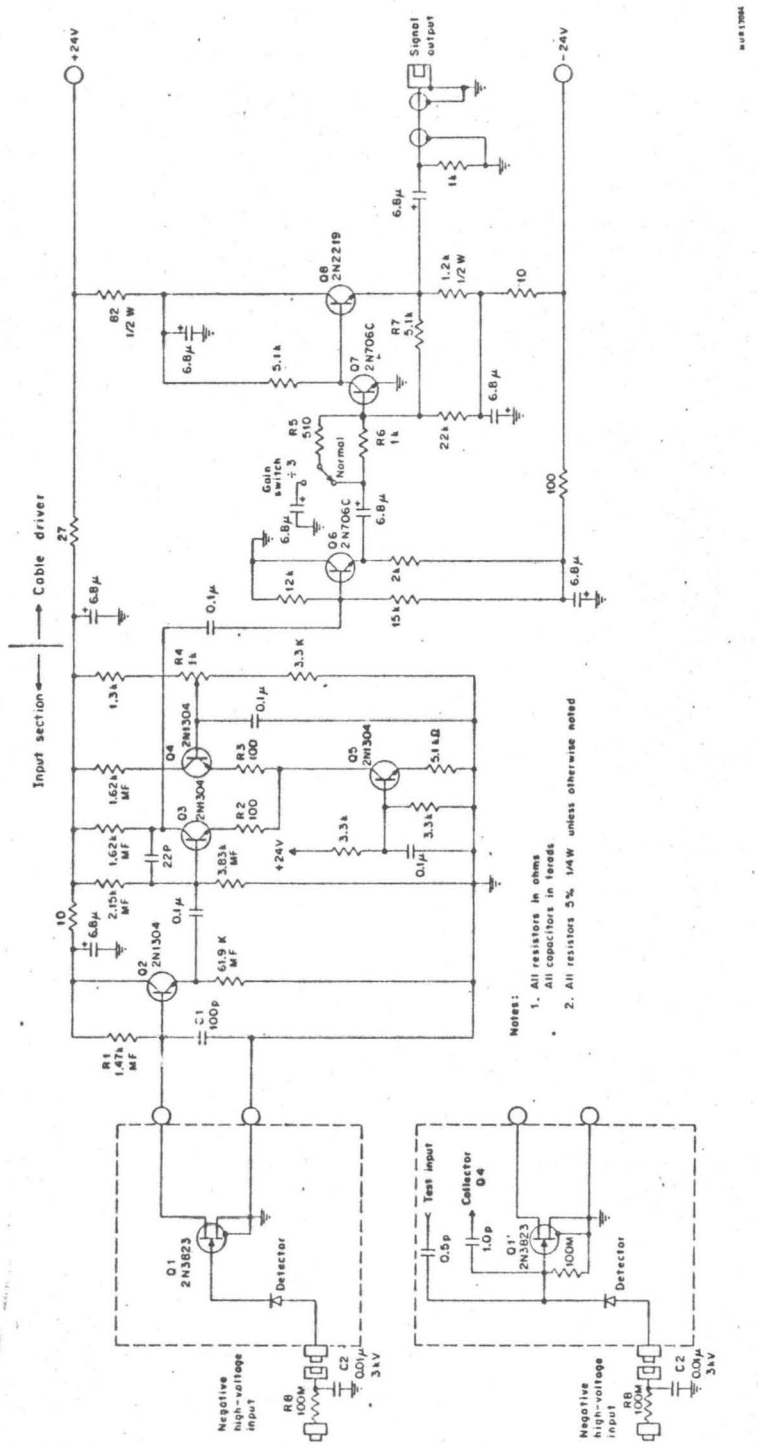

Fig. 9. Schematic diagram of field-effect transistor preamplifier designed by Elad and Nakamura.[41]

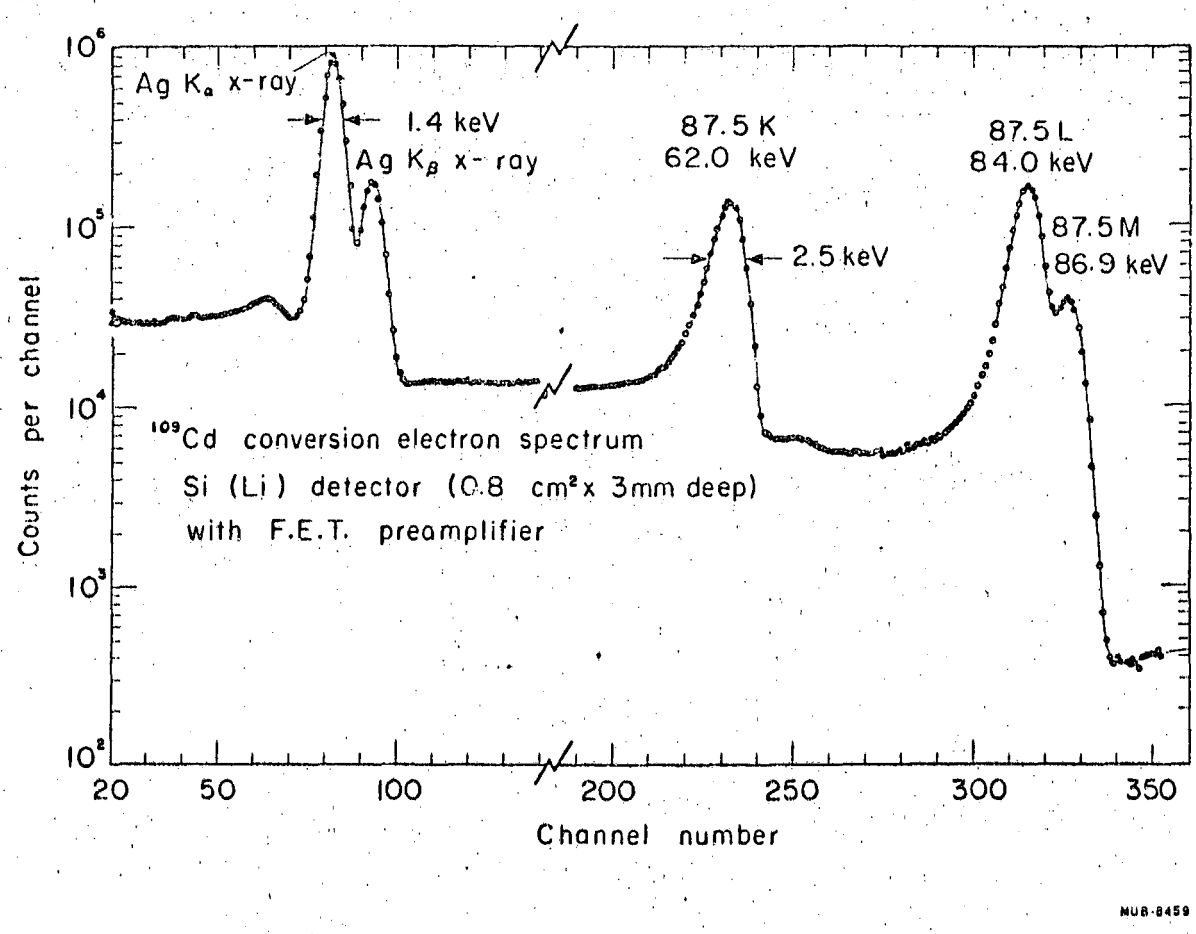

Fig. 10. Conversion-electron and x-ray spectrum from the decay of ^{109}Cd. The resolution at 62 keV is limited by source-thickness effects.

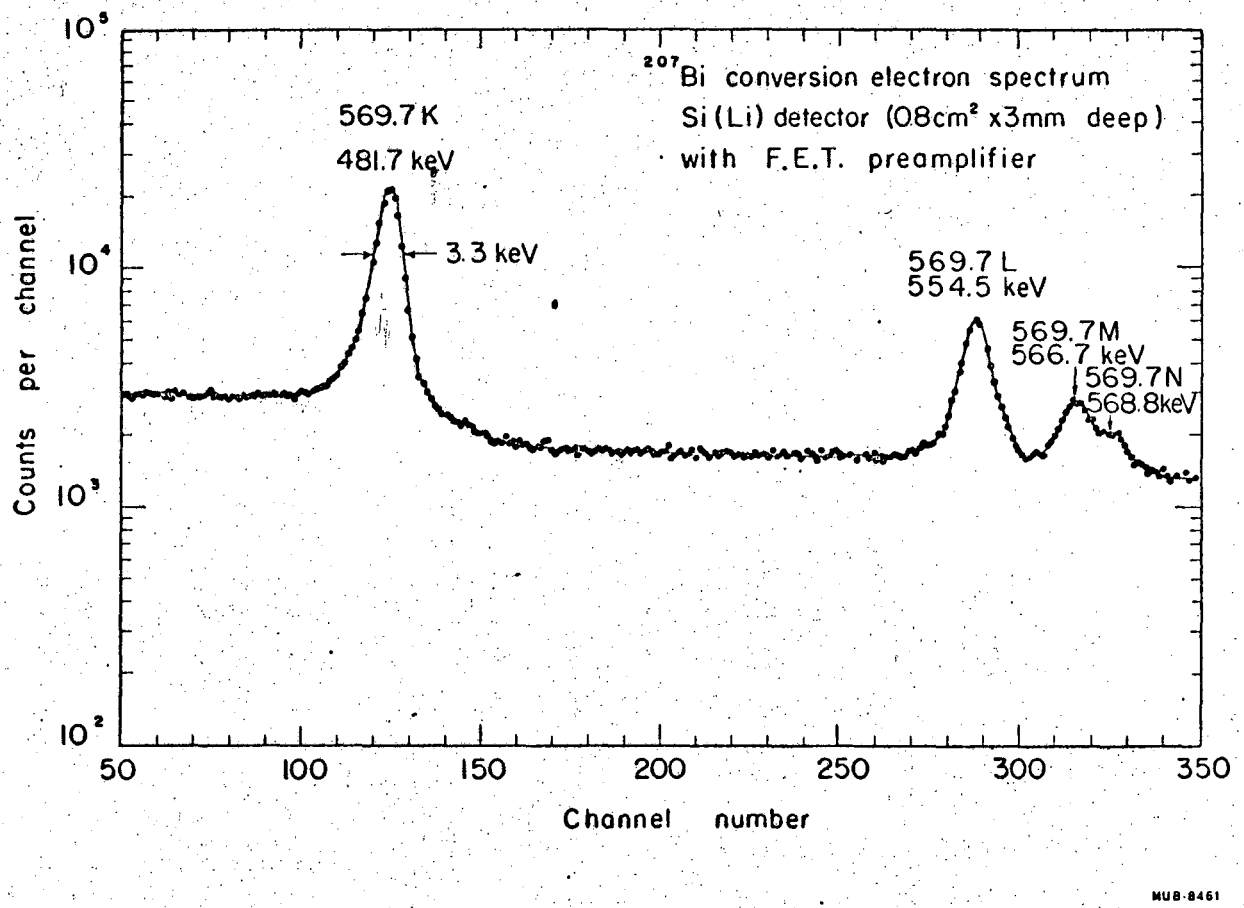

Fig. 11. Partial conversion-electron spectrum of ^{207}Bi.

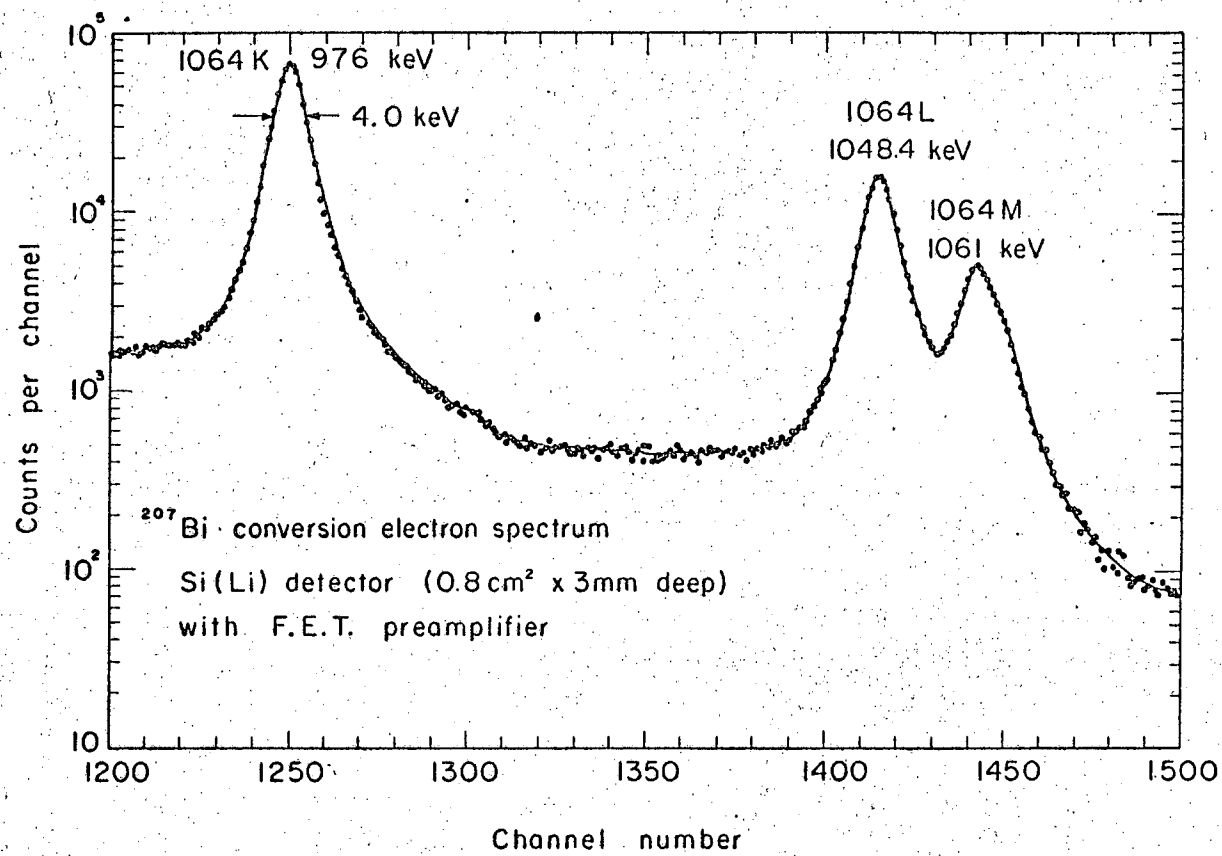

Fig. 12. Partial conversion-electron spectrum of ^{207}Bi. High-energy tailing on the peaks is due to summing effects within the detector.

detector and FET preamplifier. In Fig. 10 we show the X-ray and conversion-electron spectrum from the decay of ^{109}Cd. The resolution for the 22-keV Ag K_α X-ray is 1.4 keV, and the resolution for the 62.2-keV K line of the 87.9-keV transition is 2.5 keV (which is limited due to source thickness). Figures 11 and 12 show the conversion electron groups from the 569.6- and 1063.5-keV transitions in ^{207}Pb respectively. These spectra exhibit resolution of 3.0 and 4.0 keV at 481.6 and 975.5 keV. It is interesting to note that the optimum temperature for the Si(Li) detector used in conjunction with the FET was determined to be 143° K. This is essentially in agreement with the findings of Elad and Nakamura.[41] To attain this temperature, the contact between detector mount and cooling arm was made with 1/2-inch ceramic spacers.

In all of our work we have used amplifier-biased-amplifier systems designed by Goulding and Landis[42,43] and manufactured at this Laboratory. Pulse-height analysis of the spectra have been made with two 400-channel R.I.D.L. analyzers[44] or a Scipp 1600-channel analyzer[45] modified to operate as two independently timed 800-channel analyzers.

Sources for this spectrometer were either liquid deposited or evaporated onto 0.00025-inch gold-anodized mylar. The mylar was made structurally solid by fastening to 1-inch annular rings of aluminum with aluminum spray lacquer. The actual source deposits were typically 0.3 cm^2 or smaller in area and 10 μ Ci in strength.

3. Calibration of Apparatus

The calibration of the spectrometer was carried out in the following manner: First, the photopeak efficiency of the Ge(Li) detector for gamma rays was determined as a function of energy by the method described in Appendix B-4. Then, by utilizing nuclides with well-known conversion coefficients, the full-energy peak efficiency of the Si(Li) detector for electrons can be determined at a number of energies from

$$(\omega\epsilon)_e = \frac{A_e}{A_\gamma} \frac{(\omega\epsilon)_\gamma}{\alpha_k}$$

These points should be sufficient to determine the efficiency function of the detector. Those sources which have sufficiently well-known ICC to be used as standards are listed in Table I. This table is taken from the compilation of van Nooijen and Hamilton.[46] It is also suggested that a source which emits conversion electrons of well-known relative intensities be used as an independent check of the shape of Si(Li) efficiency function. Possible sources for such a measurement are discussed in Appendix B-5.

As an example of the efficiency observed for the Ge(Li) detectors used with this spectrometer, we present in Fig. 13 the photopeak efficiency curve for a detector having dimensions 6 cm^2 × 8 mm deep, as determined in the spectrometer configuration. In this arrangement the detector intercepts a solid angle of approximately 5.3%. The thickness of aluminum which lies between the source and Ge(Li) detector is about 0.412 g/cm^2. This amount is sufficient to reduce the intensity of a 40-keV gamma ray approximately 20%.

The Si(Li) efficiency curves determined for this apparatus are quite interesting. Previously published silicon efficiency curves for electrons (Bosch et al.[27,28] and Bundrit and Sen[47]) have been determined for detectors with depletion regions shallower than those in the detectors used with this spectrometer (3 mm - equivalent to the range of a 1.3-MeV electron). These curves have shown a decrease in efficiency with increasing electron energy, the decrease becoming quite rapid as the range of the electron approaches the depth of the depletion layer for the detector in question. Other workers (e.q. McKenzie and Ewan[48]) have determined the efficiency of these detectors by using a $\pi\sqrt{2}$ iron-free electron spectrometer to assure a "line" energy source (remove the effects of electron degradation in the source itself). These measurements have shown the full-energy peak efficiency to be essentially constant (within 10%) until the electron range surpasses the depletion depth. In Figs. 14, 15, and 16, we show the electron efficiency curves determined for the three different Si(Li) detectors used with the conversion coefficient spectrometer. While the efficiency of the detector of Fig. 15 seems to be independent of energy, those of Figs. 14 and 16 show a decrease

Table I. Internal conversion coefficient calibration standards.

Source	$t_{1/2}$	E_γ (keV)	Multipolarity	α_k	
^{109}Cd	470 d	87.7	E3	11.0	±0.3[a]
^{141}Ce	33 d	145.43	M1(E2)	0.379	±0.004[b]
^{139}Ce	140 d	165.84	M1(E2)	0.2142	±0.0015[c,d]
^{203}Hg	47 d	279.15	M1+E2	0.163	±0.002[e]
^{113}Sn	118 d	391.7	M4	0.438	±0.008[d]
^{198}Au	2.7 d	411.795	E2	0.0302	±0.0003[f]
^{137}Cs	30 y	661.595	M4	0.0894	±0.0010[g]
^{58}Co	71 d	810.46	E2	0.000295	±0.000010[h]
^{54}Mn	314 d	835.12	E2	0.000224	±0.000010[i]
^{65}Zn	245 d	1115.51	M1+E2	0.0001664	±0.0000066[i]

[a] H. Leutz, K. Schnekenberger, and H. Wenninger, Nucl. Phys. 63, 263 (1965).

[b] Weighted average of results reported in 1) J. R. Cook, Proc. Phys. Soc. 77, 346 (1961); 2) L. Nemet, Izvest. Akad. Nauk, SSSR, Ser. Fiz. 25, 68 (1961); 3) S. S. Pancholi, Bull. Am. Phys. Soc. 10, 442 (1965); 4) R. S. Dingus and W. L. Talbert, Jr., Bull. Am. Phys. Soc. 10, 93 (1965).

[c] J. G. V. Taylor and J. S. Merritt, Bull. Am. Phys. Soc. 7, 352 (1962).

[d] S. C. Misra, J. S. Merritt and J. G. V. Taylor, unpublished.

[e] W. L. Croft, B. G. Pettersson, and J. H. Hamilton, Nucl. Phys. 48, 267 (1963).

[f] Weighted average from Nuclear Data Sheets, excluding PBS results.

[g] J. S. Merritt and J. G. V. Taylor, Anal. Chem. 37, 351 (1965).

[h] W. F. Frey, J. H. Hamilton, and S. Hultberg, Arkiv Fysik 21, 383 (1962), and corrected for new photoelectric cross sections.

[i] J. H. Hamilton, S. R. Amtey, B. van Nooijen, A. V. Ramayya, and J. J. Pinajian, Phys. Letters 19, 682 (1966).

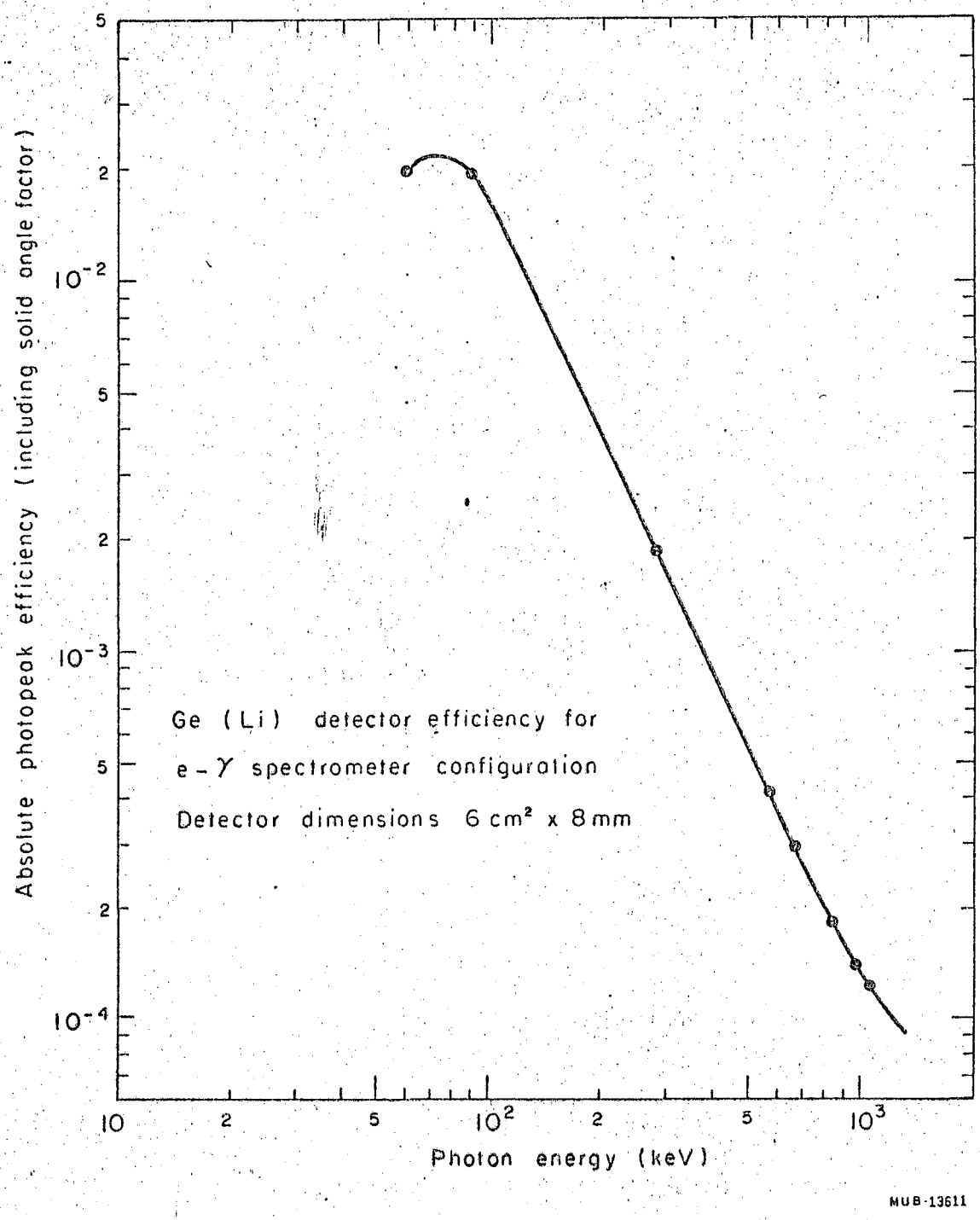

Fig. 13. Full-energy peak efficiency of 6 cm^2 x 8 mm Ge(Li) detector used in conversion-coefficient spectrometer.

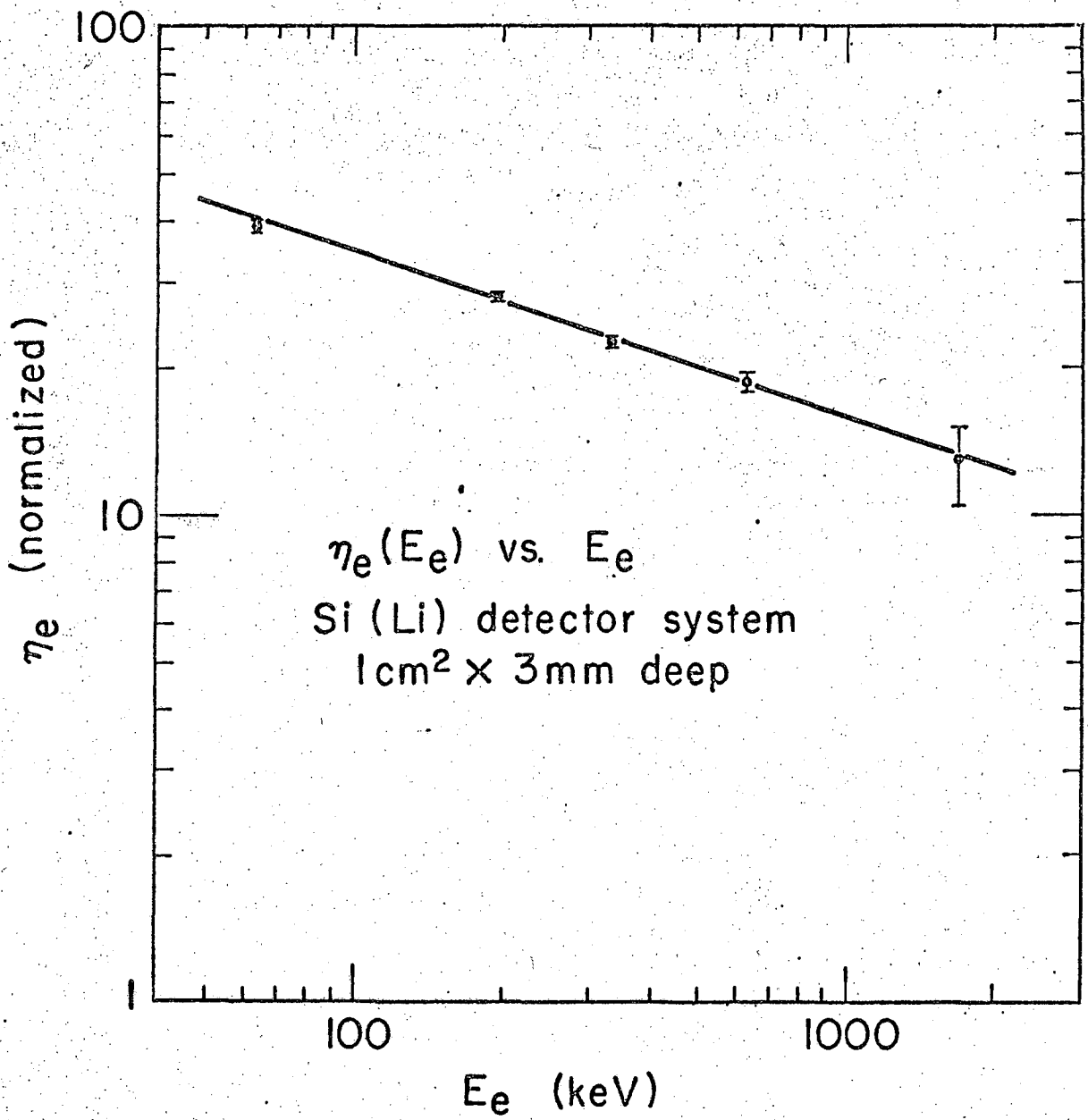

MUB-3719

Fig. 14. Full-energy electron peak efficiency of Si(Li) detector relative to Ge(Li) detector efficiency for gamma rays. The error limits indicated arise only from uncertainty in standard conversion coefficients.

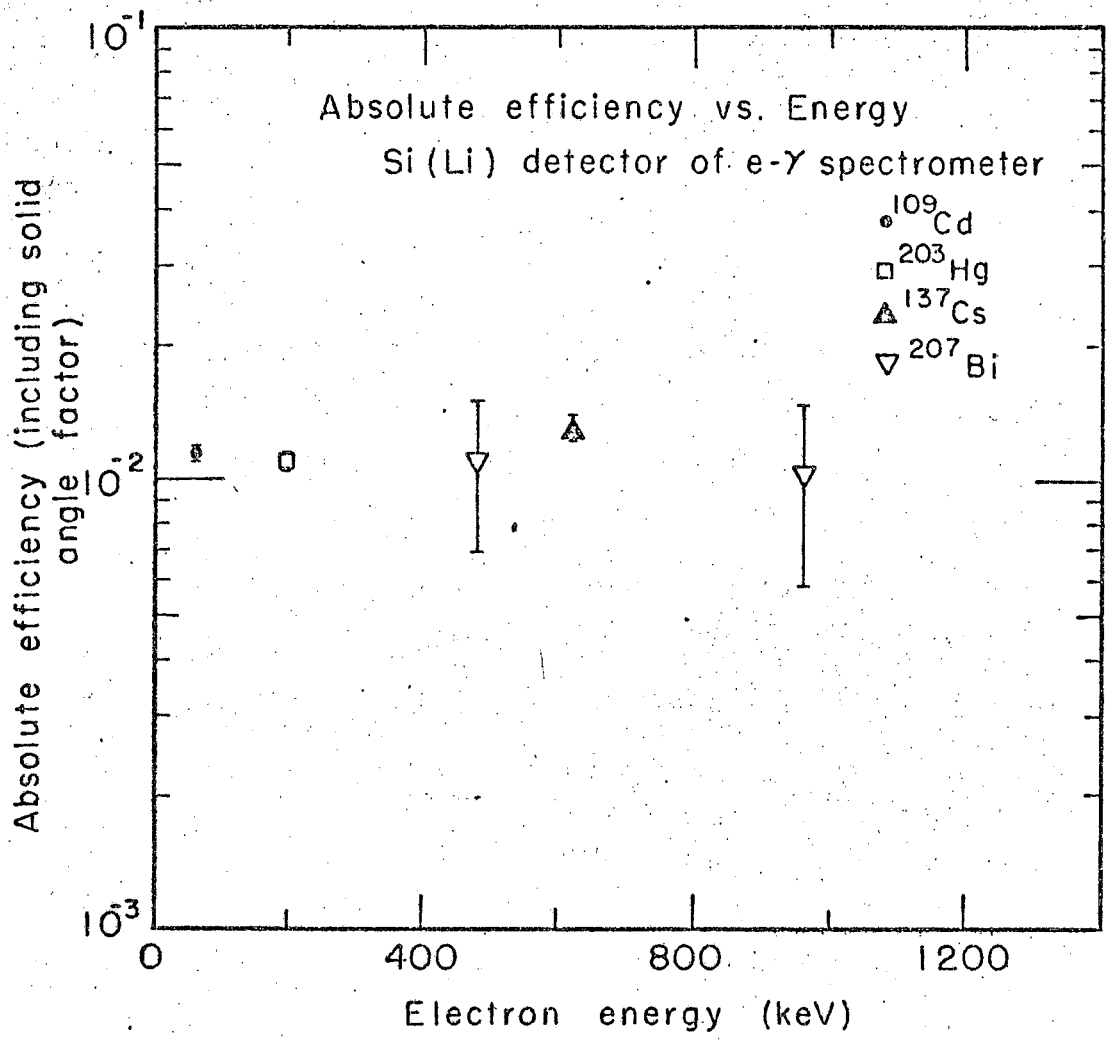

MUB 6023

Fig. 15. Absolute full-energy electron peak efficiency for Si(Li) detector. The error limits indicated arise only from uncertainty in standard conversion coefficients.

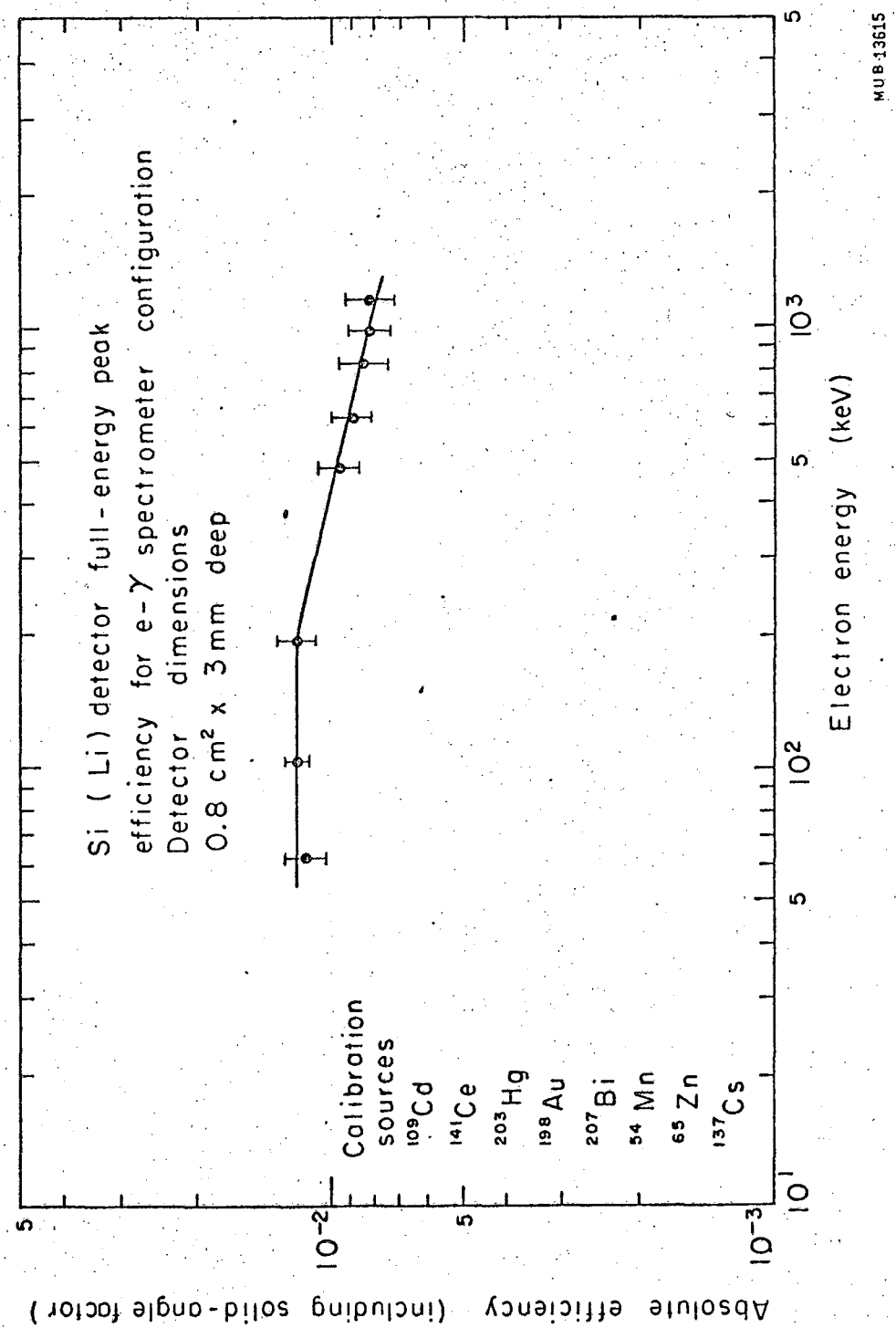

Fig. 16. Absolute full-energy electron peak efficiency for Si(Li) detector. The error limits indicated include a 5% error arising from the uncertainty in the gamma-ray efficiency of the Ge(Li) detector used in the spectrometer as well as the uncertainty in the standard conversion coefficients.

in efficiency with increasing energy. Since these curves were all taken under essentially the same experimental conditions (detector depth, source-detector geometry, collimation, etc.), it must be inferred that the detectors themselves lead to the observed differences in efficiency. While the differences have not be explained, it is thought that possible variations in depletion depth across the crystal might be a possible cause.

4. Examples of Use

While we shall present in Section III of this thesis a number of examples of the use of this spectrometer in regard to the study of the level schemes of the odd-mass gold isotopes, we feel that two examples discussed at this point would indicate the general quality of multipolarity determination obtainable with this apparatus.

The ICC of the 241-keV transition in the decay of 17-hour ^{86}Zr, which had been unknown, was determined by Hollander[17] using the above apparatus. Figures 17 and 18 show the relevant portions of the photon and conversion electron spectra, respectively, with the background to be subtracted for analysis indicated in each case. In Fig. 19, we show the conversion electron spectrum with the background subtracted. The approximate contributions of L, M and N lines to the composite line is shown in this figure. Utilizing these spectra, the experimental K-ICC was found to be $(3.5 \pm 0.3) \times 10^{-2}$, leading to an E2 (theoretical K-ICC 3.8×10^{-2}) assignment for this transition. Other subsequently measured properties of the transition, e.g. half life, agree with this E2 assignment.

Another interesting use of the conversion coefficient spectrometer in the assignment of a particular transition multipolarity has been described by Frankel.[49] In this case the desired multipolarity was that of the 168-keV transition in ^{137}La. Since this was observed in the decay of 34.4 hr. $^{137}Ce^{m}$, the high background due to "tailing" from the electron lines of the very intense 255-keV M4 $^{137m}Ce \rightarrow {}^{137g}Ce$ isomeric transition was sufficient to obscure the electron lines of the transition of interest. To determine the multipolarity, they took the gamma-ray intensity of 168-keV gamma

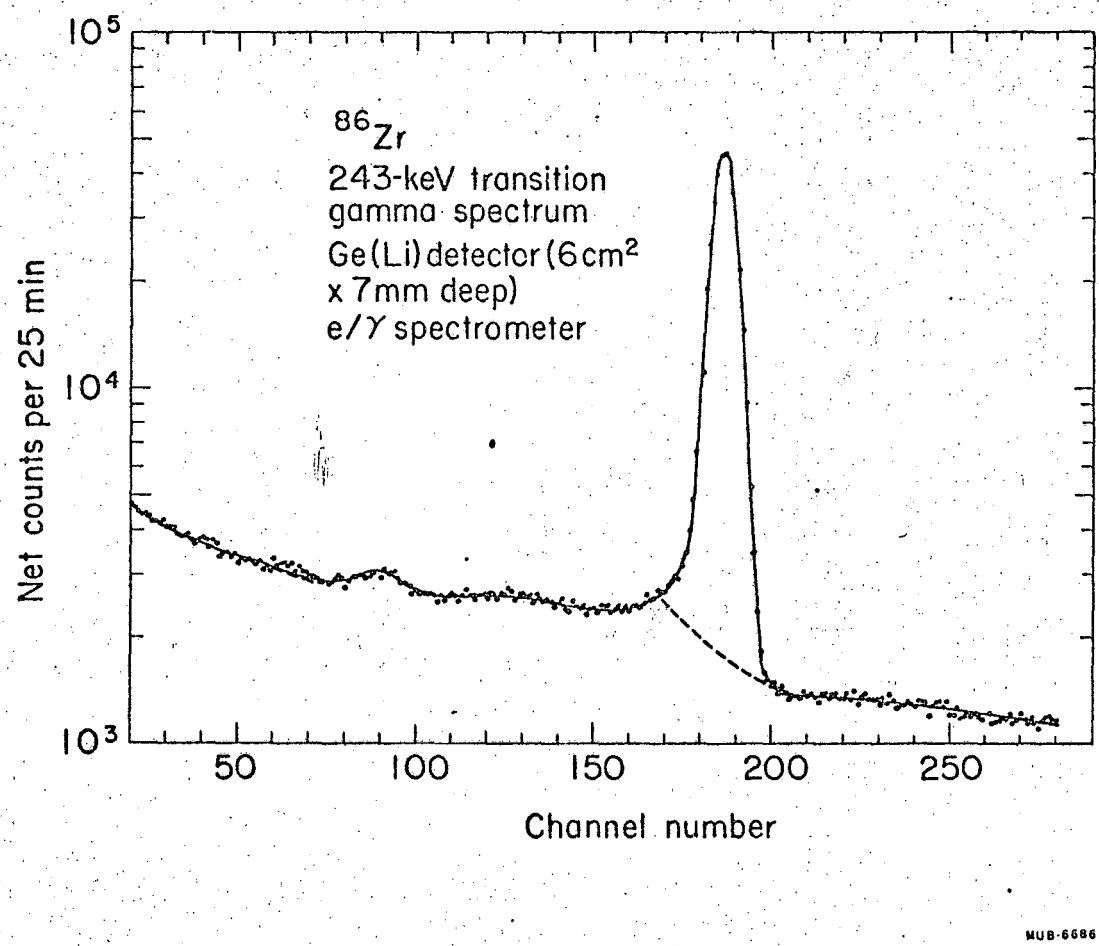

Fig. 17. Partial gamma-ray spectrum of ^{86}Zr recorded with Ge(Li) detector of conversion-coefficient spectrometer. Dashed line indicates background subtracted for area determination; from Hollander.[17]

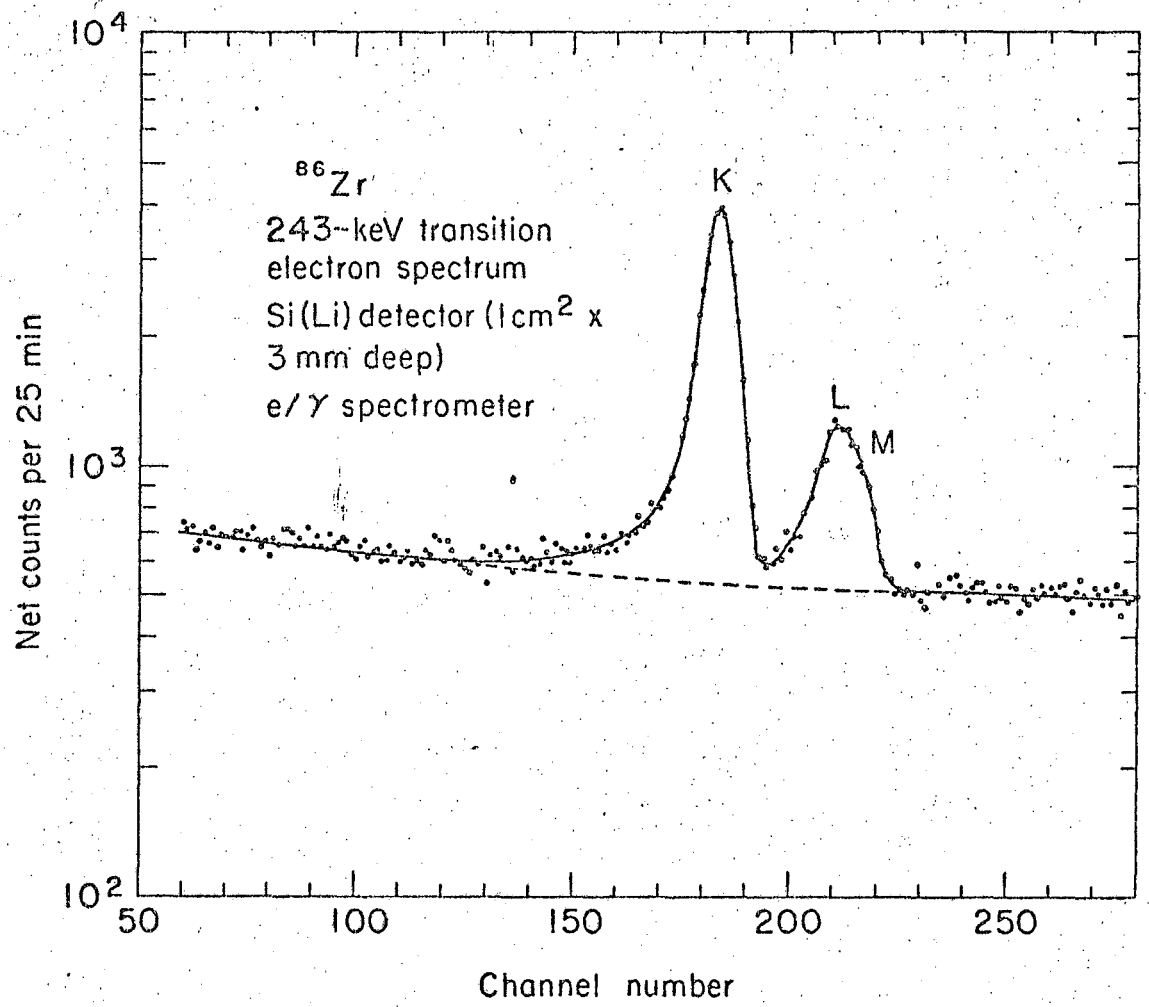

MUB-6687

Fig. 18. Partial electron spectrum of ^{86}Zr recorded with Si(Li) detector of conversion-coefficient spectrometer simultaneously with gamma-ray spectrum of Fig. 17. Dashed line indicates background subtracted for area determination; from Hollander.[17]

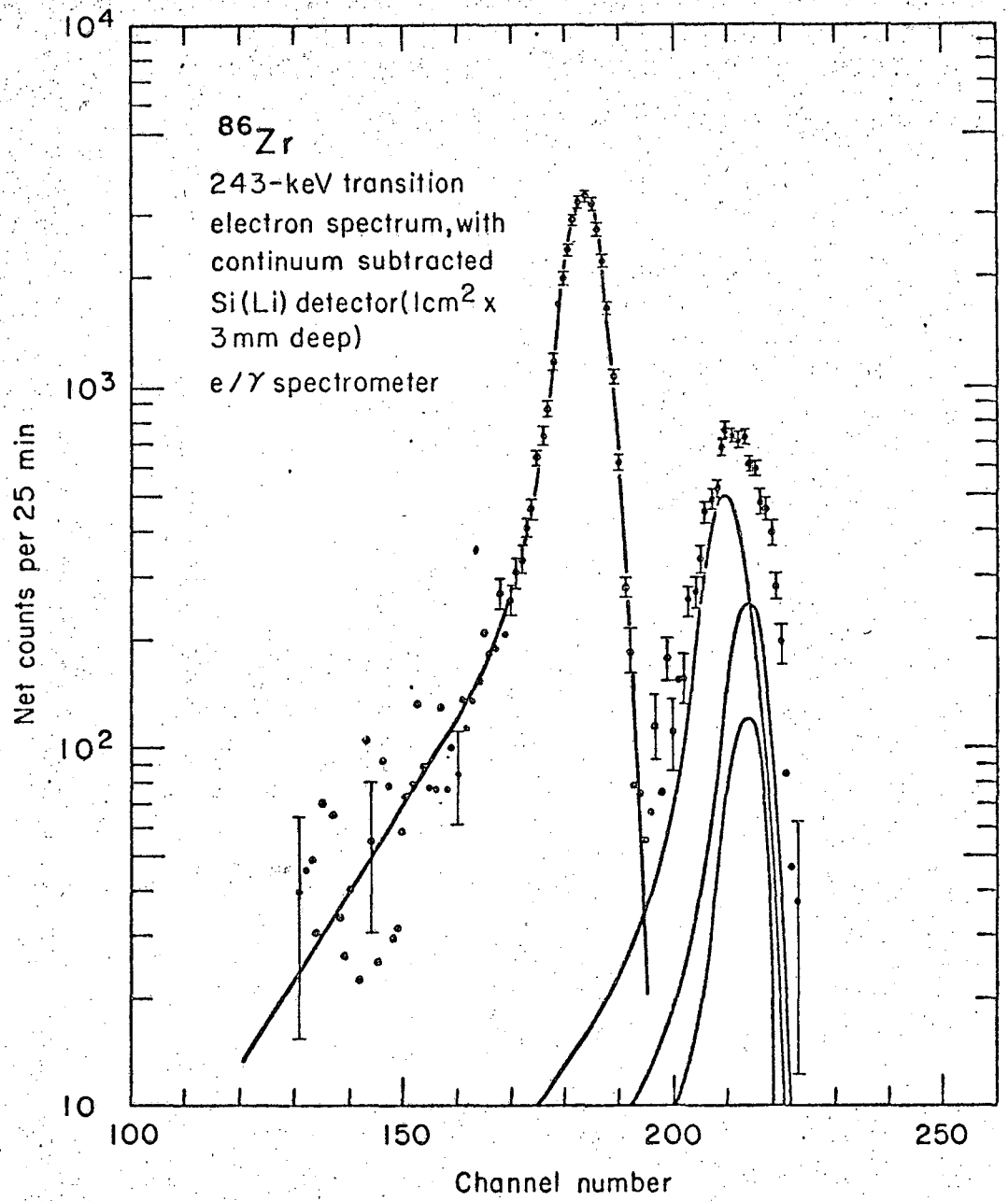

MUB-6688

Fig. 19. Analysis of electron lines of Fig. 18; from Hollander.[17]

relative to the 255-keV gamma, and using the 255 K electron line as a standard shape, subtracted the electron intensity expected for various multipolarities (calculated from theory) from the background at the position of the expected 168 K line. As is seen in Fig. 20, for all multipolarities greater than E1, the resulting background shapes were quite anomalous in appearance. Thus, an assignment of E1 was made for the transition.

5. Limits of Accuracy and Possible System Improvements

In most cases, the accuracy of the ICC determinations made using this spectrometer is limited by the accuracy of the gamma-ray and conversion-electron relative efficiency functions. The gamma-ray efficiency is, of course, doubly important due to its use in the determination of the electron efficiency. If a large number of intensity standards are used in the gamma-ray efficiency determination, it should be possible to achieve an accuracy of 5% or better for gamma-ray efficiency over most of the energy region between 100 keV and 1.5 MeV. If most of the conversion coefficient standards listed in Table I are utilized for electron efficiency determination, the accuracy of this function can be approximately 3% relative to the gamma efficiency. Thus, the two efficiency determinations limit the overall accuracy to about 7-8%.

Clearly, an effect which tends to complicate the observed spectra, or reduce the height of the peaks above background will reduce the accuracy of the measurement. Thus, the use of this device is severely limited in cases where there are intense beta or positron spectra. This background spectrum may be reduced by coincidence requirements. Another source of background is gamma-ray emission from the source. We feel that the major contribution to counts in the electron spectra lying lower in energy than the conversion lines is due to Compton-scattered photons within the Si(Li) crystal. In more advanced designs of this device, some method must be devised to reduce this gamma-ray interaction. This may be either an anti-coincidence shield to surround the Si(Li) detector (this removing a large portion of those counts from the spectrum due to scattering in which full

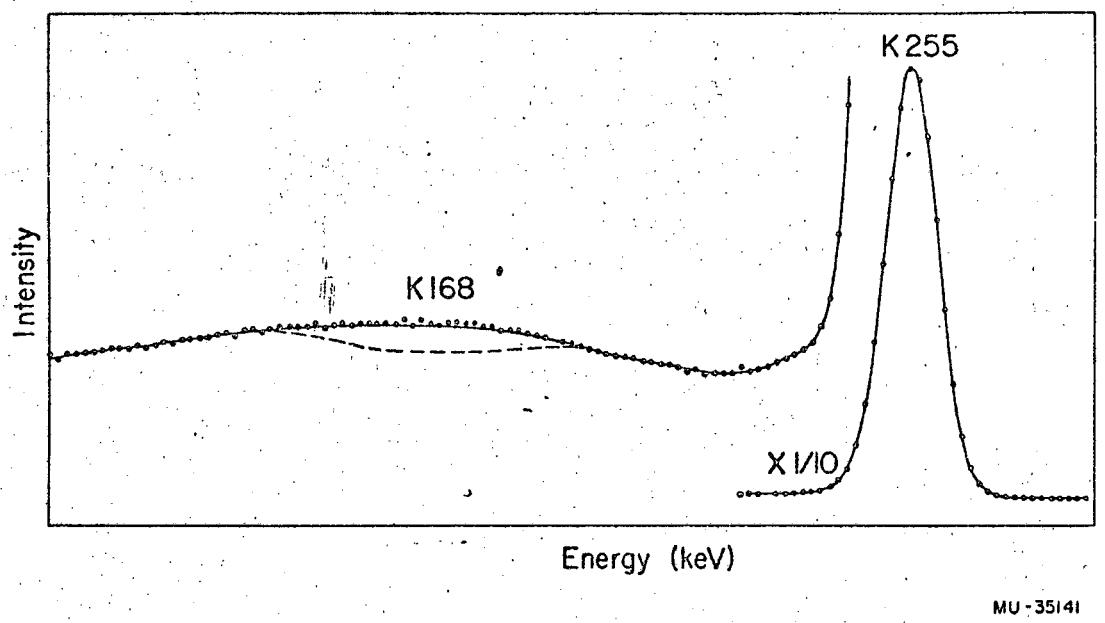

Fig. 20. 168-keV transition in ^{137}La conversion electron measurement from Frankel.[49] Solid curve is theoretical expectation for an E1 transition. The dashed curve is theoretical expection for an M1 or E2 transition.

energy is not deposited within the crystal) or some type of magnetic steering device, similar to that proposed by Malmfors[50] and utilized by Watson[51] for conversion electron-fission coincidence studies, capable of bending the electrons away from the source and refocusing them at a point which can be conveniently shielded from source gamma rays. Another appealing facet of the use of a magnetic steering device, is the removal of any positron spectrum which may accompany the nuclear decay. This would extend the use of this device to lower Z, cyclotron-produced nuclides.

Improved resolution will, of course, improve the peak-to-background ratio for both detectors. While the advances in resolution during the past two years have been great, there is no reason to think that significant advances in this area do not still lie before us. There will also be advances in the total active volume of the detectors, which should again add intensity to the full energy peak. In this regard, one should realize that for a device such as the one described here, it is not the total volume of the Ge(Li) detector alone which should be the determining factor in the selection of the detector, but rather the ratio of active to total volumes, since we wish to increase the intensity of the full-energy peak relative to its Compton distribution.

Since the most convenient method of data acquisition with this device is the simultaneous accumulation of both conversion-electron and gamma-ray spectra for a pre-set live-time interval, similar counting rates for the two spectra are quite desirable. In the case of short-lived activities, if the counting rates (and thus the analyzer dead-times) are considerably different, decay corrections are necessary for intercomparison of the spectra. High counting rates also tend to make poorer the resolution obtainable with the semiconductor detectors. With the present design of the conversion coefficient spectrometer, we find that in most cases where the decay of a moderately high Z nuclide is observed, the Si(Li) detector exhibits a higher count rate, presumably due to the efficiency of the detector for X-rays as well as electrons. Hopefully, this higher count rate would be reduced by methods discussed in the previous paragraph. There will also be cases for

which the conversion coefficients will be small. In these cases, the gamma-ray counting rate will determine the maximum useable source strength. For such cases, it would be advisable to have a variety of absorbers as part of the assembly, and have the system calibrated for each absorber. Another important variation would be a number of fixed positions for both detectors. This, if properly calibrated, would allow the optimization of counting rates for both detectors.

D. Conclusion

The semiconductor detector, with many accomplishments already to its credit, has been shown to have great potential in the area of ICC measurements. In this section we have not only reviewed this potential, but have also described an apparatus utilizing these detectors which is capable of rapidly yielding much information to the spectroscopist. The conversion coefficient spectrometer we have discussed permits ICC measurements to an accuracy which is sufficient for most multipolarity determinations. It also allows ICC measurements to be made with nuclides having quite short half lives. These two qualities mark this device as one which would be of great value in the nuclear spectroscopy laboratory. The device does, at present, however, have a number of weak points. Primary among these is the inability of the Si(Li) detector to observe any electron lines other than the most intense above a strong beta continuum. This can only be remedied with great improvements in resolution. Another weak point is the sensitivity of the Si(Li) detector to gamma rays. It is expected that a number of methods can be used to reduce this source of background. Due to these weaknesses, a spectrometer of the present design will be of greatest value to those working with nuclides which have (1) a large EC/β + ratio or, (2) low intensity beta or positron distribution in the region of the transitions of interest or, (3) highly converted transitions (e.g. isomeric transitions from levels populated in (n,γ) reactions).

III. DECAY SCHEME STUDIES OF THE ODD-MASS GOLD ISOTOPES

A. Theory

The search for systematic trends in the behavior of various nuclear properties is an important aspect of nuclear spectroscopy. Such a systematic study of the spins and magnetic moments of nuclear ground and isomeric levels led to the formulation of the shell model by Mayer[52] and Haxel, Jensen, and Suess.[53] With this model it has been possible to predict a great many nuclear phenomena, particularly near the regions of the magic numbers of nucleons. Another model which has profited from nuclear systematic studies is the so called unified model formulated by Bohr and Mottelson.[54] This model has, of course, done an excellent job in the prediction of nuclear phenomena in regions where the nucleus assumes an equlibrium nonspherical shape.

Of particular interest is the systematic study of the nuclear properties of nuclei which lie in the region between those covered by the above theories. This region is characterized by the presence of shell-model type single particle states as well as low lying states arising from collective motion of the nucleons. Since the main features of the nuclear levels of odd-mass nuclei are determined by the odd group, an effective method of study for this region is the observation of systematic trends in the set of nuclei having $(Z, N+2\nu)$ or $(Z+2\epsilon, N)$ where ν and ϵ are integers and Z is odd in the first case and N odd in the second. The levels and transitions in these nuclei can be studied to determine the extent of interaction between the odd particle and the collective motion of the other nucleons.

There has been considerable theoretical interest shown in the nuclei which occupy the region extending from the lead isotopes down in mass to the rare earth region which commences with osmium and rhenium. Those nuclides surrounding the doubly-magic isotope ^{208}Pb have shown to be amenable to shell-model calculations, while the rare earth nuclides have, of course, been extensively treated in light of the unified theory. In the midst of the region between lead and osmium lie the gold isotopes. A study of the

odd-mass gold isotopes will indicate the interaction between the odd 79th proton and the slightly deformable nucleon core. This should act as an indication of the transition taking place in the nuclear potential.

In this section we shall discuss those theories which are presently prominent in the description of the odd-mass gold isotopes.

1. Simple Shell Model

The shell model has had considerable success in the prediction of various nuclear phenomena. Its major achievement was the explanation of the additional stability associated with the "magic numbers" (2,8,20,28,50, 82, and 126) of nucleons. Despite the great simpliciation used in formulating this model and the neglect of specific internucleon interactions, the numerous quantities which are not extremely sensitive to the fine details of nuclear structure can be treated quite well. At present, however, the simple shell model is used as a base upon which to build more sophisticated models. Before we examine the simple shell model predictions for the gold region, let us discuss the basic assumptions of the model very briefly.

The primary assumption of this model is that each nucleon moves in an average field of force which is spherically symmetric and independent of the instantaneous positions of all other nucleons. This potential felt by the nucleon is assumed to have a form somewhere in between that of a three-dimensional harmonic oscillator and that of a square well. These assumptions led to nearly the proper level ordering for light nuclei and allowed prediction of the magic numbers of 2,8, and 20. The larger magic numbers, however, were not correctly predicted until a force of the form $f(r)(\vec{s}\cdot\vec{\ell})$ was included in the total potential. This is, of course, the spin-orbit interaction force which tends to lower the energy of those levels in which the nucleon spin and orbital angular momentum vectors are "parallel" ($j = l+1/2$) and increases the energy of those in which the vectors are "antiparallel" ($j = l-1/2$). The inclusion of the spin-orbit force predicts shell closures at the experimentally observed values without additional assumptions. Emperical evidence indicates that the stepwise filling of the levels within

each shell is governed to a considerable extent by pairing. Pairing means that configurations in which pairs of nucleons have zero angular momentum are energetically favored and the amount of favoring increases as the angular momentum of the single-particle level in which the pairing takes place.

In the single particle model, the low-lying levels of odd-mass nuclei are determined by those shell model states available for the odd nucleon. In the case of the odd-mass gold isotopes this is the 79th proton. The levels available for this proton within the shell occupied by the 51st to 82nd nucleons are the $1g_{7/2}$, $2d_{5/2}$, $2d_{3/2}$, $3s_{1/2}$, and $1h_{11/2}$ orbitals. The actual order of filling of the levels is $1g_{7/2}$, $2d_{5/2}$, $1h_{11/2}$, $2d_{3/2}$, $3s_{1/2}$ with the $1h_{11/2}$ filling in pairs. Thus, for the ground state of the odd-mass isotopes we expect a spin and parity of 3/2 + arising from the proton being in the $2d_{3/2}$ orbital. Low-lying excited states arising from proton excitation should then be, according to the simple shell model, 1/2+, 5/2+, 11/2-, and 7/2+.

2. Core-Excitation Model

Even-even nuclei have been shown to exhibit distinctive levels which arise from collective surface vibrations. If we think of odd-even or even-odd nuclei as consisting of a single nucleon outside an even-even core, it it tempting to consider the possibility of coupling the odd nucleon to excited states of the core. This situation would arise where the energy necessary to excite the odd nucleon to a higher lying single particle level was comparable to the energy required to excite surface oscillations in the even-even core. The energy of the states resulting from such coupling would then be dependent upon the particle state occupied by the odd nucleon, the state of the core excitation (number of phonons), the strength of particle-core coupling, and the total spin to which the particle and core angular momenta are coupled. Bohr and Mottelson[54] first treated this situation in 1953 in their general discussion of collective phenomenon. In their treatment the above situation is covered by the weak-coupling model. For this model the assumption is made that the deformation of the nucleus is small enough for perturbation methods to be used. Thus, the model only deals with nearly

spherical nuclei, and the collective modes in which there is interest are vibrations about a sphere.

In the treatment of weak coupling in the unified model, the Hamiltonian for the core plus extra nucleon is taken as

$$H = H_c + H_p + H_{int}$$

where H_c, the surface vibration Hamiltonian for the core, is expressed according to the definitions found in Preston,[55] page 231, (considering only quadrupole deformations of the core)

$$H_c = (1/2) \sum_{\mu} (B|\dot{\alpha}_{2\mu}|^2 + C|\alpha_{2\mu}|^2) \quad ,$$

H_p is the Hamiltonian for the odd nucleon with eigenvalues corresponding to the single-particle levels in the presence of a spherical core, and H_{int} is the interaction Hamiltonian which couples the particle motion to the core oscillations and is expressed

$$H_{int} = - k \sum_{\mu} \alpha_{2\mu} Y_2^{\mu} (\theta,\phi) \quad ,$$

where the Y_2^{μ} are spherical harmonics of order 2. The basis wave functions taken in this treatment are the eigenvectors of the Hamiltonian for the uncoupled system

$$H' = H_c + H_p \quad ,$$

and are specified by $|j; NR; JM\rangle$, where j denotes the quantum numbers of the odd nucleon, N is the number of phonons of collective vibrations, R is the total angular momentum associated with the core vibrations, and J and M refer to the total angular momentum ($\vec{J} = \vec{j} + \vec{R}$). The ground state of the coupled system is the state with no phonons, $|j; 00; jm\rangle$, with some admixture from those states where the matrix element

$$\langle j';\ NR;\ JM|H_{int}|j;\ 00;\ jm\rangle$$

has a nonzero value. H_{int} will connect the ground state only with states with one 2+ phonon present ($N = 1$, $R = 2$), and only for $j' = j$, $j \pm 1$, or $j \pm 2$ with the same parity and similar energy. The lowest lying excited states will be those arising from the coupling of the half-integral ground state j to one quadrupole phonon yielding levels of positive angular momentum J such that $|j+2| \geq J \geq |j-2|$. In the simplest model these levels will be degenerate, with the degeneracy being removed only by the presence of other particle states or the admixture of other phonon states.

A quite similar model was derived as an extension of the jj-coupling shell model by de-Shalit[56] in 1961. In this case the basic wave functions are $|J_c j\ JM\rangle$, where J_c stands for the core angular momentum, j for that of the odd nucleon, and J is the total angular momentum with $J_z = M$. In this case the absence of any core-particle interaction causes all states characterized by the same pair of values for J_c and j, but different values of J and M to be degenerate. These levels make up what is termed by de-Shalit as a "core multiplet". The degeneracy of the core multiplet will be split by the core-particle interaction. Since this interaction is a scalar, its form is taken to be the product of two tensors of rank k: $T^{(k)}(c)$ operating on the core and $T^{(k)}(p)$ operating on the particle. The general interaction is taken as the summation of the tensor products over all values of k. If the interaction does not involve monopole-monopole ($k = o$) effects, the "center of gravity" of each core multiplet $E_{cg} = [\sum_J E_J(2J+1)/\sum_J (2J+1)]$ should coincide with the energy of the unperturbed first vibrational level of the even-even nucleus which corresponds to the core. The "center of gravity" aspect has been discussed extensively by Lawson and Uretsky.[57] Monopole effects will show up as a shifting of the multiplet, but will not split the multiplet degeneracy.

Thus, according to the description by de-Shalit, a core multiplet should approximately satisfy the following requirements: 1) The center of

gravity of the multiplet should be at the excitation energy of the even core known from the neighboring even-even nucleus. 2) The reduced E2 transition probabilities from members of the multiplet should be equal and about the same strength as that from the first excited state of the neighboring even-even nucleus. 3) The M1 transition probability from the multiplet to ground should be very small. These requirements are based, of course, on the assumption that the core multiplet is "pure". Any admixtures of other particle wave functions to these levels or the distortion of the excited state of the core from that observed in the even-even neighbor will cause significant deviation from the above requirements.

The difference between the weak coupling treatment of the unified model and that offered by de-Shalit lies in the form of the core-particle interaction. While the weak coupling interaction is equivalent to the product of two tensors of rank two (quadrupole-quadrupole coupling), the form of the interaction in the de-Shalit model is more general, including a sum over tensor products of all ranks.

While these models have been applied to numerous nuclides, particular emphasis has been placed on their application to nuclides in the gold region. In this region the even-even nuclei maintain their spherical shape while exhibiting vibrational levels at fairly low energies (300-600 keV). In particular, Braunstein and de-Shalit[58] have discussed the levels of ^{197}Au in terms of the coupling of the 79th proton (presumably in the $d_{3/2}$ orbit) to an excited state of the core (^{196}Pt). The low lying levels of this nucleus and their interpretation in light of the de-Shalit model are shown in Fig. 21. The wave functions used in Ref. 58 are

$$
\begin{aligned}
|3/2\rangle_1 &= A|0\ 3/2,3/2\rangle + \sqrt{1-A^2}\ |2\ 3/2,3/2\rangle \\
|1/2\rangle &= |2\ 3/2,1/2\rangle \\
|3/2\rangle_2 &= A|2\ 3/2,3/2\rangle - \sqrt{1-A^2}\ |0\ 3/2,3/2\rangle \\
|5/2\rangle &= B|2\ 3/2,5/2\rangle + \sqrt{1-B^2}\ |0\ 5/2,5/2\rangle \\
|11/2\rangle &= |0\ 11/2,11/2\rangle \\
|7/2\rangle &= |2\ 3/2,7/2\rangle \quad .
\end{aligned}
$$

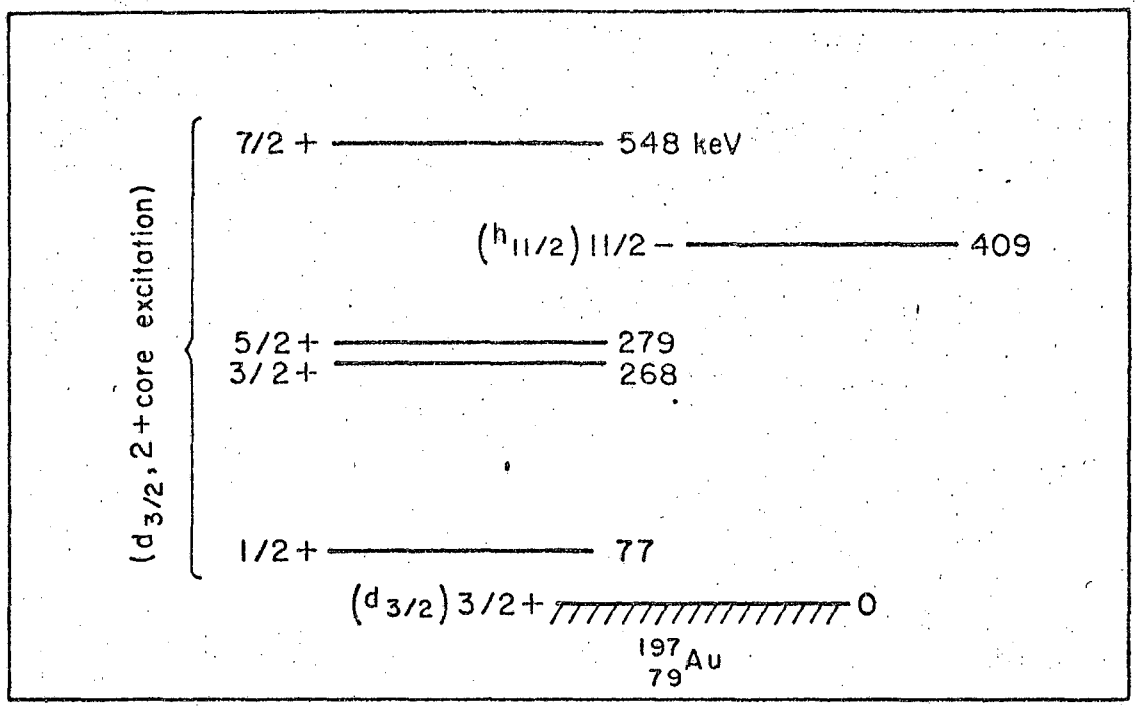

MUB-3888

Fig. 21. Energy levels of ^{197}Au arranged according to the "core-excitation" model of Braunstein and de-Shalit.[58]

The two 3/2 levels are allowed to mix through the parameter A, and B accounts for any admixture of $d_{5/2}$ single particle state into the 5/2 level. From experimentally measured values of M1 transition probabilities and the magnetic moment of the ground state, the values of A and B were determined. These derived values were then used to predict various other quantities. It was found that the fit to the experimental data was quite good. Later work by McKinley and Rinard[59] attempted to obtain a quantitative fit for the levels of ^{197}Au under the assumption of a core-particle interaction involving tensors of up to rank three.

A somewhat different approach to ^{197}Au has been taken by Thankappan and Rao,[60] who have discussed the properties of the low-lying levels in terms of the coupling of a proton hole in the $d_{3/2}$ subshell with the ground state and first excited state of ^{198}Hg. It was found that tensors up to rank three were necessary to reproduce the observed level positions. Particularly necessary was the monopole-monopole portion of the interaction (due to the center of gravity of the core multiplet falling about 48 keV below the ^{198}Hg core state at 412 keV). In this treatment it was found that the dominant part of the core-particle interaction was the dipole-dipole term.

3. Kisslinger and Sorensen Treatment

In 1963 Kisslinger and Sorensen[61] published their general theoretical treatment for spherical nuclei. Since the extent of the calculations is large, we will not cover them in detail, but rather present a general introduction and suggest a reading of the original work for further information.

In this treatment, the interaction between nucleons is taken to have both short- and long-range components. The short-range force gives rise to pairing effects. The modern approach to pairing arose from work on superconductivity by Bardeen, Cooper and Schrieffer[62] and its application to nuclear phenomena by Bohr, Mottelson and Pines.[63] The pairing force acts only on shell-model pairs of nucleons coupled to zero angular momentum, and has the effect of scattering these pairs over unfilled nucleon orbitals.

The long-range force used in this treatment is a quadrupole-quadrupole force which depends on the second-order spherical harmonic of quasi-particle coordinates and acts between both protons, neutrons, and proton-neutron pairs. Of course, the quasi-particle formalism is used throughout this treatment.

For odd-mass nuclei there exist low-lying states which are primarily one quasi-particle states. The quadrupole-quadrupole force in even nuclei gives rise to collective 2+ first excited states, which may be regarded as 1-phonon states, microscopically consisting of a coherent superposition of many 2-quasi-particle configurations. In odd nuclei the q-q force admixes configurations with one quasi-particle plus zero, one, or more such phonons. The Hamiltonian in this treatment, as in the weak coupling case, is the sum of the phonon Hamiltonian, the quasiparticle Hamiltonian, and the Hamiltonian for the phonon-quasi-particle interaction. For the final calculations, the energy parameters for the single particle levels are obtained for whole regions from single closed-shell and closed-shell ± 1 nuclei, and are assumed to vary linearly as a function of A within the shell.

While the values for the calculable quantities are not expected to be extremely accurate for the odd-mass gold isotopes, they should give an indication of the general trends within this region. In the comparison of experiment to theory we shall return to examine the results of this treatment more closely.

4. Semimicroscopic Description

An extension of the intermediate coupling theory of Choudhury[64] has been undertaken by Alaga and Ialongo[65,66] in order to apply to nuclei one, two, or three nucleon numbers away from an even single-closed-shell configuration. In the particular case of ^{197}Au, for example, the three proton holes are treated explicitly in the $S_{1/2}$ and $d_{3/2}$ orbitals with an attractive pairing force. The core excitations (mainly the neutrons) are brought in as quadrupole phonons, with particle-phonon coupling strengths taken as adjustable parameters. The vibrating core is taken to have up to two phonons of excitation. The phonons arise as collective excitations of the neutron

holes in the 126-neutron shell of lead nuclei. In separate calculations, they have included up to three phonons and also taken into account the $d_{5/2}$ hole states, as well as calculating the negative parity levels.

The eigenvectors of the Hamiltonian were then used to calculate transition probabilities, lifetimes, mixing ratios, magnetic and quadrupole moments. As an example of complexity of the eigenfunctions for this treatment, the wave function for the 3/2+ ground state is found to consist of 16 terms. We shall return to examine the predictions of this treatment, particularly with regard to the level ordering, later in this section.

B. Experimental Techniques and Apparatus

1. Source Preparation

In the following set of studies we observed transitions within the level schemes of those odd-mass isotopes of gold with mass numbers 199, 197, 195, and 193. Levels in both ^{199}Au and ^{197}Au as well as ^{197}Au are populated from mercury decay. We are therefore interested in the production of the corresponding platinum and mercury isotopes and their separation from other activities.

Samples of 31-min ^{199}Pt were prepared by neutron irradiation of isotopically enriched ^{198}Pt in the LRL research reactor at Livermore, California.† Samples were subjected to an average thermal flux of approximately 2×10^{12} n/cm^2 · sec for periods of roughly two hours. The short half life of this isotope required delivery to this laboratory by helicopter.[67] Samples of 18-h ^{197}Pt and 97-min ^{197m}Pt were prepared by irradiation of isotopically enriched ^{196}Pt in the G.E. reactor at Vallecitos, California‡ at a flux of

---

†The ^{198}Pt was obtained from Stable Isotopes Division, Oak Ridge National Laboratory, Oak Ridge, Tennessee. Isotopic analysis of this material was ^{190}Pt <0.05%, ^{192}Pt <0.05%, ^{194}Pt 4.94%, ^{195}Pt 11.54%, ^{196}Pt 26.70%, ^{198}Pt 56.82%.

‡The ^{196}Pt again was obtained from the Stable Isotopes Division and had an isotopic analysis of ^{190}Pt <0.05%, ^{192}Pt <0.05%, ^{194}Pt 6.57%, ^{195}Pt 26.18%, ^{196}Pt 65.55%, ^{198}Pt 1.70%.

1.8×10^{13} n/cm^2 · sec, and with a thermal/epithermal (E_n > 0.4eV) neutron ratio of 7.3/1.

Chemical purification of the platinum was undertaken by a method similar to that described by Smith.[68] The samples were first dissolved in hot aqua regia. The solution was then evaporated to dryness, and the residue taken up in approximately 3ml of 3N HCl. To remove the principal impurity, gold, the technique of solvent extraction was utilized. The gold, in the form of the chloride complex ion, was extracted from the HCl solution by repeated washings with amyl acetate. It is of course, easy to follow the gold extraction due to the yellow color of the ion. The HCl solution was then heated; both to remove the last traces of amyl acetate and to reduce the volume. Portions of the Pt solution were then liquid-deposited on aluminum planchets for the observation of gamma-ray spectra or on to gold-anodized mylar for the observation of conversion-electron and gamma-ray spectra.

The neutron deficient isotopes of mercury were produced by bombarding gold metal foils with deuterons in the L.R.L. 88-inch cyclotron. Thus, the actual reactions utilized were of the type ^{197}Au(d, Xn) $^{199-X}$Hg, with deuteron energies of 15 MeV for X=2, 35 MeV for X=4, and 50 MeV for X=6. For most runs, 4-5 gold foils of 0.001-inch thickness were used as a target. This thickness was sufficiently small to reduce the contribution to the total activity from the competing reactions of the type ^{197}Au(d, (X-1,2)n) arising from deuterons degraded in energy.

Due to its high volatility, mercury is quite easily separated from gold and platinum by distillation. In these experiment, the irradiated gold foils were placed into the quartz vessel of an "astatine boiler" of the type described by Fink and Thompson.[69] The quartz vessel was then clamped tightly to the boiler assembly and heated to approximately 800°C by means of a small induction furnace. The volatilized mercury was then collected on thin gold foils which were fastened to the cooled base of the boiler by means of a small end cap. The area of the mercury deposit was limited by an aluminum collimator. The time for evaporation varied from

two minutes to two hours depending upon the desired source strength. Gold foil was used to collect the mercury in order to form a mercury-gold amalgam. This amalgam served to keep the mercury from evaporating when the sample was introduced into an evacuated chamber for the observation conversion electrons.

2. Apparatus

(a) Gamma-ray spectrometers. In these experiments, gamma-ray spectra were observed utilizing lithium-drifted germanium (Ge(Li)) detectors fabricated at this Laboratory by the technique described by Goulding.[12] We have used detectors of dimensions 2 cm^2 × 5 mm deep, 6 cm^2 × 9 mm deep, 4 cm^2 × 5 mm deep, and 1 cm^2 × 5 mm deep. The first three of these detectors were coupled to low-noise preamplifier using EC 1000 vacuum tubes in their first stages. They exhibited resolutions of 2.1, 3.3, and 3.0 keV at 122 keV respectively. The 1 cm^2 × 5 mm deep detector was utilized with a field-effect transistor (FET) preamplifier of the type described by Elad,[40] and exhibited a resolution of 1.2 keV at 122 keV.

The detectors were kept at "liquid-nitrogen" temperature and were continuously pumped upon by sputtering-ion pumps of commercial manufacture.[70] The low temperature is used both to reduce detector bulk leakage current and to prevent further diffusion of lithium within the detector. The low pressure is then used at this low temperature to prevent deposition of materials on the detector surface.

Of particular importance in the observation of the gamma-ray spectrum of ^{195}Hg was an anti-Compton spectrometer utilizing a Ge(Li) detector of dimensions 3 cm × 2 cm × 1.1 cm. This apparatus was designed and built by D.C. Camp at the Lawrence Radiation Laboratory, Livermore, California. In this device, the Ge(Li) detector is positioned between two NaI(Tl) scintillation crystals of dimensions 9-inch diameter by 4.5-inches thick. A collimated (0.5 inch) beam of gamma rays is allowed to be incident upon one of of the 2 cm × 1.1 cm detector faces. Many of the Compton interactions occurring within the Ge(Li) detector lead to scattered gamma rays which

escape the crystal. In this particular apparatus, a fast coincidence is taken between the NaI(Tl) crystal (observing the scattered gamma rays) and the Ge(Li) detector. Any such coincidence will, in this case, cause the analyzer to be blocked, and the pulse from the Ge(Li) detector will not be accepted. The block diagram of the electronics used in this apparatus is shown in Fig. 22. The Ge(Li) detector used in this device exhibited a resolution of 1.5 keV at 122 keV. When used in the anti-Compton mode a reduction of approximately one order of magnitude was observed for the Compton distribution in the ^{60}Co pulse-height spectrum. A more detailed description of this device is included in the review article by Camp.[19]

(b) Conversion electron and Internal conversion coefficient measurement. The measurement of ICC in this series of experiments was undertaken with the aid of a device utilizing a Ge(Li) detector for the observation of gamma rays and a Si(Li) detector for the observation of conversion electrons. This device and its method of application is described in detail in Section II of this thesis.

In some cases where high resolution was necessary in the observation of the conversion-electron spectrum, the Berkeley 50-cm-$\pi\sqrt{2}$- iron-free spectrometer was used. With this instrument, a momentum resolution $\left(\frac{\Delta p}{p}\right)$ of 0.10% to 0.05% was obtainable. This permitted resolution of the L- subshell lines for most transitions of interest in the gold region.

C. Experimental Results

1. ^{199}Au

The decay of ^{199}Pt to levels in ^{199}Au was first examined by Le-Blanc, Cork and Burson.[71] While this work did report nine gamma rays in the decay and did formulate a decay scheme, it was not until the more extensive work of Joshi, Thosar and Prasad[72] was published that a level scheme which was systematically consistent with those of other odd-mass gold isotopes was presented. In this latter work, both gamma-gamma and beta-gamma coincidence studies were carried out and three new gamma rays added to the scheme. From relative beta branchings log ft values were derived and some assignments of

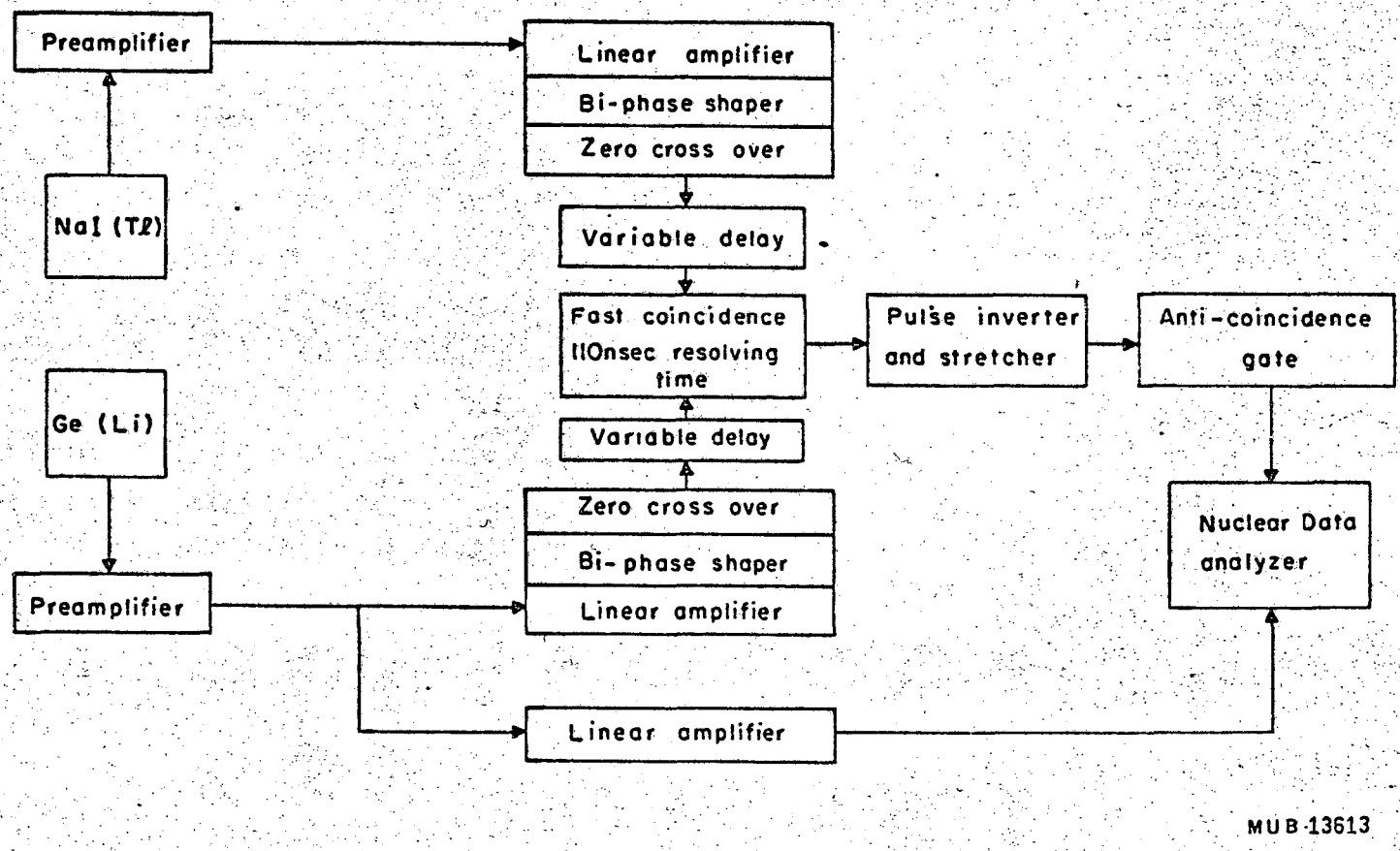

Fig. 22. Block diagram of electronic components used in anti-Compton spectrometer.

spin and parity were postulated for the gold levels. The presence of two gamma rays of approximately 320 keV as well as two of 475 keV in their postulated scheme indicated that a higher resolution study of this decay would be of value.

In the neutron irradiation of enriched ^{198}Pt both $^{199m}Pt(t_{1/2} = 15$ sec) and $^{199}Pt(t_{1/2} = 31$ min) are produced. The other impurities formed, namely ^{197}Pt, ^{195m}Pt, and ^{193m}Pt, are fairly long lived, and therefore short irradiation periods (30 min-1 hr) are utilized to reduce their production. For this reason the main peaks, not from ^{199}Pt, which will appear in the gamma-ray spectrum are those arising from the decay of the daughter of ^{199}Pt, ^{199}Au. The decay of ^{199}Au is well known and exhibits gamma rays of 49.7, 158.3, and 208.0 keV, decaying with a half life of 3.1 days.

Preliminary studies using a Ge(Li) detector of dimensions 2 cm^2 × 5 mm (resolution 2.1 keV at 122 keV) were undertaken to observe the primary gamma rays from ^{199}Pt decay. These studies determined gamma rays of approximately 185.6, 218.7, 225.8, 240.0, 246.5, 317.1, 323.7, 417.5, 425.0, 466.5, 474.5, 493.5, 505, 542.5, 714.8, 791.5, and 967.0 keV which decayed with a half life of roughly 30 minutes. The intermediate-energy region of our gamma ray spectrum is shown in Fig. 23. Since these spectra were taken primarily for the purpose of half-life determination, neither the statistics nor the amplification gain was optimum for energy measurements, and for this reason the above energies are expected to be accurate only to at best within 0.3 keV. In Table II our gamma ray data are summarized.

Very shortly after these preliminary measurements, we received a preprint of the extensive work being done by Black on this decay.[73] Using both Ge(Li) and Si(Li) detectors as well as NaI(Tl) detectors, permanent-magnet spectrographs, and γ-γ and β-γ coincidence techniques, he was able to formulate a decay scheme which was considerably more detailed than that proposed by Joshi et al. The scheme postulated by Black is shown in Fig. 24.

A close examination of the proposed ^{199}Au level scheme from Ref. 73 discloses two doublets at 541 and 789 keV with separation energies 2.5 keV in each case. Both of the lower levels of these doublets have their energies

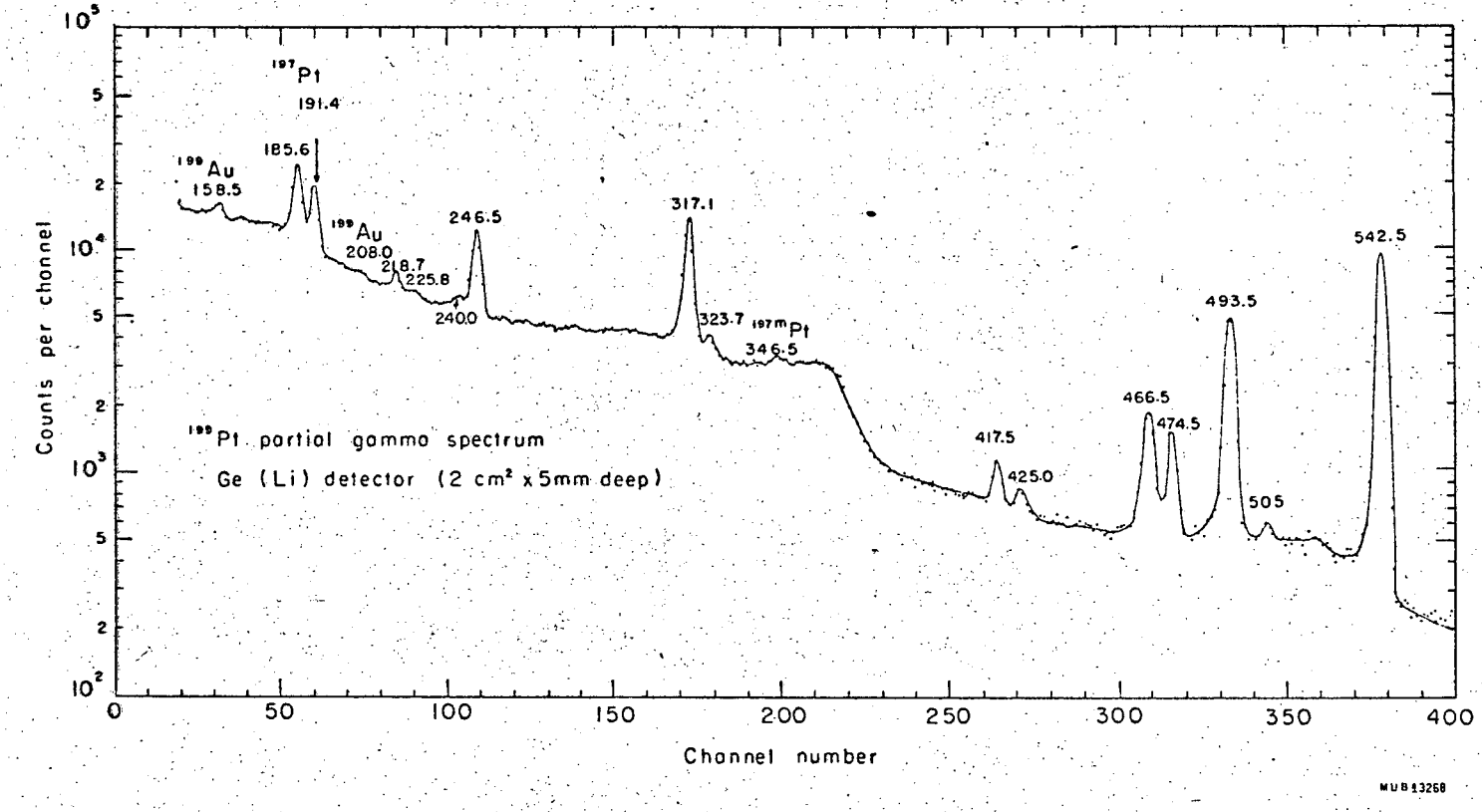

Fig. 23. Partial gamma-ray spectrum ^{199}Pt.

Table II. Photons from ^{199}Pt decay.

Energy (keV)[a]	Relative intensity
77.1[b]	---
185.6	9.7±0.9
218.7	1.3±0.2
225.8	0.3±0.1
240.0	1.3±0.2
246.5	10.2±0.5
317.1	30.7±1.5
323.7	1.9±0.3
417.5	2.2±0.2
425.0	0.9±0.2
466.5	14.0±0.6
474.5	7.7±0.5
493.5	37.1±1.6
505.0	0.7±0.2
542.5	100.0
714.8	12.2±0.5
791.5	5.8±0.7
967.0	6.3±0.8

[a]Energies are accurate to within 0.3 keV for the most intense transitions and to within 1 keV for the weakest transitions.

[b]Mixed with Au K_β x rays.

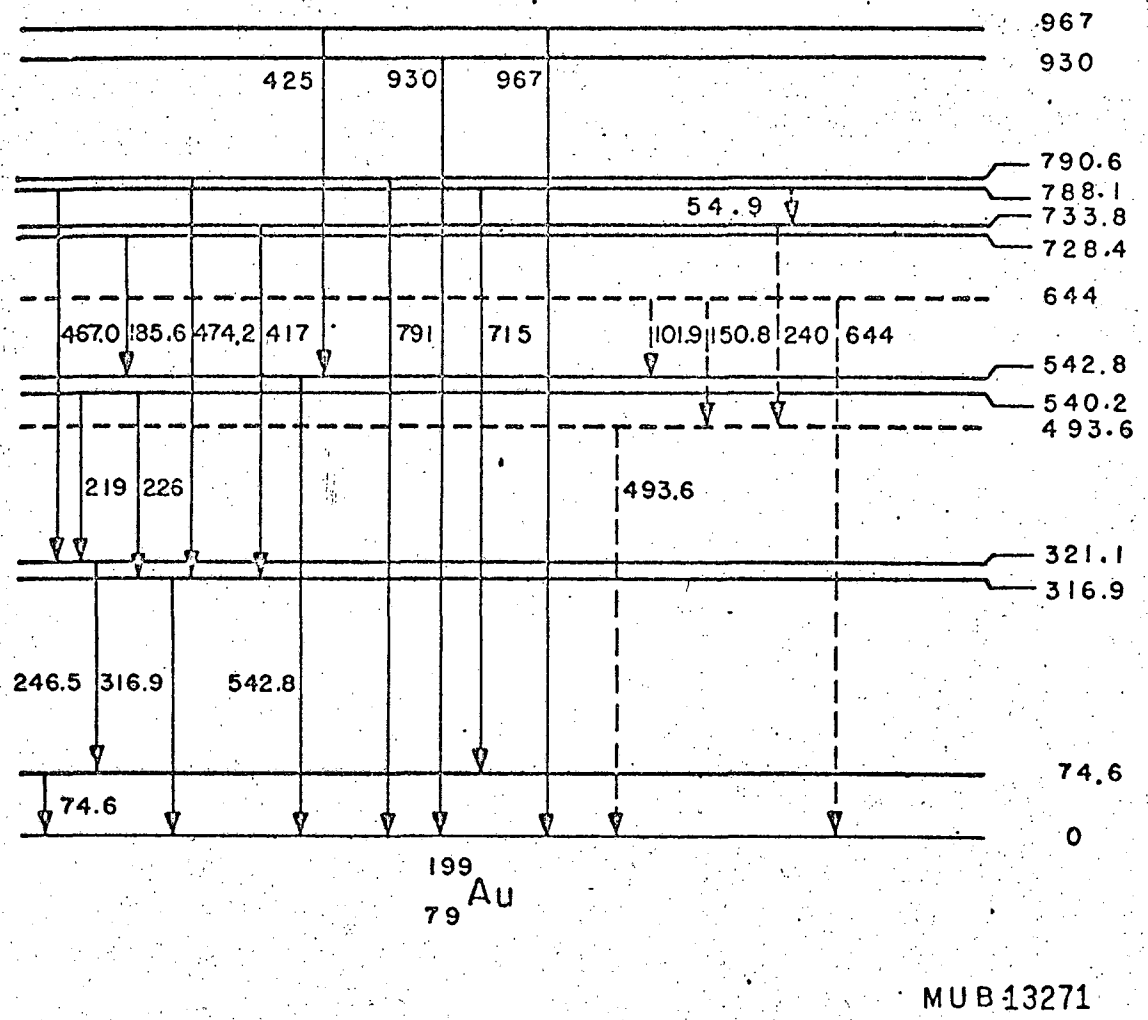

Fig. 24. Level scheme of ^{199}Au proposed by Black.[73]

determined by summing gamma-ray energies upon the energy of the first excited state at 74.6 keV. It is quite interesting to note the effect of a 2.5-keV error in the measurement of 74.6-keV transition. If the energy of the first excited state was 77.1 keV, from energy considerations the 219-keV transition would be assigned as depopulating the level at 542.8 keV along with the 226- and 543-keV transitions, and the 467- and 715-keV transitions would depopulate the level at 790.6 keV along with the 474- and 791-keV transitions. Along with these changes, the transitions we have observed at 240.0 and 323.7 keV would be interpreted as transitions from the second to the first excited and third excited to ground states respectively. These transitions were not observed by Black due to the fact that the resolution of his Ge(Li) detector was poorer than that utilized in our experiments.

The energy of the transition reported by Black at 74.6 keV was determined in high work by the measurement of conversion-electron lines at 60.26 and 62.70 keV with a permanent magnet spectrograph. These lines were interpreted as the L_I and L_{III} lines of a transition at 74.6 keV. As will be discussed later, the transition from the first excited states should be of mixed MI + E2 nature. Such a transition would be expected to have an intense L_I line with considerably weaker L_{II} and L_{III} lines. The L_{II} line should be stronger than the L_{III}. The observation of only the two lines seems to indicate that their assignment is in error. If we assume that the line at 62.70 keV is the L_I line of the transition depopulating the first excited state, the energy of this transition is then determined to be 77.05 keV. Since this energy agrees so well with the 317.1-240.0 and 323.7-246.5 gamma-ray energy differences, we must assume that Black's initial assignments are (in this case) in error. We can, however, offer no assignment for the conversion line observed by Black at 60.26 keV.

The fact that the 493.5-keV transition is not observed in any of the coincidence work done by Black indicates that it is either an isomeric transition or is directly fed by an isomeric transition. The appearance of conversion electrons from a transition of 54.9 keV in Black's permanent-magnet spectra coupled to the absence of gamma rays from this transition in

the gamma-ray spectrum led us to tentatively assign this as the isomeric transition in question. If we then assume the 493.5-keV transition goes directly to ground, the isomeric state is positioned at 548.5 keV. The isomeric levels found in the other odd-mass golds have spin and parity of 11/2-. If this holds true for the case of ^{199}Au, we expect little population of this level from direct β^- decay of ^{199}Pt (I = 1/2- or 5/2-). Since the intensity of the gamma ray depopulating the level at 493.5 keV is fairly large, we expect this level to be populated (through the 54.9-keV transition) by a fairly strong transition to the isomeric level. The 185.6-keV fits quite well, both in terms of energy and intensity, as the transition from a level at 734.3 keV to the isomeric state.

In Fig. 25 we show our modified level scheme for ^{199}Au. We have included (with the exception of the 54.9-keV transition) only those transitions observed in our work. The 467.9-keV transition depopulating the level at 791.6 keV and the 465.4-keV transition from the level at 542.5 keV are included due to the obvious unusual width of the gamma ray at 466.5 keV. It would appear that this peak is composed of two gamma rays of the above energies and approximately equal intensities.

Of particular interest in this systematic study of the odd-mass gold isotopes is the examination of those levels which may correspond to the "core-excitation" quadruplet proposed by de-Shalit and discussed in Section III-A of this thesis. As will be seen in study of the other golds, the first five excited levels are quite characteristic. They consist of a single level at 50-80 keV, a doublet at around 250-300 keV, an isomeric (11/2-) level around 400 keV, and a level of spin and parity 7/2+ lying directly above this. A very similar pattern again seems to be present in ^{199}Au. According to our proposed level scheme we find a level at 77 keV, two closely spaced levels at 317 and 324 keV, a proposed isomeric state at 549 keV, and a number of levels which might correspond to the 7/2+ level of interest.

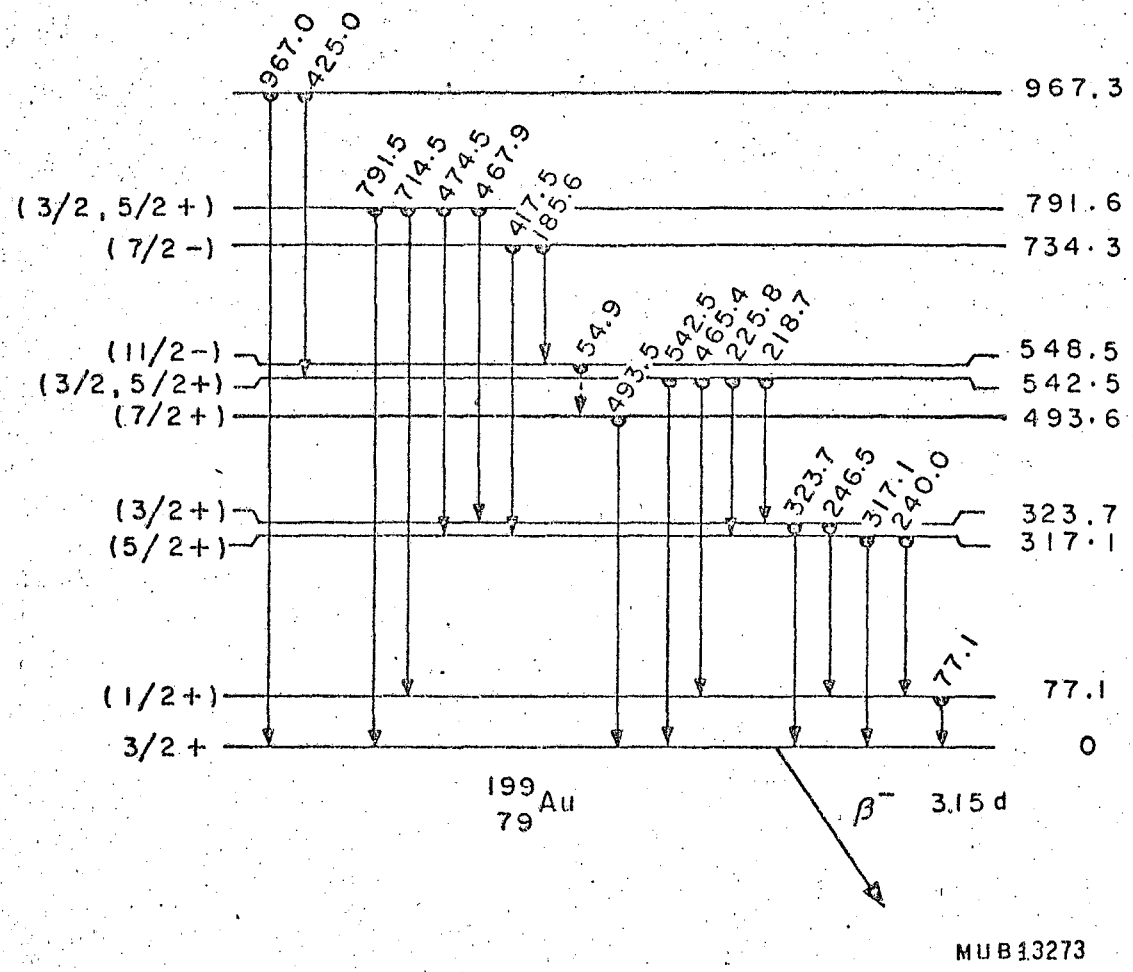

Fig. 25. Level scheme of ^{199}Au proposed from this work.

Due to the great similarity of the level structuring for the odd-mass gold isotopes, it is possible to tentatively assign spin and parity values to some of the levels in ^{199}Au. The analogies referred to in this section will become apparent later when we discuss the more neutron deficient golds.

The spin of the ground state of ^{199}Au, as well as those of ^{191}Au-^{197}Au, has been experimentally shown to be 3/2.[74,75,76] The parities of the ground states have also been shown to be positive. The first excited state (lying between 35 and 80 keV for the other odd-mass golds) by analogy can be assigned a spin and parity of 1/2+, and this value seems corroborated by the log ft value of > 8.4 derived from the data of Joshi et al. (assuming for ^{199}Pt I = 5/2-) for the decay of ^{199}Pt to this level. The two close-lying levels at 317 and 324 keV appear to correspond to the 3/2+ - 5/2+ pair which appear between 200 and 280 keV for ^{193}Au - ^{197}Au. As will be seen later, the 3/2+ level (lying lower in energy for ^{193}Au - ^{197}Au) seems to be tending to approach more closely in energy to the 5/2+ level as the neutron number increases. The question then arises as to whether the two levels have crossed by the time we reach mass 199. As will be seen in the odd-mass golds, the transitions from these levels follow a definite pattern. The 3/2+ level in the other cases is seen to decay by a strong transition to the 1/2+ level, and a weak transition to ground. For the 5/2+ level the situation is reversed, with the strong transition going to ground and the weak one going to the 1/2+. If we assume the analogy to hold for the transition strengths in this case, it would appear that the level at 317 keV with its strong transition to ground and weak transition to the 1/2+ level can be assigned a spin of 5/2, and that at 324 keV (weak transition to ground and strong transition to 1/2+ level) can be assigned a spin and parity of 3/2+. This is, of course, an important observation since it indicates a crossing of the 3/2+ and 5/2+ levels.

We have tentatively assigned an isomeric level at 548.5 keV. This should correspond to the 11/2- isomeric state found in the other odd-mass gold isotopes. As will be seen in the other gold isotopes, the strong transition (usually of around 200 keV) populating this isomeric state is of E2 character and arises from a level of spin and parity 7/2-. From analogy we would predict the 185.6-keV transition to be E2 and the level at 734.3 keV to be 7/2- (and thus would expect this level to receive considerable population from the β^- decay of ^{199}Pt). The decay of the isomeric state usually proceeds through an E3 transition to a level of spin and parity 5/2+. In the case of ^{199}Au, however, the situation is not clear. If the 54.9-keV transition was E3 in character ($t_{1/2} \approx 10^{-1}$ sec), we would expect to observe transitions from the 493.6-keV level (for this case I = 5/2) to levels of spin 1/2, 3/2, and 5/2. We have not observed transitions which would correspond to these. If the transition from the isomeric state was M2 in character ($t_{1/2} \approx 10^{-5}$ sec), the 493.6-keV level would be assigned as 7/2+ and decay primarily (as is seen in ^{197}Au coulomb excitation work) to ground. The position of the 7/2+ would then be generally what we expect from analogy to the other golds. For this reason we have given a very tentative assignment of 7/2+ to the level at 493.6-keV. The measurement of the half life of the 548.5-keV level should permit differentiation between E3 and M2 character for the 54.9-keV transition as should L- subshell measurements.

Since the transitions from the levels at 542.5 and 791.6 keV populate the four low-lying levels, we expect their spins and parities to be either 3/2 or 5/2+. The measurement of the multipolarities of the 465.4- and 714.5-keV transitions would allow differentiation between the two possible values.

While the above assignments are quite tentative, it seems quite likely, due to the very regular changes observed as one examines heavier odd-mass gold isotopes, that they are correct. Certainly more work is necessary on this decay. Accessibility of a reactor is of importance for this study, due to the fairly short half life of ^{199}Pt. Proximity to a reactor will also allow study of the 15-sec isomer ^{199m}Pt arising from the 13/2+ excited state.

Very recent measurements by K. G. Prasad, R. P. Sharma, and B. V. Thosar (Phys. Rev. 149, 980 (1966)) have confirmed many of our assignments. They found the multipolarities of the 542.5-, 317.1-, 246.5-, and 185.6-keV transitions to be M1 + E2, M1 + E2, M1 + E2 and E2 respectively. These yield spins and parities for the levels from which they originate which are in agreement with our assumed values. Their interpretation of the position of the isomeric state is also identical to ours. The conversion-electron spectrum published in this work shows no observable lines which would correspond to those from the 493.5-keV transition. Since the conversion lines from the 542.5-keV transition are quite strong, it would seem that the 493.5-keV transition has a low conversion coefficient and probable E2 character, thus giving tentative agreement to our assignment of 7/2+ for the 493.5-keV level. Due to the poor resolution of their Ge(Li) detector, they were unable to resolve the doublets at 190, 247, 320, 420, and 470 keV. They also assigned the gamma-ray observed at 191 keV to the decay of ^{199}Pt. This is in direct disagreement with our half-life measurements which show this line decaying with the half life of ^{197}Pt.

2. ^{197}Au

The low-lying levels of ^{197}Au have been studied through the decays of 18-h ^{197}Pt and 97-min ^{197m}Pt,[77,78,79,80] 65-h ^{197}Hg and 24-h ^{197}Hg,[81,82,83] as well as by Coulomb excitation and inelastic neutron scattering on ^{197}Au.[84,85,86,87] The low lying levels and their interpretation in terms of the "core excitation" model of de-Shalit[56] are shown in Fig. 21.

Prior to our work on the mass-197 isobars[88] there were a number of points of contention with regard to the ^{197}Au excited states. In particular, the spin assignment for the ^{197}Au excited level at 268 keV was not definite. This was due to the great variation in the experimentally measured values for the ICC of the 191-keV transition which connects the level at 268 keV with the 1/2 + level at 77 keV. Various measurements had led to an assignment of either 3/2+ or 1/2+ to the 268-keV level. This assignment is, of course, critical to the interpretation of the levels in terms of the core

excitation model. Another important series of observations that had not been substantiated was the work by Griesacker and Roy[80] on the decay of both ^{197}Pt and ^{197m}Pt. Their results, gained by beta-gamma and gamma-gamma coincidence techniques, suggested a more complicated level scheme for ^{197}Au than had been previously accepted, including a new level at 155 keV.

(a) ^{197}Pt and ^{197m}Pt decay. The half-lives of the various gamma rays observed in the decay of the Pt fraction of the neutron-irradiated enriched ^{196}Pt source were measured to determine whether they arise from the decay of ^{197}Pt or ^{197m}Pt. In Figs. 26(a) and 26(b) we show this spectrum taken at 3h and 12h after irradiation respectively. From these and similar spectra it was found that the 279- and 346-keV photons arise from the decay of ^{197m}Pt, and the 77-, 191-, 268-keV photons from ^{197}Pt decay, with no evidence of compound decay.

It is also seen from these spectra that the 155- and 202- keV transitions observed by Griesacker and Roy are not present with the intensities quoted by these authors. The 202-keV photon, which is observed in our early spectrum is much weaker than the 279-keV gamma-ray. This is an opposition to the results of Griesacker and Roy, where the 202 is reported to be stronger than the 279-keV photon. It is quite probable that the 155- and 202-keV photons observed by Griesacker and Roy are in reality due to the 158- and 208-keV transitions from the decay of ^{199}Au, which would have been formed from the decay of ^{199}Pt, since a radio-chemical separation was not undertaken in their experiment.

Table III summarizes our gamma-ray data for ^{197}Pt and ^{197m}Pt. In this table we also include the 52.95-keV E2 transition found by Sehgal and Emery[89] from the decay of ^{197m}Pt to levels in ^{197}Pt. The photons from this transition are not observed in our spectra due to its large conversion coefficient ($e/\gamma \approx 100$).

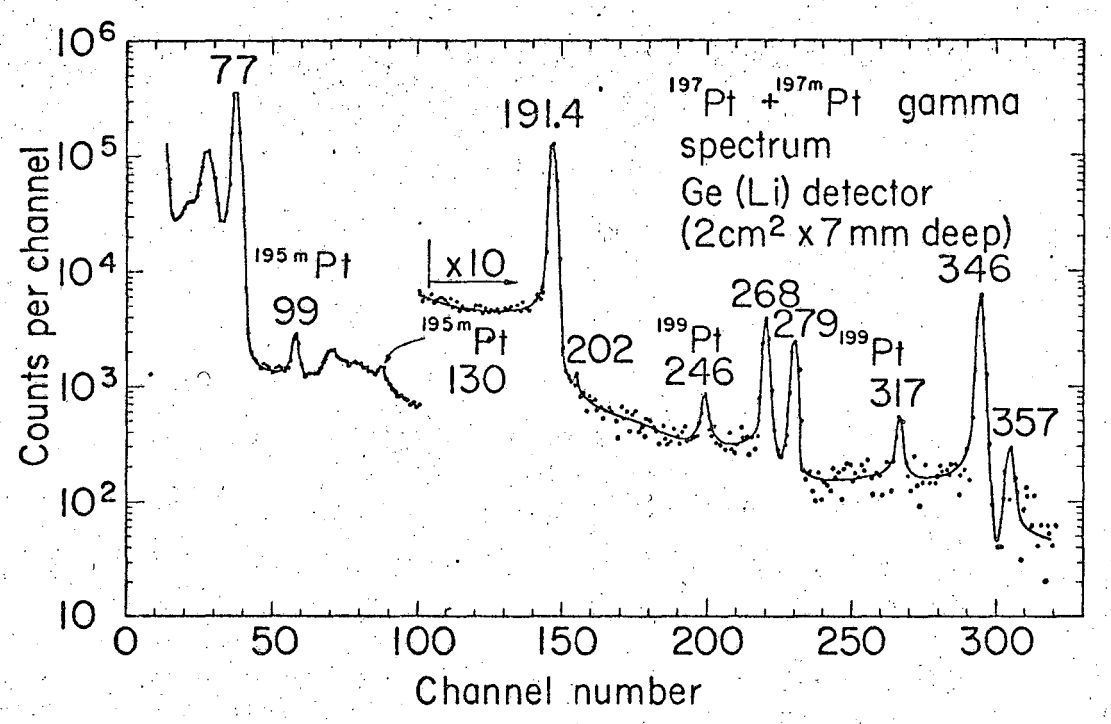

Fig. 26(a). Gamma-ray spectrum of sample containing principally ^{197}Pt and ^{197m}Pt. This spectrum, recorded for 30 min, was taken about 3 h after the end of irradiation.

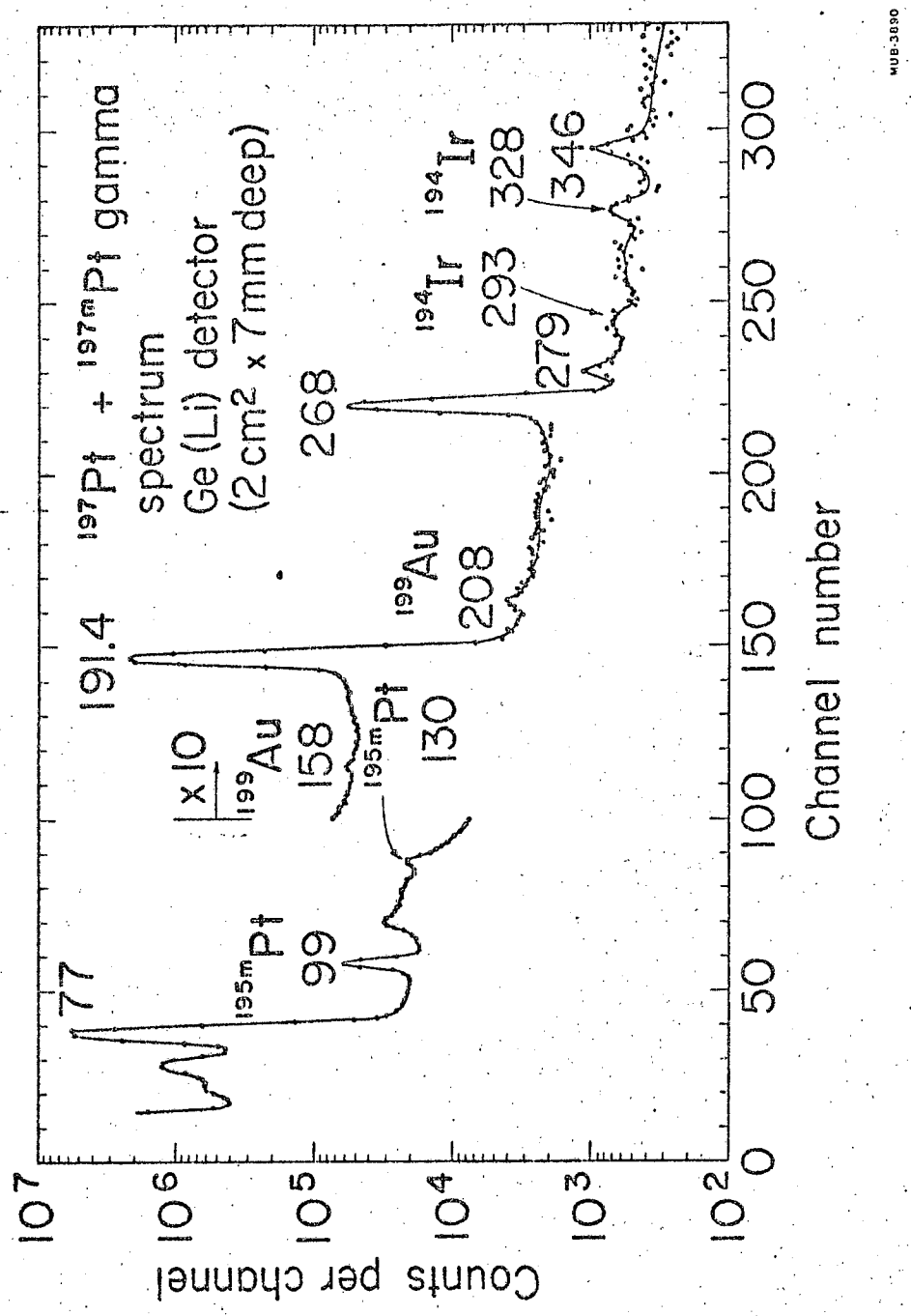

Fig. 26(b). Gamma-ray spectrum of ^{197}Pt and ^{197m}Pt, recorded for 15 h, taken at a mean time of 12 h after the end of irradiation.

Table III. Photons from ^{197}Pt and ^{197m}Pt decay.

	Energy (keV)	Relative intensity
^{197}Pt	77	330±30
	191.4	100
	268	7±1
	279 (not seen)	< 0.2
^{197m}Pt	52.95[a]	
	(130)[b]	
	202	≤ 1
	279	21±2
	346	100

[a] L subshell conversion electrons observed by Sehgal and Emery.[88]

[b] E3 transition photons not observed due to large conversion coefficient.

(b) ^{197}Hg and ^{197m}Hg. The half-lives of the photons observed from the decay of the purified Hg fraction of the Au+d bombardment were measured from a series of timed gamma-ray spectra. In Fig. 27 we show the ^{197}Hg + ^{197m}Hg gamma-ray spectrum. From this and similar spectra it was determined that the 191- and 268-keV photons decay with the half-life (66-h) indicative of ^{197}Hg, while the 134-, 164-, 202-, and 279-keV photons decay with the 22-h half-life of ^{197m}Hg. None of these photons exhibited compound decay. The 263-keV photon observed in Fig. 27 can be assigned to the decay of ^{195}Hg. In Table IV we present a summary of the gamma-ray data for ^{195}Hg and ^{197m}Hg.

From our studies, the 268-keV gamma has been observed from the decay of 66-h ^{197}Hg, as well as the weak 202-keV transition from the decay of 22-h ^{197m}Hg. Neither of these gammas had previously been reported.

(c) Conversion coefficient of the 191-keV transition. As we mentioned previously, the assignment of the multipolarity of the 191-keV transition is particularly important in order to establish the spin and parity of the level of ^{197}Au at 268 keV. The previous measurements of the K-ICC had varied widely as is shown in Table V. For a transition of this energy in gold, the theoretical K conversion coefficients of Sliv[115] are 0.95 for an M1 transition and 0.185 for an E2 transition. Thus, a measured K-ICC of greater than 0.95 will indicate an M1 + E0 admixed transition from the 77-keV 1/2+ level to the 268-keV level, and an assignment of 1/2+ to the 268-keV level. If the measured value was less than 0.95, an M1 + E2 transition and spin assignment of 3/2+ are indicated.

The measurement of the K-ICC of the 191-keV transition was made utilizing the conversion coefficient spectrometer described in Section II of this thesis. The appropriate sections of our $^{197+197m}$Pt electron and gamma spectra are shown in Figs. 28(a) and 28(b). From the areas and efficiencies of the electron and gamma-ray full-energy peaks we determined that the experimental K-ICC was 0.69 ± 0.07 which, when compared to the values of Sliv, indicated an M1 + E2 admixed transition with $\delta^2 = 0.52 \pm 0.20$. The K/L ratio, which was measured simultaneously, gave a value of

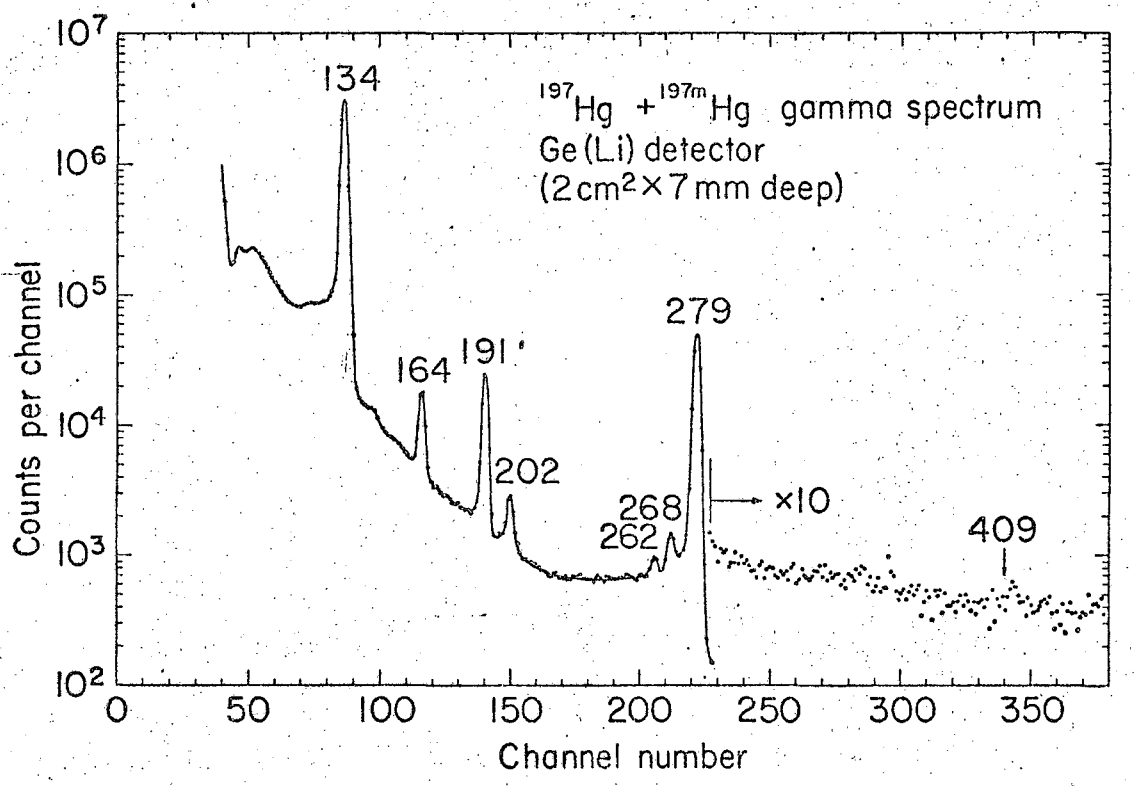

Fig. 27. Gamma-ray spectrum of sample containing ^{197}Hg and ^{197m}Hg.

Table IV. Photons from ^{197}Hg and ^{197m}Hg decay.

Energy (keV)		Relative intensity
^{197}Hg	77	
	191	100
	268	7.6±0.7
	279 (not seen)	< 2
^{197m}Hg	134	100
	165	0.95±0.1
	202	0.23±0.03
	279	15.7 ±1

Table V. Reported values of the K conversion coefficient and K/L ratio of the 191-keV transition in ^{197}Au.

α_k	K/L	Ref.
≈1.7		a
0.90±0.10	6.3	b
2.5		c
2.0 ±0.5	6 ±0.5	d
0.65±0.15		e
1.59±0.07		f,g
0.77±0.2		h
0.93±0.2		h
	6	i
	5.5±0.3	j
	5.9±0.2	k
0.69±0.07	5.2±0.6	present work

[a] O. Huber, F. Humbel, H. Schneider, A. de-Shalit, and W. Zünti, Helv. Phys. Acta 24, 127 (1951).

[b] R. Joly, J. Brunner, J. Halter, and O. Huber, Helv. Phys. Acta. 28, 403 (1955).

[c] V. R. Potnis, C. E. Mandeville, and J. S. Burlew, Phys. Rev. 101, 753 (1956).

[d] M. C. Joshi and B. C. Thosar, Proc. Int. Conf. Nuclear Structure, Kingston, ed. by D. A. Bromley and E. V. Vogt, (University of Toronto Press, 1960) p. 623.

[e] L. Feuvrais, Ann. Phys. 5, 181 (1960).

[f] V. R. Potnis, E. B. Nieschmidt, C. E. Mandeville, L. D. Ellsworth, and D. D. Bornemeier, Phys. Rev. 136, B919 (1964).

[g] D. D. Bornemeier, (Ph.D. Thesis), Kansas State University, 1965, unpublished.

continued

Table V. Continued.

[h]R. G. Helmer and L. D. McIssac, Phys. Rev. 137, B223 (1965).

[i]J. M. Cork, J. M. LeBlanc, F. B. Stumpf, and W. H. Nester, Phys. Rev. 86, 415 (1952).

[j]A. A. Bartlett and C. J. Herrlander, Research Institute for Physics, Stockholm, Annual Report, (1964) p. 28.

[k]M. Gasser, O. Huber, and L. Schellenberg, Nucl. Phys. 80, 65 (1966).

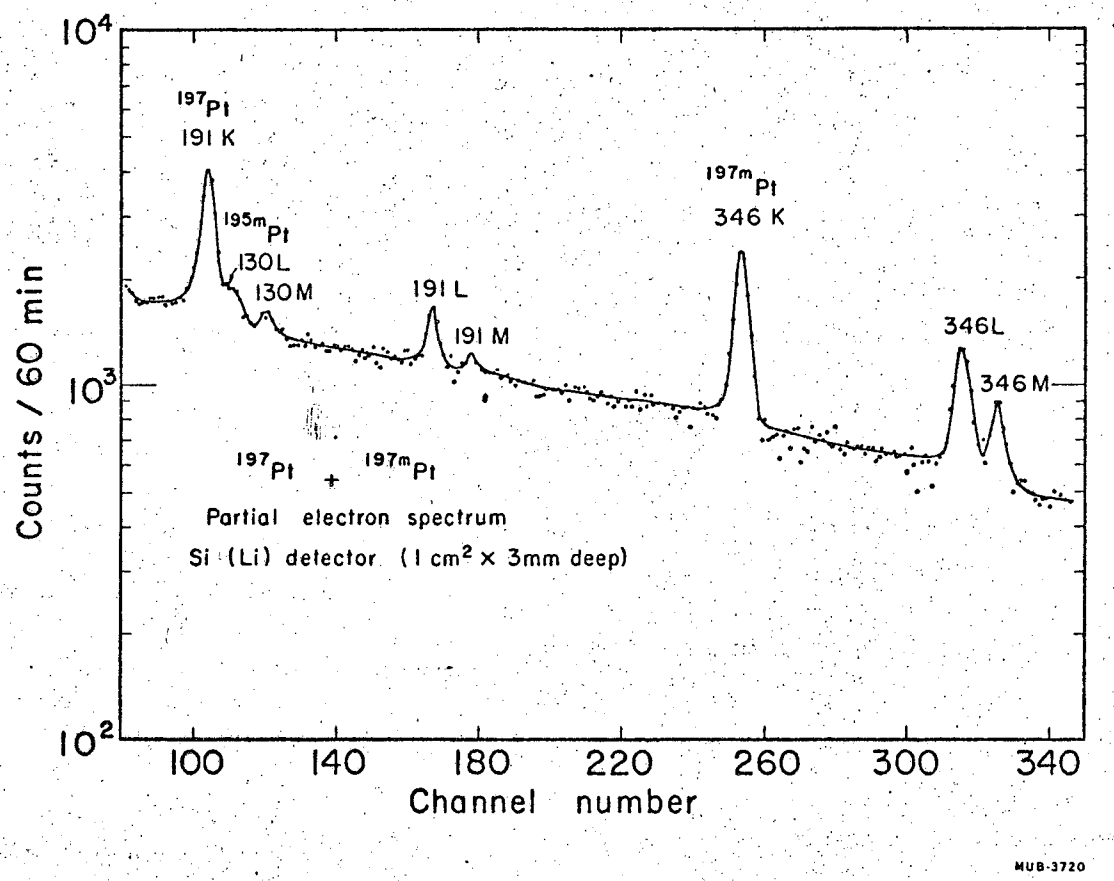

Fig. 28(a). Electron spectrum of sample containing ^{197}Pt and ^{197m}Pt, recorded with Si(Li) detector of the conversion-coefficient spectrometer.

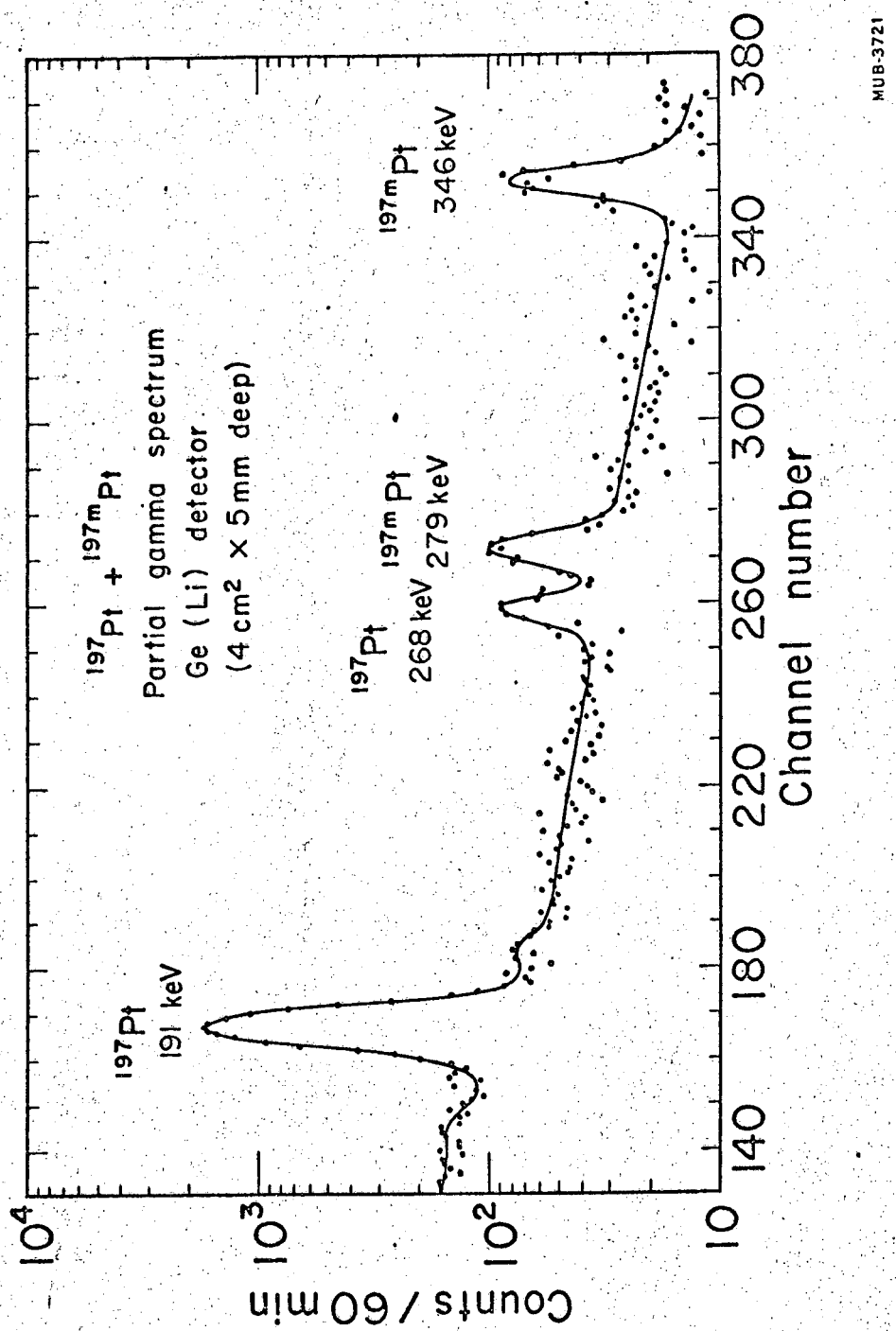

Fig. 28(b). Gamma-ray spectrum recorded simultaneously with the electron spectrum of (a) by the Ge(Li) detector of the conversion-coefficient spectrometer.

5.2 ± 0.6 and when compared to theory indicated an M1 + E2 transition with $\delta^2 = 0.19 \pm 0.16$.

To check our method, we also measured the K-ICC of the 346-keV transition in ^{197}Pt, which had previously been assigned an M4 multipolarity. Our experimental values, $\alpha_k = 3.9 \pm 0.4$ and K/L = 1.8 ± 0.2, clearly establish the multipolarity as M4 when compared to the theoretical values of β_K (M4) = 4.2, K/L = 1.75.

(d) Additional features of the decay scheme. From our observed gamma ray intensities and either measured or estimated conversion coefficients, it was possible to assign log ft values to the various beta transitions involved. In particular, our values allowed the assignment of spin and parity to the ground state of ^{197}Pt the value of which had previously been in doubt. The reported observation[77] of a weak 279-keV photon from ^{197}Pt decay and its interpretation as arising from a weak beta branch of ^{197}Pt to the 279-keV (5/2+) level of ^{197}Au had led to a 3/2+ assignment for the ^{197}Pt ground state. It is seen from our data that this observed transition is actually the 268-keV gamma ray. It is possible to set a quite small upper limit for the intensity of the 279-keV photon from ^{197}Pt decay using our gamma-ray half-life data. This upper limit leads to an upper limit of 0.013% for the beta branching to the 279-keV level. This corresponds to a log ft value of 9.7 and allows an interpretation of the beta branch as being of the "$\Delta I = 2$, yes" type, yielding a spin assignment of 1/2- for the ^{197}Pt ground state (as is observed for ^{197}Hg).

Our data are summarized in the decay scheme for these isomers shown in Fig. 29. Not shown is the 7/2+ level of ^{197}Au at 548 keV, which has been observed in coulomb excitation studies[85] and decays to ground ($E\gamma$ = 548 keV) and to the 5/2+ level at 279 keV ($E\gamma$ = 269 keV).

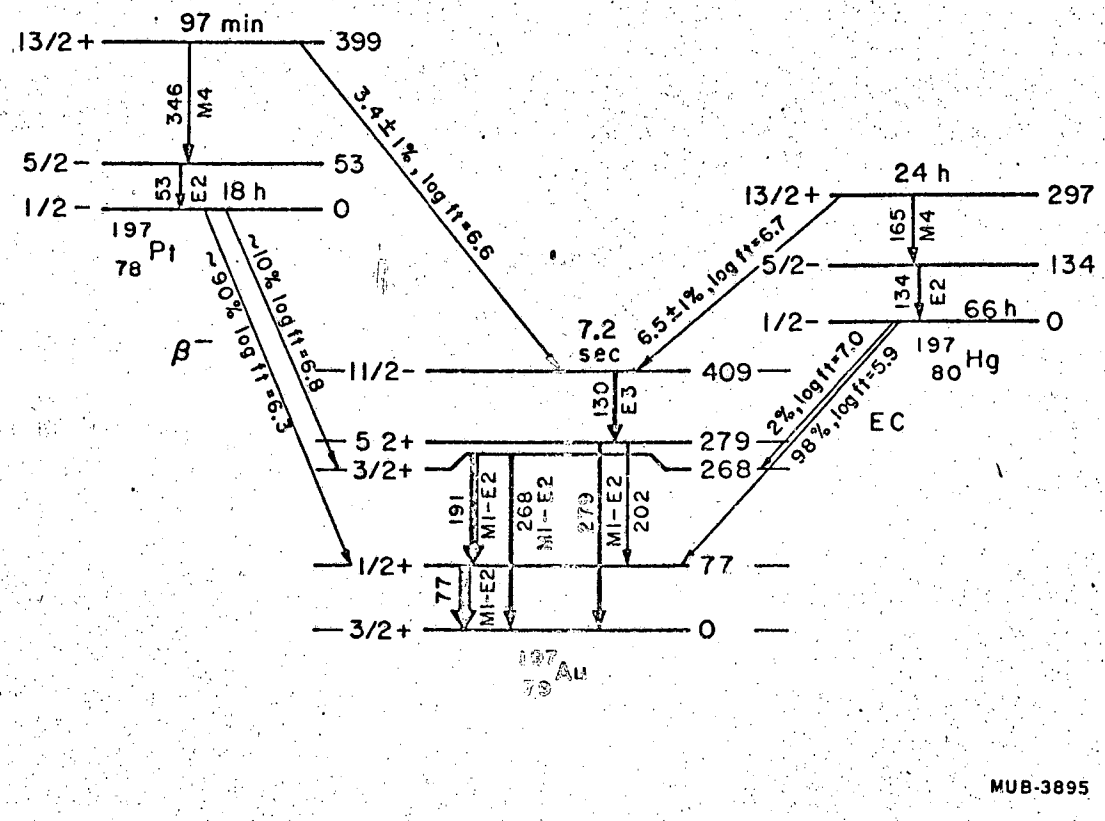

Fig. 29. Decay scheme of the A = 197 isomers of Hg and Pt. The 7/2+ level in ^{197}Au at 548 keV is not shown in this figure.

3. ^{195}Au

The early work on the electron-capture decay of both 40-h ^{195m}Hg and 9.5-h ^{195}Hg to levels in ^{195}Au was undertaken by Moon and Thompson[90] and Gillon et al.[91] The latter was the more extensive work, examining the conversion-electron spectrum below 300 keV in detail using a permanent magnet spectorgraph. From this study, Gillon et al. were able to formulate a simple level scheme for the very low lying levels in ^{195}Au. Following these early studies, Brunner, Halter and co-workers[83,92,93,94,95,96] published an extensive series of articles covering their work on the decay of the ^{195}Hg isomers. In their study, Brunner et al. utilized a NaI(Tl) spectrometer, permanent-magnet spectrographs, a double-focussing electron spectrometer, and a β-γ coincidence arrangement incorporating a "lens" spectrometer for high efficiency observation of the conversion-electron spectrum. They were able to position some 25 transitions unambiguously in a level scheme for ^{195}Au. Using K/L ratios and some absolute conversion-electron-to-gamma-ray measurements they were able to assign multipolarities to a few transitions and allow spin and parity assignments for some levels.

In our study, we produced ^{195m}Hg, and ^{195}Hg by the bombardments of ^{197}Au foils with 35-MeV deuterons. The gamma spectra of the sources produced by evaporation of the Hg from the gold target onto a "catcher" foil were examined as function of time to determine whether a given photon arose from the decay of the ground or isomeric levels of the parent ^{195}Hg. Since the half life of the isomeric state of ^{195}Hg is longer (40h) than that of the ground state (9.5h), the photons arising from the ground state decay will exhibit a complex decay pattern, while those arising from electron capture of the isomeric state will show a simple decay with a 40-h half life. From transitions known to be populated only from ground-state decay[96] we determined the shape of the decay function. The shape of this function is identical to that generated under the assumption that the isomeric state of ^{195}Hg is produced with a cross section which is a factor of two greater than that for the ground state. This finding is in accord with the results obtained by Kaufman[97] for the production of ^{195}Hg isomers from the bombard-

ment of gold with 2.8-GeV protons, where he finds $\sigma(13/2+)/\sigma(1/2-) = 2.4 \pm 0.5$. These values are in contrast to the low-energy case, where the isomeric ratio for ^{197}Hg produced by the (p,n) reaction on gold was found to be 0.23-0.36 at energies of 7.3-10.4 MeV.[161] Thus, at low energies it seems that the isomer ratio favoring the low-spin isomer is determined primarily by the predominance of compound nuclei formed with low angular momentum (target spin ^{197}Au is 3/2), while at higher energies both protons and deuterons bring in large amounts of angular momentum via the high - l partial waves that become important for higher energy reactions.

The decay curve for those transitions known to arise from mercury ground state decay was then used to determine the origin of many new lines found in the high-resolution gamma-ray spectrum observed using a Ge(Li) detector. A number of transitions observed were too weak to permit half-life determination and thus their final positioning in the decay scheme is solely from energy considerations. In Figs. 30, 31, and 32 we show the gamma-ray and conversion-electron spectra observed with moderate resolution Ge(Li) and Si(Li) detectors in the energy region 100 - 1300 keV. Portions of the gamma-ray spectrum taken with greater amplification gain, utilizing Ge(Li) detectors of quite high resolution or in the anti-Compton configuration described previously, are shown in Figs. 33-37. A summary of our gamma-ray data for the decay ^{195}Hg and ^{195m}Hg is shown in Table VI. The relative intensity values listed in Table VI are the average values obtained from many runs using a number of different detectors.

Using the relative intensities of those gamma rays listed in Table VI along with that of the 37.1-keV M1 transition in ^{195}Hg (through which 100% of the isomeric decays in ^{195}Hg must pass) and either measured or assumed ICC, it was possible to determine relative electron-capture probabilties for both ^{195m}Hg and ^{195}Hg decay. From these branching percentages, it was possible, after correction for the K/L capture ratio, to determine log ft values for the various decays. Both the K/L capture correction formula and the log ft nomograms of Wapstra[162] were utilized for these calculations.

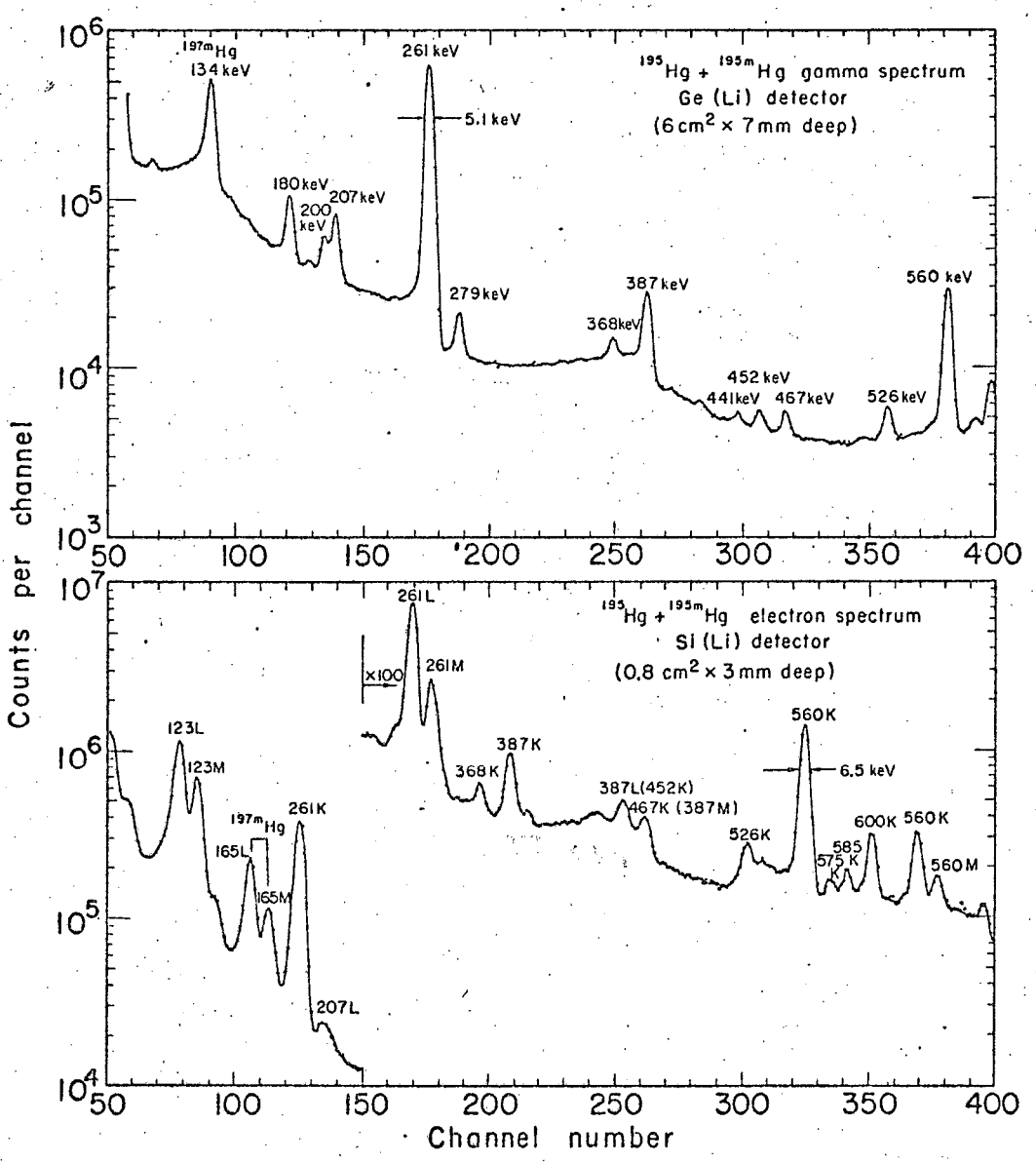

Fig. 30. Partial gamma-ray and electron spectrum from the decay ^{195}Hg and ^{195m}Hg taken simultaneously in the conversion-coefficient spectrometer.

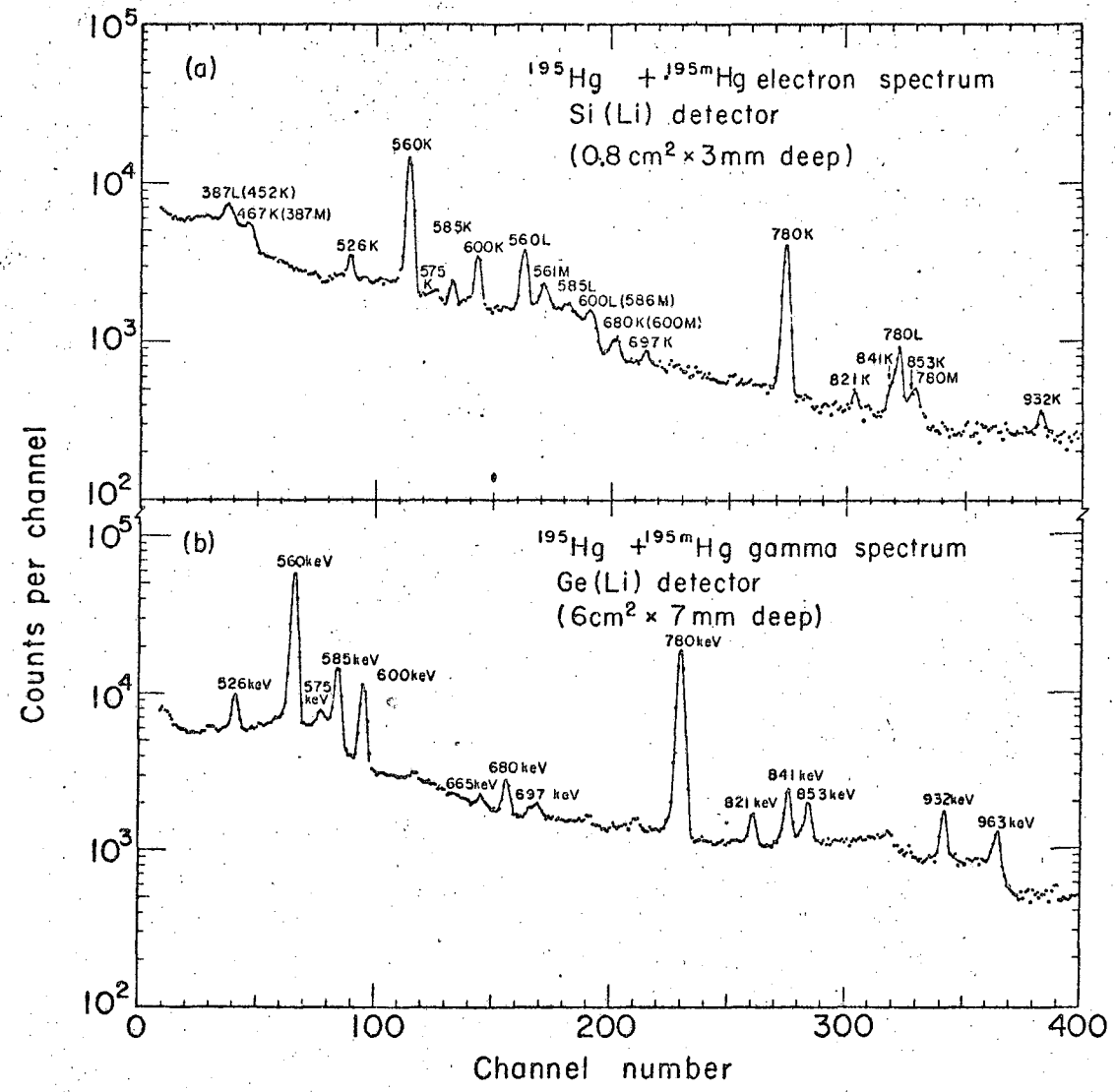

Fig. 31. Partial gamma-ray and electron spectrum from the decay ^{195}Hg and ^{195m}Hg taken simultaneously in the conversion-coefficient spectrometer.

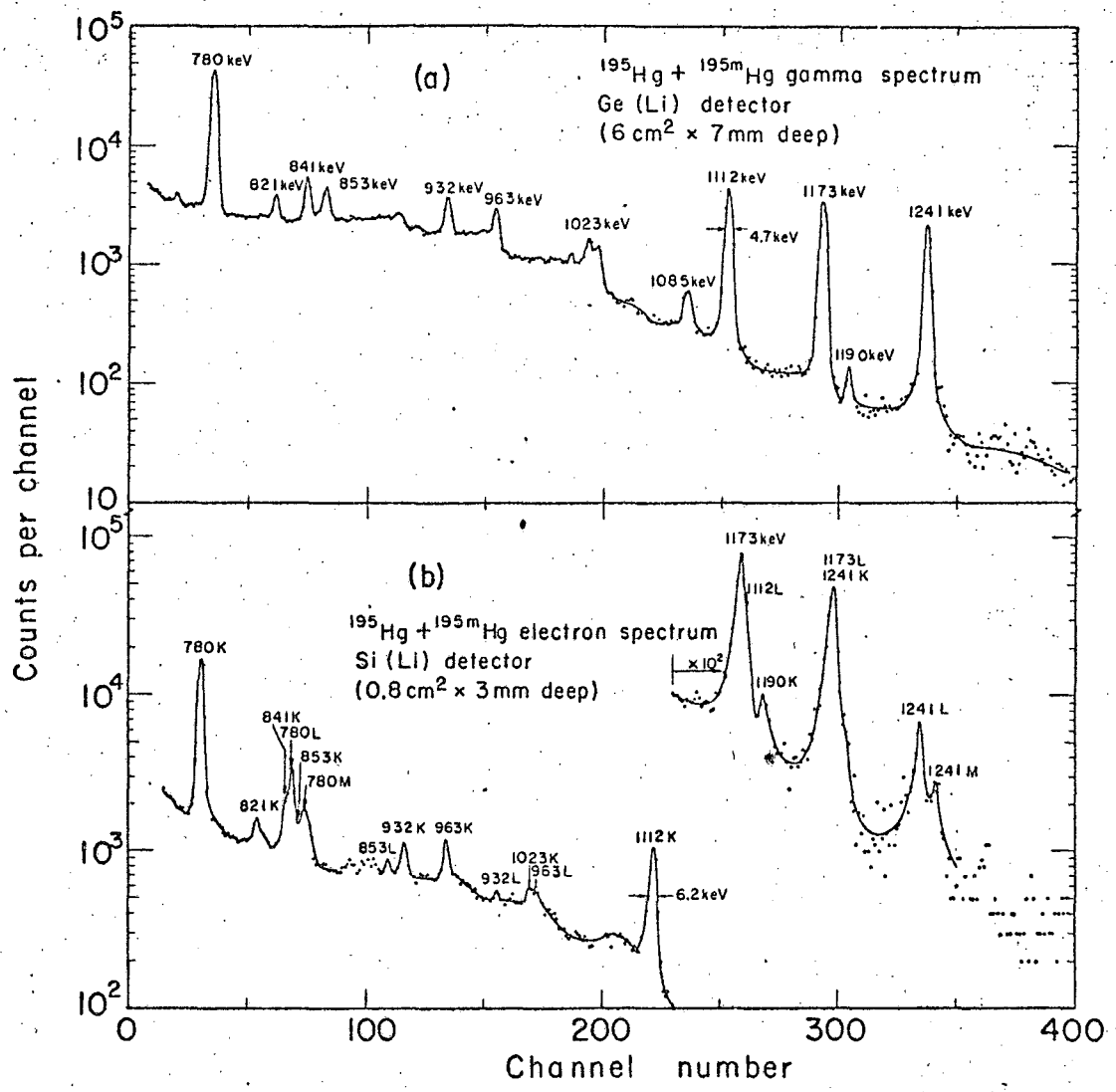

Fig. 32. Partial gamma-ray and electron spectrum from the decay ^{195}Hg and ^{195m}Hg taken simultaneously in the conversion-coefficient spectrometer.

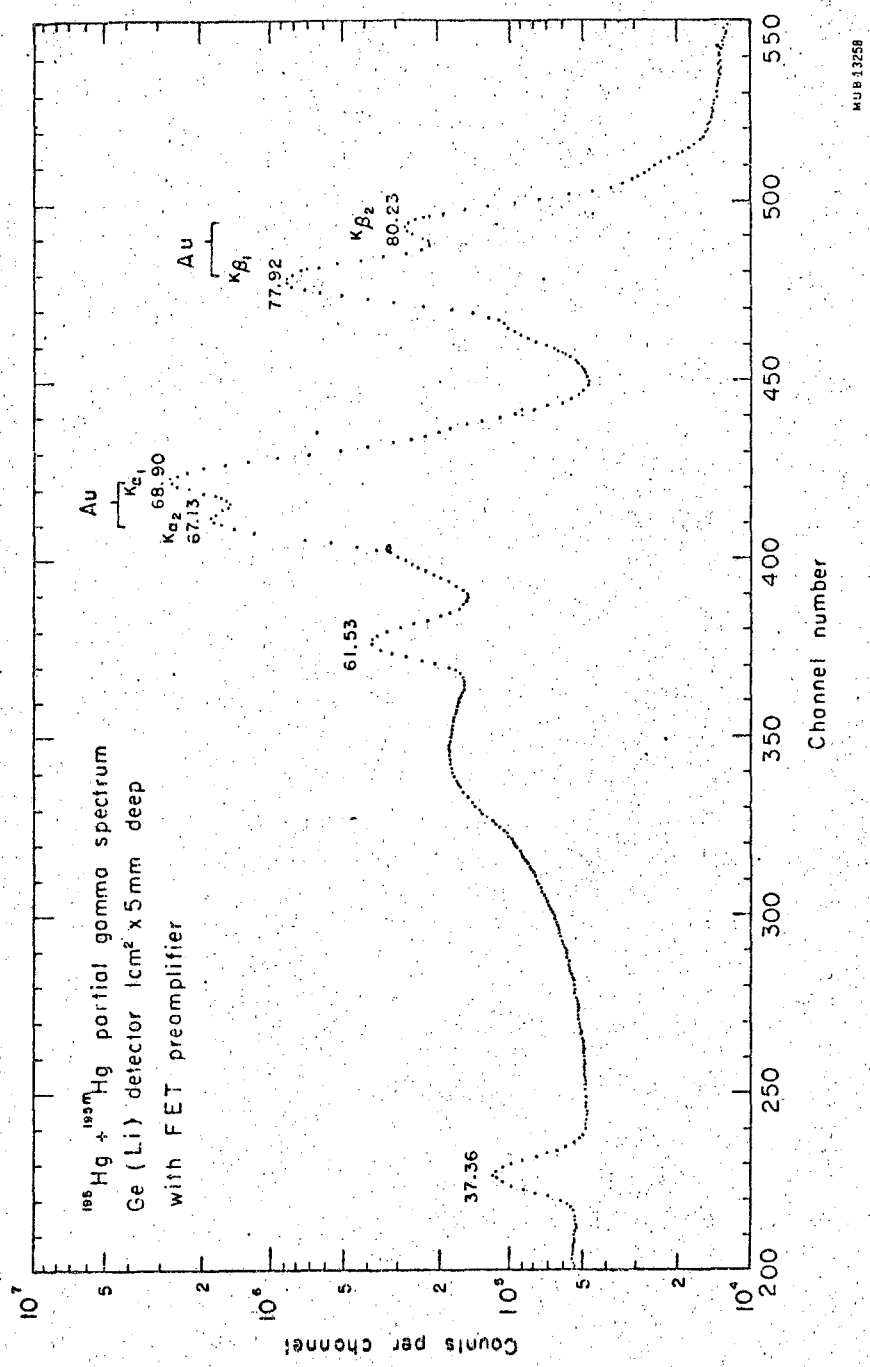

Fig. 33. Low-energy gamma-ray spectrum of ^{195}Hg and ^{195m}Hg sample recorded with high-resolution Ge(Li) detector.

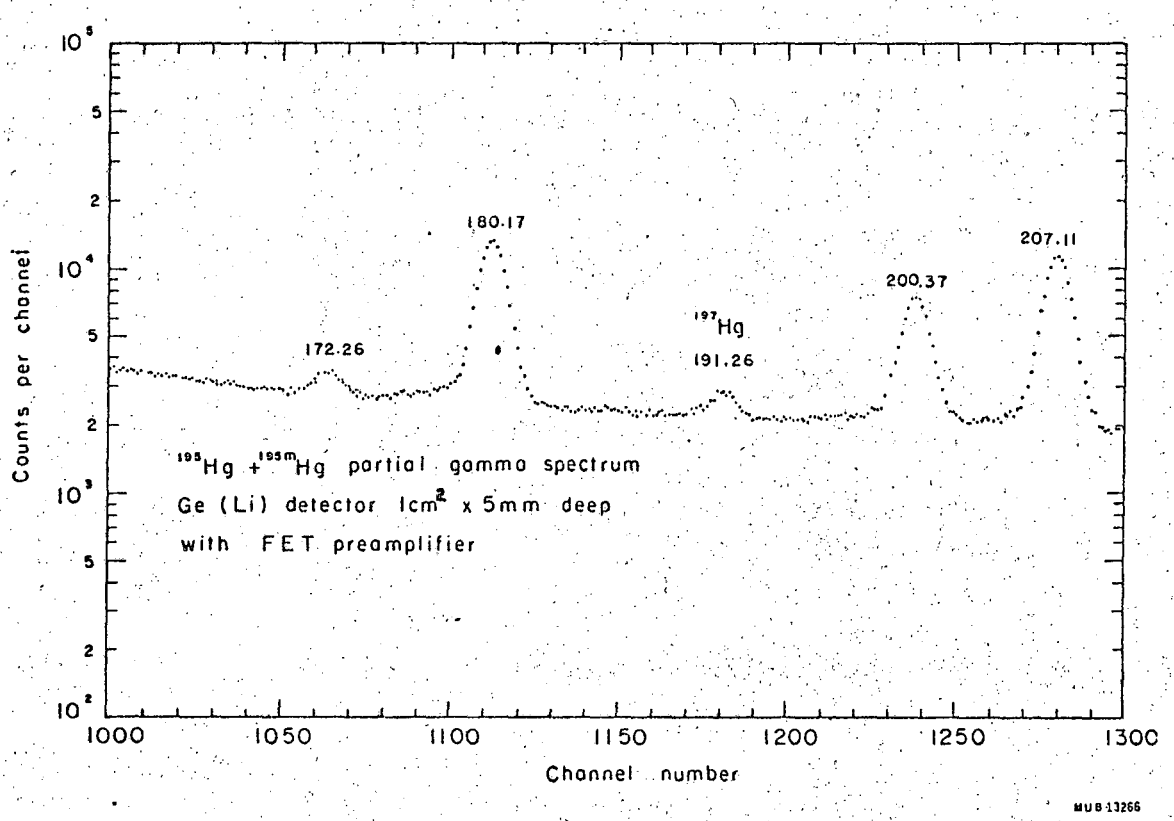

Fig. 34. Gamma-ray spectrum of ^{195}Hg and ^{195m}Hg sample in the region 160-210 keV recorded with high-resolution Ge(Li) detector.

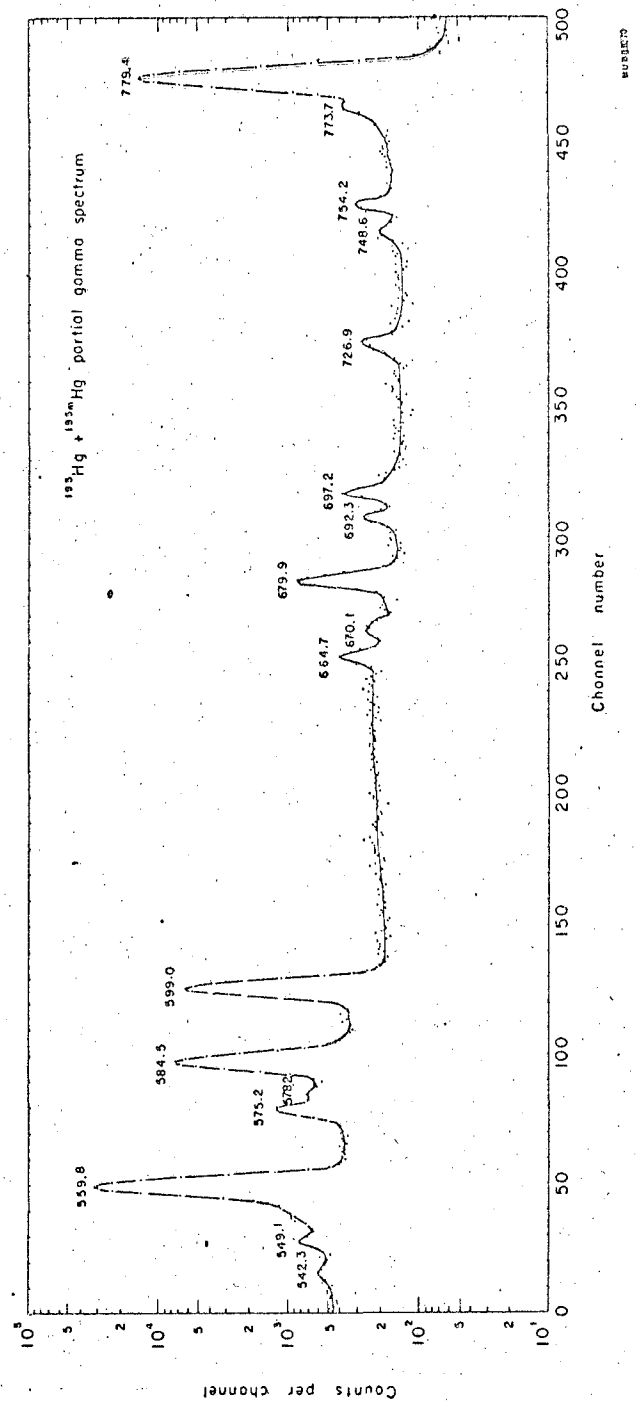

Fig. 35. Gamma-ray spectrum of ^{195}Hg and ^{195m}Hg sample in the region 540-780 keV recorded with Ge(Li) detector operating in anti-Compton mode.

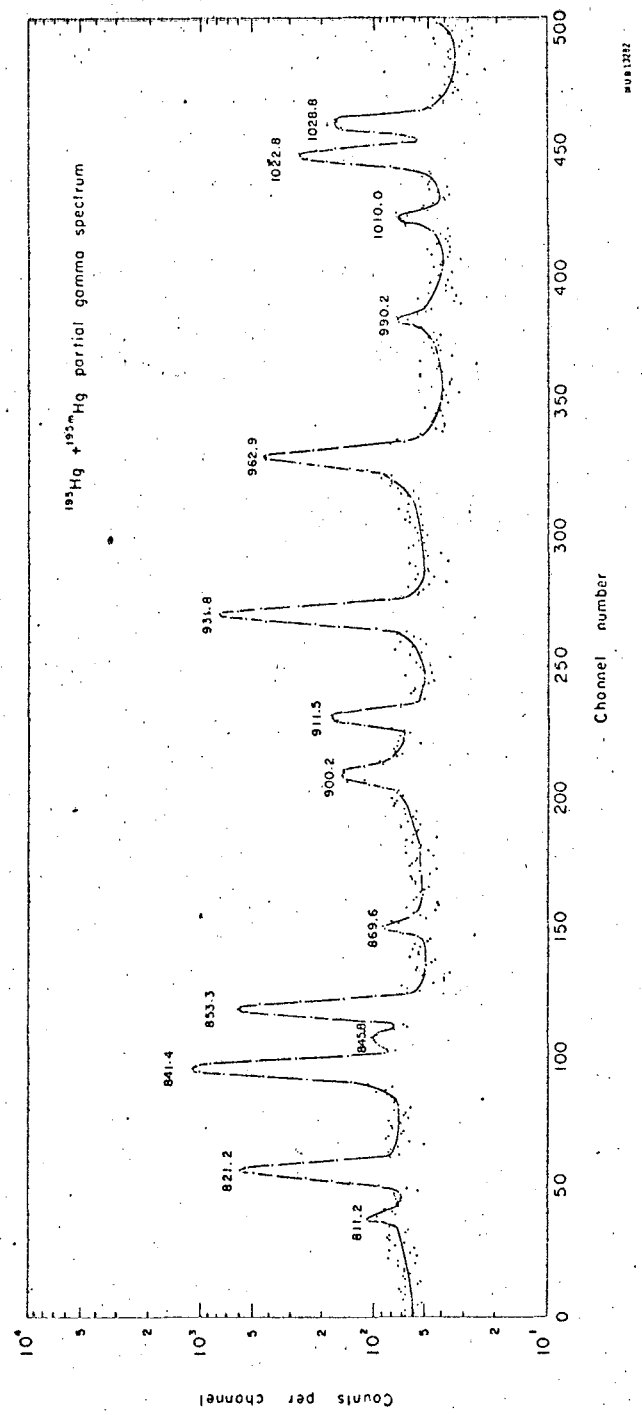

Fig. 36. Gamma-ray spectrum of ^{195}Hg and ^{195m}Hg sample in the region 800-1040 keV recorded with Ge(Li) detector operating in anti-Compton mode. The broad peaks at 900.2 and 1028.8 keV are due to Compton scattering of the 1112.1- and 1241.0-keV gamma rays. A similar peak arising from the 1173.2-keV gamma ray is obscured by the 962.9-keV gamma ray.

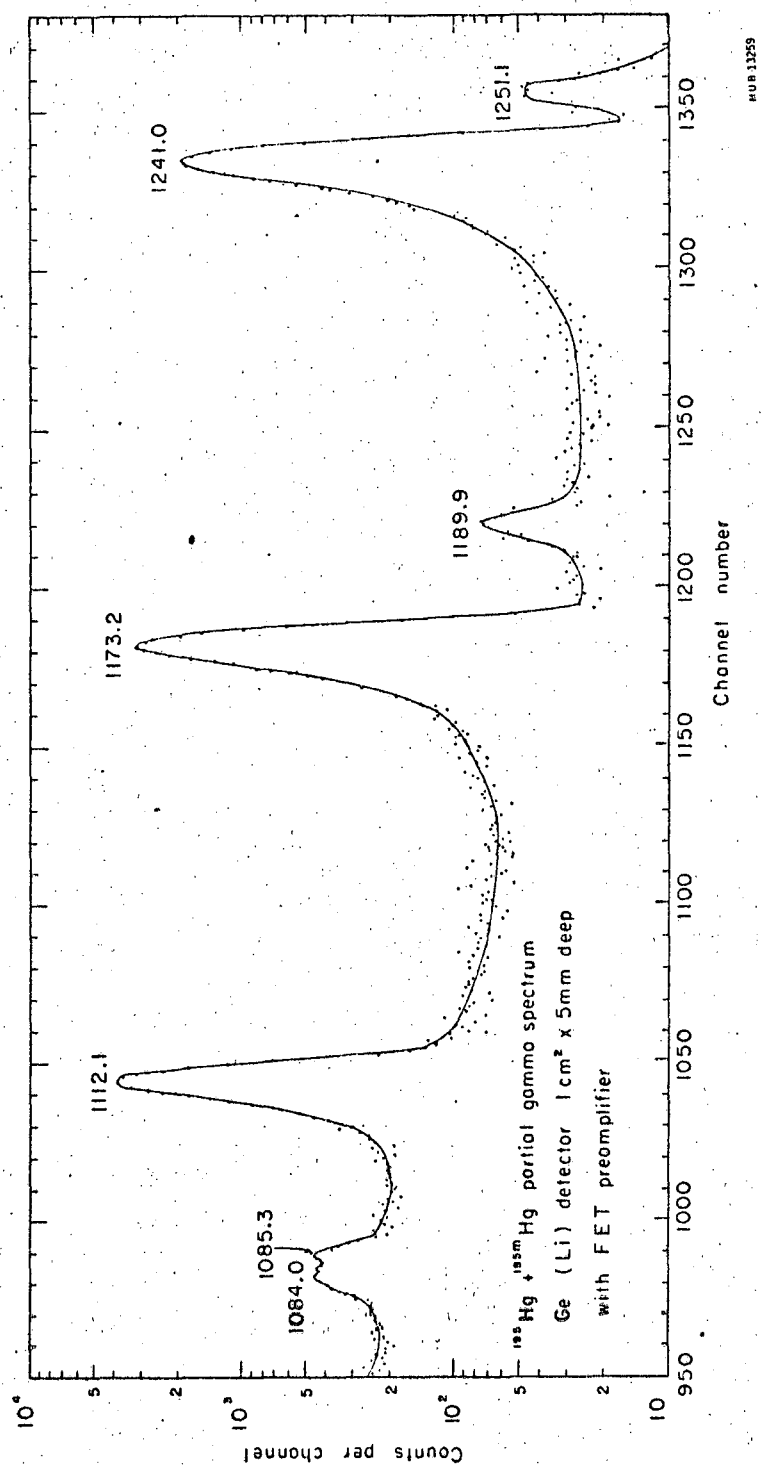

Fig. 37. High-energy gamma-ray spectrum of ^{195}Hg and ^{195m}Hg sample recorded with high-resolution Ge(Li) detector.

Table VI. Photons from ^{195}Hg and ^{195m}Hg decay.

	Energy (keV)	Parent Level (keV)	Relative Intensity
^{195}Hg	(56.7)[a]	318.2	
	61.5±0.2	61.5	366 ±20
	180.2±0.2	241.6	99 ± 6
	200.4±0.2	261.7	2.1 ± 0.2
	207.1±0.2	525.4	94 ± 7
	241.4±0.4	241.6	5.2 ± 0.6
	261.6±0.2	261.7	94 ± 7
	318.1±0.4	318.2	0.1 ± 0.02
	584.5±0.2	1109.9	118 ± 7
	599.0±0.2	840.7	100[+]
	779.4±0.2	840.7	403 ±20
	821.2±0.3	1083.7	17.9 ± 0.8
	841.4±0.3	1083.7	35.5 ± 1.6
	911.5±0.5	1173.3	5.2 ± 0.3
	931.8±0.3	1173.3	28.6 ± 1.3
	990.2±0.6	1251.5	0.8 ± 0.2
	1010.0±0.7	1251.5	0.9 ± 0.3
	1022.8±0.4	1083.7	8.0 ± 0.4
	1084.0±0.6	1083.7	3.4 ± 0.2
	1112.1±0.4	1173.3	78 ± 4
	1173.2±0.3	1173.3	72 ± 4
	1189.9±0.5	1251.5	0.9 ± 0.1
	1251.1±0.5	1251.5	0.8 ± 0.1
^{195m}Hg	37.4±0.2[b]	----	24.7 ± 1.4
	(56.7)[a]	318.2	
	61.5±0.2	61.5	5.8 ± 0.6
	172.2±0.3	877.9	0.55± 0.06

continued

Table VI. Continued.

Energy (keV)	Parent Level (keV)	Relative Intensity
200.4±0.2	261.7	9.9 ± 0.6
207.1±0.2	525.4	10.0 ± 0.6
255.3±0.5	517.4	3.5 ± 1.0
261.6±0.2	261.7	430 ±25
318.1±0.4	318.2	0.24± 0.03
368.1±0.2	893.4	4.6 ± 0.3
386.5	1280.4	25.3 ± 1.3
387.4±0.2	705.8	
451.7±0.3	1345.0	2.8 ± 0.2
466.9±0.3	1345.0	3.8 ± 0.3
517.9±0.4	517.4	0.49± 0.07
525.4±0.2	1403.1	7.2 ± 0.5
542.3±0.5	1067.1	0.28± 0.04
549.1±0.5	1067.1	0.71± 0.12
559.8±0.2	877.9	100[+]
575.2±0.4	893.4	3.7 ± 0.2
679.9±0.3	1558.7	3.4 ± 0.2
697.2±0.3	1403.1	1.1 ± 0.1
754.2±0.4	1280.4	1.0 ± 0.08
764.8±0.7	1280.4	0.3 ± 0.1
773.7±0.7	1290.7	0.29± 0.09
853.3±0.3	1558.7	4.0 ± 0.3
962.9±0.3	1280.4	3.0 ± 0.2
1085.3±0.5	1403.1	0.65± 0.05
1241.0±0.3	1558.7	8.2 ± 0.5
Unassigned gamma rays[c]		
337.4±0.4		
418.6±0.4		

continued

Table VI. Continued.

Energy (keV)	Parent Level (keV)	Relative Intensity
439.6±0.4		
441.3±0.6		
553.6±0.7		
578.2±0.6		
664.7±0.4		
670.1±0.6		
692.3±0.5		
726.9±0.5		
748.6±0.5		
811.2±0.5		
845.8±0.7		
1286 ±1.0		
1352 ±1.5		

[+]Normalized to 100 units for each isomer separately.

[a]Photons of E3 transition not observed due to large ICC.

[b]Transition in ^{195}Hg.

[c]All unassigned lines have intensities less than 5% of that of the 599.0-keV transition.

The measurement of the K-ICC of a number of transitions was undertaken using the conversion-coefficient spectrometer described in Section II of this thesis. The measured conversion coefficients are tabulated in Table VII and summarized graphically in Fig. 38.

The decay scheme of ^{195}Hg and ^{195m}Hg as developed from the work of Brunner et al.,[96] and modified by the present work is shown in Fig. 39. In the following discussion we shall describe our interpretation of the spins and parities for the various observed levels shown in Fig. 39.

(a) Ground state. The ground-state spin of ^{195}Au, as well as the spins of the other odd-mass gold isotopes mentioned in this work, has been experimentally measured to be 3/2. The level has been assigned positive parity according to the interpretation of it arising from a hole state in the $d_{3/2}$ shell-model proton orbital.

(b) 61.5-keV level. The M1 + E2 nature of the 61.5-keV transition was determined by Joly et al.[83] from its L-subshell ratio. The corresponding transition in ^{197}Au (77-keV) has been shown to originate from a level of spin 1/2 (corroborated by Mössbauer measurements). In ^{195}Au, the E3-E2 transition sequency joining the 11/2- isomeric level at 318 keV to the 61.5-keV level indicates a spin assignment for the latter level identical to that in the ^{197}Au case.

(c) 241.6-keV level. The multipolarity of the 180-keV transition is the key to the spin assignment for this level. This case is identical to ^{197}Au, where the 191-keV transition multipolarity has been the deciding factor in a 3/2+ assignment for the 268-keV level. Joly et al.[83] have determined an M1 + E2 character for the 180-keV transition, which is in agreement with our findings (as well as theirs) for the ^{197}Au case, and leads to a 3/2+ assignment for the 241.6-keV level.

(d) 261.7-keV level. The E3 transition connecting this level to the 11/2- isomeric state is again sufficient to allow the assignment of 5/2+ for the spin and parity. This assignment is supported by the M1 + E2 transition to ground.

Table VII. Internal conversion coefficients of transitions from ^{195}Hg and ^{195m}Hg decay.

Gamma-ray energy (keV)	K-ICC (exp)	Theory+ E1	E2	M1	Multipolarity
261.6	2.4±0.3(-1)	3.16(-2)	9.0 (-2)	4.0 (-1)	M1+E2
368.1	1.5±0.2(-1)	1.38(-2)	3.95(-2)	1.60(-1)	M1(M1+E2)
386.5	6.9±1.0(-2)	1.23(-2)	3.50(-2)	1.38(-1)	M1+E2
387.4					E2
467.2	8.3±1.2(-2)	8.10(-3)	2.21(-2)	8.25(-2)	M1(M1+E2)
525.4	4.0±0.6(-2)	6.50(-3)	1.75(-2)	6.00(-2)	M1+E2
559.8	3.3±0.4(-2)	5.55(-3)	1.49(-2)	5.00(-2)	M1+E2
575.2	3.1±0.5(-2)	5.30(-3)	1.41(-2)	4.70(-2)	M1+E2
584.5	8.9±1.1(-3)	5.10(-3)	1.35(-2)	4.50(-2)	E1
599.0	2.9±0.4(-2)	4.80(-3)	1.30(-2)	4.20(-2)	M1+E2
679.9	2.3±0.3(-2)	3.75(-3)	9.80(-3)	3.07(-2)	M1+E2
692.3	9.5±1.7(-3)	3.61(-3)	9.40(-3)	2.98(-2)	E2(M1+E2)
697.2	1.9±0.3(-2)	3.58(-3)	9.22(-3)	2.89(-2)	M1+E2
748.6	3.1±0.5(-2)	3.10(-3)	7.90(-3)	2.45(-2)	M1
779.4	1.5±0.2(-2)	2.88(-3)	7.30(-3)	2.21(-2)	M1+E2
821.2	1.2±0.2(-2)	2.62(-3)	6.60(-3)	1.95(-2)	M1+E2
841.4	7.0±1.0(-3)	2.49(-3)	6.22(-3)	1.78(-2)	M1+E2(E2)
931.8	5.8±0.8(-3)	2.08(-3)	5.10(-3)	1.35(-2)	M1+E2(E2)
962.9	1.2±0.2(-2)	1.94(-3)	4.76(-3)	1.25(-2)	M1(M1+E2)
1022.8	4.44±0.7(-3)	1.78(-3)	4.32(-3)	1.07(-2)	E2(M1+E2)
1112.1	5.7±0.7(-3)	1.50(-3)	3.60(-3)	8.50(-3)	M1+E2
1173.2	5.2±0.6(-3)	1.39(-3)	3.30(-3)	7.50(-3)	M1+E2
1241.0	4.0±0.6(-3)	1.25(-3)	2.95(-3)	6.40(-3)	M1+E2

+Theoretical ICC taken from Sliv and Band.

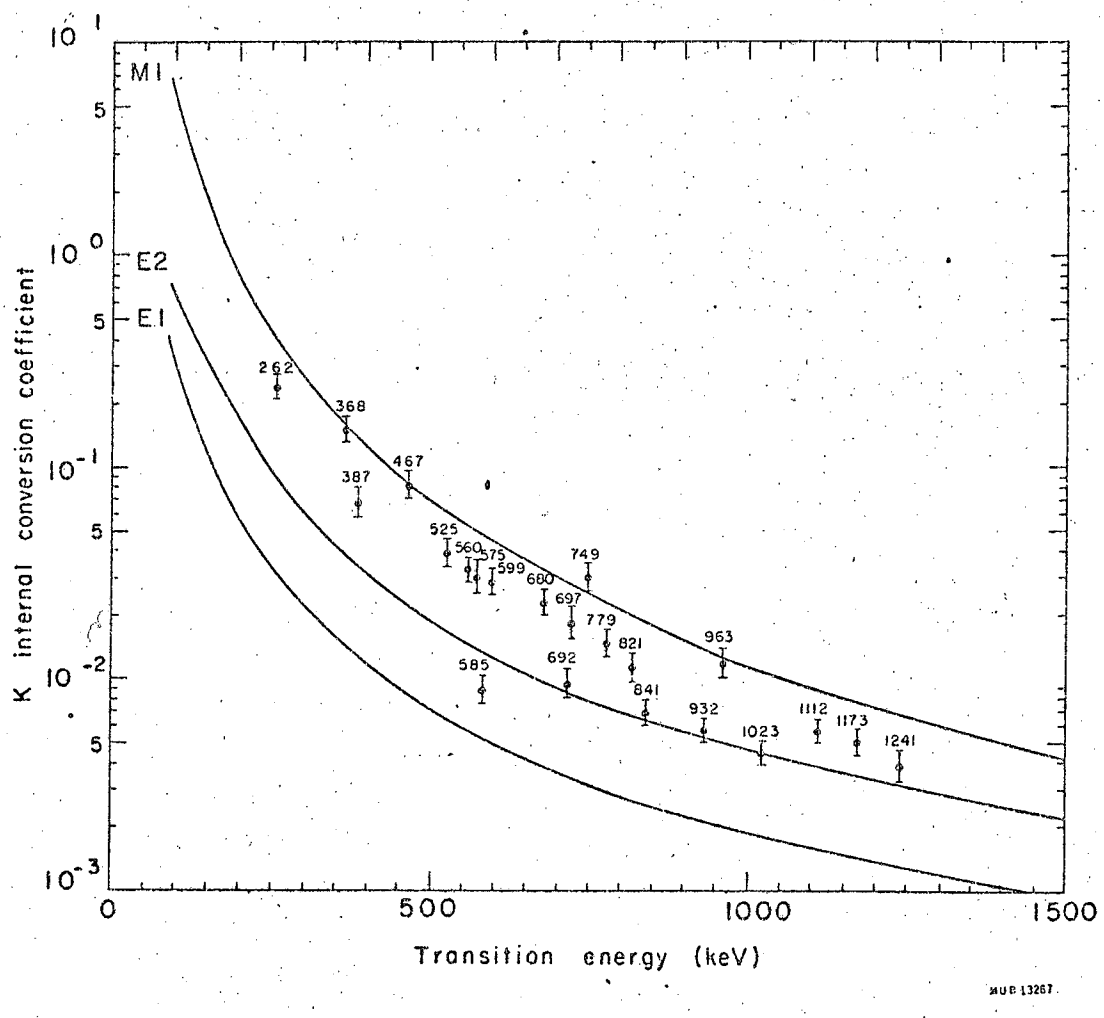

Fig. 38. Internal-conversion coefficients of transitions in the decays of ^{195}Hg and ^{195m}Hg. The solid lines are the theoretical conversion coefficients from Sliv and Band.[114]

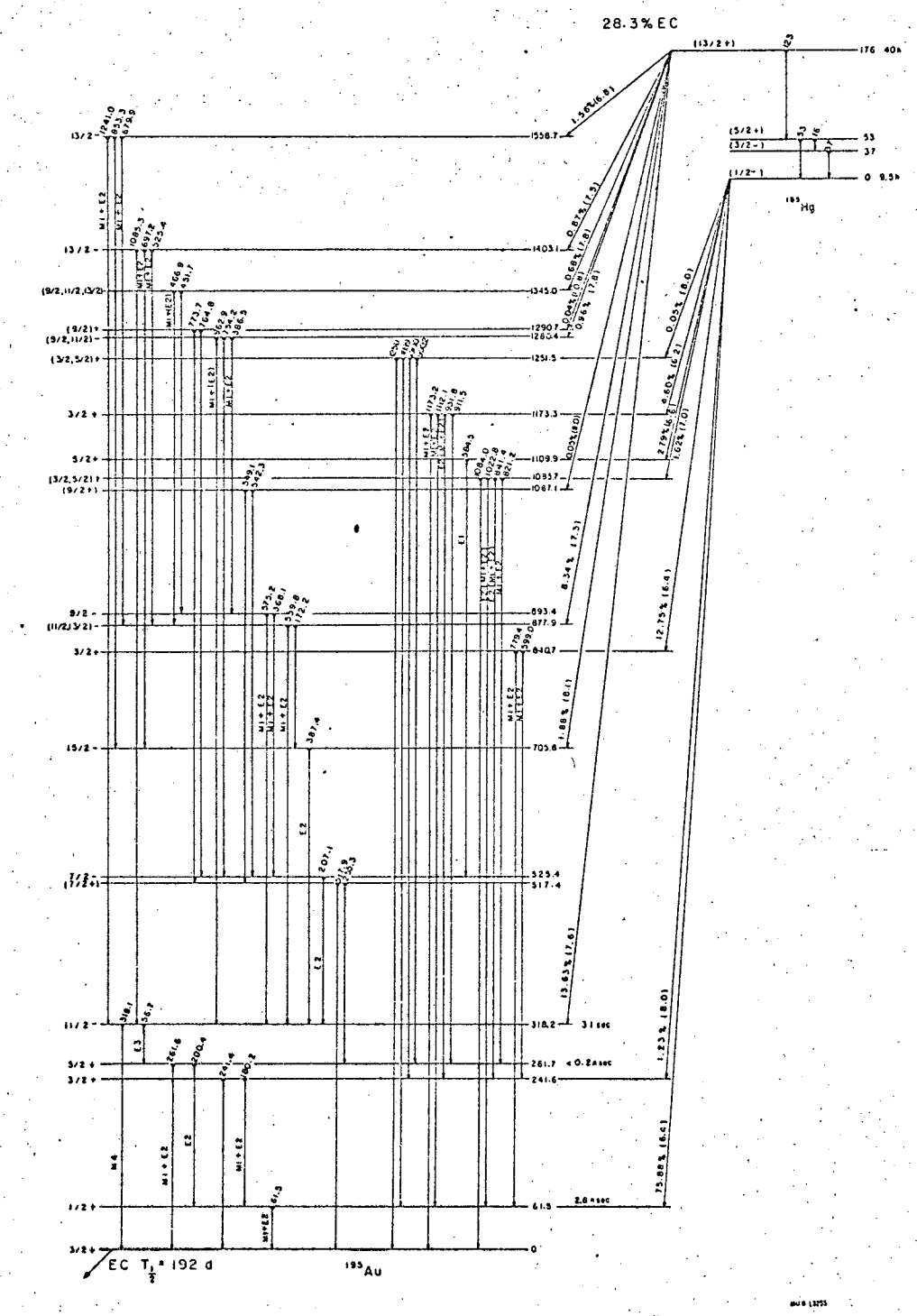

Fig. 39. Decay schemes of ^{195}Hg and ^{195m}Hg. Log ft values for the electron-capture decays are included in parenthesis after the percent EC branching value.

(e) 318.2-keV level. The 30-sec half-life of this level, along with the first-forbidden character of the electron-capture decay to this level from the 13/2+ isomeric state in ^{195}Hg, the appearance of 11/2- levels as excited states in many of the odd-proton nuclides, and the M4 transition to ground serve to indicate a spin and parity of 11/2- for this level.

(f) 517.4-keV level. The transitions we have interpreted as depopulating this level lead to the 5/2+ level and the 3/2+ ground state. A very similar pattern is observed for the depopulation of the 7/2+ level (populated in coulomb excitation studies) in ^{197}Au. Due to the weak nature of the depopulating transitions it is very difficult to undertake either coincidence or internal conversion measurements, however, from our interpretation the 517.9-keV transition should be E2 character and the 255.3 keV transition M1 or M1 + E2.

(g) 525.4-keV level. The spin and parity of this level are seen to be either 7/2- or 15/2- from the E2 character of the 207-keV transition to the 11/2- isomeric state. The population of this level by the 584.5-keV E1 transition which decays from a state of fairly low spin lends support to the interpretation of this level as 7/2-.

(h) 705.8-keV level. The 387.4-keV transition has been shown by Brunner et al.[96] to be E2 character from L- subshell measurements. Since this transition leads to the 11/2- level and the only transitions leading to the 705.8-keV level arise from levels of high spin, a spin and parity of 15/2- is assigned to this level.

(i) 840.7-keV level. The 779.4- and 599.0-keV M1 + E2 transitions depopulating this level lead to states of spin 1/2 and 3/2. An indication was seen in our spectra of a gamma ray having an energy of approximately 579.5-keV which might correspond to the transition from this level to the 5/2+ level at 261.7 keV. While these transitions permit an assignment of either 1/2 or 3/2 for the spin of the 840.7-keV level, the log ft value for electron capture from the 1/2- ^{195}Hg ground state seems to indicate a first-forbidden transition and a probable spin and parity of 3/2+ for the 840.7-keV level.

(j) 877.9-keV level. The M1 + E2 character of the 559.8-keV transition connecting this level with the 11/2- isomeric state, and the 172.2-keV transition to the 15/2- level suggest that the spin and parity of the 877.9-keV level either 11/2- or 13/2-. The absence of a photon corresponding to the 352.5-keV transition from this level to the 7/2- level at 525.4 keV tends to make an assignment of 13/2- somewhat more plausible.

(k) 893.4-keV level. Our determination of the M1 + E2 character of both the 575.2-keV and 368.1-keV transitions to the 11/2- and 7/2- levels respectively, yields an assignment of 9/2- for the 893.4-keV level.

(l) 1067.1-keV level. The 549.1- and 542.3-keV transitions to the 7/2+ and 7/2- levels suggest that the 1067.1-keV level has a spin and parity of 9/2+. The log ft value of 10.8 determined from the gamma-ray relative intensities is in agreement with an EC decay of the type "$\Delta I = 2$, no". Since this electron capture arises from the 13/2+ isomeric level of ^{195}Hg, this observation again indicates a spin and parity of 9/2+ for the 1067.1-keV level.

(m) 1083.7-keV level. We observe four transitions from this level which go to ground (spin 3/2) and the first three excited states (spins 1/2, 3/2, and 5/2). Our measurement of the multipolarity of the 1022.8-keV transition indicates E2 character, thus allowing an assignment of 5/2+ to the 1083.7-keV level. However, the error in the value of this multipolarity is such that significant M1 contribution may be present and the spin and parity for the level in question would be assigned as 3/2+. The log ft value for ^{195}Hg ground-state decay is such that neither assignment can be made with certainty.

(n) 1109.9-keV level. The work of Brunner et al.[96] has established the 584.5-keV as being in coincidence with the 207-keV gamma-ray; half-life measurements have shown that the 584.5-keV gamma decays with a period indicative of population from ^{195}Hg ground state decay; and ICC measurements have shown the 584.5-keV gamma to be E1 in character. Since the 525.4-keV level has been shown to be of spin 7/2, the E1 character of the 584.5-keV gamma leads to a 5/2+ assignment for the 1109.9-keV level. One is forced to be quite skeptical of this assignment due to the seeming very low log ft

value observed for the electron capture decay from ^{195}Hg ground state to this level. Another point against this assignment is the absence of observed transitions to any of the lower-lying 3/2+, 5/2+, or 7/2+ levels.

(o) 1173.3-keV level. We again have observed transitions to the low-lying 3/2+, 1/2+, 3/2+ and 5/2+ levels. The M1 + E2 nature of the 1173.2-, 1112.1-, and the E2 character of the 931.8-keV transition point to a spin assignment of 3/2+ for this level.

(p) 1251-keV level. The weak intensities of the four transitions depopulating this level do not permit measurement of multipolarities, but the decay pattern again points to an assignment of either 3/2+ or 5/2+ for this level. The large log ft value for the electron capture decay to this level from the 1/2- ground state of ^{195}Hg suggests that a spin of 5/2 may be quite probable.

(q) 1280.4-keV level. We observe transitions from this level to lower-lying levels of spin 9/2-, 7/2-, and 11/2-. This indicates possible assignments of 9/2- or 11/2- for this state. While the M1 or M1 + E2 nature of the transitions to the 9/2- and 11/2- levels are consistant with either of the above assignments, the multipolarity of the 754.2-keV transition to the 7/2- level at 525.4-keV is needed to decide between the two possible spin assignments.

(r) 1290.7-keV level. This level seems analogous to the level at 1067.1 keV. The two weak transitions populating both the 7/2+ and 7/2- levels at 517.4 and 525.4 keV as well as the characteristic log ft value indicate that this level may also be assigned a spin and parity of 9/2+.

(s) 1345.0-keV level. The two transitions depopulating this level lead to levels of spin 9/2- and 11/2-. Since we were only able to measure the K-ICC of the 466.9-keV transition leading to the (11/2,13/2)- level (M1 or M1 + E2 in character), we are unable to make a definite spin assignment for this level. The spins of 9/2, 11/2, or 13/2 with negative parity are possible for this level with the latter two more probable as seen from the log ft value from ^{195}Hg electron-capture decay.

(t) 1403.1-keV level. Those transitions depopulating this level lead to states of spin 11/2, 15/2, and either 11/2 or 13/2 (all with negative parity). The M1 + E2 character of the 697.2-keV transition to the 15/2- level at 705.8 keV seems to indicate that 13/2- is the best assignment for this level.

(u) 1557.8-keV level. The decay pattern of this transition is quite similar to that of the last discussed level at 1403.1 keV. In this case, however, it is the multipolarity of the 853.3-keV transition to the 15/2- level at 705.8 keV which has not been measured. The log ft value observed for electron capture from the 13/2+ level is ^{195}Hg is quite low (lowest of all observed electron-capture decays from ^{195m}Hg). This lends great support for the assignment of 13/2- as the spin and parity for the 1557.8-keV level.

4. ^{193}Au

The early work by Gillon et al.[91] and Brunner et al.[92-96] served to indicate how very similar the decays of ^{193}Hg and ^{193m}Hg were to the ^{195}Hg isomers. These measurements used double-focussing spectrometers to examine the conversion-electron spectra at high resolution. A high-resolution instrument is particularly necessary in the study of the ^{193}Hg isomers due to the very complex spectrum arising both from the numerous transitions in the mercury decay and from the large number of transitions in the decay of the radioactive daughter ^{193}Au. The decay of ^{193}Au has been shown by Ewan[98] to lead to some 25 transitions having energies between 0 and 500-keV. The work by Brunner et al.[96] led to the establishment of some 50 transitions in ^{193}Au with the observation of an additional 100 unassigned weak conversion electron lines.

We have produced ^{193}Hg and ^{193m}Hg by the bombardment of gold foils with 50-MeV deuterons. The gamma-ray spectra were taken with a Ge(Li) detector of high resolution. A series of timed spectra was taken in order to determine half lives for some of the photopeaks. Pairs of these spectra taken approximately 12 h apart are shown in Figs. 40 and 41. These cover

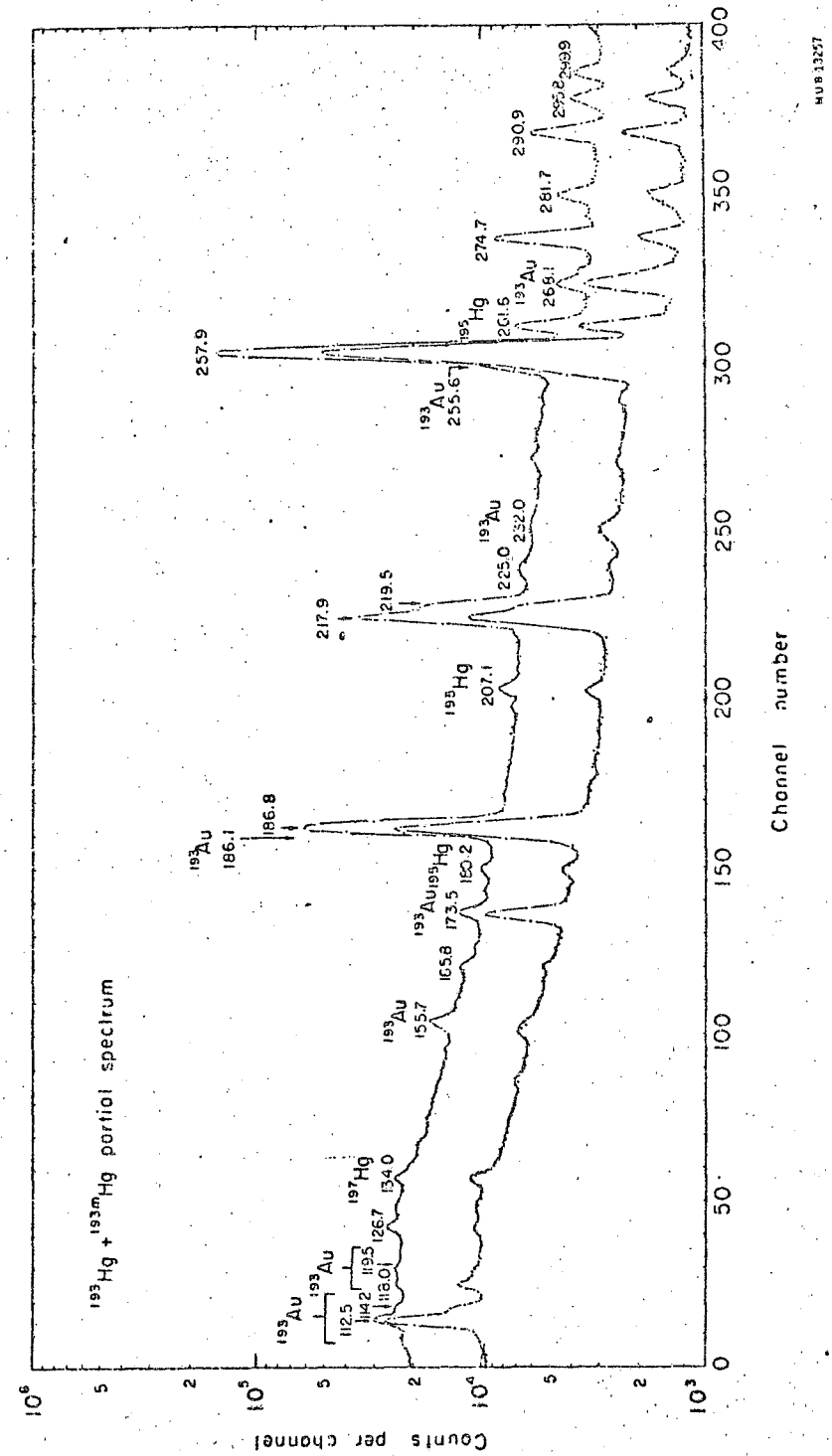

Fig. 40. Gamma-ray spectrum of ^{193}Hg and ^{193m}Hg in the energy region 110-300 keV. Lower spectrum was recorded approximately 12 h after the upper.

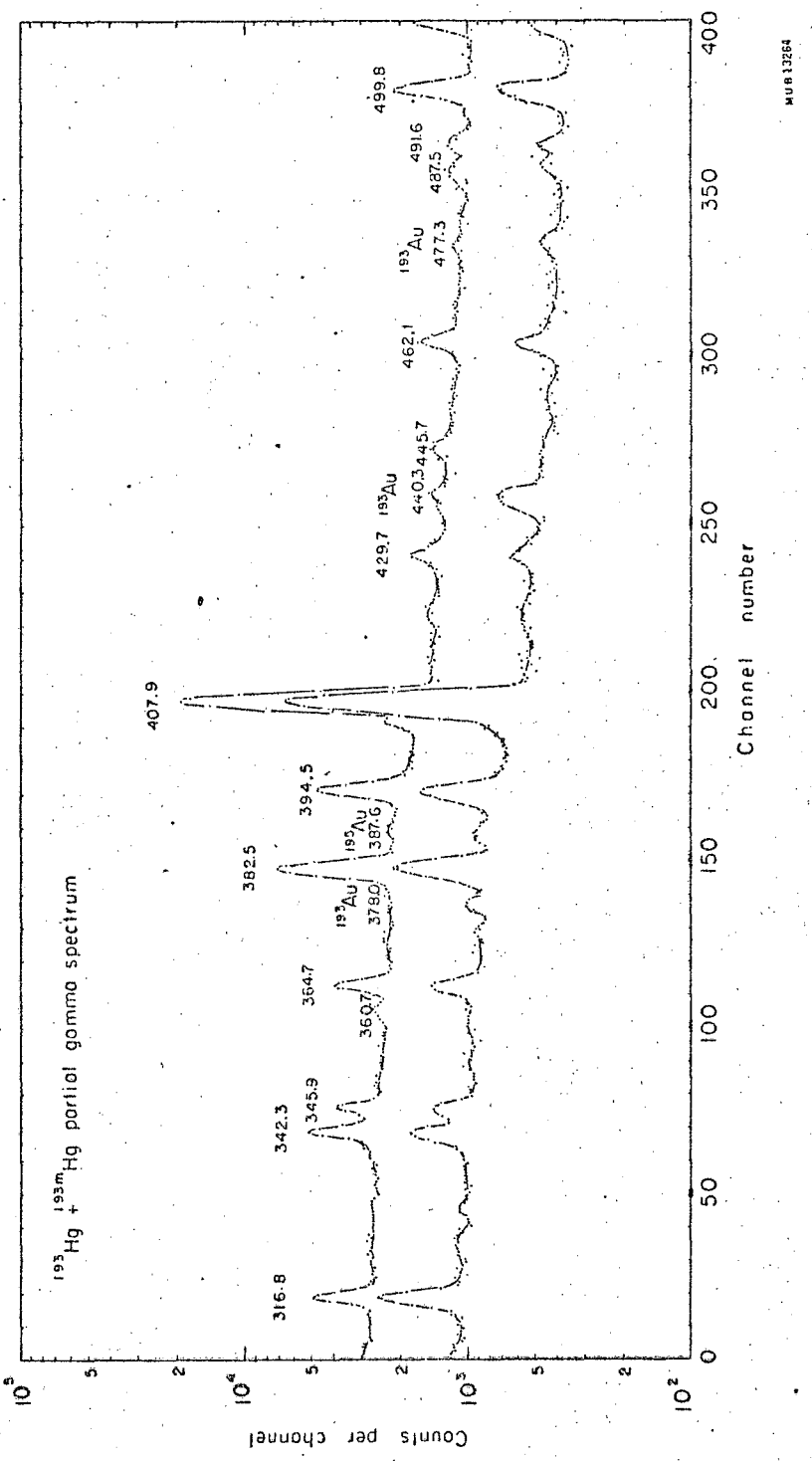

Fig. 41. Gamma-ray spectrum of ^{193}Hg and ^{193m}Hg sample in the energy region 300-510 keV. The lower spectrum was recorded approximately 12 h after the upper.

the energy region of 100-500 keV. From these and similar spectra the half life of ^{193m}Hg was determined to be approximately 11 h which is in good agreement with the values determined by both Gillon et al.[91] and Brunner et al.[96] Our observed half life for those transitions arising from ^{193}Hg positron and electron-capture decay is 3 h which is a factor of two less than the value measured by Gillon et al. (6 h). This may well be the reason no conversion lines of energy > 500 keV could be assigned to ^{193}Hg ground state decay by Brunner et al.[96] In their studies all measurements of conversion lines having energies greater than the above value were not undertaken until approximately 10 h after bombardment. Recent measurements by Kaufman[97] support this shorter value for the half life of ^{193}Hg.

Our primary goal in examining the gamma-ray spectrum of ^{193}Hg and ^{193m}Hg was the measurement of the relative intensities for the gamma rays depopulating those low-lying levels which might be interpretable as members of the "core multiplet". In Fig. 42 we show the low-lying levels of ^{193}Au as determined by Brunner et al.[96] The complete analogy to the levels of ^{195}Au is quite obvious. We have utilized our gamma-ray energy measurements to assign energies to those levels below the 890-keV level. Our energy and intensity values for the transitions of interest below 800 keV are shown in Table VIII.

Utilizing our gamma-ray relative intensity values and the relative conversion-electron intensity values from Brunner et al., we may calculate K-ICC values for many of the transitions of interest. To derive the ICC values of those transitions populated only from ^{193m}Hg decay, we normalize the two sets of data by means of the 407-keV E2 theoretical K-ICC. This transition has been shown by Brunner et al. to have an E2 multipolarity from L-subshell line intensities. For those transitions which have a compound decay (11 h + 3 h) we normalize the intensity data from the intensities of the 218 + 219.7 peaks. These have both been shown to be of E2 character. The derived ICC are displayed in Table IX along with the assigned multipolarities. These multipolarities have been used in the assignment of spins and parities to the low-lying levels of ^{193}Au as shown in Fig. 42.

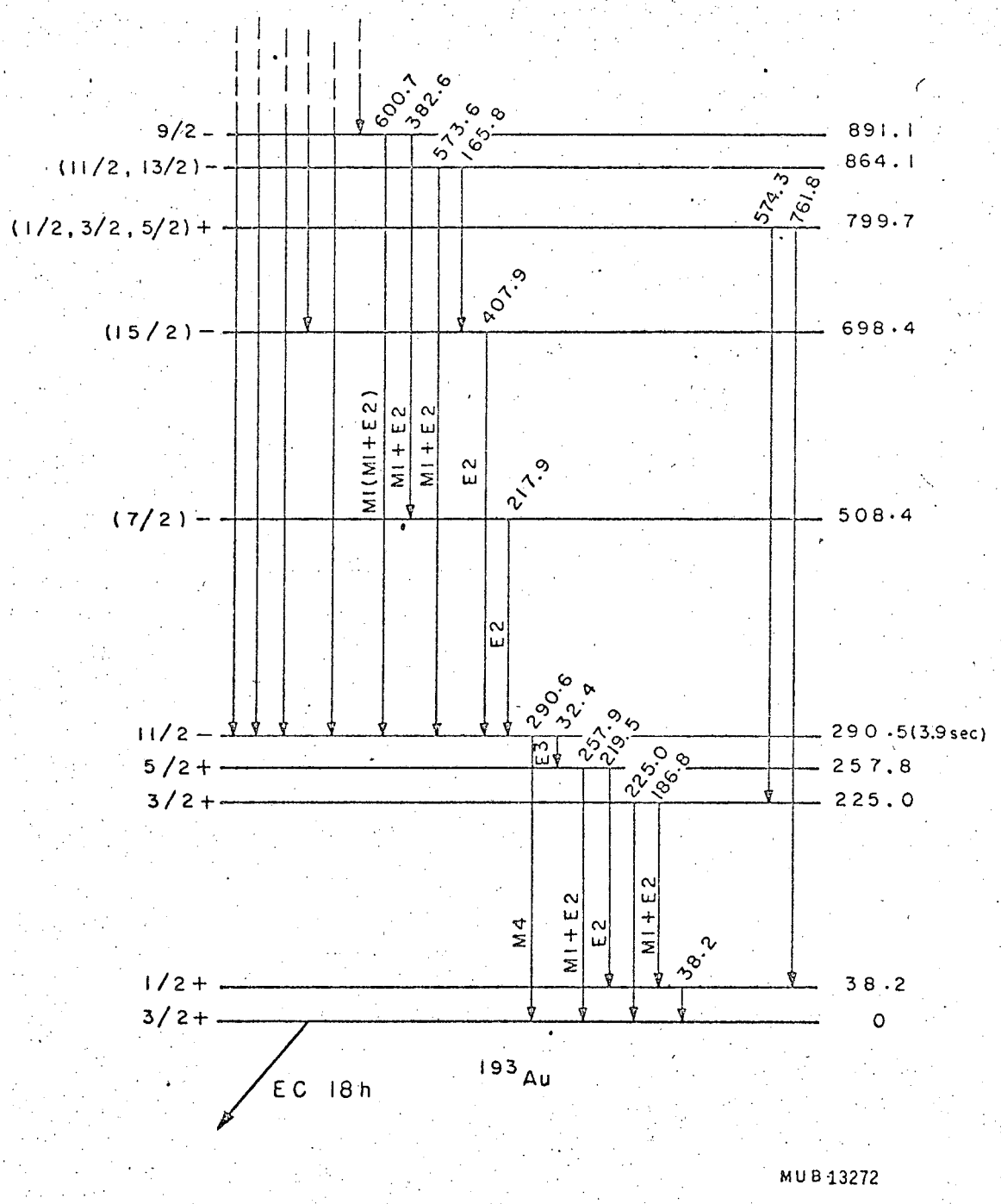

Fig. 42. Portion of ^{193}Au level scheme below 900 keV.

Table VIII. Some photons from ^{193}Hg and ^{193m}Hg decay.

Energy (keV)	Relative intensity
38.2±0.3	2.31±0.15
165.8±0.3	0.40±0.05
186.8±0.2	20.5 ±1.5[a]
217.9±0.4	17.0 ±1.2
219.5±0.4	7.9 ±0.6
225.0±0.3	1.0 ±0.1
257.9±0.2	144 ±8
290.9±0.3	4.8 ±0.3
381.8	16.2 ±0.9
382.6±0.3	
407.9±0.2	60 ±3
573.6±0.3	100[+]
600.7±0.4	7.1 ±0.4

[+]Normalized to 100 units.

[a]Corrected for contribution from $^{193}Au \rightarrow {}^{193}Pt$ 186.1-keV gamma ray.

Table IX. Conversion coefficients of transitions observed in the decay of ^{193}Hg + ^{193m}Hg.

Energy	K-ICC	E1	E2	M1	Multipolarity
217.9	1.36(-1)+		1.36(-1)		E2
219.5					E2
257.9	3.76(-1)	3.2 (-2)	9.0 (-2)	4.19(-1)	M1+E2
381.8	6.34(-2)	1.27(-2)	3.55(-2)	1.41(-1)	M1+E2
382.6					
407.9	3.0 (-2)+		3.0 (-2)		E2
573.6	1.4 (-2)	5.45(-3)	1.39(-2)	5.08(-2)	E2(M1+E2)
600.7	2.1 (-2)	4.98(-3)	1.26(-2)	4.57(-2)	M1+E2

+Determined to be E2 transitions by Brunner et al.[96]

Of particular importance in our measurements was the observation of the 224.9-keV gamma-ray which may be interpreted as the transition between the first excited 3/2+ level at 225 keV and ground. Thus, for the transitions within the "core multiplet" of ^{193}Au, our work leaves still either unobserved or uninterpreted the transitions from the 7/2+ level. A number of possible pairs of transitions which appeared as though they might populate both the 225-keV and ground states were examined, but none of the pairs differed by the proper energy.

D. Comparison of Experiment and Theory

1. Energy levels

The comparison of experiment and theory is of prime importance in judging the relative merits of those theoretical treatments suggested for the gold region. Perhaps the easiest comparison to be made is that between the theoretically predicted and experimentally observed ordering of the energy levels. The variation in energy of the experimentally observed low-lying levels of the odd-mass gold isotopes with increasing neutron number is shown in Fig. 43. The regularity of the level motion shown by these gold isotopes is quite remarkable. Particular points to notice in this figure are the decreasing energy of the 1/2+ level after the addition of the 118th neutron, the crossing of the 3/2+ and 5/2+ levels at approximately the same nuetron number, and the decreasing energy of the 7/2+ level (if our interpretation is correct) again beyond 118 neutrons.

The core excitation model of de-Shalit,[56] while not capable of a detailed prediction of the gold excited levels, does predict the existence of the low-lying 1/2, 3/2, 5/2, and 7/2 levels of positive parity arising from the coupling of the odd $d_{3/2}$ proton to the 2+ excited state of the even-even core. These levels are observed in the odd-mass gold isotopes, but the interpretation of their arising from strict particle-core coupling is open to question. According to the core excitation model, the "center of gravity" of the multiplet should fall at an energy equal to that of the 2+ excited state of the nucleus corresponding to the even-even core. In the

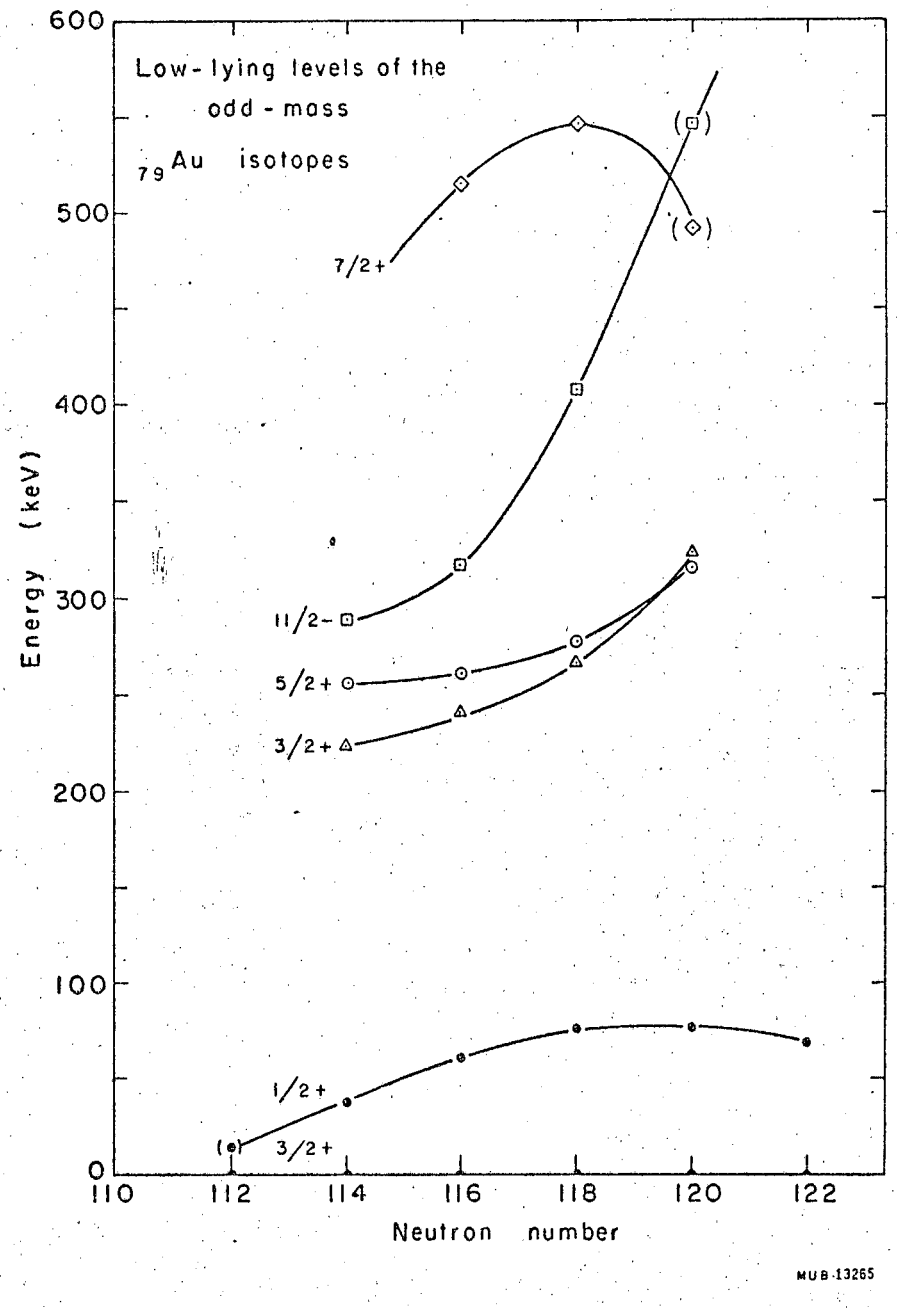

Fig. 43. Variation of the energies low-lying levels of the odd-mass Au isotopes with changing neutron number.

case of the odd-mass gold isotopes, the even-even core has been assumed to be represented by the platinum isotope having an equal number of neutrons. In Fig. 44 we show the trend of the multiplet center of gravity energy with increasing neutron number. It is seen that while the center of gravity does follow the same trend as the 2+ level of the Pt core for neutron numbers 116 and 118, it tends to decrease after 118 nuetrons (if our assignment for the 7/2+ state in ^{199}Au is correct). For all cases, however, it is observed that a weak monopole-monopole interaction term must be included in the deShalit model if either the even-mass Pt or Hg isotopes are taken as the core. It is particularly interesting to note the near coincidence of the center of gravity for the multiplet in ^{199}Au (again if our assignment of the 7/2+ level is correct) with the anomalously low 2+ level in ^{200}Hg.

If the actual situation in the odd-mass gold nuclei is described well by the de-Shalit model, we would expect few major changes in the multiplet level structure with changing neutron number. Those that would occur, should arise from (1) variation of the energy required to excite the 2+ core state, and (2) changes in the contribution from admixed single particle states. These changes would be expected to be quite regular as the neutron number is varied. In Figs. 45 and 46 we show the low-lying levels of the odd-mass thallium and copper isotopes. These nuclides have also been discussed in terms of the core-excitation model of de-Shalit.[56,99] The 3/2+ and 5/2+ levels of the odd-mass thallium isotopes have been described[56] as arising from the coupling of the odd proton in the $3s_{1/2}$ single-particle orbital to a 2+ excited state of the even-even mercury core. Due to the presence of only two "core-excited" levels in this case, there are insufficient data to undertake an extensive treatment of the levels. However, if the "core-excitation" model holds we would still expect some admixture of $d_{3/2}$ and $d_{5/2}$ to these levels, and perhaps any distinctive pattern arising from these admixtures could also be observed in the gold isotopes. As is seen in Fig. 45 the 3/2+ level in Tl increases very smoothly in energy as the neutron number is decreased. The 5/2+ level increases in an almost identical manner with the exception of the dip between

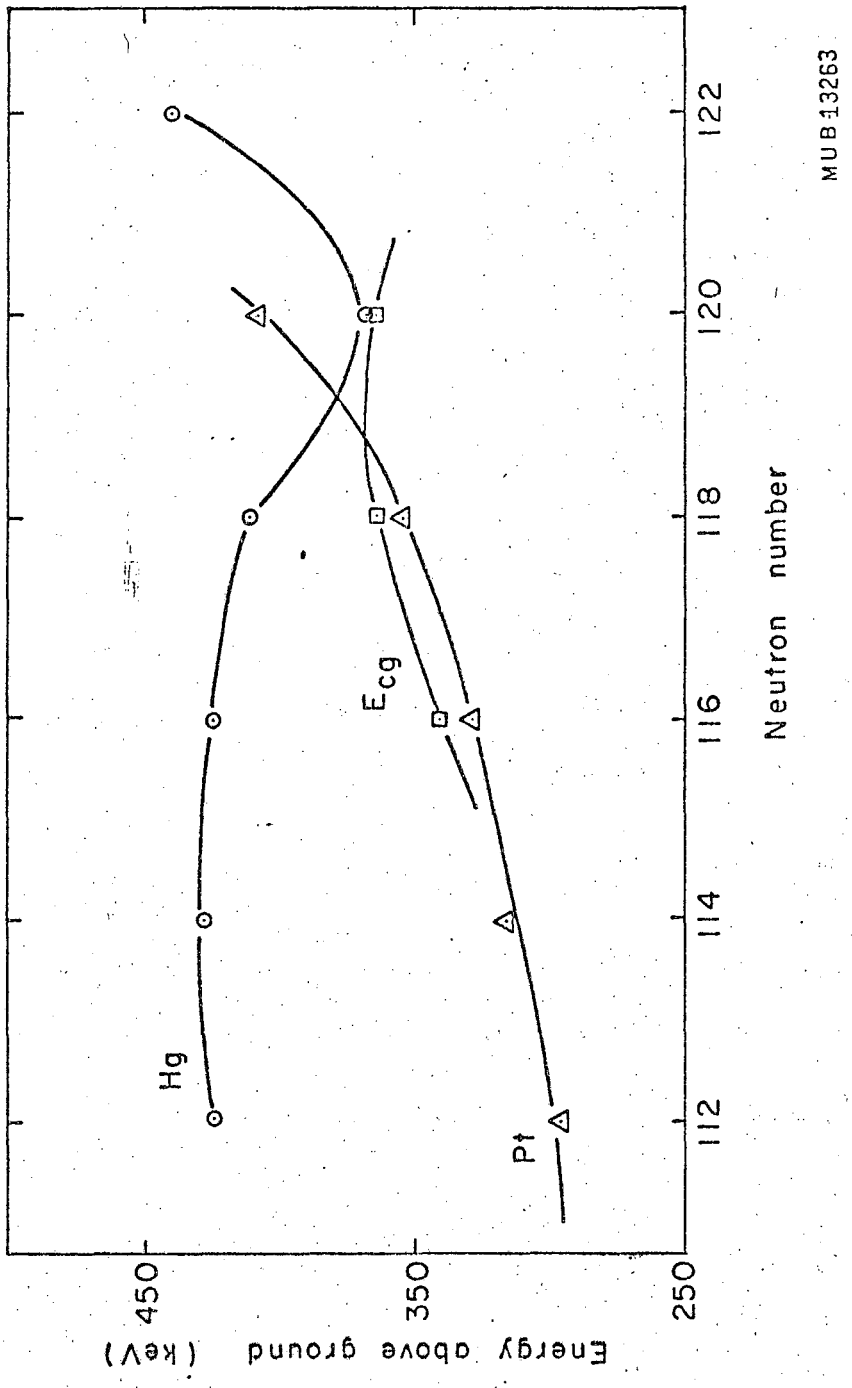

Fig. 44. Variation of the energy of the "core multiplet" center of gravity as a function of neutron number. Also shown are energies of the first 2+ excited states in both the Pt and Hg isotopes.

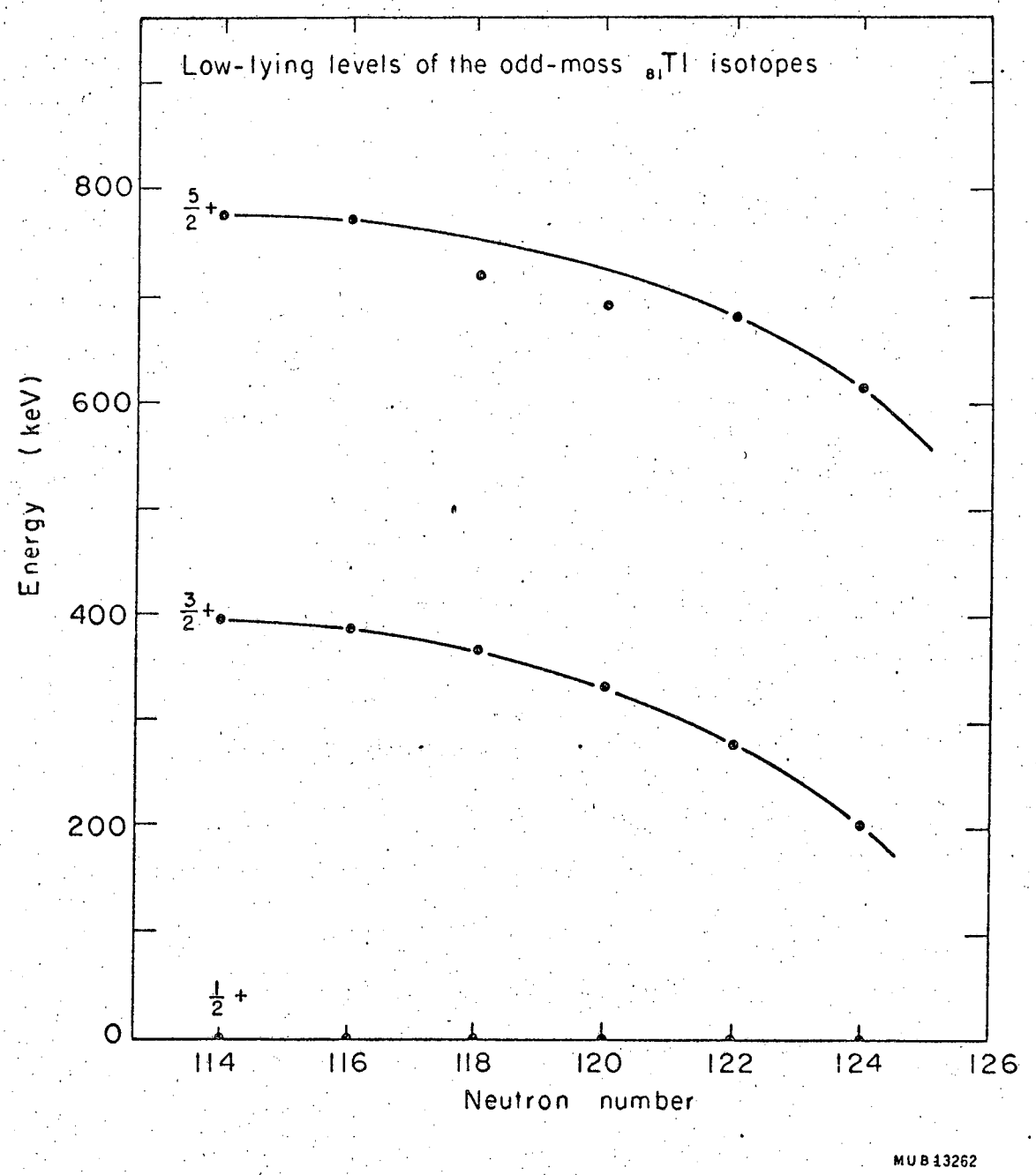

Fig. 45. Variation of the energies of the low-lying levels of the odd-mass Tl isotopes as a function of neutron number.

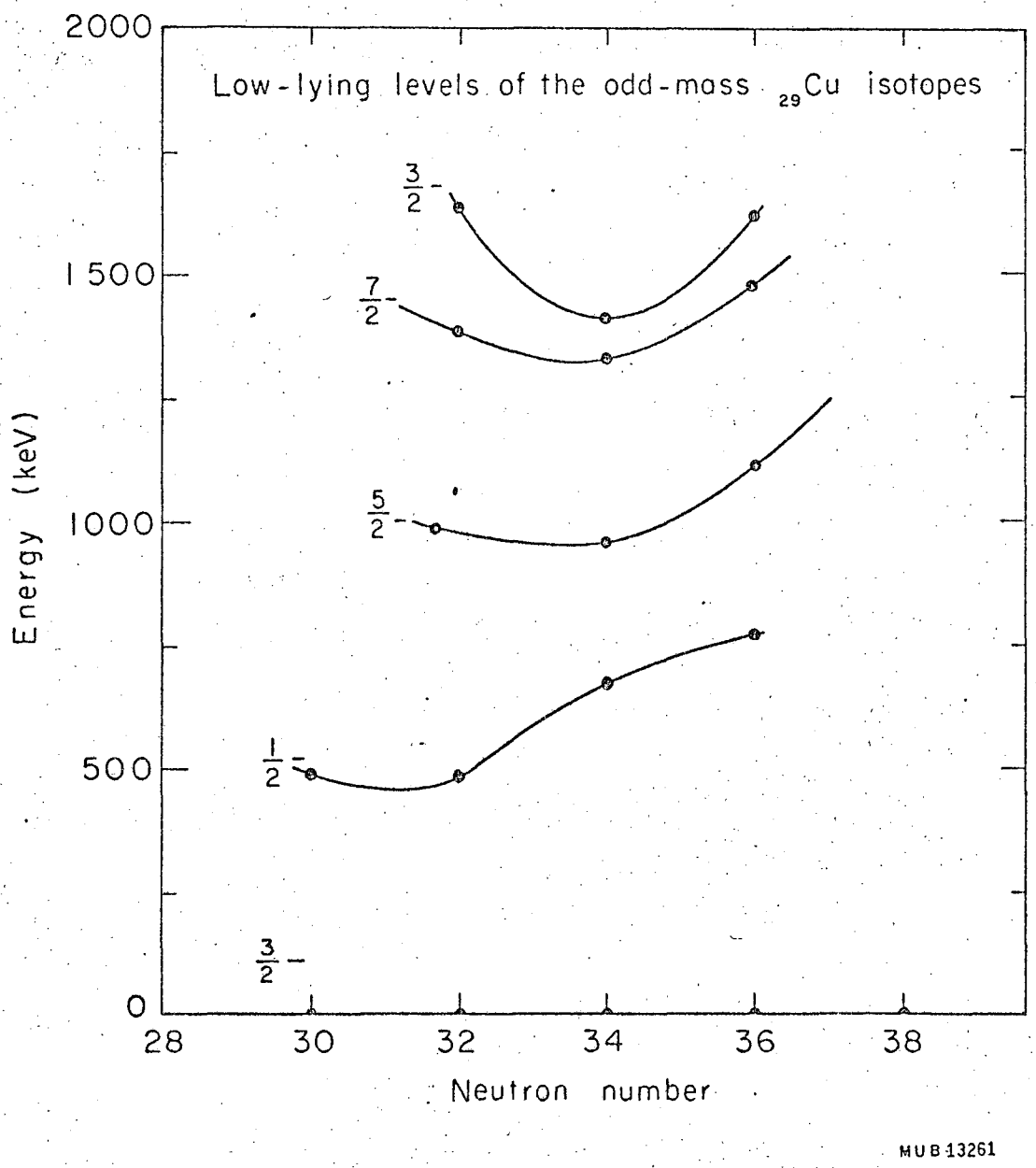

Fig. 46. Variation in the energy of the low-lying levels of the odd-mass Cu isotopes as a function of neutron number.

neutron numbers 118 and 120. This dip seems to correspond to a similar reduction in the energy of the 2+ excited state of ^{200}Hg (having 118 neutrons). The low-lying levels of the odd-mass Cu isotopes, discussed by Thankappan and True[99] in terms of the coupling of a $2p_{3/2}$ proton to the 2+ excited state of the even-even nickel core, are shown in Fig. 46. While the 5/2-, 7/2-, and 3/2- levels follow the same general pattern (minimum energy at 34 neutrons and increasing values for either addition or subtraction of enutrons), the 1/2- level acts quite differently. It has been shown by Blair[100] through (^{3}He,d) experiments, that the 1/2- level has approximately 70% $p_{1/2}$ single-particle admixture. Since the other states of the proposed multiplet have been shown to have 40% or less single-particle admixture, we might expect a fairly significant difference in the action of the 1/2- level with increasing neutron number.

The general energy trends of the odd-mass gold levels with changing neutron number, then, seem to indicate significant admixtures of single particle levels to the wave functions for these states. The treatments of ^{197}Au by both de-Shalit[101] and McKinley and Rinard[59] have treated the 3/2+ excited state as the only one of the core multiplet which contains single-particle admixed components. In these two treatments, the amount of $d_{3/2}$ single-particle admixture which gives the best fit to the total data is approximately 4-15%. It is difficult to believe that under the assumption of such a small amount of single-particle admixute, the addition or removal of two neutrons from the core would cause the level changes shown in Fig. 43. We must conclude that although the model de-Shalit does indicate the importance of phonon-particle coupling in the odd-mass gold isotopes, it does not allow us to predict the variance of the low-lying gold isotopes with changes in neutron number. In particular, since no description of the nature of the core 2+ excited state is given in this model, the changes which occur between 118 and 120 neutrons cannot be explained.

The work of Kisslinger and Sorensen[61] has included a treatment of the 2+ phonon states of the even-even spherical nuclei in the Hg-Pt region as well as a treatment of the low-lying levels of the odd-mass gold isotopes.

In general, for the gold isotopes, they find the ground 3/2+ level and the first excited 1/2+ level to be predominantly single-particle in nature. They do, however, calculate approximately 15% and 5% $d_{3/2}$ + phonon admixtures for these levels respectively. While they do not discuss the components of the second 3/2+ state, the lowest-lying 5/2+ level is found to have approximately 76% $d_{3/2}$ + phonon character. The low-lying levels vary little with respect to each other as the neutron number changes in this teatment. The general character of the levels does become more photon dependent as the neutron number decreases. A comparison of the level ordering predicted by the Kisslinger and Sorensen treatment for ^{197}Au and that ordering observed in ^{195}Au is shown in Fig. 47. The levels of ^{195}Au were chosen for comparison both because of the large number populated in the radioactive decay of ^{195}Hg and ^{195m}Hg and the fact that little change in ordering is expected between ^{197}Au and ^{195}Au. The group of levels falling at 300-500 keV in the Kisslinger and Sorensen prediction arise primarily from particle-phonon coupled admixtures. It seems, as stated by the authors, that in an increase in the strength of the quadrupole interaction taken for these calculations would yield a significantly better fit to the experimental data by causing a lowering of these levels.

The predictions of Kisslinger and Sorensen for the 2+ excited states of the even-even Pt and Hg isotopes are quite good. The low energies of these states are predicted and a change in the trend of energy vs. neutron number for the Hg isotopes is predicted at 118 neutrons. This particular point will be discussed later.

Also shown in Fig. 47 is the level scheme predicted by Ialongo[66] for ^{197}Au. This particular ordering of the positive parity levels was the result of a calculation taking into account the $s_{1/2}$ and $d_{3/2}$ single-hole states and up to two phonons of neutron core excitation. While the actual energetic fit to the experimentally observed levels is only fair, the ordering of the levels is quite good. For all values of the strength parameter for the hole-phonon interaction, the 5/2+ level is predicted to lie lower in energy than the first 3/2+ excited state. This situation has been

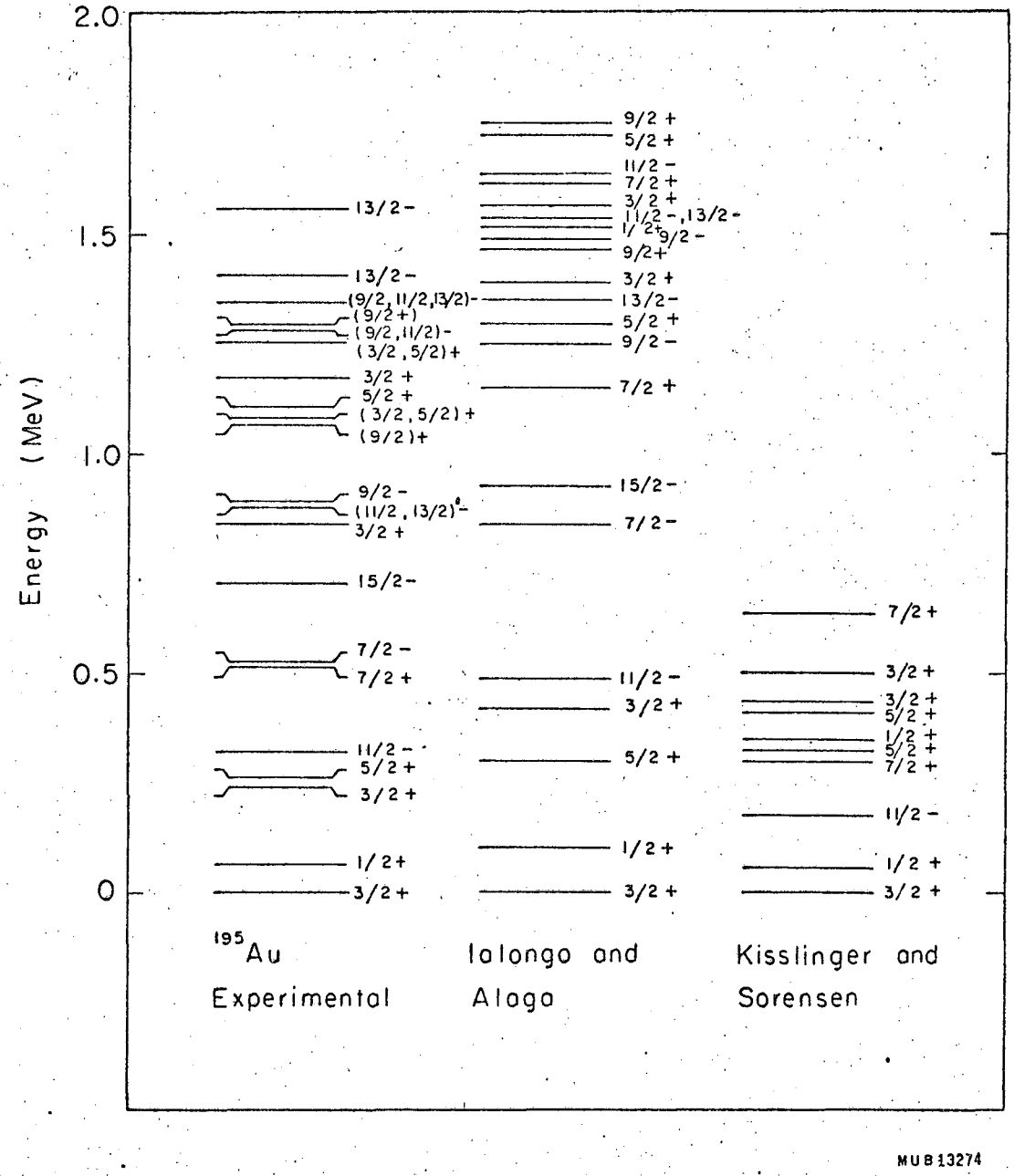

Fig. 47. Theoretical predictions of the level ordering of ^{197}Au from the treatments of Alaga and Ialongo[65,66] and Kisslinger and Sorensen.[61] The observed levels of ^{195}Au are shown for comparison.

observed in the case of ^{199}Au, but not for the more neutron deficient gold isotopes. The lowest-lying negative parity levels are predicted quite well by taking into account $h_{11/2}^{+}$ phonon wave functions.

While the wave functions for the low-lying states are fairly complex, we shall indicate in Table X the major (> 5%) admixed components to the total eigenfunctions. The unperturbed functions are written in the form $|(j_1 j_2)_{J_{12}} j_3, J; NR\rangle$. The importance of seniority-three components is quite apparent.

All of the above treatments have emphasized the role played by the phonon states of the excited core in the determination of level ordering in the odd-mass gold isotopes. We have noted a significant change in the trends of the low-lying excited states of both the gold and the even-even mercury isotopes as we increase the neutron number beyond 118. These changes may indicate a change either in the character of the core phonon or in the interaction between phonon and particle. If we assume that pairs of neutrons fill the $i_{13/2}$, $p_{3/2}$, $f_{5/2}$, and $p_{1/2}$ orbitals in order as the magic number of 126 neutrons is approached, 118 neutrons correspond to the complete filling of the $i_{13/2}$ and $p_{3/2}$ orbitals. A 2+ excitation of this core would most likely be attained by promotion of two neutrons into the $f_{5/2}$ orbital and their subsequent coupling to a spin of 2. No work has yet been undertaken to examine the difference in interaction between the odd proton of Au or Tl and the neutron phonons predominantly formed from $p_{3/2}$ or $f_{5/2}$ quasi-particles.

Since the de-Shalit model depends in no way upon the manner in which the core phonons are created, we would expect it to be incapable of predicting the fine-structure effect we have observed here. Thus, even though the de-Shalit model may fit the observed energies of the low-lying levels of ^{197}Au quite well, it is much too inflexible to predict the different variation of each level with changing neutron number. The more sophisticated treatment by Alaga and Ialongo, on the other hand, would appear to be a more realistic approach to energy level predictions in the transition region. However, since this treatment is still only semi-microscopic in nature, we

Table X. Major components of wave functions for low-lying levels of ^{197}Au from theoretical treatment by Ialongo.[66]

$\|3/2_1^+\rangle$	46.6%	$\|(s_{1/2}^{-2})_0 \quad d_{3/2}^{-1}, \quad 3/2;0\ 0\rangle$
	18.9%	$\|(d_{3/2}^{-2})_2 \quad s_{1/2}^{-1}, \quad 5/2;1\ 2\rangle$
	11.3%	$\|(s_{1/2}^{-2})_0 \quad d_{3/2}^{-1}, \quad 3/2;1\ 2\rangle$
	6.2%	$\|(d_{3/2}^{-3})_{3/2};0\ 0\rangle$
$\|1/2^+\rangle$	52.6%	$\|(d_{3/2}^{-2})_0 \quad s_{1/2}^{-1}, \quad 1/2;0\ 0\rangle$
	14.9%	$\|(d_{3/2}^{-2})_2 \quad s_{1/2}^{-1}, \quad 5/2;1\ 2\rangle$
	10.0%	$\|(d_{3/2}^{-2})_2 \quad s_{1/2}^{-1}, \quad 3/2;1\ 2\rangle$
	9.7%	$\|(s_{1/2}^{-2})_0 \quad d_{3/2}^{-1}, \quad 3/2;1\ 2\rangle$
$\|5/2^+\rangle$	38.4%	$\|(d_{3/2}^{-2})_2 \quad s_{1/2}^{-1}, \quad 5/2;0\ 0\rangle$
	25.6%	$\|(s_{1/2}^{-2})_0 \quad d_{3/2}^{-1}, \quad 3/2;1\ 2\rangle$
	12.3%	$\|(d_{3/2}^{-3})_{3/2};1\ 2\rangle$
	9.5%	$\|(d_{3/2}^{-2})_0 \quad s_{1/2}^{-1}, \quad 1/2;1\ 2\rangle$
$\|3/2_2^+\rangle$	22.5%	$\|(d_{3/2}^{-3})_{3/2};0\ 0\rangle$
	19.7%	$\|(d_{3/2}^{-2})_0 \quad s_{1/2}^{-1}, \quad 1/2;1\ 2\rangle$
	16.4%	$\|(d_{3/2}^{-1})_2 \quad s_{1/2}^{-1}, \quad 3/2;0\ 0\rangle$

continued

Table X. Continued.

$\|3/2_2^+\rangle$	11.6%	$\|(d_{3/2}^{-3})_{3/2};1\ 2\rangle$
	7.6%	$\|(d_{3/2}^{-2})_2\ \ s_{1/2}^{-1},\ \ 5/2;2\ 4\rangle$
	7.3%	$\|(d_{3/2}^{-2})_2\ \ s_{1/2}^{-1},\ \ 5/2;1\ 2\rangle$
	6.8%	$\|(s_{1/2}^{-2})_0\ \ d_{3/2}^{-1},\ \ 3/2;1\ 2\rangle$
$\|7/2^+\rangle$	59.4%	$\|(s_{1/2}^{-2})_0\ \ d_{3/2}^{-1},\ \ 3/2;1\ 2\rangle$
	10.2%	$\|(s_{1/2}^{-2})_0\ \ d_{3/2}^{-1},\ \ 3/2;2\ 4\rangle$
	8.3%	$\|(d_{3/2}^{-2})_2\ \ s_{1/2}^{-1},\ \ 5/2;2\ 4\rangle$
	5.4%	$\|(d_{3/2}^{-2})_2\ \ s_{1/2}^{-1},\ \ 5/2;2\ 2\rangle$
	5.4%	$\|(d_{3/2}^{-3})_{3/2};1\ 2\rangle$

would not expect close agreement with the changes observed upon the addition of the 119th and 120th neutrons.

2. Transition Probabilities

The various photon transition probabilities observed in the odd-mass gold isotopes offer further tests of theory. We again shall examine primarily the low-lying levels, paying particular attention to those transitions which connect members of the de-Shalit "core excitation" multiplet to ground or to other multiplet members. The relative photon intensity measurements made possible through the use of Ge(Li) detectors have permitted the measurement of relative transitions probabilities in cases where the lifetimes of the states have not been measured.

The first-excited states (1/2+) of the gold isotopes of mass 193, 195, and 197 have been shown to decay to the 3/2+ ground state by transitions of mixed M1 + E2 character. Since both the half-lives and mixing ratios of these transitions have been measured,[102-106] it is possible to calculate both the magnetic-dipole and electric-quadrupole reduced-transition probabilities (B(M1) and B(E2)) for all three cases. These transition probabilities along with the factors showing the hindrance or enhancement of the transition when compared to the single-particle estimate calculated from the formulas given by Moszkowski[107] (except that a nuclear radius of $1.2 \times A^{1/3}$ fm is used instead of $1.45 \times A^{1/3}$ fm) are displayed in Table XI. In Table XII we show the other reduced-transition probabilities which have been determined for the other levels of ^{197}Au. Some of these values have been determined from Coulomb excitation studies. For all of the odd-mass gold isotopes we have studied, the lowest-lying excited 3/2+ level decays by a strong M1(M1 + E2) transition to the 1/2+ level and a weaker M1 + E2 transition to the ground state. Neither the half lives nor the mixing ratios of these transitions have been well measured. For this reason we have plotted in Fig. 48 as a function of neutron number, the ratio of the intensity of the gamma ray to ground to the intensity of the gamma ray to the 1/2+ level weighted inversely as the third-power of the energy ratio. If both transitions were pure M1 in character or had constant E2 admixture,

Table XI. Transition probabilities for 1/2+ → 3/2+ transitions in odd-mass Au isotopes.

Isotope	E_γ (keV)	$T_{1/2}$[a] (nsec)	δ^2	α_T[b]	B(M1) ($e^2 x10^{-24}$ cm^2)	$\frac{B(M1)}{B(M1)_{sp}}$	B(E2) ($e^2 x10^{-48}$ cm^4)	$\frac{B(E2)}{B(E2)_{sp}}$
^{193}Au	38.2	2.9±0.4	0.16	96	$9.10x10^{-3}$	$1.37x10^{-3}$	0.333	48.5
^{195}Au	61.5	2.8±0.3	0.17	12	$1.65x10^{-2}$	$2.48x10^{-3}$	0.258	37.4
^{197}Au	77.3	1.9±0.2	0.12	4.2	$3.23x10^{-2}$	$4.85x10^{-3}$	0.221	31.5

[a] J. Lindskog, T. Sundström, and P. Sparrman, Table of Lifetime Measurements of Excited Nuclear States, in Alpha-, Beta-, and Gamma-Ray Spectroscopy, ed. by K. Siegbahn, (North-Holland Publishing Co., Amsterdam, 1965), Vol. 2, p. 1599.

[b] Values obtained from the tables by Sliv and Band.

Table XII. Reduced transition probabilities in ^{197}Au.

I_i	I_f	E_γ (keV)	$T_{1/2}$ (nsec)	B(M1) ($e^2 x10^{-24}$ cm^2)	$\frac{B(M1)}{B(M1)_{sp}}$	B(E2) ($e^2 x10^{-48}$ cm^4)	$\frac{B(E2)}{B(E2)_{sp}}$
1/2+	3/2+	77	1.9	$3.2x10^{-2}$	$4.85x10^{-3}$	$2.2x10^{-1}$	31.5
$3/2_2$+	3/2+	268	---	---	---	$6.6x10^{-2*}$	9.4
$3/2_2$+	1/2+	191	---	$\approx 1.8x10^{-2*}$	$2.67x10^{-3}$	≈ 4 $x10^{-2*}$	5.7
5/2+	3/2+	279	$1.6x10^{-2}$	$3.0x10^{-1}$	$4.56x10^{-2}$	$2.3x10^{-1}$	30.3
5/2+	1/2+	202	$1.6x10^{-2}$	---	---	$1.1x10^{-1}$	16.1
7/2+	3/2+	548	$5.2x10^{-3}$	---	---	$2.0x10^{-1*}$	28.6
7/2+	5/2+	270	$5.2x10^{-3}$	$\approx 1.6x10^{-1*}$	2.4 $x10^{-2}$	≈ 6 $x10^{-2*}$	8.6

*Values based upon Coulomb excitation work as reported in Nuclear Data Sheets

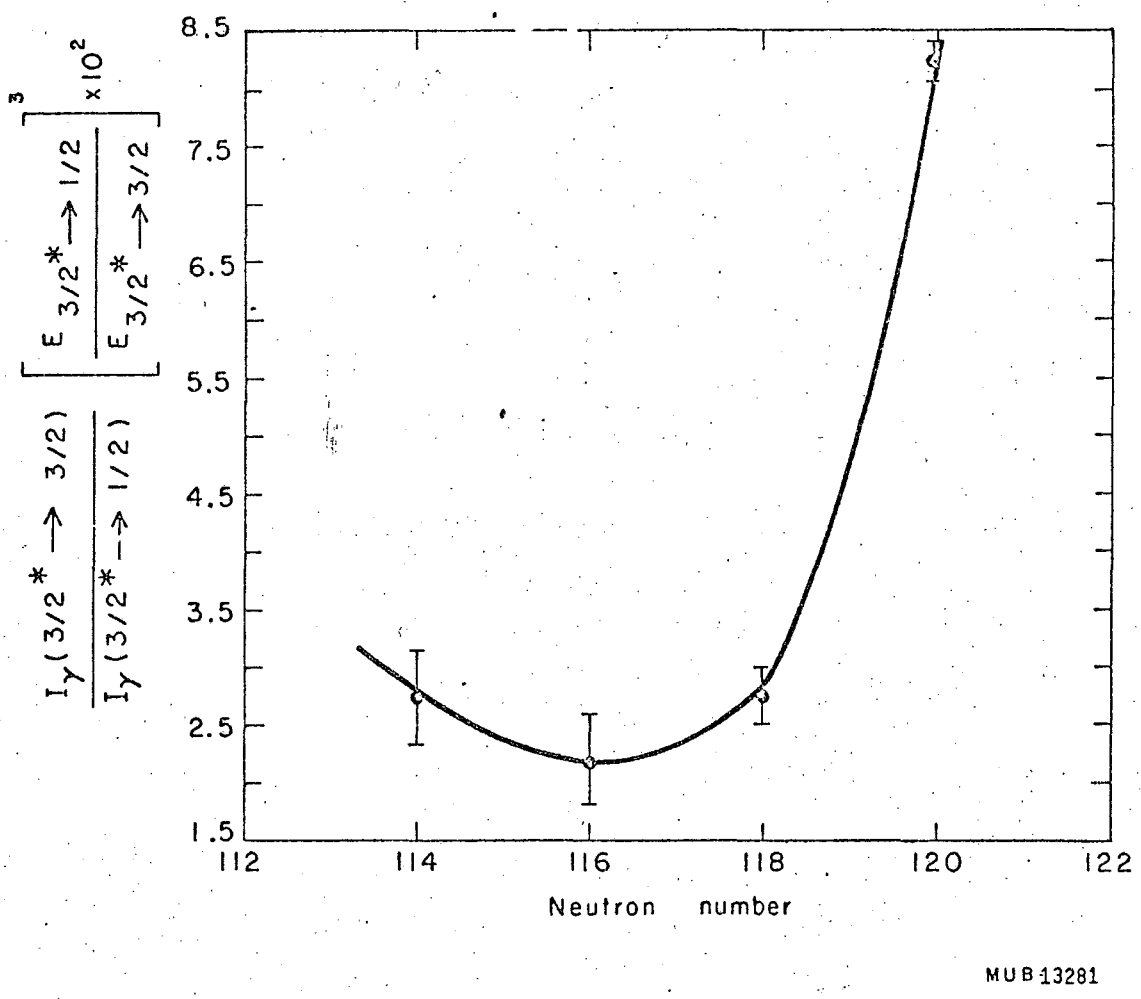

Fig. 48. The ratio of gamma-ray intensities for the transitions from the 3/2+ excited state to ground and to the 1/2+ excited level in the odd-mass Au isotopes, weighted inversely as the third power of the energy.

this plot would indicate relative B(M1) values. This could, in turn, yield information on the changing character of both the ground and first-excited states. The reverse situation exists for transitions from the lowest-lying 5/2+ level. For this case, the strong transition (M1 + E2 in character) goes directly to ground, while the weaker transition (pure E2) goes to the 1/2+ level. For these pairs we have plotted, as a function of neutron number, the ratio of the intensity of the transition to ground to that of the transition to the 1/2+ level, weighted inversely as the fifth power of the energy ratio. This is shown in Fig. 49. If the 5/2+ → 3/2+ transition had an M1 component which remained constant as a function of neutron number this plot would indicate relative B(E2) values. This particular figure seems to indicate a reduction in the electric-quadrupole transition probability for the 5/2+ → 3/2+ transition with decreasing neutron number. Both Figs. 48 and 49 show a distinct discontinuity in the plotted ratio upon the addition of the 119th and 120th neutrons. This again corresponds to the neutron number at which changes are observed in the trends of the energy levels

The "core excitation" model of de-Shalit predicts that the reduced E2 transition probabilities from the members of core multiplet to ground should be equal and approximately the same as the one found from the 2+ first-excited state to ground in the even-even nucleus which corresponds to the core. As is seen in Tables XI and XII the B(E2) values from the "core-excitation" states to ground in ^{197}Au are very nearly equal. As is expected, the 3/2+ → 3/2+ B(E2), which is very sensitive to single-particle admixtures, is considerably reduced from the other transitions to ground. Braunstein and de-Shalit[58] have shown that this value of B(E2) could be obtained with the inclusion of only 3% single-particle $d_{3/2}$ admixture to the 3/2+ excited state. With regard to the comparison of the above B(E2) values with those of the 2+ → 0+ transitions of the even-even nuclei which correspond to the gold core, we have plotted in Fig. 50 the B(E2) for the 2+ → 0+ transitions in both the even-even Pt and Hg isotopes as well as those from the 1/2+ to 3/2+ ground state for the odd-mass gold isotopes.

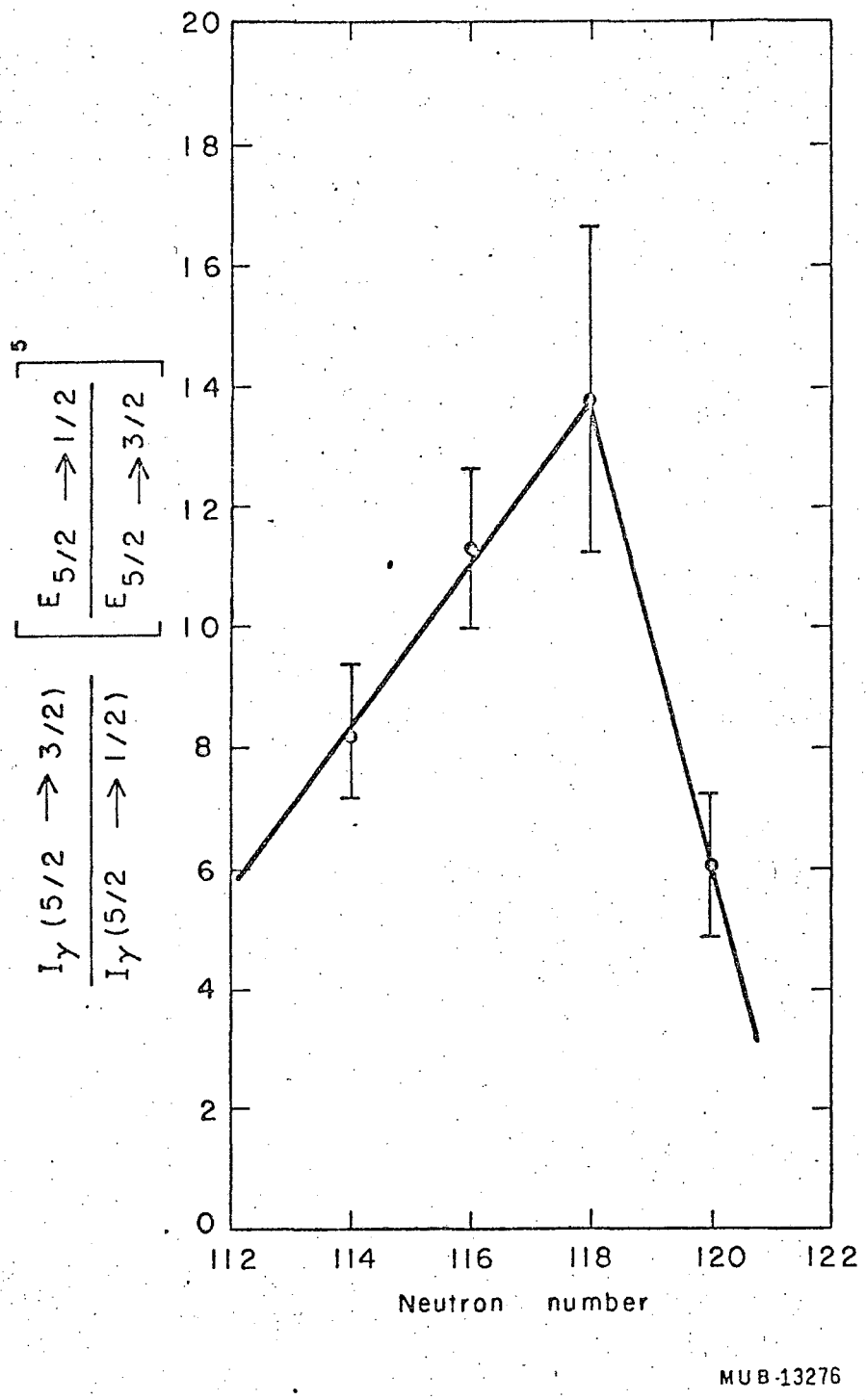

Fig. 49. The ratio of gamma-ray intensities for the transitions from the 5/2+ excited state to ground and to the 1/2+ excited level in the odd-mass Au isotopes, weighted inversely as the fifth power of the energy.

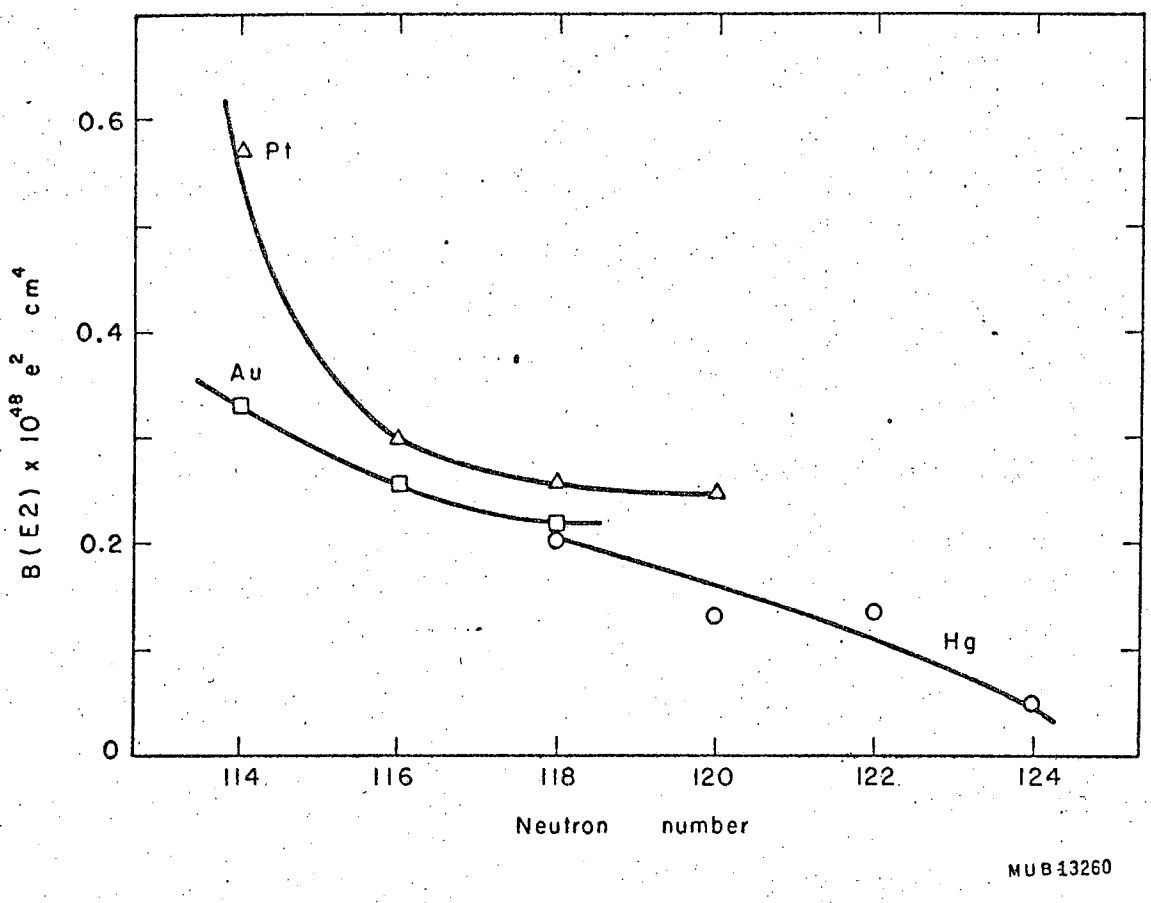

Fig. 50. Reduced E2 transition probabilities for the 1/2+ first excited state to ground state transitions of the odd-mass Au isotopes. Also shown are the reduced E2 transition probabilities for the 2+ to ground transitions of the even-mass Pt and Hg isotopes.

It is seen that the reduced transition probabilities all increase as the neutron number decreases, indicating an increasing collective nature for these E2 transitions. One can also see that the transition strengths do not increase as rapidly for the odd-mass gold isotopes as they do for the Pt isotopes.

Another prediction of the de-Shalit model is that of a negligible M1 transition strength from core multiplet states to ground. As is seen in Tables XI and XII the M1 transition rates to ground are indeed hindered with respect to single particle estimates, particularly those transitions from the 1/2+ level to ground. These findings are in good agreement with the core excitation picture. However, it must be noted that in the single-particle model we would expect a vanishingly small M1 transition rate for the $1/2^+ \rightarrow 3/2^+$ transition, since it would correspond to an l - forbidden ($s_{1/2}$ - $d_{3/2}$) proton transition. Thus, any model which would include large components of $s_{1/2}$ or $s_{1/2}{}^+$ phonon for the low-lying states would predict the hindered M1 transitions to ground. McKinley and Rinard[59] have fit seven transition probabilities along with seven other experimental results with an average error of 7.4% by using the de-Shalit model employing 9 adjustable parameters. If no attempt was made to fit the reduced M1 transition probability for the $5/2 \rightarrow$ ground transition, the average per cent error is reduced to 1.7%. Without the inclusion of an additional parameter describing the amount of $d_{5/2}$ single-particle admixture to the 5/2+ level it seems impossible to fit any of the transition probabilities involving the 5/2+ level with the exception of the B(E2)$5/2 \rightarrow$ ground value.

The work of Thankappan and Rao,[60] involving the coupling of a $d_{3/2}$ hole to the levels of ^{198}Hg, does not significantly improve the quality of the theoretical transition probability predictions. While the transitions to ground, with the exception again of the $5/2 \rightarrow 3/2$ M1 transition probability, are explained quite well, the predicted E2 transition probabilities within the multiplet are much too small when compared to experiment (under the assumption of a positive quadrupole moment for the 2+ core state as determined from the $7/2 \rightarrow 3/2$ B(E2)). On the other hand, if the charge distribution

inside the core is assumed to follow the mass distribution, the quadrupole moment of the core can be calculated from the B(E2, 2+ →0+) of the ^{198}Hg core. Utilizing this technique, Thankappan and Rao have calculated a negative quadrupole moment for the 2+ core state and this value has also been used for transition probability calculations. With this alternative choice, the fit for the transitions within the multiplet is good, but the fit for the transitions to ground is considerably worse than the first case. Thus, an experimental measurement of the quadrupole moment of the first 2+ level of ^{198}Hg would be of great aid in the fitting of the transition probabilities for this particular calculation.

In the treatment by Kisslinger and Sorensen[61] the retardation of electromagnetic transitions is dependent upon both pairing and phonon considerations. The pairing considerations are particularly important since a transition between two quasi-particle states involves transitions of both particles and holes in the shell model states. They have shown that their treatment does a good job in predicting the systematic trends of retardation for the M4 isomeric transitions in both the odd-mass Hg and Pt isotopes. The information available on the odd-mass gold isotopes is capable of yielding only qualitative predictions of transition rates. Of particular interest is the 5/2+ → 1/2+ E2 transition which we have found in both ^{197}Au and ^{199}Au and which had been previously known in ^{193}Au and ^{195}Au. Since the Kisslinger and Sorensen wave functions for the 1/2+ and 5/2+ states in ^{197}Au contain 92% $s_{1/2}$ and 8% $s_{1/2}{}^{+}$ phonon respectively, we would expect a large contribution to the E2 transition rate from the fast transition between these components. From the work of McKinley and Rinard[59] we can see that the "best parameter" core-excitation model predicts a B(E2) for this transition which is a factor of seven smaller than the experimentally observed value. Thus, significant admixtures of $s_{1/2}$ and $s_{1/2}{}^{+}$ phonon may be needed for a careful analysis of the transition probabilities. The Kisslinger and Sorensen treatment utilizes only very small changes in the various parameters as a function of neutron number. There are, therefore, no abrupt changes of the types observed in Figs. 48 and 49 which can be predicted on the basis of their model.

The model utilized by Ialongo[66] has given good agreement for the electric-quadrupole transitions observed in ^{197}Au. In general, however, the magnetic-dipole transition rates are found to differ by a rather large amount from the experimentally observed values. It is important to note that this treatment was accomplished with only 4 adjustable parameters in comparison to the nine used by McKinley and Rinard for the core-excitation model. From the wave-function components shown in Table X we can see that many of the experimentally observed results are qualitatively predicted in this treatment. The very sizable $|(s_{1/2}^{-2})_0\ d_{3/2}^{-1},\ 3/2,\ 0\ 0\rangle$ and $|(d_{3/2}^{-2})_0\ s_{3/2}^{-1},\ 1/2,\ 0\ 0\rangle$ components to the ground and first excites states respectively, do allow the prediction of a highly hindered M1 transition between these two levels. Although it is not calculated specifically in this treatment, we would expect the $5/2+ \rightarrow 1/2+$ transition to be quite fast due to admixtures of 38% $|(d_{3/2}^{-2})_2\ s_{1/2}^{-1},\ 5/2,\ 0\ 0\rangle$ and 53% $|(d_{3/2}^{-2})_2\ s_{1/2}^{-1},\ 1/2,\ 0\ 0\rangle$ in the 5/2 and 1/2 levels respectively. The neutron-proton interaction, as presently treated in this model offers no help in the prediction of the various trends in transition probabilities we have observed with varying neutron number.

3. Magnetic Moments

The magnetic moment of the ground state of ^{197}Au has been measured[108] to be 0.1439 nuclear magnetons. This corresponds very closely to the "Schmidt limit" for an odd proton in a $d_{3/2}$ single-particle state (0.126 nuclear magnetons). The magnetic moment of the first excited 1/2+ state has also been measured[108] and found to be 0.38 nuclear magnetons. This is considerably smaller than the value expected from the "Schmidt limit" for an odd proton in the $s_{1/2}$ orbital (2.79 nuclear magnetons).

The fitting of the magnetic moments for the two lowest-lying states in ^{197}Au is one of the major triumphs of the core-excitation model. Both moments are fit extremely well in the treatment by McKinley and Rinard,[59] with the fitted values being 0.1437 and 0.381 nm for the ground and 1/2+ states respectively. These values were fitted simultaneously with 8 transition probabilities.

The predictions of Kisslinger and Sorensen[61] yield a value of 0.84 - 0.92 nm for the ground state magnetic moment of ^{197}Au. This is, of course, much greater than the experimentally observed value. In spite of the fact that their predicted 1/2+ state in ^{197}Au is interpreted as being 92% $s_{1/2}$ single particle in nature, they find a quite low magnetic moment for this level of 0.25 nm. This value is in quite good agreement with the observed value. The quadrupole moment of the ground state is, like the ground state magnetic moment, predicted to be considerably greater than the observed value. Thus, with the exception of predicting the low value for the 1/2+ magnetic moment, the Kisslinger and Sorensen treatment does not seem capable of accurate moment predictions for the odd-mass gold isotopes.

The treatment by Ialongo[66] also fails in its attempt to predict magnetic moments for the low-lying gold levels. The same set of parameters that yield good predictions of level ordering and electric transition probabilities predict a magnetic moment of 0.3 nm for the ground state of ^{197}Au and 2.32 nm for the 1/2+ excited state. It has been shown by Blin-Stoyle[109] that the main cause for the deviation of the magnetic moments from the predicted single-particle values in spherical nuclei is the admixture of small amounts of higher seniority functions. They may well explain the serious disagreement between Ialongo's values and experiment. As we have seen in Table X there is an extremely large contribution of seniority three admixed states to the ground and first excited states of ^{197}Au in this treatment.

4. Log ft Values

Another very interesting comparison which can be made is the variation of electron capture probability from the odd-mass mercury ground states to low-lying levels in gold. While the present results, as indicated in Figs. 29 and 39, are limited to ^{197}Au and ^{195}Au there are some important things to note. Foremost among these is the absence of a detectable electron-capture or positron branch from the Hg 1/2- ground state to the Au 3/2+ ground state. There is, however significant branching to both the 1/2+ and

3/2+ excited states. Also there is a rather large increase in the log ft values for the above branches as well as the 13/2+→11/2- branch as the neutron number decreases.

The observation of no ground state-ground state branch indicates a great disimilarity in the state wave functions. This may indicate the presence of large phonon coupled components in one of the states and not in the other. Kisslinger and Sorensen predict greater than 80% $d_{3/2}$ single particle character for the ^{197}Au ground state. The ground 1/2- level of ^{197}Hg is predicted to have almost equal admixtures of $p_{1/2}$, $f_{5/2}^{+}$ phonon, and $p_{3/2}^{+}$ phonon. This type of difference in character may explain the retardation of electron capture between the levels. The Kisslinger and Sorensen treatment states that the ft value for the type of decay observed between Hg and Au is proportional to $(U_n\ U_p)^{-2}$, where the U's are the non-occupation probabilities for the neutron and proton orbitals respectively. Using the wave functions provided by Kisslinger and Sorensen, we find that the ft values are expected to decrease with decreasing neutron number. The opposite effect is observed. Considerable work remains to be done on the prediction of the change of log ft values as a function of neutron number.

5. Rotational Model

While we have not mentioned it previously, there is still an alternate interpretation of the low-lying gold levels. If we consider the gold nucleus to be slightly deformed, the levels of gold may be examined in terms of the unified model.[54] It would then be possible to consider the low-lying levels of ^{197}Au to be a series of rotational states built upon two Nilsson[110] single particle states. Thus, the 3/2+, 5/2+, and 7/2+ levels would correspond to a rotational band built upon the 3/2+ [402] Nilsson orbital, and the 1/2+ and 3/2+ levels to an anomalous band built upon the 1/2+ [400] orbital. This would yield an explanation for the observed gamma-ray intensity pattern. The intense transitions (7/2+→3/2+, 5/2+→3/2+, and $3/2_2^{+}$ → 1/2+) would be considered intra-band transitions, while the weaker ones (5/2+→1/2+ and $3/2_2^{+}$→3/2+) would be inter-band transitions. This might also explain the absence of the 7/2+→$3/2_2^{+}$ transition, which would be an inter-band E2.

This application of the unified model has been discussed by both Brunner et al.[96] and Jastrzebski.[111] Brunner et al. used the magnitude of the rotational level spacing constant as a criterion of the spherical character of the gold nucleus. Using semiempirical relationships, it was found that if $3\hbar^2/I$ for the spacing of the low-lying levels is greater than $13\hbar^2/I_{rig}$, where I_{rig} is the rigid-rotor moment of inertia, the nucleus is considered spherical. As they state, the values for the odd-mass gold isotopes are two to three times larger than the critical value and should be considered spherical. Jastrzebski examined the M1 transition rate for the $1/2+ \rightarrow 3/2+$ transition as a function of neutron number. From his treatment it is seen that the M1 transition probability should increase as the deformation increases. This effect has been observed in the Eu isotopes. Of course, a reduction of the B(M1) is observed as the neutron number is decreased. Since one would expect ^{193}Au to be considerably more deformed than ^{197}Au, it seems as though the rotational model does not hold.

Since the rotational model is capable of predicting relative gamma-ray intensities, coulomb excitation B(E2) values, M1 + E2 mixing ratios, etc., we have tested much of the available experimental data against these predictions. In particular, if we examine the ratio $B(E2, 7/2+\rightarrow 3/2+)/B(E2, 5/2+\rightarrow 3/2+)$ using the formulas from Bohr and Mottelson[54] the rotational model predicts a value of 0.417. The experimentally observed value is 0.905 as determined from Coulomb excitation work. Also the relative M1 + E2 mixing ratios for the $5/2+\rightarrow 3/2+$ and $7/2+\rightarrow 5/2+$ transitions can be predicted if we assume the intrinsic quadrupole moment and g factors remain constant within the "band". The value of $\delta^2(5/2+\rightarrow 3/2+)/\delta^2(7/2+\rightarrow 5/2+)$ is predicted from the formulas of Bohr and Mottelson[54] to be 2.32. The observed ratio of 0.163. Thus, it appears that while the rotational model is qualitatively inviting, actual quantitative predictions seem quite badly in error.

E. Conclusion

The development of high-resolution Ge(Li) detectors has permitted a careful analysis of many gamma-ray spectra previously thought too complex for detailed analysis. The ability to accurately measure gamma-ray energies has been of great value in positioning weak gamma rays in cases where the level schemes are fairly well known. Coincidence studies have been ruled out for most of the new transitions found in our studies due both to their weak nature and the need for maintaining highest possible resolution. As Ge(Li) detectors of large volume become available coincidence studies should be undertaken to verify our assignments.

The level schemes of the odd-mass gold isotopes examined in this study have been shown to be very similar. Much of the experimental data has pointed to the sizeable effect of collective contributions to these levels. The theoretical treatments we have discussed are, of course, greatly concerned with the character and magnitude of the particle-collective phonon coupling. While the relatively simple core-excitation model of de-Shalit seems to be capable of fitting much of the data for ^{197}Au, it does have a number of serious failures. It would also appear very difficult for this model to predict the systematic trends we have observed with changing neutron number without greater admixing of single particle configurations into the various wave functions. The Kisslinger and Sorensen predictions are by their nature much too general to expect quantitative agreement with experiment. The work by Ialongo and Alaga seems quite promising. The observed level ordering is predicted quite well, as are the electric-quadrupole transition probabilities. The problem of magnetic moment and transition probability agreement is still to be overcome. These latter values are very sensitive to the large amounts of high senority components present in the wave functions.

We have shown that there seems to be a significant change in the structure of the nucleus upon the addition of the 119th and 120th neutrons. Any further theoretical treatment for the gold region should be capable of including a method of describing the residual interaction between the proton and specific neutron pairs. This region of nuclei appears to be too complex for the presently applied theoretical treatments to explain comprehensively.

ACKNOWLEDGMENTS

I wish to extend my most sincere thanks to both Professor John O. Rasmussen, who directed this work, and Dr. Jack M. Hollander, who supervised and generated many of the ideas for this research.

Particularly valuable have been many discussions with members of the staff of the Lawrence Radiation Laboratory. Special thanks must go to Drs. Harry T. Easterday, George T. Ewan, Toshimitsu Yamazaki, and Stanley G. Prussin for their aid, encouragement, and friendship.

I would also like to thank Dr. David C. Camp of the Lawrence Radiation Laboratory in Livermore, California, both for allowing me to use his anti-Compton spectrometer and for his timely and helpful comments on this thesis.

It is impossible to leave the Lawrence Radiation Laboratory without expressing my gratitude to the many support groups which have made this work possible. I am greatly indebted to the Semiconductor Instrumentation Group, and in particular to Drs. Fred S. Goulding and Richard H. Pehl and Messrs. Blair V. Jarrett and Robert P. Lothrop, for making the best of a difficult situation. I also wish to acknowledge the excellent help given me by the electronics groups of Messrs. George W. Killian and Michyuki Nakamura. An expression of thanks must also go to the members of the Health Chemistry Division both for their day-to-day assistance and for their thelp in scheduling helicopter deliveries of short-lived activities.

The assistance of Messrs. Charles J. Butler, James A. Harris, C. Eugene Miner, Richard E. Parsons, and Donald F. Malone in solving many of the technical problems that arose during the course of this work has also been greatly appreciated.

My association with Drs. Rand Watson, John Cooper, Michael Lederer and Messrs. Fred Bernthal, Martin Holtz, James Lamb, and Jerry Wilhelmy has been extremely enjoyable and moderately profitable.

I also wish to thank my mother for her encouragement throughout my scholastic career.

I would especially like to thank my wife, Jeanne, for her encouragement, interest, patience, and for typing the original manuscript of this thesis.

This work was done under the auspices of the U. S. Atomic Energy Commission.

APPENDICES

A. The Internal Conversion Coefficient as a Means of Multipolarity Determination

1. Basic Theory

The nucleus in an excited state will normally proceed to a state of lower energy by one of two competitive processes. These are gamma-ray emission and internal conversion. It is within the scope of this work to give a brief description of the latter process and discuss its importance in the area of nuclear spectroscopy.

In the internal conversion process, the energy involved in the transition between nuclear levels is transferred directly to an orbital electron. This electron is then ejected from the atom with a kinetic energy equal to the transition energy minus the binding energy of the electron in its original atomic orbital. This process may take place in any shell of the atom provided the electron binding energy is less than the transition energy. In a given transition, the internal conversion coefficient (ICC), α_i, for a particular shell or subshell i, is defined by:

$$\alpha_i = \frac{N_e(i)}{N\gamma}$$

where $N_e(i)$ is the rate of ejection of electrons from shell i and $N\gamma$ is the rate of gamma emission.

The numerical value of the ICC will strongly depend on a number of parameters. They are as follows: the electron shell in which conversion is taking place; the atomic number, Z, of the atom in which conversion is occurring; the transition energy; the angular momentum change, L, of the radiation field; and the change in parity, $\Delta\pi$, between the initial and final nuclear levels. In general, for a transition with energy well above the binding energy of any of the shells, the following trends occur. As the major shell becomes farther removed from the nucleus, the ICC decreases. The ICC increases as Z increases, decreases as the energy increases, and increases as L increases. It is strong dependence of the ICC on L and $\Delta\pi$ that has made ICC such a valuable tool in the formulation of decay schemes.

If we consider a transition between two nuclear levels charactarized by initial and final angular momenta and parity J_i, J_f, π_i, and π_f, the gamma ray or conversion electron emitted will carry away angular momentum L according to the following restrictions

$$J = J_i - J_f \leq L \leq J_i + J_f \text{ and } \Delta\pi = (\pi_i)(\pi_f) \quad .$$

The electromagnetic field of this transition is said to be of a particular multipole character. This is either electric 2^L - pole, EL, if the change in parity is $(-)^L$, or magnetic 2^L - pole, ML, if the parity change is $(-)^{L-1}$.

As the L selection rule indicates, the observed ICC will usually be a mixture of ICC for fields of pure L. This is stated

$$\alpha = \sum_L |a_L|^2 \alpha(L) \quad \text{where} \quad \sum_L |a_L|^2 = 1$$

where L is limited by the above restrictions. The mixing coefficients, a_L. are the relative amplitudes of photon radiation associated with angular momentum L. Due to the parity selection rule, the $\alpha(L)$ above will alternately be from pure electric and pure magnetic multipole fields. From the theory of multipole radiation it can be shown that the relative intensity of multipoles with L and L + 2 units of angular momentum will be roughly

$$\left|\frac{a_{L+2}}{a_L}\right|^2 \approx \left(\frac{R}{\lambda}\right)^4 \ll 1$$

where R is the nuclear radius and λ is the wave length of the radiation. In some cases, however, the ratio of a_{L+1}/a_L will not be so small. For this reason, the observed ICC are usually limited to at most the mixture of two multipoles, $L = \Delta J$ and $L = \Delta J + 1$, and in some cases to one multipole, $L = \Delta J$. If as an example we take a transition between levels of $J_i = 3/2$, $\pi_i = +$, $J_f = 1/2$, $\pi_f = +$, the multipole field would be expected to be an MI, E2 mixture, with

$$\alpha = |a_1|^2\alpha(M1) + |a_2|^2\alpha(E2) \quad \text{where } |a_1|^2 + |a_2|^2 = 1 \quad .$$

The ratio $|a_2/a_1|^2$ is defined as the mixing ratio, δ^2. In this case $\delta^2 = \gamma_{E2}/\gamma_{M1}$ and it is simple to show that

$$\delta^2 = \frac{\alpha(M1)-\alpha}{\alpha-\alpha(E2)}$$

Since the pure-multipole gamma-ray transition probability between two levels is a model - dependent, calculable quantity, values of δ^2 are very important in the comparison of experiment and theory.

2. Theoretical Calculations of ICC

It is not the purpose of this discussion to go into a detailed treatment of the actual method used in calculation ICC, but rather to briefly describe the basic models used in these calculations. For a complete description of the methods involved, one should consult the original works [112,113,114,115] or an excellent review article by Rose.[116]

All modern calculations of ICC have been done essentially in the same manner. First-order perturbation theory has been used to calculate the rate of gamma-ray emission. This involves the coupling of the nucleus to the electromagnetic field and the subsequent emission of real quanta. The rate of conversion electron ejection must be treated by second - order perturbation theory since it involves the coupling of the orbital electron as well as the nucleus to the electromagnetic field. The electron wave functions have been those obtained by solving the Dirac equation in a given central potential. The various calculations have differed in the form of the central potential as well as those approximations used along with this potential.

The first computed values of Rose[112] were done using a point nucleus and a pure Coulomb potential. These were for the K - shell only. Rose's later calculations[117] used a Thomas - Fermi - Dirac screened potential. The effect of screening is to lower the ICC, especially at low Z values.

Sliv and Band[114] were the first to include the effects of finite nuclear size in the calculation of ICC. These effects are twofold. The first (static effect) is the actual alteration of the electron wave functions, notably the removal of the singularity at the origin. This effect can easily be taken account of by assuming a constant charge density for the nucleus. The second effect (dynamic effect) arises from the penetration of the electron orbitals within the nuclear radius. Nuclear matrix elements, which cancel in ICC calculations under the point nucleus approximation, no longer do so if this dynamic effect is considered. The evaluation of these nuclear matrix elements depends on the formulation of a particular nuclear model. Thus, only under the finite nucleus assumption does the ICC depend on nuclear wave functions. In the latest calculations of Rose,[113] results are given for K - shell and L_I - and L_{II} - subshell conversion with screening and the static effects of nuclear size taken into account. The L_{III} - subshell ICC include screening, but no nuclear size effects (since they are not expected to be important). Rose also includes M-shell ICC calculated for a point nucleus with no screening. For M-shell screening corrections to the tables of Rose it is suggested that the reader consult the work of Chu and Perlman.[118] The tables of Sliv and Band[114,115] give K-shell and L-subshell ICC calculated with screening as well as both static and dynamic nuclear size effects. The dynamic effects are accounted for through the assumption of a uniform surface transition current density. In most cases the values found in these tables differ little from those of Rose, although differences of 9 percent in the K-shell and 35 percent in the L_I - subshell occur for high Z M1 - transitions.

In general, where the effects of nuclear structure are small, the errors expected in the theoretical ICC values are about 2-3 percent for the K-shell and about 5 percent for the L-shell.

3. Experimental Methods of ICC Measurement

Since we are placing primary emphasis on the ICC as a means of determining transition multipolarity, the following discussions will not dwell on those refinements to experimental methods which have brought the ICC into play as an indicator of nuclear structure effects on the conversion process. The present discussion will not cover the various methods in great detail, but will, it is hoped, give the reader a feel for the great variety of ICC measurements which can be used to determine multipolarities. This section is organized in the following manner. We first will examine those measurements which involve observation of conversion electrons alone. This will be followed by those methods which involve observation of gamma rays (or associated events) as well as conversion electrons or secondary events. The final methods to be discussed are those which involve the use of coincidence techniques.

(a) Determination of K/L ratio. In many instances the ratio of internal conversion taking place in the K shell to that taking place in the L shell may be used as an indicator of multipolarity. Thus, for a given array of nuclei, one must experimentally determine the relative intensities of K and L electrons ejected in the conversion of a particular transition. This measurement requires only a piece of apparatus capable of sorting the conversion electrons by energy. This, of course, permits the differentiation of K and L electrons due to the different binding energies of the corresponding atomic shells. The separation of K and L lines varies from approximately 0.68 keV(Z=10) to 116.65 keV(Z=100). From the preceeding values it is seen that the instrumental resolution qualities necessary for these measurements will depend upon the nuclide of interest. In general, present measurements of these ratios are being made with magnetic spectrometers or, as indicated in the main portion of this work, semiconductor detectors.

The observed K/L ratio may be compared to theoretical values derived from the tables of Rose[113] or Sliv and Band[114,115]. Rose et al.[119] have presented convenient graphs of K/L ratios as a function of energy for various Z values and multipolarities which should be quite useful in decay scheme work.

The main drawback to the use of K/L ratios is the general insensitivity of this value to changes in multipolarity. Figures 51 and 52 indicate K/L ratios as a function of energy for Z=40 and Z=80. One should note that the K/L ratio is a better indicator of multipolarity for high Z than for low Z nuclides. Particularly noticeable in Fig. 51 for Z=40 is the fact that the K/L ratio will be of little value in M1 + E2 mixing ratio determinations for energies greater than approximately 300 keV. However, in general if the parity change and an upper and lower limit to the angular momentum change are known from independent data, the K/L ratio can be quite useful in determining multipolarity.

(b) L - subshell ratios. The L-shell conversion coefficient, α_L, is comprised of three subshell ICC. These are the L_I, L_{II}, and L_{III} ICC which arise from the ejection of $2s_{1/2}$, $2p_{1/2}$, and $2p_{3/2}$ electrons respectively. The ratios of these subshell electrons ejected in a particular transition are often quite sensitive to the multipolarity of the transition. If the L_I/L_{III} ratio does not conclusively give the multipolarity, the L_I/L_{II} ratio can be used to choose between alternatives. In general, it is very difficult to give approximate values for the ratios due to their great variation with Z and energy. Perhaps the only multipolarity that can be easily recognized from its L - subshell pattern is M1, where $L_I \gg L_{II}$ and usually $L_{II} \gg L_{III}$. For other multipolarities, one should consult the tables of Sliv and Band[115] or Rose[113] for the Z and energy in question. Also Rose et al.[119] has published convenient graphs of L - subshell ratios as a function of Z and E.

The measurement of L - subshell ratios requires a high-resolution electron spectrometer. This requirement is seen from the fact that the L_I - L_{III} separation varies from 0.05 keV(Z=20) to approximately 7 keV(Z=100). This high resolution also requires sources of very low mass. This means that L - subshell measurements are very difficult for transitions of low energy and/or low intensity. Thus, according to Ewan and Graham[120] L - subshell measurements are practical for heavy elements only up to transition energies of approximately 1 MeV, for rare earths to about 500 keV, and

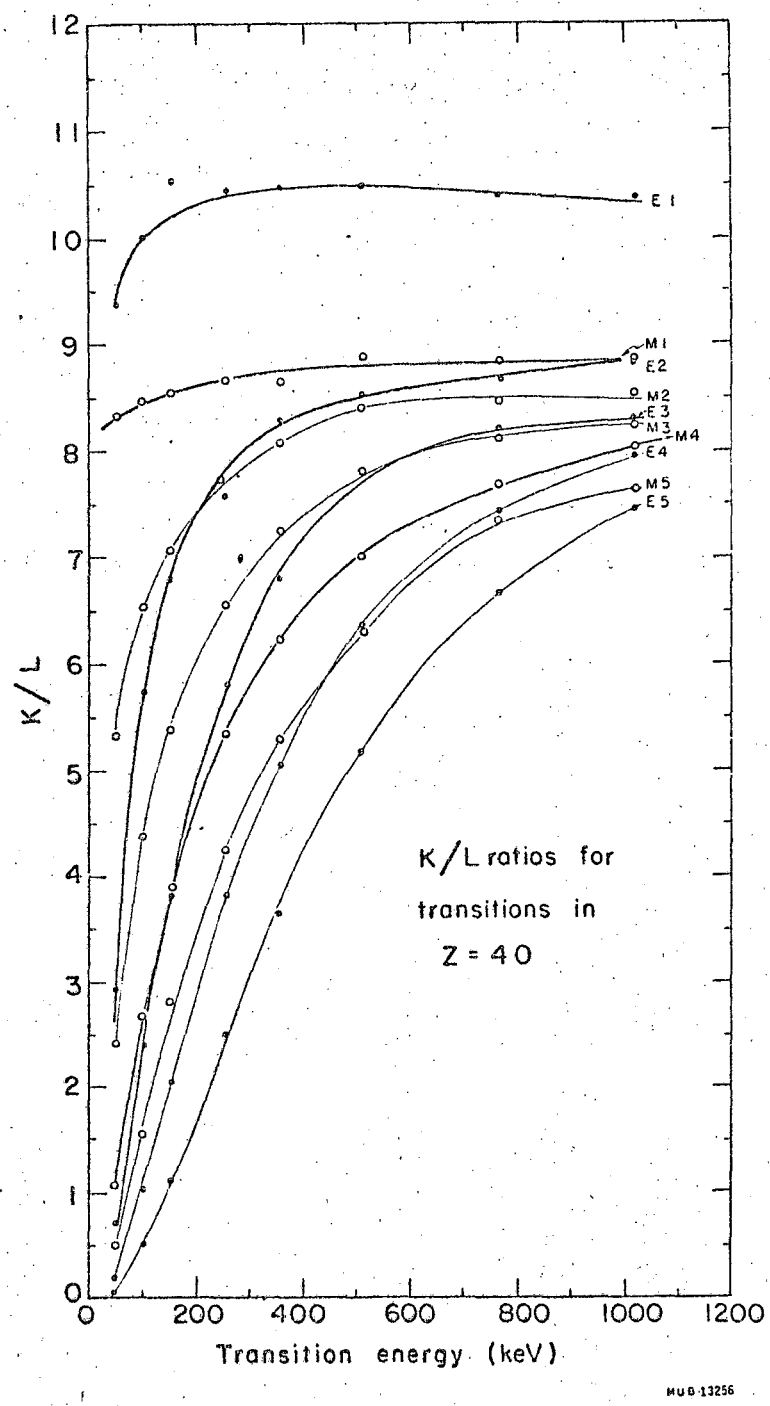

Fig. 51. K/L ratio for various multipolarity transitions in Z = 40 isotopes.

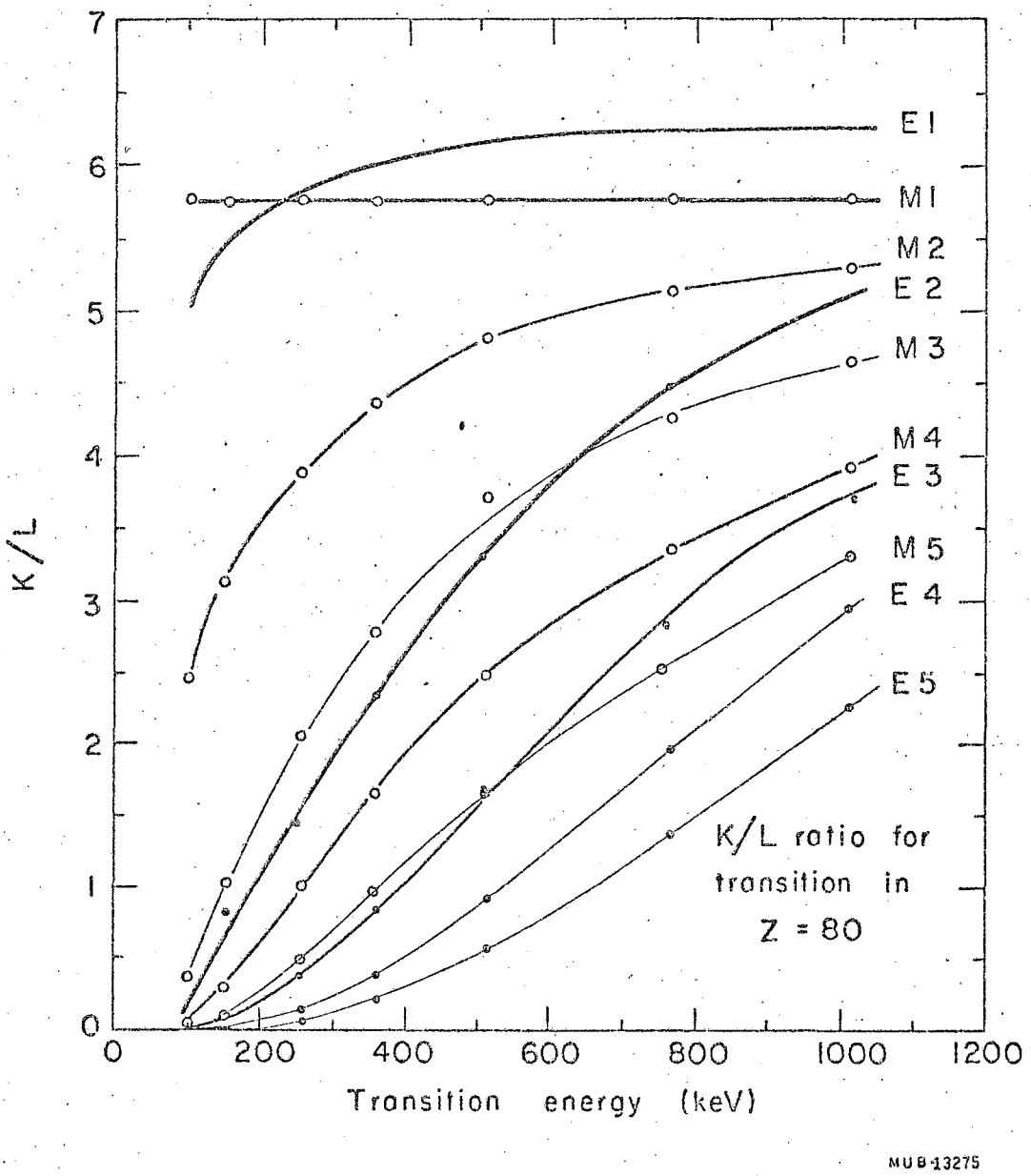

Fig. 52. K/L ratio for various multipolarity transitions in Z = 80 isotopes.

for light elements to about 200 keV. The slow-scanning magnetic spectrometers allow one to make measurements only on isotopes having fairly long half lives.

For a general discussion of the method of analysis for L - subshell ratios the reader is directed to the paper by Novakov and Hollander.[121]

(c) Conversion - electron-peak-to-beta-distribution ratio. One important method of ICC measurement which requires the use of only one major piece of experimental apparatus is the K - conversion peak-to-beta-spectrum method, or, as it is abbreviated, the PBS method. If one considers a simple scheme in which beta decay leads to a single excited state which then proceeds to ground by either gamma-ray emission or internal conversion, a measurement can be made of the relative intensities of K - conversion electrons and beta particles using a magnetic spectrometer. One then can determine

$$\frac{A_K}{A_\beta} = \frac{N_K}{N\gamma(1+\alpha)} = \frac{\alpha_K}{(1+\alpha)}$$

where α is the total conversion coefficient. The K - ICC is then found from

$$\alpha_K = \frac{A_K}{A_\beta - (A_K + A_{L_I} + A_{L_{II}} + \ldots)}$$

In cases where the decay scheme is as simple as above the PBS method can be useful. The chief problem in using this method is obtaining a good value for the intensity of the beta continuum. The scattering of low-energy electrons from both source and source holder tend to distort the beta spectrum. To obtain a true value for A_β one must make a Fermi-Kurie plot and extrapolate to zero electron momentum. Fermi-Kurie plots require knowledge of the so-called "shape factor" for the beta transition in question. While there are good values available for the shape factors of allowed and unique first-forbidden transitions, there is considerable uncertainty in shape factors for nonunique first-forbidden transitions. A good example of the uncertainties in ICC caused by this is shown in the work of Parsignault.[22]

For a general discussion of the experimental procedures involved in this method the reader is advised to read the review article by Hamilton et al.[123]

In general, this method of ICC measurement loses its applicability where the decay scheme becomes complex. It also is not useful in cases where the transitions of interest are weak in comparison to high-energy beta distributions. Since this method requires the observation of electrons only, one is at the mercy of the slow measurements made by scanning with a magnetic spectrometer. Thus, the PBS method will be of greatest value in cases where the decay scheme is simple and the half life long.

(d) Conversion-electron-to-gamma-ray ratio. From the definition of the ICC, it would seem that the most direct method for its measurement would be the relative measurement of the intensity of the gamma ray and its corresponding conversion electron line. This method has indeed been of importance. It has been most generally applied in the following manner. The relative intensities of the gamma rays emitted by the nuclide in question are determined. The relative intensities of the conversion electron lines are also determined. If the ICC of one transition in the decay has been accurately determined by some other means, or if the multipolarity of a particular transition can be assumed and the theoretical ICC used, this "standard" transition can be used to normalize the electron intensities to those of the gamma rays. The various ICC are then found from

$$\alpha = \left(\frac{I_e}{I_{e\text{-std.}}}\right)\left(\frac{I_{\gamma\text{-std.}}}{I_\gamma}\right) \alpha_{\text{std.}} \quad .$$

One regularly used variation to this method has been the mixing of a nuclide having a very well known ICC with the actual experimental source. If this procedure is undertaken and electron and gamma measurements are not made simultaneously, corrections must be made for the difference in half lives between standard and the nuclide in question.

In the past, electron relative intensities have usually been measured using a magnetic spectrometer and gamma-ray relative intensities using NaI(Tl) scintillation spectrometers. Since the advantages and disadvantages of using

these as well as other spectrometer combinations are discussed in Section II of this thesis, it seems sufficient to say that the rapid development of semiconductor detectors has given this general method a significant boost in importance.

(e) X-ray-to-gamma-ray ratio. The ejection of an internal conversion electron is followed by a rearrangement of the orbital electrons. For example, immediately after K-conversion takes place, the vacancy in the K-shell will be filled by an electron dropping down from a higher shell. The energy released in this process may then either be emitted as a K X-ray or transferred to an outer electron which is ejected into the continuum. These ejected electrons are called Auger electrons.

If one corrects for those conversions which lead to the Auger process, it is possible to determine the K-ICC by a measurement of the relative intensities of the K X-rays and the gamma ray corresponding to the transition being converted. This can be expressed

$$\alpha_k = \frac{I_{KX}}{I_\gamma \omega_K}$$

where I_{KX} is the K X-ray intensity, I_γ the gamma-ray intensity, and ω_K is the K-fluorescent yield (the fraction of K-conversion electrons giving rise to K X-rays). The K-fluorescent yield may be determined from the semi-empirical formula of Hagedoorn and Wapstra[124] to an accuracy of from 4% to about 0.5% depending upon the Z value.

The method in question is another which requires the use of only one detection system. In this case, normal gamma-ray scintillation crystals have been used. Since this device is a multichannel one, this method lends itself to measurements on short half-life nuclides.

Clearly, any occurrence which will lead to an increased intensity for the K X-ray will yield an incorrect value for the K ICC. Other transitions which convert will, of course, add K-X-rays to the spectrum, as will the process of electron capture. Thus, this method is most suitable for very simple decay schemes fed by beta decay.

Due primarily to photomultiplier noise it is very difficult to measure photopeak efficiency and accordingly X-ray intensity with NaI(Tl) detectors at energies below 15 keV. Thus, one must work at Z values above approximately 37 to be able to determine the X-ray intensities. The poor resolution of NaI(Tl) spectrometers has also contributed to the uncertainties in α_K values determined by this method. With these spectrometers, it is difficult to analyze the gamma and X-ray peaks if the gamma rays are low in energy. The satellite low-energy peaks caused by iodine X-ray escapes must be carefully considered in the analysis of the low-energy region. Pile-up of pulses and summing effects also affect the results. It has been suggested by Jansen and Wapstra[125] that backscattering will also affect the results using NaI(Tl) detectors yielding ICC values that are too great, and that perhaps the best configuration would be the well-type crystal. Many of these problems are overcome by using Ge(Li) detectors for both X-rays and gammas as is discussed in Section II of this thesis.

(f) Internal - external conversion. The internal - external conversion method takes advantage of the high resolution of the magnetic spectrometer to study the gamma-ray emission rate in a particular nuclear decay. The internal conversion electrons are detected in the normal manner with the intensity proportional to the area under the peak observed in the electron spectrum. A thin layer of high Z material is then placed in front of the source in a position identical to that originally occupied by the source during internal conversion measurements. The gamma rays emitted from the source may then interact with this converter material through the photoelectric process with the subsequent ejection of a photoelectron. The photoelectron spectrum is then observed and the intensity of the K photoelectron (found at an energy equal to that of the gamma ray minus the K-binding energy in the converter material) is measured. The K ICC can then be found from the following relation.

$$\alpha_K = \left[(A_{in})_K/(A_{ex})_K\right] k\tau_K f_K \text{ db}$$

where $(A_{in})_K$ and $(A_{ex})_K$ are the areas of the internal and external K conversion lines respectively, k is the strength of the external conversion source relative to the internal conversion source (thus correcting for either natural decay or different sources), τ_K is the K-shell photoelectric cross section for the converter, f_K is the factor which takes into account the anisotropy of photoelectrons ejected from the converter, d is the thickness of the converter in mg/cm^2, and b is a constant which depends on the converter material. Values of τ_K can be obtained from the calculations of Hultberg et al.[15] and values of f_K from calculations of the type discussed by Hultberg.[16] The value of b is $6.025 \times 10^{-4}/M$ (atoms cm^2 $barns^{-1}$ mg^{-1}), where M is the atomic weight of the converter element. Uranium and gold are the most commonly used converter materials.

While this method is one of the most accurate, it suffers from the maladies of slow speed and low efficiency. Thus its use is restricted to fairly long-lived isotopes or to prominent transitions. Also associated with this method are the standard source requirements for high-resolution electron spectrometers, namely thin sources of high specific activity. The source used for external conversion may, of course, be thicker than that used for internal conversion, but the converter must be kept thin to prevent energy loss of the photoelectrons. For a detailed discussion of this method the reader is directed to the articles by Hultberg and Stockendal[128] and Mitchell.[129]

(g) Coincidence methods. Coincidence methods have been applied to ICC measurements in many different ways. They generally require gating upon the particular radiation populating that state from which the transition in question is emitted. Thus, one may gate on alpha particles, betas, X-rays from electron capture, gammas, or other internal conversion electrons. If one then counts the number of gate pulses, the ratio of the intensity of a coincident gamma ray to gate pulses will be equal to $1/(1 + \alpha)$ where α is the total ICC. From a measurement of the K/(L+M+....) ratio one may determine the K ICC. As an alternative method, one might observe the relative intensities of gamma and K X-rays in the coincident spectrum, thus,

still using the method described in part e while removing some of the X-ray intensity arising from other transitions. The variations on the general method are numerous. For particular examples of the coincidence method it is suggested that the reader consult articles by Gerholm,[130] Lewin et al.,[131] and Dingus et al.[132]

As in all coincidence experiments, to obtain valid results, one must take some pains in the setting of the gate. Inclusion of unwanted Compton distribution, if one is gating on a portion of a gamma-ray spectrum, will add incorrect counts to both gate and coincident spectra. Backscattering will also complicate analysis of the results, as will summing and pile-up effects. However, in some cases this method can be quite accurate, and can in addition give the absolute source strength if the decay scheme is simple.

B. Spectrometer Calibration

1. Introduction

The high-resolution characteristics of semiconductor detectors have placed a considerable burden upon those data previously used for spectrometer energy and efficiency calibration. With NaI(Tl) gamma-ray spectrometers, for example, one could make energy measurements accurate to approximately 1% of the photopeak energy fairly routinely. With great precautions, some workers have claimed an accuracy of around 0.1%. Using Ge(Li) gamma-ray spectrometers, with their order-of-magnitude better resolution, most energy measurements have been made to an accuracy of 0.1% - 0.2% with some measurements being made to a few parts in ten thousand. To take full advantage of this increased accuracy, one must use standards which have extremely well known energies. For this reason we include in this section a discussion of calibration methods and standards which are of sufficient accuracy to be used with semiconductor detectors.

2. Gamma-Ray Energy Calibration

In general, the best method of gamma-ray energy measurement is the simultaneous measurement of a large number of gamma rays having well-known energies along with the unknown spectrum. In practice, however, the standards are usually measured separately. If one takes care to maintain approximately equal counting rates between sample and standards, this should cause very little error. One then determines the centroids of the standard peaks. From adjacent peaks one may then obtain values for the number of keV per channel in each region of the spectrum. At this point we find that the most convenient method of analysis is to average all measured keV-per-channel values and plot E_o as a function of channel number from the relation

$$E = E_o + (\text{keV/Channel})(\text{Channel Number}).$$

If the system were completely linear E_o would have a constant value, but with most systems non-linearities show up as some continuous function for E_o. For example, Fig. 53 shows the E_o function for one particular experiment in which an average gain of 0.26746 keV/Channel was used. The large value of E_o is due to the presence of a biased (window) amplifier in the system. The full deflection of this curve corresponds to nearly three channels (out of 1600).

There are, of course, numerous other methods of energy calibration. Among the most interesting are those described by Kennett[133] and Heath et al.[134] The first is particularly applicable in measurements of high-energy gamma-ray spectra where the "double-escape" peaks are quite prominent. Both references concern calibration methods suitable for use with an experiment which is "on line" with a small computer. Another interesting reference is the work of Dolan et al.[135] in which an alternative method of numerically handling the standard calibration procedure is described.

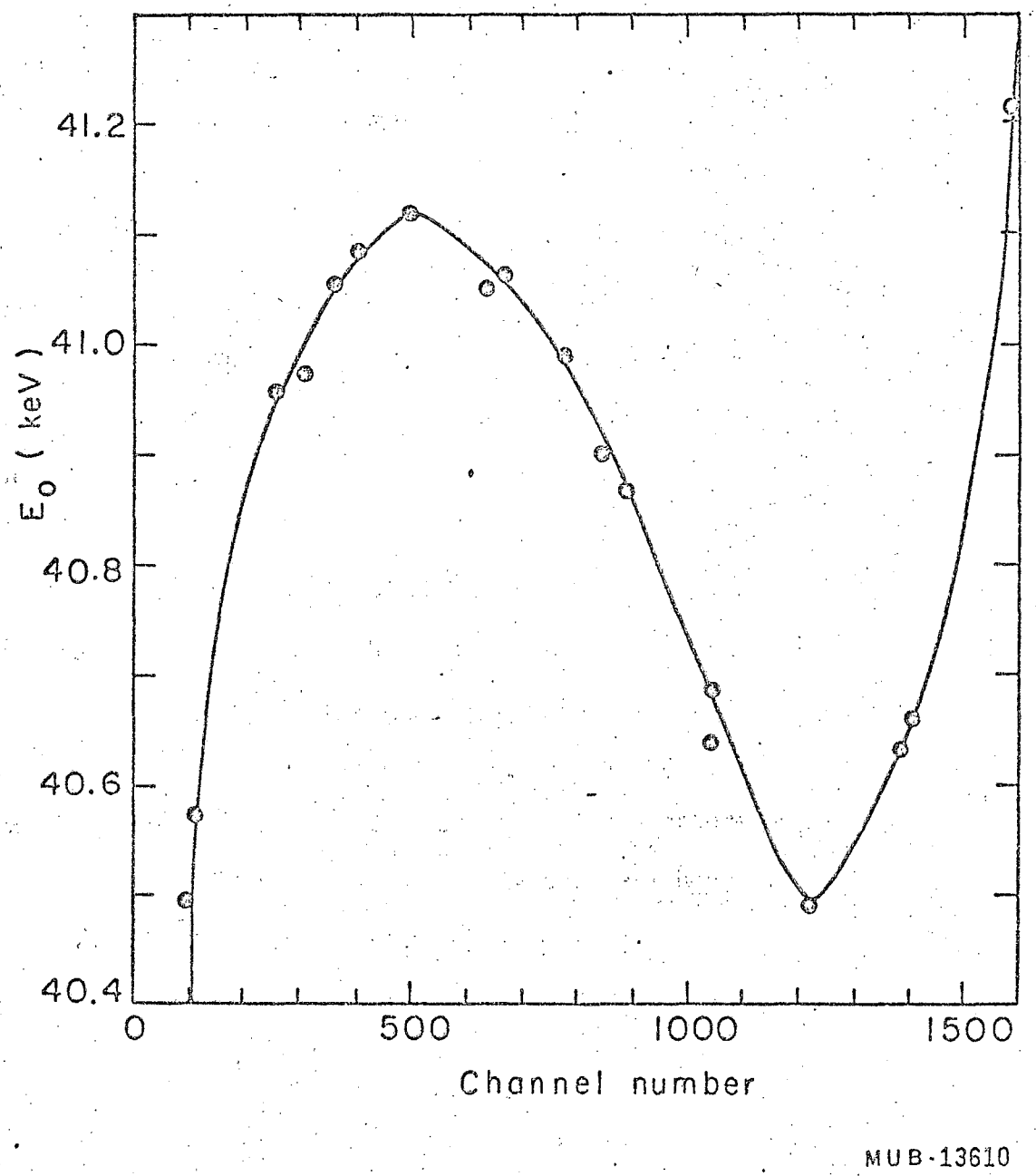

Fig. 53. Non-linearity correction function for gamma-ray energy determination.

With the exception of those mehtods in which a precision pulse generator is used for calibration, it is most advantageous to have a large number of gamma rays with well-known energies for use in each spectral region of interest. As an aid to the experimenter, we have included in Tables XIII and XIV a compilation of those gamma-rays with well-enough known energies to be conveniently used as standards. These tables come primarily from the compilation by Marion[136] and include his weighted error values. For the detailed references, it is suggested that the reader consult this compilation. We have included the energies of a number of X-rays which occur in the gamma-ray spectra of selected standards. The X-rays of In are included in this table due to their presence in many Ge(Li) gamma-ray spectra. They arise from fluoresence in the In foil used as thermal and electrical contact between the Ge(Li) detector and its mounting block. Also included are many of the prominent gamma rays from the decay of ^{177m}Lu, the energies of which have been determined in this laboratory[137] using Ge(Li) detectors. This source, with its many low-energy (100 - 400 keV)lines, and its fairly long half-life, is particularly suited for a calibration standard in this energy range. The decay scheme and gamma-ray spectrum of this isomer are included in part 6 of this appendix.

Table XIII. Gamma-ray energy standards.

Source	Gamma-ray energy (keV)	Half-life	Comments	Reference
^{241}Am	11.887±0.004	458 y	Np L	a
^{241}Am	13.9 ±0.1	458 y	Np L_α	a
^{57}Co	14.36 ±0.05	268 d		b
^{241}Am	17.8 ±0.1	458 y	Np L_β	a
^{241}Am	20.8 ±0.1	458 y	Np L_γ	a
^{109}Cd	22.11 ±0.08	470 d	Ag K_α	a
In	24.14 ±0.08	---	In K_α	a
^{109}Cd	25.03 ±0.10	470 d	Ag K_β	a
^{241}Am	26.348±0.010	458 y		26
In	27.37 ±0.10	---	In K_β	a
^{137}Cs	32.07 ±0.08	30 y	Ba K_α	a
^{137}Cs	36.52 ±0.10	30 y	Ba K_β	a
^{241}Am	59.543±0.015	458 y		26
^{203}Hg	70.833±0.001	47 d	Tl K_{α_2}	a
^{203}Hg	72.873±0.001	47 d	Tl K_{α_1}	a
^{131}I	80.164±0.009	8.05 d		136
^{203}Hg	82.572±0.004	47 d	Tl K_{β_1}'	a
^{203}Hg	84.918±0.004	47 d	Tl K_{β_2}'	a
^{109}Cd	87.7 ±0.2	470 d		140
^{182}Ta	101.101±0.012	115 d		136
^{177m}Lu	105.31 ±0.05	155 d		137

continued

Table XIII. Continued.

Source	Gamma-ray energy (keV)	Half-life	Comments	Reference
^{177m}Lu	112.95 ±0.05	155 d		137
^{177m}Lu	121.63 ±0.05	155 d		137
^{50}Co	121.97 ±0.03	268 d		136
^{177m}Lu	128.50 ±0.05	155 d		137
^{57}Co	136.33 ±0.03	268 d		136
^{141}Ce	145.43 ±0.02	32.5 d		141
^{182}Ta	152.429±0.003	115 d		159,160
^{177m}Lu	153.29 ±0.06	155 d		137
^{182}Ta	156.389±0.004	115 d		159,160
^{139}Ce	165.84 ±0.03	140 d		136
^{182}Ta	179.392±0.005	115 d		159,160
^{177m}Lu	204.08 ±0.06	155 d		137
^{177m}Lu	208.34 ±0.06	155 d		137
^{182}Ta	222.104±0.005	115 d		159,160
^{177m}Lu	228.44 ±0.06	155 d		137
^{182}Ta	229.317±0.008	115 d		159,160
Th B	238.61 ±0.01	1.91 y	^{228}Th	142
^{182}Ta	264.068±0.009	115 d		159,160
^{203}Hg	279.15 ±0.02	47 d		136
^{177m}Lu	281.78 ±0.07	155 d		137
^{131}I	284.307±0.049	8.05 d		136

continued

Table XIII. Continued.

Source	Gamma-ray energy (keV)	Half-life	Comments	Reference
^{51}Cr	320.11 ±0.03	27.8 d		158
^{131}I	364.467±0.050	8.05 d		136
^{113}Sn	391.7 ±0.4	118 d		143
^{198}Au	411.795±0.009	2.70 d		136
^{7}Be	477.57 ±0.05	53 d		139
m_0c^2	511.006±0.002	---		136
^{207}Bi	569.62 ±0.06	30 y		136
Th C"	583.139±0.023	1.91 y	^{228}Th	136
^{110m}Ag	657.61 ±0.15	249 d		157
^{137}Cs	661.595±0.076	30 y		136
^{110m}Ag	677.36 ±0.20	249 d		157
^{110m}Ag	686.80 ±0.25	249 d		157
^{110m}Ag	706.28 ±0.25	249 d		157
^{110m}Ag	743.99 ±0.25	249 d		157
^{110m}Ag	763.77 ±0.20	249 d		157
^{58}Co	810.46 ±0.10	71 d		136
^{110m}Ag	817.87 ±0.30	249 d		157
^{54}Mn	835.12 ±0.21	314 d		c
^{56}Co	846.5 ±0.2	77.3 d		136
Th C"	860.47 ±0.06	1.91 y	^{228}Th	136
^{110m}Ag	884.46 ±0.25	249 d		157

continued

Table XIII. Continued.

Source	Gamma-ray energy (keV)	Half-life	Comments	Reference
^{88}Y	898.01 ±0.07	108 d		139
^{110m}Ag	937.2 ±0.3	249 d		157
^{207}Bi	1063.63 ±0.07	30 y		139
^{65}Zn	1115.51 ±0.07	245 d		139
^{60}Co	1173.226±0.040	5.26 y		136
^{56}Co	1238.6 ±0.2	77.3 d		136
^{22}Na	1274.58 ±0.10	2.58 y		158
^{60}Co	1332.483±0.046	5.26 y		136
^{24}Na	1368.526±0.044	15.0 h		136
^{110m}Ag	1383.8 ±0.4	249 d		157
^{110m}Ag	1475.5 ±0.4	249 d		157
^{110m}Ag	1504.6 ±0.5	249 d		157
^{110m}Ag	1561.8 ±0.4	249 d		157
^{58}Co	1674.9 ±0.3	71 d		136
^{56}Co	1770.8 ±0.3	77.3 d		136
^{88}Y	1836.17 ±0.12	108 d		158
^{56}Co	2034.7 ±0.3	77.3 d		136
^{56}Co	2598.9 ±0.3	77.3 d		136
Th C"	2614.47 ±0.10	1.91 7	^{228}Th	136
^{24}Na	2753.92 ±0.12	15.0 h		136
^{56}Co	3202.3 ±0.5	77.3 d		136

continued

Table XIII. Continued.

Source	Gamma-ray energy (keV)	Half-life	Comments	Reference
^{56}Co	3254.0 ±0.5	77.3 d		136
^{56}Co	3273.6 ±0.4	77.3 d		136
^{56}Co	3452.6 ±0.5	77.3 d		136

[a]Calculated from the binding energies of Ref. 138, and weighted according to known intensity ratios.

[b]Calculated from energy difference between 136.33 keV and 121.97 keV transitions.

[c]Weighted average value from Ref. 136 in doubt due to spread of measured values.

Table XIV. Gamma-ray energy standards listed by source.

Source	Gamma-ray energy	Source	Gamma-ray energy
m_oc^2	511.006±0.002	^{60}Co	1173.226±0.040
^{7}Be	477.57 ±0.05		1332.483±0.046
^{22}Na	1274.58 ±0.10	^{65}Zn	1115.51 ±0.07
^{24}Na	1368.526±0.044	^{88}Y	898.01 ±0.07
	2753.92 ±0.12		1836.17 ±0.12
^{51}Cr	320.11 ±0.03	^{109}Cd	22.11 ±0.08
			25.03 ±0.10
^{54}Mn	835.12 ±0.21		87.7 ±0.2
^{56}Co	846.5 ±0.2	^{110m}Ag	657.61 ±0.15
	1770.8 ±0.3		677.36 ±0.20
	2034.7 ±0.3		686.80 ±0.25
	2598.9 ±0.3		706.28 ±0.25
	3202.3 ±0.5		743.99 ±0.25
	3254.0 ±0.5		763.77 ±0.20
	3273.6 ±0.4		817.87 ±0.30
	3452.6 ±0.5		884.46 ±0.25
^{57}Co	14.36 ±0.05		937.2 ±0.3
	121.97 ±0.03		1383.8 ±0.4
	136.33 ±0.03		1475.5 ±0.4
^{58}Co	810.46 ±0.10		1504.6 ±0.5
	1674.9 ±0.3		1561.8 ±0.4
		^{113}Sn	391.7 ±0.4

continued

Table XIV. Continued.

Source	Gamma-ray energy	Source	Gamma-ray energy
^{131}I	80.164±0.009	^{198}Au	411.795±0.009
	284.307±0.049	^{203}Hg	70.833±0.001
	364.467±0.050		72.873±0.001
^{137}Cs	32.07 ±0.08		82.572±0.004
	36.52 ±0.10		84.918±0.004
	661.595±0.076		279.15 ±0.02
^{139}Ce	165.84 ±0.03	^{207}Bi	569.62 ±0.06
^{141}Ce	145.43 ±0.02		1063.63 ±0.07
^{177m}Lu	105.31 ±0.05	^{228}Th	238.61 ±0.01
	112.95 ±0.05		583.139±0.023
	121.63 ±0.05		860.47 ±0.06
	128.50 ±0.05		2614.47 ±0.10
	153.29 ±0.06	^{241}Am	11.887±0.004
	204.08 ±0.06		13.9 ±0.1
	208.34 ±0.06		17.8 ±0.1
	228.44 ±0.06		20.8 ±0.1
	281.78 ±0.07		26.348±0.010
^{182}Ta	101.101±0.012		59.543±0.015
	152.429±0.003		
	156.389±0.004		
	179.392±0.005		
	222.104±0.005		
	229.317±0.008		
	264.068±0.009		

3. Electron Energy Calibration

For the general measurement of conversion electron spectra with Si(Li) detectors there is not a great need for precise energy standards. Under most circumstances the gamma-ray spectrum will have been previously measured, and if one knows the approximate energy region being observed in the electron spectrum, rapid assignment of K and L internal conversion lines from the gamma-ray data will allow an adequate calibration. However, since experimental situations will arise where it may be difficult to observe the gamma-rays (conversion electrons from nuclear reactions, fission, etc.), it is convenient to have a number of well-known electron energy standards. Fortunately, many of the gamma-ray standards have sufficiently large ICC values to permit their use as electron standards as well. Table XV lists those K- and L- IC lines which are useful in the calibration of Si(Li) detectors. The energies are computed from the corresponding gamma-ray energy (Table XIII this Appendix) minus the electron-binding energy as found in the tables by Hagstrom et al.[138] The L-IC line energy has been determined by weighting the L-subshell line energies according to the intensity ratios for the multipolarity in question. The errors indicated for the L lines do not reflect errors in knowledge of the L-subshell energies. These errors are placed in the table to indicate that the actual energy will depend on the resolution of the crystal and also on the experimenter's definition of peak center. This is due to the separation in energy between $L_1 + L_2$ and L_3 increasing as one goes to higher Z values.

The reader should note the absence from this table of one of the primary β-spectrometer calibration standards, Th(B + C + C''). This is due to the fact that one of the daughter products is the emanating isotope ^{220}Rn, would cause serious contamination in any Si(Li) chamber.

It has been noted by a number of workers that low energy X-rays or gamma rays cannot be used to calibrate the Si(Li) detector for electrons. This is due to the finite "window" (i.e., dead layer at the surface) thickness through which the electrons must pass. The energy loss for electrons above approximately 40 keV observed in our Si(Li) detectors is about 1 keV.

Table XV. Electron energy standards.

Source	Conversion-electron energy (keV)	Assignment
^{109}Cd	62.19±0.20	^{109}Ag 87.7 K (E3)
^{109}Cd	84.2 ±0.2	^{109}Ag 87.7 L (E3)
^{141}Ce	103.44±0.02	^{141}Pr 145.43 K (M1+E2)
^{139}Ce	126.91±0.03	^{139}La 165.84 K (M1+E2)
^{141}Ce	138.63±0.08	^{141}Pr 145.43 L (M1+E2)
^{139}Ce	159.61±0.08	^{139}La 165.84 L (M1+E2)
^{203}Hg	193.62±0.02	^{203}Tl 279.15 K (M1+E2)
^{203}Hg	264.47±0.10	^{203}Tl 279.15 L (M1+E2)
^{198}Au	328.69±0.01	^{198}Hg 411.795 K (E2)
^{113}Sn	363.8 ±0.4	^{113}In 391.7 K (M4)
^{113}Sn	387.6 ±0.4	^{113}In 391.7 L (M4)
^{198}Au	397.68±0.08	^{198}Hg 411.795 L (E2)
^{207}Bi	481.61±0.06	^{207}Pb 569.62 K (E2)
^{207}Bi	554.37±0.10	^{207}Pb 569.62 L (E2)
^{137}Cs	624.15±0.08	^{137}Ba 661.595 K (M4)
^{137}Cs	655.88±0.10	^{137}Ba 661.595 L (M4)
^{58}Co	803.35±0.10	^{58}Fe 810.46 K (E2)
^{58}Co	809.62±0.10	^{58}Fe 810.46 L (E2)
^{54}Mn	829.13±0.21	^{54}Cr 835.12 K (E2)
^{54}Mn	834.44±0.21	^{54}Cr 835.12 L (E2)
^{88}Y	881.91±0.07	^{88}Sr 898.01 K (E2)
^{88}Y	895.81±0.07	^{88}Sr 898.01 L (E2)
^{207}Bi	975.63±0.07	^{207}Pb 1063.63 K (M4)
^{207}Bi	1048.10±0.10	^{207}Pb 1063.63 L (M4)
^{65}Zn	1106.53±0.07	^{65}Cu 1115.51 K (M1+E2)
^{65}Zn	1114.41±0.07	^{65}Cu 1115.51 L (M1+E2)

4. Gamma-Ray Relative-Intensity Calibration

While gamma-ray energies are quite important in the formulation of a valid level scheme for a particular nuclear decay, it is the relative intensity relationship between the gamma-rays which is often more directly comparable to nuclear theory. This, of course, puts prime importance on the ability to measure accurately these intensities. The improved resolution of the Ge(Li) detector has greatly simplified these measurements. Other methods of measurement which have equal or superior resolution qualities, specifically curved crystal or external conversion measurements, require very strong sources and lengthy scanning periods. These methods also have much poorer peak-to-background ratios than that of the Ge(Li) detector. These problems make the determination of intensities of weak transitions (which may be among the most interesting in the scheme) quite difficult. The NaI(Tl) spectrometer, which has a good peak-to-background ratio, has such poor resolution that, for a fairly complex gamma-ray spectrum, analysis of relative intensities usually requires some type of sophisticated, computer-oriented spectrum-stripping procedure and will still fall short of detecting weak transitions. In this section we will discuss the relatively simple method of relative intensity calibration and measurement which the Ge(Li) detector has made possible.

For NaI(Tl) detectors, two primary methods have been used for photopeak efficiency calibrations. The first involves the use of computed intrinsic efficiencies (the intrinsic efficiency is that fraction of gamma-rays within a given solid angle which are detected in the pulse height spectrum). One determines experimentally the ratio of counts in the full-energy (photo) peak to the total counts in the spectrum for a number of sources in a particular geometry. This peak-to-total ratio is then multiplied by the intrinsic efficiency to evaluate the photopeak efficiency. Since the peak-to-total ratio varies quite smoothly with energy, this method is quite satisfactory. It is quite tempting to apply this method to Ge(Li) calibration. However, since the development of these detectors has been so rapid, there has not, as of this time, been a standard detector configuration

(both detector shape and backing material) established. Thus, those calculations of intrinsic efficiency which have been undertaken[144,145,147] have differed in the shape of detector considered. This method, however, will become convenient when a standard configuration is established.

The second method of efficiency calibration for NaI(Tl) detectors is that suggested by Åström et al.[148] and is the one which we have applied to Ge(Li) detectors. In this method, sources are used which have two or more transitions the relative intensities of which are well known. Particularly useful for this purpose are sources which have transitions in cascade without the presence of crossover, or single gammas with well known K-ICC (thus permitting use of gamma-to-K-X-ray ratio). If it is assumed that one of the transitions is detected with 100% efficiency, the relative photopeak areas of the other transitions can be used to determine the relative efficiency of the detector at the particular transition energies. By plotting these sets of points on double logarithmic paper and adjusting the efficiency axis the points should form a smooth curve. One may then measure a few standards, the absolute disintigration rates of which are known, to place the efficiency curve on an absolute scale. Particularly useful for this purpose are commercially* available sets of 8 standards (^{241}Am, ^{57}Co, ^{203}Hg, ^{22}Na, ^{137}Cs, ^{54}Mn, ^{65}Zn, ^{60}Co) the disintegration rates of which are known to an accuracy of 1% - 3%. The sources may be ordered in either 1μCi or 10μCi strengths.

In Tables XVI and XVII we present the relative intensity standards used for calibration of our detectors. Table XVI has been taken from Ref. 139. Table XVII lists the main transitions in the decays of ^{152}Eu and ^{154}Eu and their present intensity values from the work of Reidinger, Hamilton and Johnson[149] using a well-calibrated Ge(Li) detector. It should be emphasized that ^{152}Eu is potentially the finest single efficiency calibration source available. Its long half life (12 yr.) and numerous intense transitions spaced well in energy make it perfect for a rapid

---

*Source sets available from International Atomic Energy Agency, Division of Research and Laboratories, Kärntner Ring 1113, Vienna 1, Austria.

Table XVI. Relative-intensity standards used to calibrate the gamma-ray spectrometers.

Isotope	Photon energy[d] (keV)	Relative intensity	Method[a]
^{241}Am	11.9 Np L	2.2	PROP[b]
	14.0 Np L_α	37.5	
	17.8 Np L_β	51.2	
	20.8 Np	13.8	
	26.35	7.0	
	59.55	100	
^{109}Cd	22.2 Ag K_α	25.5	SSD
	24.9 Ag K_β	5.5	
	87.9	1.00	
^{57}Co	14.4	11	SSD
	122.0	100	
	136.3	13	
^{188}Re	63.0 Os K_α	24.2	ICC
	71.4 Os K_β	6.6	
	155.0	100	
^{203}Hg	72.9 Tl K_α	11.9	ICC
	82.6 Tl K_β	3.44	
	279.2	100	
^{198}Au	70.8 Hg K_α	2.24	ICC
	80.3 Hg K_β	0.643	
	411.8	100	
^{137}Cs	32.2 Ba K_α	6.85	ICC
	36.4 Ba K_β	1.54	
	661.6	100	

continued

Table XVI. Continued.

Isotope	Photon energy[d] (keV)	Relative intensity	Method[a]
^{180m}Hf	55.8 Hf K_α	25.2	ICC and DS
	63.2 Hf K_β	7.4	
	93.3	16.8	
	215.3	80.6	
	332.5	94.8	
	443.6	83.0	
	501.2	14.2	
^{160}Tb	46.0 Dy K_α	116	ICC
	51.1 Dy K_β	28.8	
	86.8	100	
^{22}Na	511.0	180	DS[c]
	1274.6	100	
^{60}Co	1173.2	100	DS[c]
	1332.5	100	
^{88}Y	898.0	93	DS[c]
	1836.2	99	
^{24}Na	1368.5	100	DS[c]
	2753.9	100	

[a]Abbreviated as follows: PROP - Proportional counter spectrometry; SSD - Solidstate detector spectrometry; ICC - Assuming K internal conversion coefficient of a pure E2 transition from negatron emitter, and use of K-fluorescence yield; DS - Well established from decay scheme.

[b]Reference 150.

[c]Reference 151.

[d]The quoted x-ray energies are $K\alpha_1$ and $K\beta_1$.

Table XVII. ^{152}Eu and ^{154}Eu gamma-ray relative intensities from Reference 149.

^{152}Eu (12.4 yr)		^{154}Eu (16 yr)	
E_γ [a] (keV)	I_γ [b] (Rel.)	E_γ [a] (keV)	I_γ [b] (Rel.)
122.1	125	123.1	100
244.7	29	247.8	18
295.7	1.3	444.3	1.3
343.7	100	558.1	0.6
366.8	2.1	592.5	16
410.5	8.1	693.0	6.0
443.4	13	724.2	56
687.6	2.7	759.1	12
779.4	52	817.1	1.5
868.3	15	848.0	1.8
957.4	2.0	876.0	31
965.0	55	906.2	2.1
1006.1	3.5	999.6	31
1086.8	44	1008.2	50
1113.0	50	1249.3	3.2
1213.0	4.6	1278.0	100
1249.0	1.5	1495.8	1.8
1263.7	1.1	1540	0.1
1298.4	6.1	1595.9	4.6
1406.5	79		
1454.9	1.7		
1524.6	1.2		

[a] Energy measurements are good to 1 keV or better.

[b] Relative intensity errors are about 5% for strong transitions increasing to about 30% for weak transitions.

calibration source for Ge(Li) detectors. The data presented are perhaps somewhat tentative and we are anxiously awaiting them in their final form. It is suggested that, in order to obtain the best possible values, other groups should measure the intensities of the transitions in both of the above isotopes due to their potential importance as standards (as well as for the actual physics of the decay schemes in question).

Figures 54 and 55 display photopeak efficiency curves for two Ge(Li) detectors, of dimensions 1cm × 1cm × 0.5cm and 3cm × 2cm × 1.1cm respectively, determined in the above manner. These show the characteristic reduction in efficiency as one approaches low energy. This is due, of course, to photon absorption in the cryostat chamber window as well as in the surface "dead layer" of the crystal itself. The fact that the efficiency of the detector of Fig. 54, in comparison to that of Fig. 55, reaches a maximum at a lower energy as well as falling off less rapidly as the energy gets even lower is due both to its "thin window" construction[152] and to the 0.010 in. Be window on the cryostat. This makes the smaller detector quite useful for relative intensity measurements in the X-ray region.

For a comparison of the observed efficiency to theory, we have included in Figs. 54 and 55 the curves of efficiency versus $E^{-2.5}$ and $E^{-1.5}$. Theoretical calculations of the photo-electric cross section[146] suggest that the photopeak efficiency should fall off as $\sim E^{-2.5}$ between 100 - 500 keV and as $\sim E^{-1.5}$ between 500 keV and 3 MeV. The fact that the small detector of Fig. 54 follows this prediction fairly well is not unexpected, since the small active volume does not permit sizeable contribution to the full-energy peak from multiple events. The larger detector, however, is seen to closely follow $E^{-1.5}$ over a broad energy range. This indicates the sizeable contribution of reabsorption of the Compton scattered gammas to the full-energy peak. The detector in question shows this large photopeak efficiency due to its particular experimental arrangement. The photon beam is collimated, and is incident upon one of the 2cm × 1.1cm crystal faces,

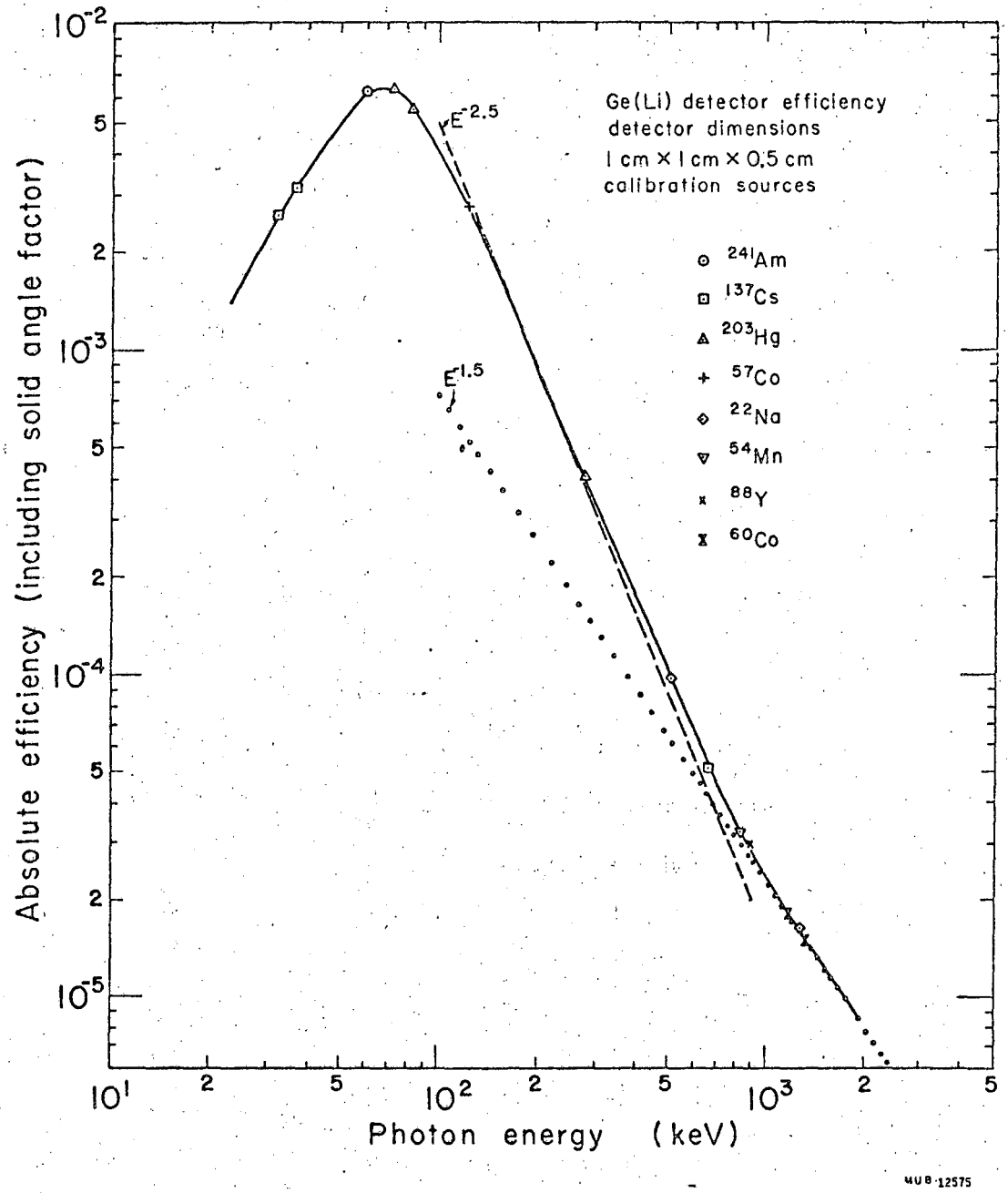

Fig. 54. Full-energy peak efficiency for gamma rays observed in a Ge(Li) detector of dimensions 1 cm^2 x 5 mm.

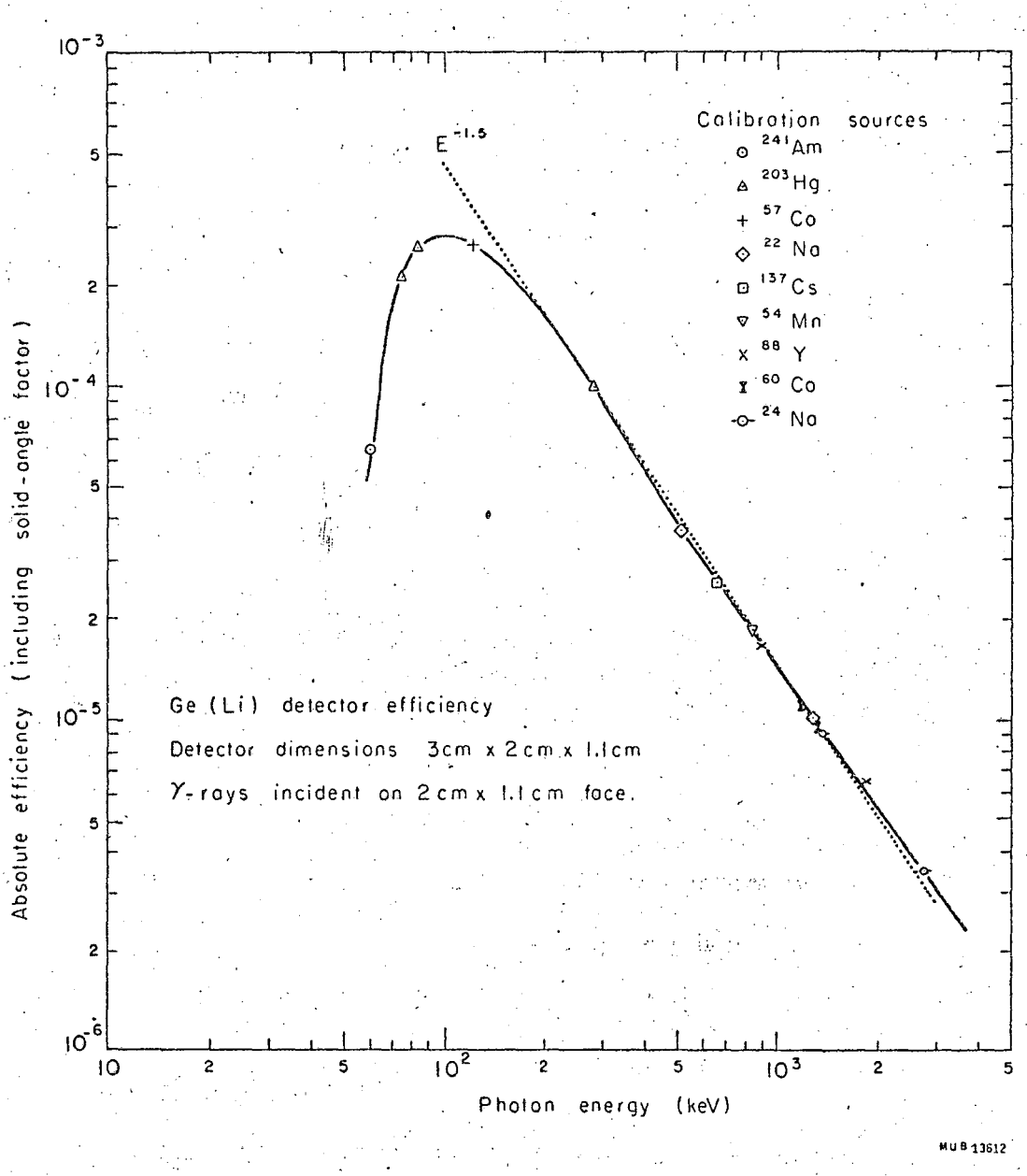

Fig. 55. Full-energy peak efficiency for gamma rays observed in a Ge(Li) detector of dimensions 6 cm^2 x 11 mm deep, with photons incident on one of the 2 cm x 11 mm faces.

thus presenting an effective depletion depth of 3cm. The proportionality between the efficiency and the gamma-ray energy raised to a specific power suggests a convenient method plotting the efficiency data. While the double logarithmic plot shown above is quite useful, it has been suggested[153] that one may take better advantage of the efficiency determinations by plotting the function Eff. $\times E^{1.5}$($E^{2.0}$ or $E^{2.5}$) versus E on a linear scale for the energy range 200 keV - 1 MeV. This function will closely follow a straight line and one may read the desired values from the curve much more accurately than with the double logarithmic plot.

This entire discussion of photopeak efficiency determination has been predicated on the experimenter's ability to accurately determine the areas of the photopeaks in question. Of course, it is not essential that some absolute peak be defined. However, it is very important for one to be consistent in the manner in which photopeaks are analyzed. If all peaks were situated on a flat background there would be little problem in determining a background value to subtract point-by-point from the total spectrum yielding the desired peak area. With single-peak spectra or spectra in which a given transition is very intense, the situation is more complex. The loss of electron energy from within the crystal through bremsstrahlung and other means tends to fill in the region between the photopeak and Compton distribution. For this reason, the region just lower in energy than the photopeak may be more than one order of magnitude more intense than that higher than the photopeak. At this point a very important question arises. What background shape should be taken in such a situation? The problem is shown in Fig 56.

Spectrum A in this figure is that of ^{113}Sn, showing the two photopeaks at 255.1 and 391.7 keV and the Compton edge associated with the higher energy photopeak. Spectrum B is spectrum A with a background from ^{60}Co added in until the region under the photopeak becomes essentially flat. In a normal experimental situation, the background for spectrum B indicated by the solid line beneath the photopeak would be used to determine

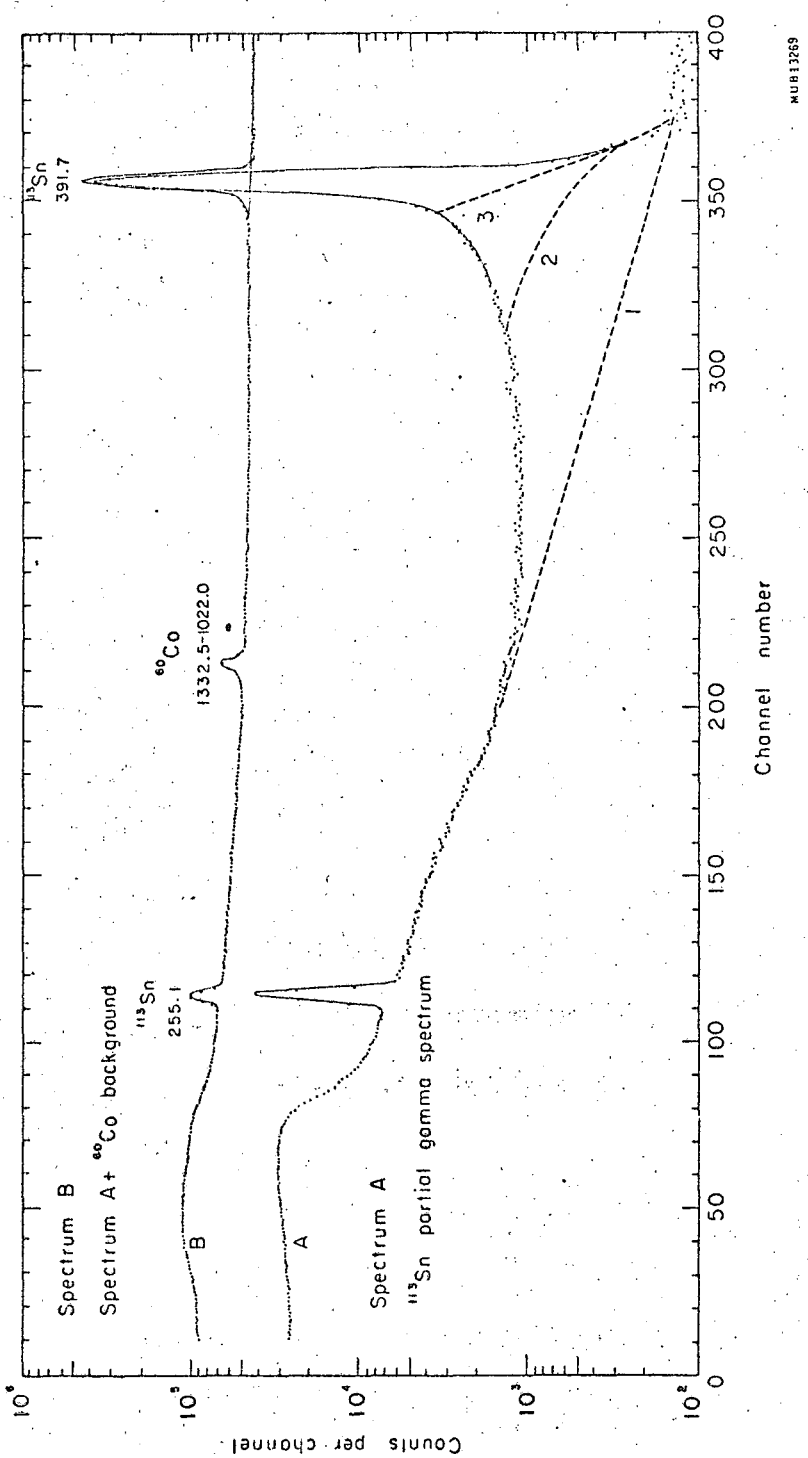

Fig. 56. ^{113}Sn partial gamma-ray spectrum showing background subtraction line shapes.

the area. Three of the possible alternatives for the photopeak background of spectrum A are shown by the dashed lines numbered 1, 2, and 3. Line 1 extends from the edge due to multiple Compton processes to the high-energy base of the photopeak. Line 2 was determined by replotting the region surrounding the photopeak on linear paper and joining the point of maximum radius of curvature on the low-energy side to the base on the high-energy side. Line 3 is that background which, as it will be shown, reproduces the peak shape from spectrum B.

In Fig. 57 we show the peak shapes obtained by subtracting the three background lines in spectrum A of Fig. 56 channel-by-channel from the total spectrum. The solid line peak shape is that obtained from spectrum B. It is seen that background 3 of Fig. 56 gives a peak shape almost identical to that of spectrum B. If we include only that portion of the peak greater than 1% of the peak height, we find that background 1 yields 2.5% greater area and background 2 yield 1.3% greater area than that obtained from spectrum B. In practice it is not possible to consistantly determine those points from which to draw background lines 1 and 3. Thus, in order to insure reproducibility, we use a background like that of line 2. Our method of background subtraction should then be consistent to within 1 - 1.5%.

If we use a background like that of line 2 in Fig. 56 when determining standard peak shapes for peak-shape analysis of complex spectra, the general form of the standard peak is found to be Gaussian with a low-energy exponential tail. The height on the peak at which this tail starts is a function of the gamma-ray energy and is due to incomplete charge collection in the detector. The tail can be lowered if the bias voltage on the detector can be increased. The use of standard peak shapes is shown in Fig. 58, where the shape of the 780 keV peak from the decay of ^{195}Hg is used to analyze near-by peaks.

For well-resolved, fairly-intense photopeaks in the energy range 300-1300 keV we feel that relative intensities can be determined to approximately 3-5% with normal precautions. It is possible to do better than this, but only with <u>extreme</u> care. There are many effects which must be

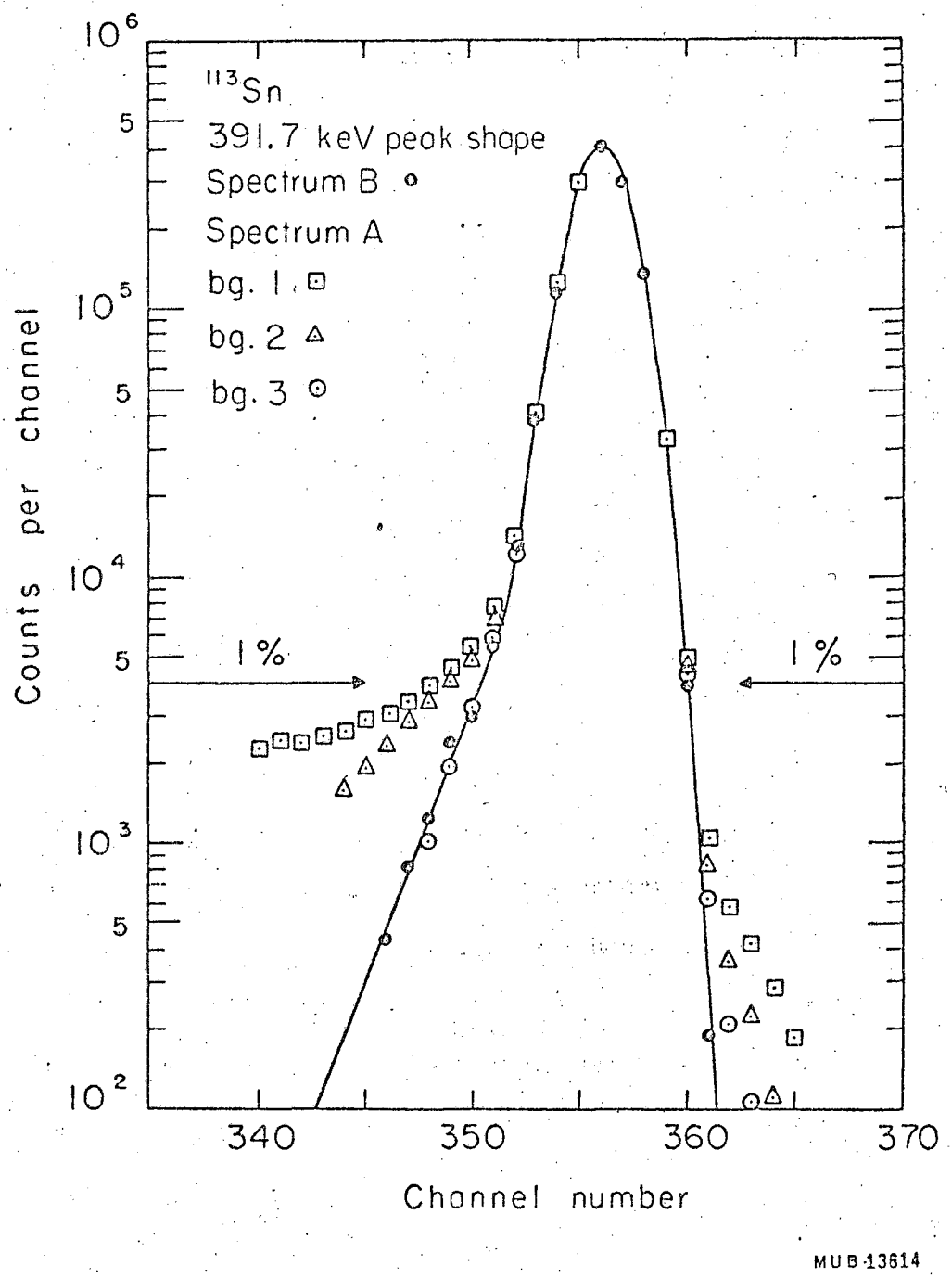

Fig. 57. Peak shapes determined from subtraction of the background values shown in Fig. 56.

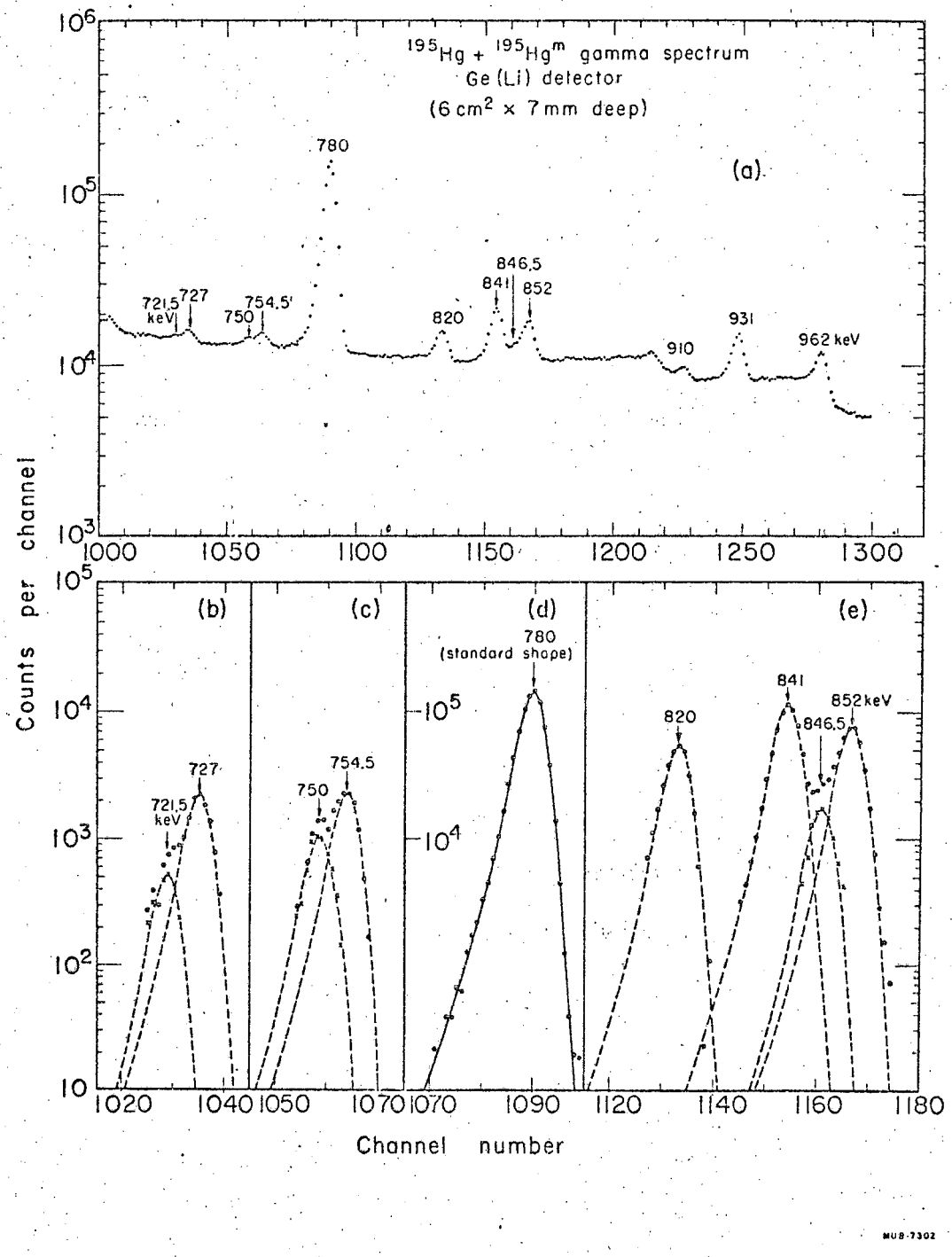

Fig. 58. Peak-shape analysis of a portion of the gamma-ray spectrum of ^{195}Hg and ^{195m}Hg. The 780-keV full-energy peak is used as a standard shape for the analysis of the other peaks.

considered if one wishes to push intensity measurements to their limits of accuracy, but the two major problems still lie in the number of useful standards available and the method of photopeak analysis.

5. Conversion-Electron Relative-Intensity Calibration

Since the best method of full-energy electron peak efficiency determination for Si(Li) detectors has been extensively discussed in Section II of this thesis, we present here only those sources which will be of value in obtaining rough shapes for the efficiency curves. Table XVIII lists the sources in question. The nuclide ^{243}Cm is included not only for its electron relative intensities but also for the fact that the known alpha-to-conversion-electron ratio* can be used to place the electron efficiency on an absolute scale if the alpha disentegration rate is known. There are a very large number of transitions in the spectrum of ^{205}Bi + ^{206}Bi. In Table XVIII, we have included only those peaks which are fairly intense and are relatively well separated from neighboring electron lines. The errors on the intensities of the Bi lines are probably on the order of 6-10% in most cases. It should be noted here that an accurate measurement of the relative intensities of the electron lines in the decay of the long-lives isomer, ^{166m}Ho, would be quite valuable; for the large number, as well as the wide energy span, of transitions in this decay make it a likely candidate for an intensity standard. This is also one of the few reactor produced nuclides where the beta spectrum will not seriously interfere with the observation of conversion electrons (due to the low energy of the beta endpoint).

For the convenience of the reader, we also include here, as Table XIX the table of standard internal conversion coefficients from Ref. 157, which has been previously discussed in Section II of this thesis.

---

*The alpha-to-277.6 keV K line intensity ratio is given in Ref. 156 as 0.157.

Table XVIII. Conversion-electron relative intensity standards.

Source	E_γ (keV)	Line	E_e (keV)	I_e (Rel)
^{243}Cm	209.8	K	87.9	5.1 ±0.4[a]
(35 y)	228.2	K	106.3	11.9 ±1.0
	277.6	K	155.8	9.8 ±1.0
	209.8	L_1+L_2	186.7	0.94±0.12
	228.2	L_1+L_2	205.1	2.45±0.24
	277.6	L_1+L_2	254.6	1.99±0.13
^{205}Bi	282.3	K	194.3	201[b]
(15 d)	284.2	K	196.2	
	550.0	K	462.0	6.3
	703.3	K	615.3	100
	910.8	K	822.8	9.8
	1043.7	K	955.7	32.5
	1190.3	K	1102.3	7.6
	1766.4	K	1678.4	43.6
^{206}Bi	343.4	K	255.4	760[b]
(6.3 d)	398.1	K	310.1	210
	497.1	K	409.1	170
	516.1	K	428.1	250
	537.5	K	449.5	280
	803.3	K	715.3	100
	880.5	K	792.5	60
	895.1	K	807.1	44

[a]Relative intensities taken from Ref. 154 for the same transitions observed in the β decay of ^{239}Np.

[b]From Ref. 151.

Table XIX. Internal conversion coefficient calibration standards.[a]

Source	$t_{1/2}$		E_γ (keV)	Multipolarity	α_k	
^{109}Cd	470	d	87.7	E3	11.0	±0.3
^{141}Ce	33	d	145.43	M1(E2)	0.379	±0.004
^{139}Ce	140	d	165.84	M1(E2)	0.2142	±0.0015
^{203}Hg	47	d	279.15	M1+E2	0.163	±0.002
^{113}Sn	118	d	391.7	M4	0.438	±0.008
^{198}Au	2.7	d	411.795	E2	0.0302	±0.0003
^{137}Cs	30	y	661.595	M4	0.0894	±0.0010
^{58}Co	71	d	810.48	E2	0.000295	±0.000010
^{54}Mn	314	d	835.12	E2	0.000224	±0.000010
^{65}Zn	245	d	1115.6	M1+E2	0.0001664	±0.0000066

[a]For References consult Table I, page 28 of this thesis.

6. ^{177m}Lu

The 155-day isomer of Lu is of great importance from the standpoint of nuclear theory. Its decay scheme is shown in Fig. 59. The presence of such a large number of transitions in the region of 100-500 keV also make it important as a standard for energy calibration. In anticipation of its general use, we present here, as Table XX a listing from Ref. 137 of the energies and relative intensities of gamma-rays in this decay. Also included in this table are the values determined by Alexander et al.[155] using a bent-crystal spectrometer. To aid the experimenter in rapid assignment of peaks in the calibration spectrum we also, include, as Figs. 60, 61, 62, and 63 the gamma-ray spectrum of ^{177m}Lu taken with a Ge(Li) detector having a resolution of 1.2 keV at 122 keV.

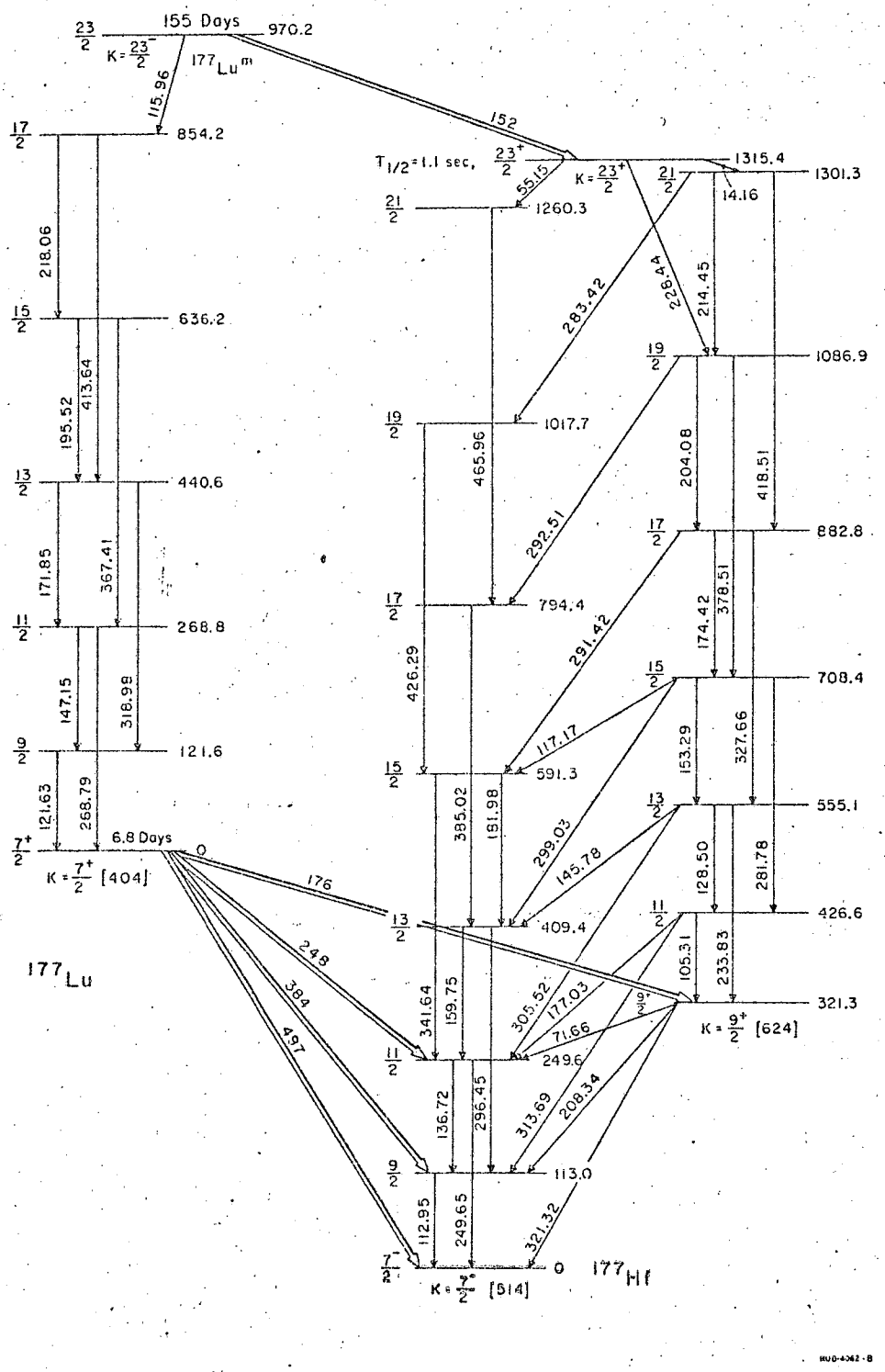

Fig. 59. Decay scheme of 155-d ^{177m}Lu.

Table XX. Energies and relative intensities of gamma rays from the decay of 155-day ^{177m}Lu.

Reference 137		Alexander et al.[155]	
Gamma-ray energy (keV)	Relative intensity	Gamma-ray energy (keV)	Relative intensity
71.66 (6)	6.8 (4)	71.64 (2)	9 (2)
105.31 (5)	100*	105.36 (2)	100*
112.95 (5)	179 (13)	112.97 (2)	251 (13)
115.96 (10)	5.0 (4)	115.83 (4)	9 (2)
117.17 (13)	1.8 (2)	117.01 (4)	12 (2)
121.63 (5)	52 (4)	121.56 (3)	62 (3)
128.50 (5)	127 (8)	128.48 (2)	125 (6)
136.72 (5)	11.7 (8)	136.68 (2)	17 (3)
145.78 (10)	6.6 (6)	145.59 (6)	11 (2)
147.15 (8)	29 (2)	147.10 (6)	27 (3)
153.29 (6)	133 (8)	153.25 (4)	134 (7)
159.75 (8)	5.4 (5)	159.92 (8)	5 (1)
171.85 (10)	37 (4)	171.84 (8)	41 (4)
174.42 (6)	96 (8)	174.37 (6)	110 (6)
177.03 (8)	26 (3)	177.05 (8)	34 (3)
181.98 (10)	0.75 (13)		
195.52 (6)	7.0 (6)	195.4 (1)	9 (2)
204.08 (6)	114 (8)	204.00 (8)	130 (13)
208.34 (6)	485 (40)	208.36 (6)	610 (31)
214.45 (6)	48 (4)	214.3 (1)	79 (8)
218.06 (6)	27 (3)	218.0 (1)	37 (6)
228.44 (6)	287 (26)	228.48 (8)	340 (17)
233.83 (6)	45 (4)	233.75 (10)	43 (4)
249.65 (6)	47 (4)	249.69 (10)	62 (6)
268.79 (6)	25 (3)	268.4 (1)	32 (5)

continued

Table XX. Continued.

Reference 137		Alexander et al.[155]	
Gamma-ray energy (keV)	Relative intensity	Gamma-ray energy (keV)	Relative intensity
281.78 (7)	108 (9)	281.77 (10)	32 (5)
283.42 (13)	4.7 (7)		
291.42 (10)	7.7 (9)	291.7 (3)	20 (4)
292.51 (10)	7.8 (9)		
296.45 (8)	38 (4)	296.1 (2)	65 (7)
299.03 (10)	12 (2)	299.1 (3)	10 (2)
305.52 (8)	14 (1)	306.0 (3)	13 (3)
313.69 (8)	9.4 (7)	313.5 (3)	12 (2)
318.98 (8)	78 (8)	318.8 (2)	86 (4)
321.32 (12)	9 (1)	321.4 (2)	12
327.66 (8)	136 (8)	327.7 (3)	149 (15)
341.64 (8)	13 (1)	341.8 (4)	14 (4)
367.41 (8)	23 (2)	367.4 (4)	25 (5)
378.51 (8)	222 (17)	378.4 (3)	223 (22)
385.02 (8)	24 (2)	385.0 (4)	37 (7)
413.64 (12)	131 (10)	413.7 (5)	163 (16)
418.51 (10)	161 (12)	418.6 (5)	185 (19)
426.29 (10)	3.4 (4)		
465.96 (12)	19 (2)	466 (1)	23 (7)

*Normalized to 100.

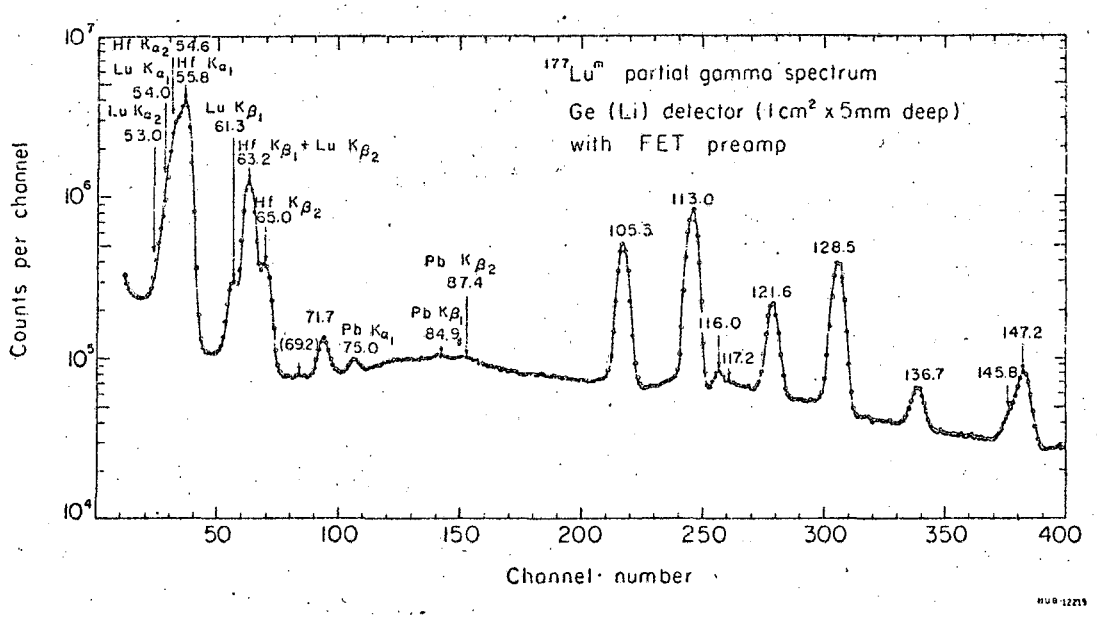

Fig. 60. Gamma-ray spectrum of ^{177m}Lu in the energy region 50-150 keV.

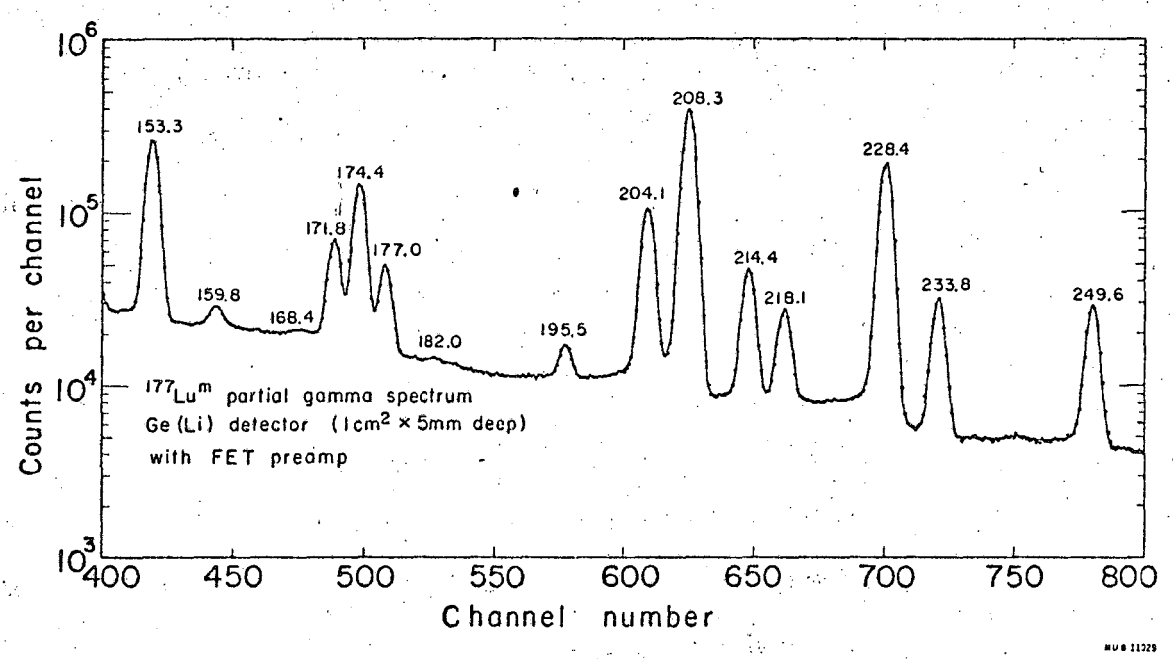

Fig. 61. Gamma-ray spectrum of ^{177m}Lu in the energy region 150-250 keV.

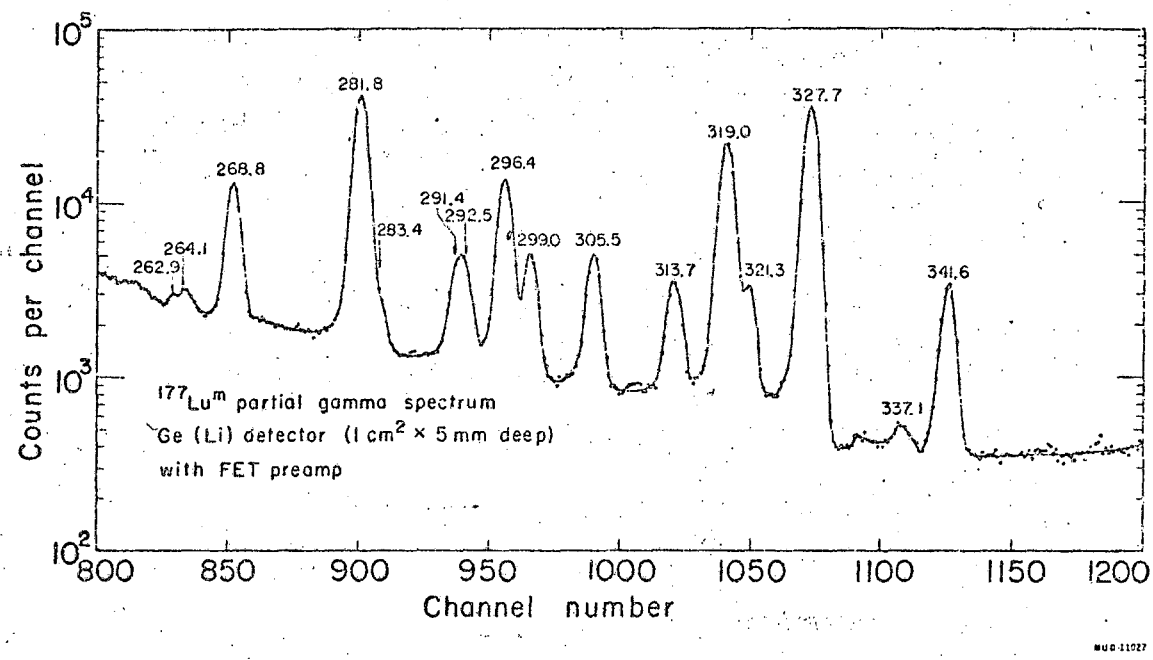

Fig. 62. Gamma-ray spectrum of ^{177m}Lu in the energy region 250-360 keV.

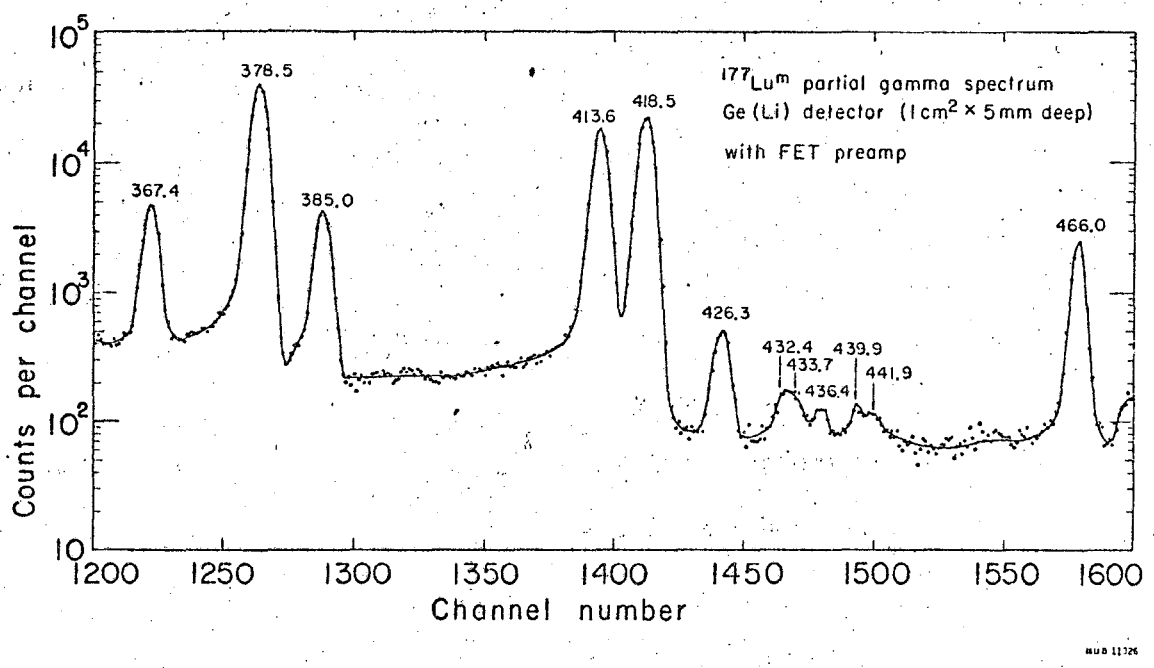

Fig. 63. Gamma-ray spectrum of ^{177m}Lu in the energy region 360-470 keV.

REFERENCES

1. E. M. Pell, J. Appl. Phys. 31, 291 (1960).
2. D. J. Freck and J. Wakefield, Nature 193, 669 (1962).
3. P. P. Webb and R. L. Williams, Nucl. Instr. Methods 22, 361 (1963).
4. G. T. Ewan and A. J. Tavendale, Nucl. Instr. Methods 25, 185 (1963).
5. N. A. Baily, R. J. Grainger, and J. W. Mayer, Radiology 76, 116 (1961).
6. J. H. Elliot, Nucl. Instr. Methods 12, 60 (1961).
7. J. L. Blankenship and C. J. Borkowski, IRE Trans. Nucl. Sci. NS-9, No. 3, 181 (1962).
8. J. M. Taylor, Semi-Conductor Particle Detectors, (Butterworth Inc., Washington, D. C., 1963).
9. G. Dearnaley and D. C. Northrop, Semi-Conductor Counters for Nuclear Radiations, (John Wiley, Inc., New York, 1963).
10. G. Dearnaley and D. C. Northrop, Semi-Conductor Counters for Nuclear Radiations, 2nd Edition, (John Wiley, Inc., New York, 1966).
11. W. J. Price, Nuclear Radiation Detectors, (McGraw-Hill Book Co., Inc., New York, 1964).
12. F. S. Goulding, Nucl. Instr. Methods 43, 1 (1965).
13. G. T. Ewan and A. J. Tavendale, Can. J. Phys. 42, 2286 (1964).
14. D. A. Shirley, Nucleonics 23, No. 3, 62 (1965).
15. W. M. Gibson, G. L. Miller, and P. F. Donovan, Alpha-, Beta-, and Gamma-Ray Spectroscopy, ed. by K. Siegbahn, Vol. 1, (North-Holland Publishing Co., Amsterdam, 1965), p. 345.
16. H. Jungclaussen, Kernenergie 8, 513 (1965).
17. J. M. Hollander, Nucl. Instr. Methods 43, 65 (1966).
18. G. T. Ewan, Progress in Nuclear Instrumentation and Techniques, ed. by F. J. M. Farley, (to be published, 1967).
19. D. C. Camp, Lawrence Radiation Laboratory Report UCRL-50156, 1966, (to be published).

20. M. A. Listengarten, Izv. Akad. Nauk SSSR, Ser. Fiz. 22, 759 (1958); (English trans: Bull. Acad. Sci. USSR 22, 755 (1958)).

21. J. W. C. Harpster, (M. S. Thesis), Western Reserve University, 1963, (unpublished).

22. I. O. Durosinmi-Etti, D. R. Bundrit, and S. K. Sen, Internal Conversion Processes, ed. by J. H. Hamilton, (Academic Press, New York, 1966), p. 201.

23. B. vanNooijen, A. V. Ramayya, J. H. Hamilton, J. J. Pinajian, and N. R. Johnson, Internal Conversion Processes, ed. by J. H. Hamilton, (Academic Press, New York, 1966), p. 193.

24. R. A. Brown and G. T. Ewan, Nucl. Phys. 68, 325 (1965).

25. T. Yamazaki and J. M. Hollander, unpublished data as reported by J. M. Hollander in Ref. 17.

26. T. Yamazaki and J. M. Hollander, Nucl. Phys. 84, 505 (1966).

27. H. E. Bosch, F. Krmpotic, and A. Plastino, Nucl. Phys. 48, 292 (1963).

28. H. E. Bosch, F. Krmpotic, and A. Plastino, Nucl. Phys. 56, 689 (1964).

29. S. K. Sen and B. G. Hogg, Nucl. Instr. Methods 15, 209 (1962).

30. D. R. Bundrit and S. K. Sen, Nucl. Phys. 68, 287 (1965).

31. T. Yamazaki, D. A. Landis, R. S. Stone, and J. M. Hollander, Lawrence Radiation Laboratory Report UCRL-16580, 1966 (unpublished).

32. G. Bertolini, F. Cappellani, R. Gantechi, and G. Restelli, Nucl. Instr. Methods 27, 281 (1964).

33. P. Charoenkwan, Nucl. Instr. Methods 34, 93 (1964).

34. J. Reynolds and B. Persson, Nucl. Instr. Methods 33, 77 (1965).

35. E. Sakai, Electronique Nucleaire, (ENEA, Paris, 1964), p. 205.

36. H. T. Easterday, A. J. Haverfield, and J. M. Hollander, Nucl. Instr. Methods 32, 333 (1965).

37. Liquid nitrogen reservoirs were obtained from Linde Oxygen Co., Inc.

38. C. E. Miner, Lawrence Radiation Laboratory Report-11946, 1965 (unpublished).

39. A similar pump is commercially available from Linde Oxygen Co., Inc., R. E. Parsons, Lawrence Radiation Laboratory Report, 1966 (to be published).

40. E. Elad, Nucl. Instr. Methods 37, 327 (1965).

41. E. Elad and M. Nakamura, Nucl. Instr. Methods 41, 161

42. F. S. Goulding and D. Landis, Proceedings of Conference on Instrumentation Techniques in Nuclear Pulse Analysis, Monterey, April 1963, NAS-NRC publication 1184.

43. F. S. Goulding, Lawrence Radiation Laboratory Report UCRL-11302, 1964 (unpublished).

44. Manufactured by Radiation Instrument Development Laboratories, Inc., Melrose Park, Illinois.

45. Manufactured by Tullamore Division, the Victoreen Instrument Company, Oak Lawn, Illinois.

46. B. vanNooijen and J. H. Hamilton, Internal Conversion Processes, ed. by J. H. Hamilton, (Academic Press Inc., New York, 1966), p. 642.

47. D. R. Bundrit and S. K. Sen, Nucl. Instr. Methods 34, 225 (1965).

48. J. M. McKenzie and G. T. Ewan, IRE Trans. Nucl. Sci. NS-8, No. 1, 50 (1961).

49. R. B. Frankel, (Ph.D. Thesis) Radiation Laboratory Report UCRL-11871, 1965 (unpublished).

50. K. G. Malmfors, Arkiv Fysik 13, 237 (1957).

51. R. L. Watson, (Ph.D. Thesis) Lawrence Radiation Laboratory Report UCRL-16798, 1966 (unpublished).

52. M. G. Mayer, Phys. Rev. 74, 235 (1948).

53. O. Haxel, J. H. Jensen, and H. E. Suess, Phys. Rev. 75, 1766 (1949).

54. A. Bohr and B. R. Mottelson, Kgl. Danske Videnskab. Selskab Mat.-Fys. Medd. 27, No. 16 (1953).

55. M. A. Preston, Physics of the Nucleus, (Addison-Wesley Publishing Co., Inc., Reading, Mass., 1962).

56. A. de-Shalit, Phys. Rev. 122, 1530 (1961).

57. R. D. Lawson and J. L. Uretsky, Phys. Rev. 108, 1300 (1957).

58. A. Braunstein and A. de-Shalit, Phys. Letters 1, 264 (1962).

59. J. M. McKinley and P. M. Rinard, Nucl. Phys. 79, 159 (1966).
60. V. K. Thankappan and Y. S. T. Rao, private communication (1966).
61. L. S. Kisslinger and R. A. Sorensen, Rev. Mod. Phys. 35, 853 (1963).
62. J. Bardeen, L. N. Cooper, and J. R. Schrieffer, Phys. Rev. 108, 1175 (1957).
63. A. Bohr, B. R. Mottelson, and D. Pines, Phys. Rev. 110, 936 (1958).
64. D. C. Choudhury, Kgl. Danske Videnskab. Selskab. Mat.-Fys. Medd. 28, No. 4 (1954).
65. G. Alaga and G. Ialongo, Lawrence Radiation Laboratory Report UCRL-16385 (1965).
66. G. Ialongo, (Ph.D. Thesis) New York University, 1966 (unpublished).
67. Helicopter service provided by General Air Service, Buchannan Field, Concord, California.
68. W. G. Smith, (Ph.D. Thesis) Lawrence R diation Laboratory Report UCRL-2974, 1955 (unpublished).
69. R. W. Fink and S. G. Thompson, "Chemical Procedures Used in Bombardment Work at Berkeley," ed. by W. W. Meinke, AECD-2738, p. 232, 1949.
70. Vacion pumps available from Vacuum Products Division, Varian Associates, 611 Hansen Way, Palo Alto, California.
71. J. M. LeBlanc, J. M. Cork, and S. B. Burson, Phys. Rev. 104, 1670 (1956).
72. M. C. Joshi, B. V. Thosar, and K. G. Prasad, Nucl. Phys. 52, 301 (1964).
73. W. W. Black, AEC Research and Development Report IDO-17081, p. 59, 1965.
74. G. Wessel and H. Lew, Phys. Rev. 92, 641 (1953).
75. R. L. Christensen, D. R. Hamilton, A. Lemonick, F. M. Popkin, J. B. Reynolds, and H. H. Stroke, Phys. Rev. 101, 1389 (1956).
76. W. B. Ewbank, L. L. Marino, W. A. Nierenberg, H. A. Shugart, and H. B. Silsbee, Phys. Rev. 120, 1406 (1960).
77. V. R. Potnis, C. E. Mandeville, and J. S. Burlew, Phys. Rev. 101, 753 (1956).

78. M. C. Joshi and B. V. Thosar, Proc. Int. Conf. Nuclear Structure, Kingston, ed. by D. A. Bromley and E. V. Vogt, (University of Toronto Press, Toronto, 1960), p. 623.

79. R. G. Halmer, Phys. Rev. 131, 2597 (1964).

80. P. B. Griesacker and R. R. Roy, Nucl. Phys. 50, 41 (1964).

81. J. W. Mihelich and A. de-Shalit, Phys. Rev. 91, 78 (1953).

82. O. Huber, F. Humbel, H. Schneider, A. de-Shalit, and W. Zünti, Helv. Phys. Acta 24, 127 (1951).

83. R. Joly, J. Brunner, J. Halter, and O. Huber, Helv. Phys. Acta 28, 403 (1955).

84. C. F. Cook, C. M. Class, and J. T. Eisinger, Phys. Rev. 96, 658 (1954).

85. P. H. Stelson and F. K. McGowan, Phys. Rev. 99, 112 (1955).

86. V. K. Fischer, Phys. Rev. 99, 764 (1955).

87. F. Smend, W. Weirauch, W.-D. Schmidt-Ott, and A. Flammersfeld, Z. Physik 191, 1 (1966).

88. A. J. Haverfield, H. T. Easterday, and J. M. Hollander, Nucl. Phys. 64, 379 (1965).

89. G. T. Emery and M. L. Sehgal, Bull. Am. Phys. Soc. 10, 83 (1965).

90. J. H. Moon and A. L. Thompson, Phys. Rev. 83, 892 (1951).

91. L. P. Gillon, K. Gopalakrishnan, A. de-Shalit, and J. W. Mihelich, Phys. Rev. 93, 124 (1954).

92. J. Brunner, H. Guhl, J. Halter, and O. Huber, Helv. Phys. Acta 28, 85 (1955).

93. J. Brunner, H. Guhl, J. Halter, H. J. Leisi, Helv. Phys. Acta 28, 475 (1955).

94. J. Brunner, J. Halter, H. J. Leisi, Helv. Phys. Acta 29, 237 (1956).

95. J. Brunner, J. Halter, C. Perdrisat, Helv. Phys. Acta 30, 269 (1957).

96. J. Brunner, J. Halter, P. Scherrer, Helv. Phys. Acta 31, 335 (1958).

97. S. B. Kaufman, Annual Progress Report, Nuclear Chemistry Research at Princeton University, PPAD-2137-566, p. 27, 1965.

98. G. T. Ewan, Can. J. Phys. 35, 672 (1957).

99. V. K. Thankappan and W. W. True, Phys. Rev. 137, B793 (1965).

100. A. G. Blair, Phys. Letters 9, 37 (1964); and private communication as quoted in Ref. 99.

101. A. de-Shalit, Phys. Letters 15, 170 (1965).

102. A. W. Sunyar, Phys. Rev. 98, 653 (1955).

103. I. J. vanHeerden, D. Reitman, H. Schneider, Nuovo Cimento 11, 167 (1959).

104. P. Reyes-Suter, T. Suter, Arkiv Fysik 20, 187 (1961).

105. J. Sant'Ana Dionisio, Compt. rend. 254, 1972 (1962).

106. J. Jastrzebski and P. Kilcher, Compt. rend. 254, 1411 (1962).

107. S. A. Moszkowski, "Theory of Multipole Radiation," in Beta- and Gamma-Ray Spectroscopy, ed. by K. Siegbahn, (North-Holland Publishing Co., Amsterdam, 1955), p. 391.

108. H. H. Woodbury and G. W. Ludwig, Phys. Rev. 117, 1287 (1960).

109. R. J. Blin-Stoyle, Proc. Phys. Soc. (London) 66, 1158 (1953).

110. S. G. Nilsson, Kgl. Danske. Videnskab. Selskab Mat.-Fys. Medd. 29, No. 16 (1955).

111. J. Jastrzebski, Phys. Letters 3, 289 (1963).

112. M. E. Rose, G. H. Goertzel, B. I. Spinrad, J. Harr, and P. Strong, Phys. Rev. 83, 79 (1951).

113. M. E. Rose, Internal Conversion Coefficients, (North-Holland Publishing Co., Amsterdam, 1958).

114. L. A. Sliv and I. M. Band, Coefficients of Internal Conversion, Acad. of Sci. USSR, 1956; also published as Reports 57ICCKI, and 58ICCLI, Phys. Dept., University of Illinois, 1957.

115. L. A. Sliv and I. M. Band, "Tables of Internal Conversion Coefficients," in Alpha-, Beta-, and Gamma-Ray Spectroscopy, ed. by K. Siegbahn, (North-Holland Publishing Co., Amsterdam, 1965), Vol. 2, p. 1639.

116. M. E. Rose, "Theory of Internal Conversion," in Alpha-, Beta-, and Gamma-Ray Spectroscopy, ed. by K. Siegbahn, Vol. 2, (North-Holland Publishing Co., Amsterdam, 1965), p. 887.

117. M. E. Rose, "Tables of Internal Conversion Coefficients," in Beta- and Gamma-Ray Spectroscopy, ed. by K. Siegbahn, (North-Holland Publishing Co., Amsterdam, 1955), p. 905.

118. Y. Y. Chu and M. L. Perlman, Phys. Rev. 135, B319 (1964).

119. M. E. Rose, W. H. Brantley, J. Hamilton, and A. V. Ramayya, "K/L, L_1/L_2, and L_1/L_3 Conversion Coefficient Ratios," in Internal Conversion Processes, ed. by J. H. Hamilton, (Academic Press, New York, 1966), p. 616.

120. G. T. Ewan and R. L. Graham, "Internal Conversion Studies at Very High Resolution," in Alpha-, Beta-, and Gamma-Ray Spectroscopy, ed. by K. Siegbahn, (North-Holland Publishing Co., Amsterdam, 1965), Vol. 2, p. 951.

121. T. Novakov and J. M. Hollander, Nucl. Phys. 60, 593 (1964).

122. D. Parsignault, "The Beta Spectrum of Au^{198}, and the Conversion Coefficients of the 412-keV Line in Hg^{198}," in Internal Conversion Processes, ed. by J. H. Hamilton, (Academic Press, New York, 1966), p. 173.

123. J. H. Hamilton, A. V. Ramayya, B. vanNooijen, R. G. Albridge, E. F. Zganjar, S. C. Pancholi, J. M. Hollander, V. S. Shirley, and C. M. Lederer, Nuclear Data 1, 521 (1966).

124. H. Hagedoorn and A. H. Wapstra, Nucl. Phys. 15, 146 (1960).

125. J. F. W. Jansen and A. H. Wapstra, "Determination of the Conversion Coefficient in Yb^{170} with Scintillation Methods," in Internal Conversion Processes, ed. by J. H. Hamilton, (Academic Press, New York, 1966), p. 237.

126. S. Hultberg, B. Nagel, and P. Olsson, (to be published).

127. S. Hultberg, "Recent Developments in the Internal-External Conversion (IEC) Method," in Internal Conversion Processes, ed. by J. H. Hamilton, (Academic Press, New York, 1966), p. 125.

128. S. Hultberg and R. Stockendal, Arkiv Fysik 14, 565 (1959).

129. A. C. G. Mitchell, "Procedures for the Investigation of Disintegration Schemes: General Procedures," in Alpha-, Beta-, and Gamma-Ray Spectroscopy, ed. by K. Siegbahn, (North-Holland Publishing Co., Amsterdam, 1965), Vol. 1, p. 467.

130. T. R. Gerholm, Arkiv Fysik 11, 55 (1956).

131. W. H. G. Lewin, B. vanNooijen, and A. H. Wapstra, Nucl. Phys. 27, 681 (1961).

132. R. S. Dingus, W. L. Talbert, Jr., and E. N. Hatch, Iowa State Univ. Report IS-1032 (1965).

133. T. J. Kennett, Physics Today 19, 86 (1966).

134. R. L. Heath, W. W. Black, and J. E. Cline, Nucleonics 24, No. 5, 52 (1966).

135. K. Dolan, D. K. McDaniels, and D. O. Wells, Phys. Rev. 148, 1151 (1966).

136. J. B. Marion, Gamma-Ray Energy Standards, (to be published).

137. A. J. Haverfield, F. M. Bernthal, and J. M. Hollander, Lawrence Radiation Laboratory Report UCRL-16862, 1966.

138. S. Hagström, C. Nordling, and K. Siegbahn, "Table of Electron Binding Energies," in Internal Conversion Processes, ed. by J. H. Hamilton, (Academic Press Inc., New York, 1966), p. 644.

139. W. W. Black and R. L. Heath, Nucl. Phys. (in press).

140. J. Moreau, J. Phys. Radium 15, 380 (1954).

141. J. S. Geiger, R. L. Graham, I. Bergström, and F. Brown, Nucl. Phys. 68, 352 (1965).

142. K. Siegbahn, "Beta-Ray Spectrometer Theory and Deisgn," in Alpha-, Beta-, and Gamma-Ray Spectroscopy, ed. by K. Siegbahn, (North-Holland Publishing Co., Amsterdam, 1965), Vol. 1, p. 198.

143. S. C. Misra, J. S. Merritt, and J. G. V. Taylor, (unpublished).

144. H. P. Hotz, J. M. Mathiesen, J. P. Hurley, U. S. Naval Radiological Defense Laboratory Report USNRDL-TR-817.

145. K. M. Wainio, (Ph.D. Thesis) University of Michigan, 1965.

146. E. Storm, E. Gilbert, and H. Israel, AEC-report LA-2237 (1958).

147. E. S. Fry, J. M. Palms, R. B. Day, Los Alamos Report LA-3456.

148. B. Åström, A. H. Wapstra, S. Thulin, and I. Bergström, Arkiv Fysik 7, 247 (1954).

149. L. L. Riedinger, J. H. Hamilton, N. R. Johnson, private communication.

150. L. B. Magnusson, Phys. Rev. 107, 161 (1957).

151. Nuclear Data Sheets, Nuclear Data Group, Oak Ridge National Laboratory.

152. F. S. Goulding and B. V. Jarrett, Lawrence Radiation Laboratory Report UCRL-16480.

153. G. T. Ewan, private communication.

154. G. T. Ewan, J. S. Geiger, R. L. Graham, and D. R. MacKenzie, Phys. Rev. 116, 950 (1959).

155. P. Alexander, F. Boehm, and E. Kankeleit, Phys. Rev. 133, B284 (1964).

156. I. Ahmad, (Ph.D. Thesis) Lawrence Radiation Laboratory Report UCRL-16888, 1966 (unpublished).

157. J. A. Moragues, T. Suter, P. Reyes-Suter, W. Scheuer, private communication.

158. D. H. White and D. J. Groves, Nucl. Phys. (to be published).

159. V. Gruber, R. Koch, B. P. Maier, and O. W. B. Schultz, Z. Naturforsch. 20, 929 (1965).

160. E. J. Seppi, H. Henrikson, F. Boehmand, and J. W. M. DuMond, Nucl. Instr. Methods 16, 17 (1962).

161. R. Vandenbosch and J. R. Huizenga, Phys. Rev. 120, 1313 (1960).

162. A. H. Wapstra, G. J. Nijgh, and R. Van Lieshout, Nuclear Spectroscopy Tables, (North-Holland Publishing Co., Amsterdam, 1959).

This report was prepared as an account of Government sponsored work. Neither the United States, nor the Commission, nor any person acting on behalf of the Commission:

A. Makes any warranty or representation, expressed or implied, with respect to the accuracy, completeness, or usefulness of the information contained in this report, or that the use of any information, apparatus, method, or process disclosed in this report may not infringe privately owned rights; or

B. Assumes any liabilities with respect to the use of, or for damages resulting from the use of any information, apparatus, method, or process disclosed in this report.

As used in the above, "person acting on behalf of the Commission" includes any employee or contractor of the Commission, or employee of such contractor, to the extent that such employee or contractor of the Commission, or employee of such contractor prepares, disseminates, or provides access to, any information pursuant to his employment or contract with the Commission, or his employment with such contractor.